Bulletin 39
Part 6
(of 6 Parts)

THE SHOCK AND VIBRATION BULLETIN

MARCH 1969

A Publication of
THE SHOCK AND VIBRATION
INFORMATION CENTER
Naval Research Laboratory, Washington, D.C.

Office of
The Director of Defense
Research and Engineering

Reproduced by the
CLEARINGHOUSE
for Federal Scientific & Technical
Information Springfield Va. 22151

DISCLAIMER NOTICE

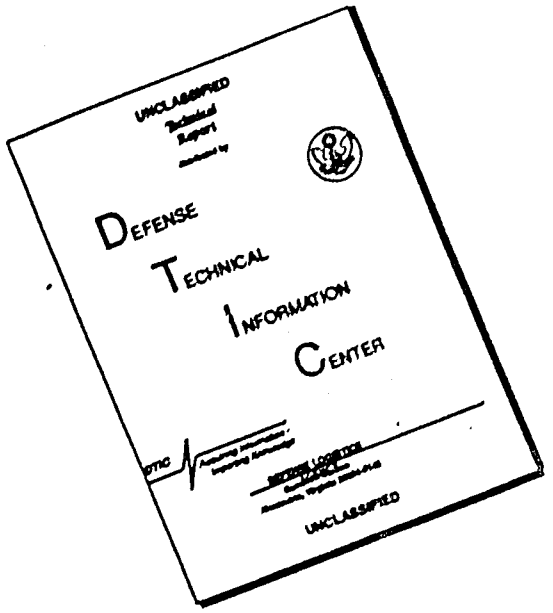

THIS DOCUMENT IS BEST QUALITY AVAILABLE. THE COPY FURNISHED TO DTIC CONTAINED A SIGNIFICANT NUMBER OF PAGES WHICH DO NOT REPRODUCE LEGIBLY.

SYMPOSIUM MANAGEMENT

THE SHOCK AND VIBRATION INFORMATION CENTER

William W. Mutch, Director
Henry C. Pusey, Coordinator
Rudolph H. Volin, Coordinator
Katherine G. Jahnel, Administrative Secretary

Bulletin Production

Graphic Arts Branch, Technical Information Division,
Naval Research Laboratory

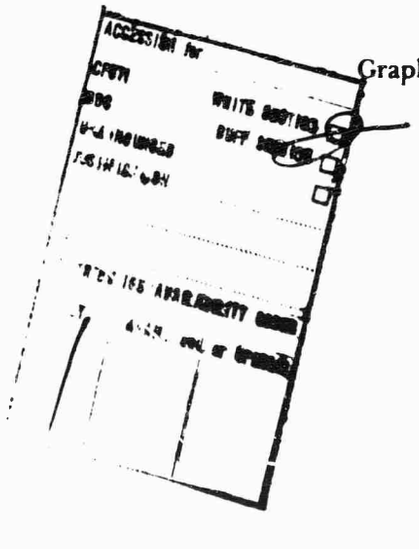

Bulletin 39
Part 6
(of 6 Parts)

THE SHOCK AND VIBRATION BULLETIN

MARCH 1969

A Publication of
THE SHOCK AND VIBRATION
INFORMATION CENTER
Naval Research Laboratory, Washington, D.C.

The 39th Symposium on Shock and Vibration was held in Pacific Grove, California, on 22-24 October 1968. The U.S. Army was host.

Office of
The Director of Defense
Research and Engineering

CONTENTS

PAPERS APPEARING IN PART 6

PAPERS APPEARING IN PART 1

Part 1 - Classified
(Unclassified Titles)

*This paper not presented at Symposium.

PAPERS APPEARING IN PART 2

Vibration

*This paper not presented at Symposium.

*This paper not presented at Symposium.

PAPERS APPEARING IN PART 4

Damping

*This paper not presented at Symposium.

Isolation

*This paper not presented at Symposium.

PAPERS APPEARING IN PART 5

Shock

PAPERS APPEARING IN THE SUPPLEMENT

*This Paper not presented at Symposium.

INTRODUCTORY PAPERS

THE IMPACT OF A DYNAMIC ENVIRONMENT ON FIELD EXPERIMENTATION*

Walter W. Hollist†

U.S. Army Combat Developments Command
Experimentation Command
Fort Ord, California

Gentlemen:

Let me first thank you for the invitation to speak to you this morning. It is an honor and a pleasure to be a part of this 39th Symposium on Shock and Vibration. Since some of you may not be familiar with the organization of which I am a part, I have divided my remarks into two parts. First, I will discuss the U.S. Army Combat Developments Command Experimentation Command and its mission, after which I shall discuss some aspects of the interaction between our field instrumentation and a dynamic environment.

The U.S. Army Combat Developments Command Experimentation Command, located at Fort Ord, is a major subordinate command of the Army's Combat Developments Command. Our parent command is charged with the mission of determining the answers to three seemingly simple, but really very complex questions:

1. How should the Army by organized?
2. How should the Army fight?
3. How should the Army be equipped?

As you can appreciate, the magnitude of this task is enormous since these questions must be answered not only for today, but for next year and succeeding years for more than 20 years into the future. To assist in this task, the Combat Developments Command has many subordinate commands, of which the Combat Developments Command Experimentation Command, called CDEC for ease, is one.

We are the field laboratory of our parent command. It is our task to generate scientifically-derived data which will assist in providing answers to those three salient questions I mentioned earlier. Military field experimentation is an adaptation of the well known and well utilized academic investigative technique. As with any experiment, our data must satisfy three basic tests of value — objectivity, validity, and reliability. Since the medium with which we are experimenting is a complex interrelationship between the soldier, his environment, his materiel, the doctrine by which he fights, and the organization within which he fights, the problems associated with satisfaction of these tests of value are unique, as you can imagine.

Just as our problem of experimental design is unique, so is the laboratory in which we conduct our experiments. The CDEC Laboratory is spread over a 120-mile range. The Laboratory Headquarters and most of our personnel are located at Fort Ord; however, most of our experiments are executed at the Hunter Liggett Military Reservation. Hunter Liggett includes some 175,000 acres of ranges and maneuver area. Representative terrain at Hunter Liggett is shown in Figs. 1-3. Our attempt is, however, to be flexible in our response to the demands of experimentation. We have, for example, conducted a field experiment in Panama and one in Texas. The spectrum covered by our experimentation program is broad. Recently we concluded an evaluation of the utility of a new chaplain's kit for use in conflicts such as the current one in Southeast Asia, and we are now engaged in an experiment intended to provide insights into the most effective means of organizing and arming the basic infantry element.

With this brief explanation of what CDEC is and why CDEC is, let me move into the primary

*An introductory address given at the 39th Shock and Vibration Symposium.
†Scientific Advisor

Fig. 1 - Hunter Liggett Military Reservation (mountains)

Fig. 2 - Hunter Liggett Military Reservation (valleys)

Fig. 3 - Hunter Liggett Military Reservation (rolling terrain)

subject of my discussion — the impact of a dynamic environment on field experimentation. In addressing this subject I will give you a broad qualitative rather than quantitative view since the balance of your program will, I am sure, provide you with sufficient mathematics.

To meet the test of validity, our investigations must be conducted under conditions which duplicate as closely as possible those of actual field or combat operations. Therefore, almost by definition, our experimental environment is dynamic. Instrumentation used in our experiments can generally be placed in one of two categories. The first of these categories includes all instrumentation which is carried by players in our experiments and the second category includes all instrumentation which is a part of the targets against which our players operate.

In the first category of instrumentation, we must have equipment which is capable of functioning reliably and accurately in spite of the rough and tumble treatment it will receive in the course of the tactical play of the experiment and which, at the same time, is not of such weight and volume as to interfere with the execution of normal operating procedures or tactical maneuvers by the player personnel. In the second category of instrumentation the weight and volume constraints are not as stringent, but the environment is more severe since the instrumentation is subjected to the induced shock, vibration, and temperature environment resulting from a projectile hit on the target. As you can appreciate, the task of the instrumentation design envineer in first identifying the appropriate environmental limits and then designing equipment to function in that environment is substantial.

Those responsible for this task at CDEC, our Instrumentation Support Group, have been quite successful. The unit shown in Fig. 4 is the man portable responder unit which can both send and receive information pertinent to player activity. This unit is a part of a system by which a record of player position, event, occurrence, and time of event occurrence is maintained. One component of this unit, not shown in Fig. 4, is a probe which extends into the path of the muzzle blast, senses the firing of a round and causes an appropriately coded signal to be transmitted by the transponder unit. I think all of you can appreciate the need for careful consideration of the dynamic environment in the design of such a device.

In the area of instrumentation for the individual soldier, we are now engaged in a development program for a direct fire weapon simulator, Fig. 5, which will permit us to conduct more realistic two-sided maneuvers than can be conducted at the present time. This device will be based upon the use of a pulse-coded gallium arsenide laser beam which will be used as the "bullet" of the simulator. For realism, the soldier firing the simulator will simultaneously fire a blank cartridge from his weapon.

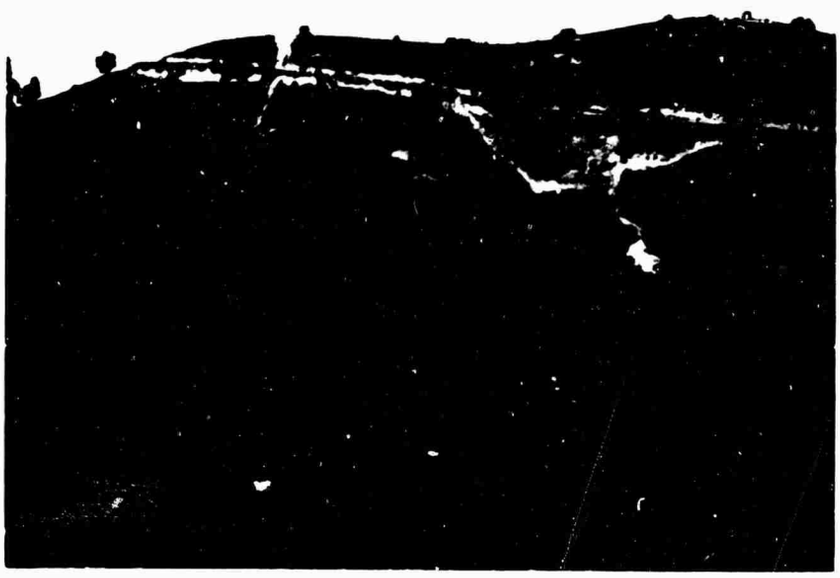

Fig. 4 - Man portable responder unit

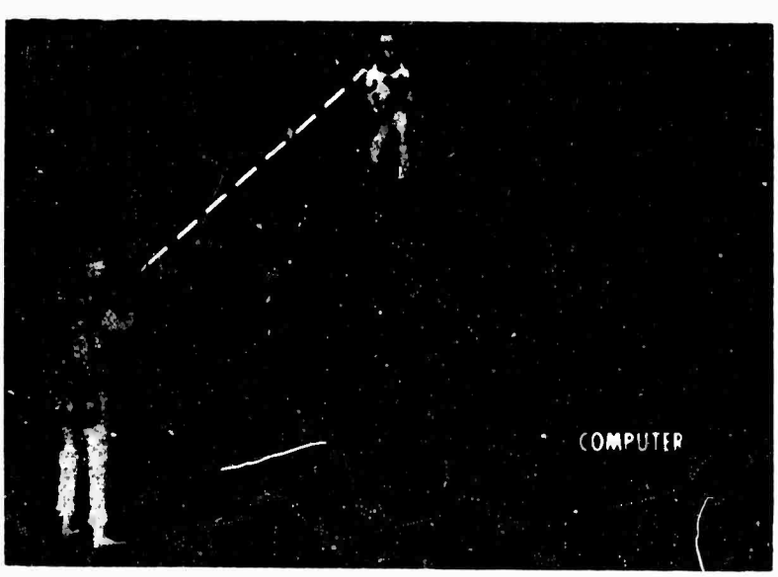

Figure 5

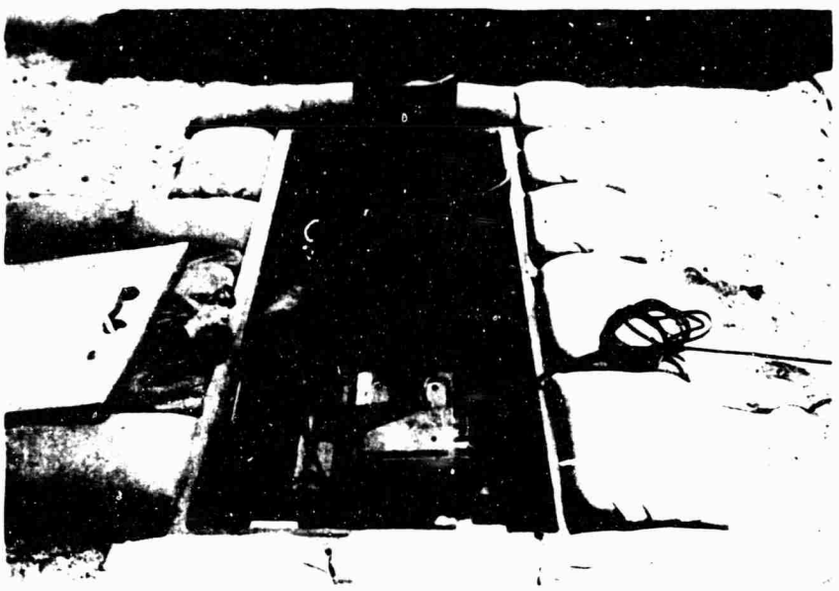

Fig. 6 - "Pop-up" personnel target

The recoil of the weapon and force of the hammer striking the firing pin cause vertical accelerations to the weapon which may cause the laser beam to miss the target since the logic of the simulator requires that three messages be transmitted by the weapon and received by the target in order to register a hit. The problem here, of course, is to identify accurately the timing sequence of all the actions which cause the vertical accelerations, identify the amount of time during which the hammer is falling, and then transmit the necessary laser messages in that time interval.

In the second category, I mentioned one of our principal items of instrumentation in the "pop-up" personnel target, Fig. 6. This target is the target we now employ on our "live fire" ranges. The target is instrumented to record hits and/or near misses from rifle fire, machine gun fire, and from the shrapnel caused by the detonation of 40-mm grenades. The construction of this target system permits protection of most of the instrumentation within the coffin; however, the target itself is aluminum and any vibration induced in the target as a result of a projectile hit could cause the registration of "false hits." Study of this potential problem led to the overcoating of the forward side of the target with a cellular rubber which effectively damps the induced vibration below a level to which the hit sensing mechanism is sensitive.

In the same category of instrumentation a potentially more difficult problem to solve is associated with our requirement for a vehicular target system which will be representative of a so-called "hard target," that is, a tank or armored personnel carrier. This vehicular "pop-up" target must be capable of withstanding the shock impact resulting from a direct hit from a projectile fired by a tank in main armament, be capable of sustaining more than one hit without destruction, and, of course, be economical to acquire. Our preliminary investigation into this problem indicates that a target constructed of fluted cardboard may be the answer; however, this investigation is far from complete as I speak to you today.

TRANSCRIPT OF PANEL DISCUSSION ON PROPOSED USASI STANDARD ON METHODS FOR ANALYSIS AND PRESENTATION OF SHOCK AND VIBRATION DATA

Julius S. Bendat
Measurement Analysis Corporation
Los Angeles, California

and

Allen J. Curtis
Hughes Aircraft Corporation
Culver City, California

DR. BENDAT

We want this panel discussion to be an informal, extemporaneous, and informative discussion about work that has been going on for the last six years. This is the first public presentation on the results of this particular S2 Standards Committee to document and recommend standard methods for analyzing and presenting shock and vibration data, based on current usage and current understanding of the activities and the developments in the field. This work started in 1962 and the first Chairman was Dr. Charles Crede from Cal Tech. Dr. Crede headed a committee of which Dr. Curtis, Dr. Rubin, myself and others were members. Unfortunately when Dr. Crede died some four years ago, the work was still in an early phase, so we continued, and I was asked to take over as Chairman.

Many other people assisted us who represented a cross section of different interest groups from Government and Industry in the U.S. As the writing proceeded, it was necessary to send preliminary drafts to these people for their comments, criticism and suggestions. This work went quite slowly and its only been in the last two days that we can now finally state that our work is just about over. There was a meeting of the full S2 Committee here in Asilomar on Tuesday afternoon and at that time the last material that had been submitted by this committee was approved, to be transmitted to the U.S.A. Standards Institute for final action and ultimate distribution as a USASI Standard.

I might mention that besides the three of us who were going to give this presentation today (we're sorry that Dr. Rubin is unable to attend), other people who have been involved reviewing and approving the work include L. L. Beranek. S. Edelman, C. A. Golueke, H. H. Himelblau, D. C. Kennard, D. Muster, W. W. Mutch, M. L. Stoner, H. E. von Gierke, representing groups from the Department of Defense, the American Society of Mechanical Engineers, the Acoustical Society of America, National Bureau of Standards, Institute of Electrical-Electronic Engineers, Society of Automotive Engineers, Institute of Environmental Sciences, National Electric Manufacturers Association, and so on.

Now, what has resulted from this effort is a Standard of some 49 pages that includes a definite statement of the purpose and scope, every word carefully chosen. There is a listing of some 50 symbols which are used repeatedly. This does not constitute standardization of the symbols, it just means that we use them, we recomment them, others are using them. This list doesn't replace the use of other symbols found elsewhere in some other Standard or in some other work. Also, there is a list of some hundred definitions of different terminology that appears throughout the literature and a great deal of current work. This includes definitions of some terms which have appeared in previous Standards, so that we merely followed previous work; other definitions have had to be written for the first time. These are in alphabetical order and go all the way from "acceleration" through many of the terms that we will mention later this morning up to the last term

of Weakly Self Stationary Data." Some of these may be new to certain people here but they have become well enough understood now to be incorporated in such a Standard.

We also have a fairly comprehensive block diagram of recommended data analyses and presentations - sort of overall considerations that you should have in mind regardless of your application. This has been distributed to each of you here for reference (see slides). It doesn't necessarily mean that you will follow every block in the diagram, but you should be aware of them and should use those that are pertinent to a particular application. This is one of some twenty diagrams in the Standard. The other diagrams in the Standard give greater details for individual blocks, different ways to compute certain of the functions or ways in which to display the results.

There is no attempt in this Standard to restrict anyone in the use of any particular equipment, analog, hybrid or digital, or to use any special computer data analysis program. There is no attempt to state specifically what parameters you should choose; these matters have to be determined as a result of a great deal of other work that would go along with these ideas. There are some references given to pertinent literature, and there is a great deal of emphasis on requirements that you should keep in mind.

These particular types of analyses and presentations are the ones that we consider fairly basic, fairly standard, and we feel there is no reason any more for people to be using these concepts in different ways. Confusion exists when the same term has a different interpretation on the part of different people. There were a number of points of view that had to be considered in this Standard and we tried as hard as we could to reconcile the various groups. Different people, of course, you know, have different needs and it is quite difficult as we learned over a four year history to get the agreement that we finally did achieve, so we are very pleased at the acceptance that has been obtained.

I want to emphasize again the fact that this Standard contains a number of very basic analysis procedures and basic data presentation methods. Deviations are going to occur and will legitimately occur for many special applications, but I think the requirement on people in the future who deviate from some of these recommendations will be that they must justify their deviations. It is not a wholesome situation anymore when people are computing, for example, correlation functions or spectral density functions by a number of different methods without taking into consideration some of the basic requirements to make sure that other people who will examine their work can properly interpret it. The analysis must be conducted in an accepted fashion and enough parameters must be made available to the analyst so he can do some appropriate error analysis for the displayed results if he so desires. Error analysis considerations are implied in the Standard. However, the exact procedures for carrying out error analysis were not in a state where they could be standardized as such.

The document, I think, will strike a very responsive chord in the mind of many people who have long felt a need for this material. It's our hope that as it becomes circulated, it will facilitate the application of these techniques to not only problems in shock and vibration but in many other fields as well. As a matter of fact, although there are many terms here that are restricted to shock and vibration, the actual scope of the Standard is broader, and would refer to random data regardless of the field in which it's obtained. I might briefly read a few words that state the purpose and scope of this document.

PURPOSE

"This Standard is designed to acquaint the user with general principles of the analysis and presentation of shock and vibration data, and to describe concisely several methods of reducing data to forms that can be applied and used in subsequent analyses. The Standard includes references to the technical literature for elucidation of applicable mathematical principles or where ready explanations are not available in the literature, an outline of applicable principles."

SCOPE

"This Standard covers vibration in the following idealized classes which are defined in Section 2.2. a. periodic vibration, b. aperiodic vibration, c. random vibration, and d. transient vibration (including shock). It is assumed that the data are available as time-histories of a variable

associated with shock and vibration, for example, acceleration, velocity, force, and so forth and that any distortion resulting from the transducer, recording system, etc., has been eliminated. It is recognized that in many instances the vibration does not conform to this classification but rather consists of combinations of two or more classes. Suggestions are given for separating classes as a necessary step in data analysis."

The purpose, the scope, and other details in the Standard represent the results on which we were able to obtain this general agreement that I mentioned. How Dr. Curtis or myself might apply some of these ideas, or how some of you might apply these ideas might be worthwhile additions, but they were not in a form, in a general enough way to be included in the Standard. I think, in our later discussion, we will have to be very careful to state what is in the Standard, as opposed to other practices not in the Standard (that we are aware of) which are used by some people.

We have only three slides that we want to show and then we will open up the session to discussion. The three slides are a breakdown of the figure which has been passed out to you. You will note that there are, first of all, many steps involving classification and data qualification prior to the time that you actually do any specific analysis. Then there are six blocks across of different types of analysis. I would like to start out by discussing the initial preparation and classification of data, and then Dr. Curtis will go into some details of specific types of analysis and presentations.

SLIDE NO. 1

You will note that we start out with some time-history. The word time-history is descriptive only. You may prefer to call it the vibration, record, waveform or signal, it really doesn't matter. I think time-history is used by enough people, and we understand that it is some indication of behavior of the particular phenomena in question. It's a function of an independent variable which may be time or any other variable which can take the place of time. Our job is to analyze in as much detail as is needed for a particular application, the amplitude properties, frequency properties, and time related properties as might be contained in the data.

There are many extensions of ideas that are not in the Standard - we are very careful to restrict ourselves in the Standard to analysis of either individual records or to pairs of records. You may want to get more information about an individual record as a result of being able to duplicate the analysis on similar results from other experiments. There is some discussion here of joint statistical properties such as cross-correlation and cross-spectral density analysis, but we don't go into discussion of transfer functions or frequency response functions which represent important applications that you might want to make of spectral or cross-spectral results.

In the first part of the Standard, the top part of this diagram, you will note that the data needs to be separated out into three main types. The first type of data is transient, which means that its properties will die down. Next is periodic data, as defined classically, which goes on forever. Third is data which visually at least may not appear to be periodic or transient, so it needs to be studied further. We call this third type continuing non-periodic data.

There are three special test blocks that may be required, but the actual procedure for carrying out the test for randomness, or the test for stationarity, or the test for normality, are not in the Standard. There are different ways that people are currently using for these tests and we didn't feel it appropriate at this stage of the game to standardize any of these tests. We merely wanted to indicate here that there is a need for such tests. It is necessary, in general, to qualify the data before you can do the later analysis to be sure that you are analyzing what you think you are analyzing.

A test for randomness is to separate out the random from the non-random components in the continuing nonperiodic data. It might be ignored by some trained analysts, but this omission is seldom recommended. It doesn't have to be a statistical test, it can be a practical test, fairly elementary. The actual ways in which you might carry out the test for randomness are not a part of the Standard.

The most important test requirement is probably the test for stationarity. Again this test is not in a

form that can be standardized, but here we definitely want to separate out non-stationary components from stationary components. All of these terms are defined in the Standard and we don't have time here to give a course or to go into these matters. I hope it will still be clear what's involved in our discussion. If the data is non-stationary, it must be analyzed by special methods which would be peculiar to the particular type of non-stationarity. One such method which we felt is in pretty good shape has been included in the Standard, namely, a magnitude-time analysis which Dr. Curtis will discuss. There are many other procedures for analyzing non-stationary data - which are not in the Standard - that should be used where appropriate in current work. If the data does pass the test for stationarity, considering a single record, we really have the idea of weakly self-stationary data in mind. For usual cases of self-stationarity, this means that we are considering only the stationarity of this one record rather than the stationarity of a collection of records.

For weakly self-stationary data, there are certain types of accepted well-known analyses that have been in the field now for many years: statistical analysis, correlation analysis, spectral analysis. Basic results for these types of analyses are described in the Standard, the definitions of various terms, typical displays; results that we feel are so well established that there is a requirement on the part of everybody concerned to use these methods. Where you might go further into applications of these particular results, or in developing other special functions, you would be doing your own individual creative work.

Periodic data is deterministic data for which fairly classical well-known procedures are available, since there are explicit mathematical formulas to describe the properties, as opposed to random data which must be handled by probability or statistical techniques. Some of these accepted recognized procedures are in the Standard for analyzing periodic data. Finally, the analysis and presentation of transient data, also aperiodic data and shock data, can be standardized by means of Fourier or shock spectrum analysis techniques which are widely used, as discussed in the Standard.

The first discussion, and the first emphasis on data classification, is really the guideline for overall considerations. After applying needed tests, as you perform the subsequent analysis, we point out in the Standard the importance of keeping track of various parameters, so that somebody that follows you who wants to do some further detailed error analysis of a statistical sort would have the necessary parameters. I would like to turn over the discussion now to Dr. Curtis who will go into some of the detailed analysis and presentation recommendations.

DR. CURTIS

SLIDE NO. 2

This slide again is just a certain part of the road map, if you will, that we handed out to you and includes all the blocks under weakly self-stationary data. It says that you've gone through this classification process, you've determined that it is weakly self-stationary data, and under here we try to indicate the kinds of analyses that can, possibly should, be done. Now you can separate these into three major kinds: statistical analysis, correlation analysis, and spectral analysis. Now these three are interrelated, as I am sure you are aware, since the performance of correlation analysis gives you some indication of the statistical characteristics of the signal and so in effect helps you in the statistical analysis. Likewise, for stationary data, it's possible to derive the spectral density plot from an autocorrelation analysis, and so they are again interrelated.

Under each of these three major classifications we indicate again sub-classifications of data analysis and the last line then describes the ways in which data after it has been analyzed in the prescribed way, should be presented. Now, we have not suggested what coordinate scales you should use or even particularly what physical units you should use, but we have indicated the kinds of units you should use. More particularly, we have said and we hope through this document that we can help standardize the information which is included on a particular data plot. For example, an incomplete spectral density plot is one that does not give you some information about the bandwidth used for analysis, that does not tell you the length of the data sample, or if you used a sweep filter, for instance, that does not define the sweep rate of the filter. We have indicated throughout

the Standard the requirements for complete data presentation so that somebody else can interpret what you did. Presumably if you do analysis, it's for understanding not only by yourself, but somebody else as well.

Under statistical analysis, we describe the principles, or some principles by which, this may be conducted. These principles apply equally well whether you are interested in the statistical nature of the instantaneous value of this time history, or the peak or maxima of the time-history. You can do this in two ways: you can look at the probability density of the signal which, for example, says what percentage of the time is the signal within a certain magnitude window, or you can look at the probability distribution which says what percentage of the time does the signal exceed a certain value. As I am sure you will remember, the probability distribution can be obtained as the integral of the probability density. When you have conducted such an analysis, then we indicate that probably a desirable analysis to perform is to compare the probability density or the distribution to the normal distribution to indeed check that you have a Gaussian distribution or how far you've strayed from that.

The third block is a little more exotic, the joint probability analysis, where you take two signals and you are computing their joint statistical or common statistical properties. The data presentation here, of course, becomes a three dimensional plot which is a little more difficult, but the Standard does indicate what is necessary to do.

The correlation analysis breaks down into two types. First, autocorrelation, where one looks at the relationship for a single record between the values that it obtains a certain time interval apart as one varies that time interval. Whereas, for cross-correlation, you have two signals and you are looking for the relationship as a function of a time shift, between the values of those two signals.

Spectral analysis breaks down into two kinds of analyses and a third one which is sort of a product of the other two. We have a power spectral density function shown as the first analysis. The word power, of course, can sometimes be questioned. It is perhaps a matter of personal taste and there is some thought that perhaps we should make this more symmetrical by calling it autospectral analysis. We don't require this in the Standard but autospectral density analysis is related to the autocorrelation function analysis, and here we are looking to find out what are the frequency characteristics of the signal. In cross-spectral analysis, it's a similar type except we have two records and we want to look at the frequency characteristics of these two signals simultaneously, and this kind of analysis is closely related to cross-correlation analysis. In other words, for correlation analysis you do things in the time domain whereas for spectral density analysis you do things in the frequency domain.

Coherence function, which may not be familiar to all of you, is a function of frequency which is numerically the ratio of the square of the magnitude of the cross-spectral density to the product of the autospectral densities (or power-spectral densities) of the individual signals. In all cases, we have indicated how you ought to present these kinds of data after you have conducted the analyses shown in the middle row.

SLIDE NO. 3

This was to be Sheldon Rubin's slide until about half an hour ago. I'll try to walk you through what is the remaining part of the road map in a few minutes. We have one class of data, and have indicated that a simple analysis that can be done with this type of data is magnitude-time analysis. Here one is saying the magnitude of the signal, or the intensity of the signal, is varying as a function of time and you wish to examine the way in which it does vary. What you would like to do then is look at the variation of some representative characteristic of the signal as a function of time. This might be the overall RMS value, it might be the spectral density within some restricted bandwidth, or any other characteristic of your choice. You can do this in two ways: you can break up the signal into successive small time increments and calculate the value for each increment and look at this as a function of time, or you can look at a sort of a running average, if you will.

If you examine the right side of the slide, you see we have periodic data and aperiodic data both feeding into spectral analysis, but in this case it is spectral analysis for a deterministic signal rather than the random signal shown on the last slide. You can break these types of data into periodic data or multi-sinusoidal data.

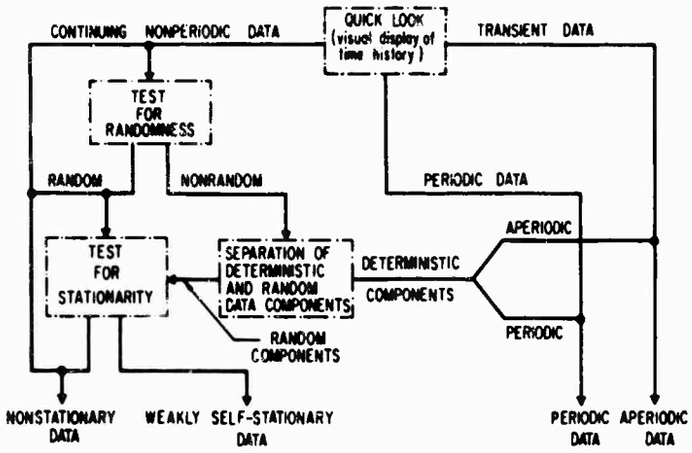

Slide 1

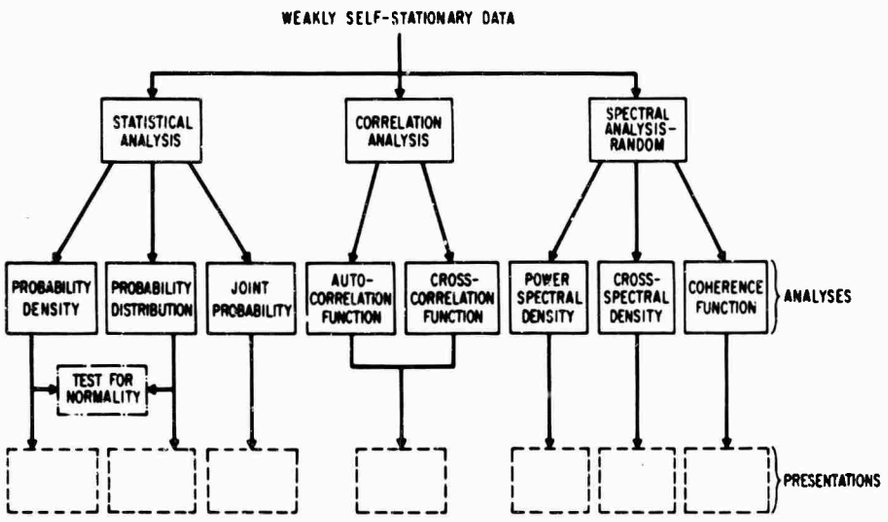

Slide 2

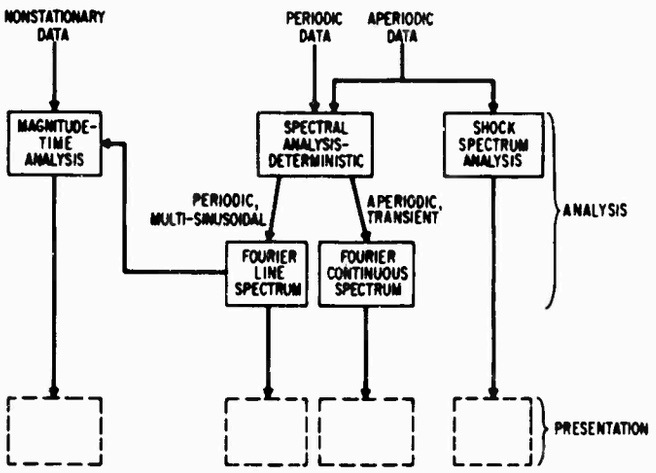

Slide 3

Now by multi-sinusoidal data, we mean a signal which is composed of the superposition of a number of sine waves; however, they are not harmonically related, and so it then is an aperiodic signal though composed of sine waves. Periodic and multi-sinusoidal data classically give you a Fourier line spectrum and one computes the magnitude and phase for each of these sinusoidal components.

Aperiodic data and transient data on the other hand yield a continuous spectrum and one conducts a Fourier transform analysis here and the data may be presented as the real and imaginary parts of the Fourier continuous spectrum or if you wish, the magnitude and phase as a function of frequency.

The last kind of analysis included in the road map and described in the Standard is shock spectrum analysis. We have described the way in which the shock spectrum analysis is conducted. You can plot several types of shock spectra. For instance, you can look at only the positive values of the spectra, or you can look at both the positive and the negative values. Also, you can look at what is called the primary shock spectrum (in other words, the shock spectrum which one obtains while the transient is in process), you can look at the residual shock spectrum which is a plot of the response maxima after the transient has died away, or you can look at the overall shock spectrum (the shock spectrum which includes the maxima both during and after the transient).

We point out in the Standard that with any shock spectrum analysis, one has to select the damping factor or the Q for the single-degree-of-freedom systems used in the analysis. The Q used in the shock spectrum analysis has to be defined on the data presentation and if you like, of course, you can repeat the analysis several times and come up with a family of curves for different Q's. Basically, two kinds of presentation are described: the first is a response-frequency plot in Cartesian coordinates. The second kind requires a four coordinate plot which is particularly useful for shock spectrum presentation wherein, as a function of frequency, there is displayed the pseudo-velocity, the maximum relative displacement, and the equivalent static acceleration.

QUESTIONS AND ANSWERS

Question: Attendee from TRW
Can you explain to us exactly how and perhaps more important why we should discriminate between non-stationary data and transient data?

Answer: Dr. Bendat
This is a good question. Transient data can be considered to be a special type of non-stationary data for certain applications and can be treated by some particular non-stationary analysis method. The fact remains, however, that many people do analyze transient data by taking a Fourier transform, or perform some shock spectrum analysis without getting involved in more advanced considerations of non-stationarity. On the other hand, non-stationary data in general would not have Fourier transforms and must be analyzed differently than the usual transient data.

Answer: Dr. Curtis
I can give an example where a non-stationary signal would certainly not be considered a transient. You all know what a shock is - but if we had a recording of the vibration in a missile, a continuous recording during which the flight conditions of the missile or perhaps the airplane were changing continuously - I think that would be a non-stationary kind of signal but where I rather doubt you would treat it as a transient.

Answer: Dr. Bendat
There are overlapping areas here where you may take certain data and put it in more than one category. We stated that at the very beginning of this discussion. You can analyze the data by different approaches as appropriate to the given application. In this Standard, we list accepted methods for analyzing data which would be classified as transient, periodic or non-periodic. The non-periodic would be divided down further into finding out really why it is non-periodic. The distinction between stationary and non-stationary is a critical one because anybody that analyzes non-stationary data by the accepted techniques of weakly stationary data is doing incorrect work, is losing sight of vital information. If data is non-stationary, it would have statistical properties which vary as a function of time, whereas weakly stationary methods, on the other hand, give you results which are independent of time. There is a complete separation in techniques and interpretations between these two classes of data.

Question: Attendee from NSRDC
Will the guide or Standard as published assume that the user knows

why he will use this Standard or do you provide guidance and examples of why you would do certain types of analysis in order to get certain types of presentations?

Answer: Dr. Bendat

The Standard does not replace the need for understanding basic concepts or practical knowledge on the part of the user. It is very restricted in scope. The user must supply his own justification for why he wants to do any part of the analysis that he might conduct. Application areas as such are not included in the Standard.

This Standard can be used for many different application areas. I know of other work going on in Oceanography, Communications, Seismology, etc., which also require the same ideas that are included in the Standard. I think that it would be very difficult, if not impossible, to get agreement on these matters from as many people who have been involved in this over the past six years if we tried to standardize particular applications or particular interpretations. I am amazed and really very pleased at the final results of this sustained effort, that we were able to get agreement on what is contained in the Standard. There are many guidelines here, many valuable ideas, and many things are implied besides what is actually stated in the Standard, but what is stated is very specific on recommended ways in which to use certain terms and the recommended ways to carry out certain analyses, listing important parameters and displaying results.

Question: Attendee from Aerospace Corporation

The joint probability distribution that is included, is it for two signals or for more than two signals?

Answer: Dr. Curtis

You asked if the joint probability was for more than two signals. The material in the Standard restricts itself to how to compute the joint probability distribution for two signals only. It does not explore the more general case.

Question

When do you hope to have this Standard in effect?

Answer: Dr. Bendat

Well, as I mentioned, two days ago we received approval here from the S2 Committee on our last draft of the Standard, and were authorized to submit it to the United States of America Standards Institute for their final action and distribution. I don't know how fast they are able to move. We ourselves are now essentially through with our contributions and expect to send this material to the Standards Institute within the next thirty days. Those of you that may be interested in getting a copy because of your current work can obtain one by writing to me in Los Angeles.

There is a lot of room that's still left in this field in the way of future Standards and future applications. There are many challenges and opportunities for different people who have different facilities who will actually carry out the work. There is no restriction in this Standard at all - as we said - on the use of any particular instruments or any particular digital computer programs. However, if you want to have a comprehensive capability, then clearly we have stated here at least the minimum requirements that should be available to you. Which particular types of analyses you would conduct will vary considerably from user to user. Nobody in his right mind should ever take any raw data and go through and compute all of these functions. It would be a waste of a great deal of effort. On the other hand, if you only collect data and immediately do a power spectral density analysis, that would also be wrong because nobody could interpret the results. You must qualify data along the way to make sure that any particular analysis is appropriate to that particular data for some specific application.

On this positive note, the session is adjourned.

TRANSPORTATION AND PACKAGING

THE BUMP TESTING OF MILITARY SIGNALS EQUIPMENT IN THE UNITED KINGDOM

W. Childs
Signals Research and Development Establishment,
Ministry of Technology, United Kingdom.

The paper explains the need for mechanical proofing tests on equipments, sub-assemblies and components and briefly describes the first bump test machine built to carry out such tests, and the machine's shortcomings.

The characteristics of the current British bump test and the reasons for its form are dealt with, leading to the design and manufacture of the 50lb and 250lb machines currently used in the U.K. capable of applying the test. The design, operation and performance testing of these machines is dealt with in some detail.

The need for ruggedised equipment need hardly be stressed; for whatever its use, military or commercial, at some stage it will be subjected to rough treatment while being transported by road, rail or air.

However my remarks today centre mainly on the standards required for military equipment and give some account of the circumstances which have led to the adoption of what the U.K. classify as a "Bump" Test.

During the early part of World War II there was a high failure rate of signal equipment caused by transportation. Equipment was frequently carried unpacked, loose, on the floors of trucks travelling cross-country. The same hazard applied to equipments, normally fixed, but removed and taken loose in trucks to base workshops for repair. Under these conditions the most severe bumping was experienced, and the most serious damage occurred.

This high failure rate showed the need for mechanical proofing tests for new equipments, sub-assemblies and components.

The responsibility for these tests was handled by the Inspectorate of Electrical and Mechanical Engineering (I.E.M.E.), who produced the first bump test machine.

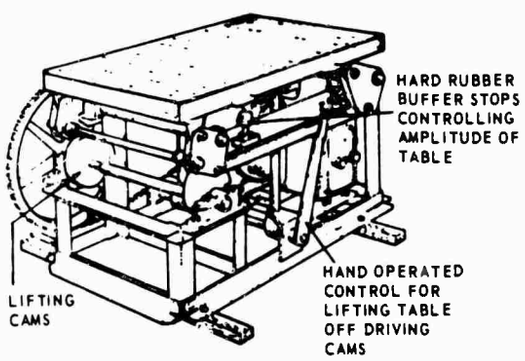

FIGURE 1. THE FIRST BUMP TEST MACHINE

This machine, shown at Figure 1 was in use for several years and the experience gained from it demonstrated the necessity to rationalise the test. Engineers had criticised the machine's performance, mainly on the ground that test results were not repeatable.

This criticism was justified when the machine's performance characteristics were examined. The machine produced secondary shocks varying in magnitude and duration during the free drop and cam pick-up periods. Such a random test negates the whole concept of controlled laboratory environmental tests within defined parameters, fully instrumentated to produce positive evidence of an equipment's capability.

Environmental tests must be designed to simulate with reasonable accuracy, certain characteristics likely to be met in service, and provide repeatable consistent measurement. It is imperative that a bump test machine should be capable of producing repeatable results.

The British Bump Test is one in which the equipment is subjected to a specified number of shocks, in other words it is a periodic bump test, although each individual bump is a separate entity and the shock applied is a non-periodic function.

Machines capable of providing the required performance are the S. R. D. E. Bump Test Machines. Two machines were designed, the 50lb and 250lb machines, the weights referring to the maximum pay load. These machines are now widely known and used in a number of countries as a standard for robustness testing for military signals equipment.

The performance requirements for the new machines were based on the experience gained during the use of the early machine and the results of field investigations, and these in turn were written into the Ministry of Defence, Specification DEF. 133 as the performance requirements for Bump Test Machines. The specification states briefly, "The waveform of the impact deceleration shall approximate to one half-cycle of a sine wave, mean peak value 40g $\pm$ 4g. The duration shall be 6 $\pm$ 1 milliseconds. The amplitude of any waveform distortion shall not exceed 20 per cent of its fundamental waveform. At all other points in the cycle the maximum acceleration shall not exceed 10g".

The S. R. D. E. 50lb Bump Test Machine at Figure 2 was designed for the robustness testing of small equipments, sub-assemblies and components with a maximum weight of 50lb. The cast aluminium test table, 12 x 12 inches and integral ram are freely mounted by two parallel motion link arms to vertical members of the base frame so as to drop freely with a rectilinear motion onto a specifically designed rubber anvil. The anvil and link arms are so positioned that at the instant of impact the ram motion is vertical and the link arms parallel to the face of the anvil.

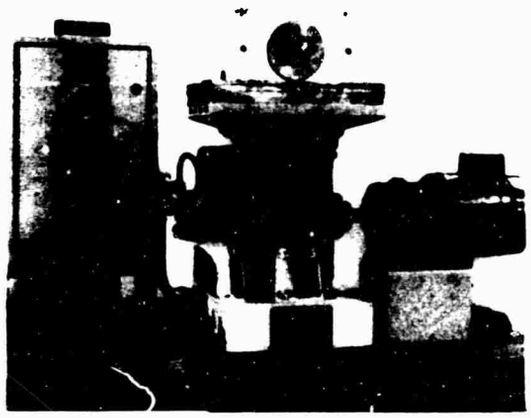

FIGURE 2. THE 50lb BUMP TEST MACHINE

The drop height and lift of the table is controlled by the setting of an adjustable tappet fixed to the ram. The tappet, has a nylon tip and is lifted by the cam, the bearings of which are resiliently mounted. The driving force is applied through a torsional resilient coupling. These precautions, nylon tip, resilient mountings and coupling assist in the smooth pick up and release of the table necessary to reduce impact between the cam and tappet to an acceptable level.

The machine is calibrated under full pay load conditions, ballast weights totalling 50lb being firmly secured to the table. The ballast weights must be smooth and flat so as to eliminate contact vibrations. In some instances it has been found necessary to have the interfaces of the weights nylon coated.

The accelerometer response illustrated at Figure 3 was obtained from a piezo-electric transducer mounted on the table and it covers one complete cycle of operation. Secondary impacts due to cam pick-up and release are negligible and well within specification requirements. On close examination they can however, be detected. This fact is most useful in that it enables the machines performance to be closely controlled. The amplitude of the cam impact on pick-up can be observed, and if excessive, be reduced to acceptable level by adjusting the running speed so that the cam meets the tappet more or less on the peak of its bounce rise. The cam release can also be identified and the measure-

ment of the time between release and impact is the time taken to drop one inch, from which the velocity on impact can be calculated.

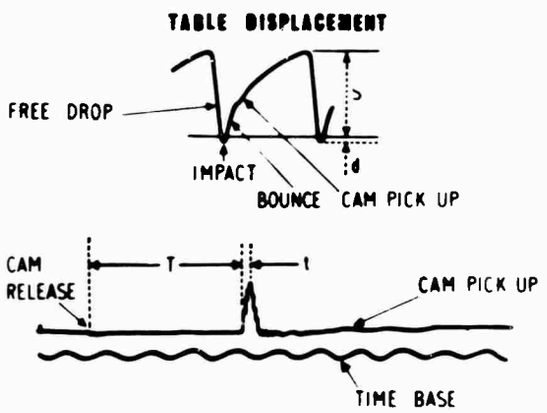

FIGURE 3. ACCELEROMETER RESPONSE

This information provided by the accelerometer response enables the performance of the machines on delivery, installation, and during use to be closely controlled and standardised. For example, if the drop time was too slow one would immediately examine the link arm bearings for stiffness, lack of oil, etc.

The 250lb Bump Test Machine, shown at Figure 4, has a 2ft square cast aluminium top, box sectioned with fabricated integral ram, and is freely mounted by two parallel link arms to the base frame in a similar manner to the 50lb machine. Ballast weights, ten 25lb units, nylon coated on interface surfaces are carried inside the ram thus leaving the whole of the table area free of obstructions, unlike the 50lb machine where the ballast is carried on the table.

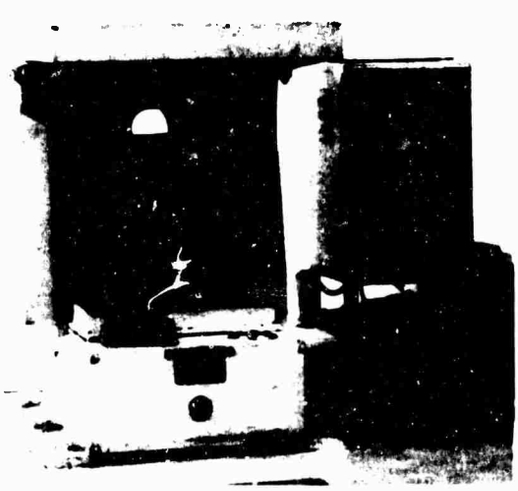

FIGURE 4. THE 250lb BUMP TEST MACHINE

The table lift is governed by a variable pivot, rocker motion cam, actuated and driven by a geared ½ H.P. D.C. motor. The cam is designed to pick up the table at a predetermined rebound position following the impact and to lift it to the required drop height. The rocker mechanism is incorporated to ensure the same smooth lift characteristics over the adjustable drop height, range 0.25 to 1.25 inches. The drop height is preset by a coin slot screw situated at the foot of the base frame. Bump repetition rate is governed by a motor speed control and enables correct synchronisation of cam lift with table bounce within the impact repetition rate of 2 to 4 bumps per second for a particular test condition. A foot pedal is provided to determine the table pay load by reading a calibrated gauge situated at the base of the machine when the pedal is pressed with the machine at rest. A preset counter with "cut out" switch incorporated is used to control the number of bumps per test. Within limits, other bump impact conditions can be obtained by varying the heights of drop, the pay load including ballast, or the Shore hardness of the anvil.

The project, the rationalisation of the Bump Test and Bump Test Machine was undertaken by S.R.D.E. successfully to the extent that a performance specification for a test machine is now published by the British Standards Institution, BS. No. 3585. Interest in such a test requirement has been stimulated internationally via International Electrotechnical Committee (I.E.C.) and N.A.T.O. and naturally opinions on the value of the test are divided, not so much on technical grounds, but largely because individual countries were deeply committed to alternative forms of testing, mainly one form of shock test or another. However there is reason to believe that a large measure of agreement exists in that the bump and shock tests are complementary, for example, there is no suggestion that the bump test reproduces the characteristics of a parachute landing, but does more readily simulate shocks experienced by electronic equipment during Service Use, handling, cross country transport and the effects of shunting (railroad humping) as confirmed by a study in the U.K. by Export Packaging Services (E.P.S.) and the Fighting Vehicle Research and Development Establishment (F.V.R.D.E.).

The results of this investigation revealed

that loose pieces of equipment up to 100 lb in weight experience shock levels of up to 100 g when transported under hazardous conditions, across rough country. Duration of significant impacts range from 5 to 35 milliseconds. The occurrence of bumps above the 40g level are relatively few and we consider that these would be adequately covered by the Drop and Push-over Tests. By far the greater number of bumps experienced during these trials which covered several types of Army transport vehicles driven at various speeds over poor road, pave and rough cross country terrain were of the order of 40g and less. Thus it would appear that the choice of the 40g impact, duration 6 milliseconds, would be of sufficient severity for use as a standard for robustness testing. The results obtained from transporting a piece of equipment loose in a 3 ton truck over rough country are graphically illustrated in Figure 5.

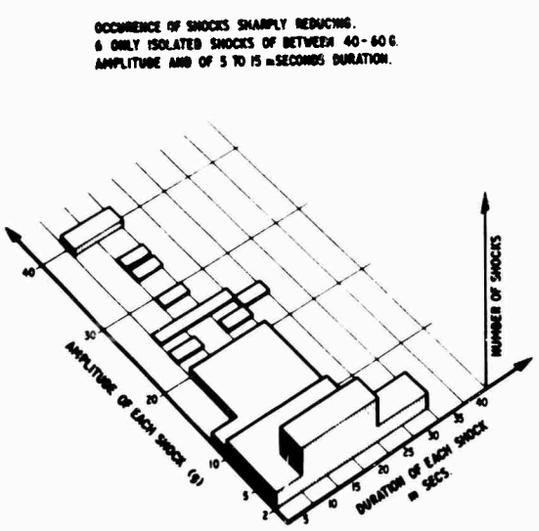

FIGURE 5. GRAPHIC REPRESENTATION OF SHOCK LEVELS MEASURED ON AN EQUIPMENT TRANSPORTED LOOSE IN A 3-TON TRUCK OVER ROUGH TERRAIN.

Many of you may feel concerned that the adoption of such a bump test universally might adversely effect the economics of equipment development. Experience in the U.K. has shown that this is not so, since, in fact, any equipment structure built on sound engineering principles will certainly survive the 40g condition. Any higher levels, for example 80g, would, we agree, result in a severe rise in development costs. It is interesting to note that certain manufacturers, mainly of domestic equipment have adopted a 20g test. The number of bumps, 4,000 has been the basis of an acceptable relationship between the life of the equipment and cost of construction - good engineering construction in relation to cost factor.

The Bump Test is included in all our environmental specifications for new equipments which are liable to be transported loosely and not permanently fixed in the vehicle. It is applied at temperature extremes -40°C and +50°C with solar radiation covering transport in open vehicles.

It is also used in an abbreviated form, 100 bumps, as a shake down test during factory inspection. This augments the removal of foreign matter, for example loose bits of solder, nuts and etc., and helps to reveal faulty workmanship, dry soldered connections, poor welding, loose nuts and bolts and badly mounted components. The production qualification tests are then applied and finally we should have a robust equipment capable of reliable performance in the field. This is the British Bump Test.

DISCUSSION

Mr. Swanson (MTS Systems Corp.): Could you elaborate on the transverse bumping? For instance, in service the radio looked as though it got a few sideways jolts. How do you check out the transverse effects?

Mr. Childs: You only saw part of the bump test. It is applied in each of three planes. If there are three planes on which it can stand, it gets 3000 bumps in each of those planes.

Mr. Swanson: All to the same g-level?

Mr. Childs: Yes.

NLABS SHIPPING HAZARDS RECORDER STATUS AND FUTURE PLANS

Denis J. O'Sullivan, Jr.
U. S. Army Natick Laboratories
Natick, Massachusetts

The paper describes the basic recorder unit developed by NLABS to measure the shipping hazards that packages encounter in worldwide distribution and storage. Also described are the transducers used with the basic recorder to measure velocity, temperature, humidity, static load, dynamic load and acceleration. The status of the program is presented along with future plans and the results of the limited test shipment.

INTRODUCTION

There is a continuing need within the Department of Defense for reliable information on conditions encountered by military supplies during worldwide distribution and storage. In 1955 an Ad Hoc Committee was established to collect the information but was deactivated in 1963 due to the lack of suitable recording instrumentation to measure the desired conditions. As a result today's packaging design engineer has to rely on "empirical and nebulous criteria" established through experience, to design effective packages. In most instances the packages have excellent protective qualities but are overpacked, resulting in excessive material and labor cost. In some instances they are underdesigned resulting in damaged contents.

About 5 years ago, in an attempt to provide the packaging engineer the necessary information, the U. S. Army Natick Laboratories established a design criteria program to devise the ways and means required to measure and record the shipping hazards encountered by military supplies during worldwide distribution and storage. A contract was awarded to determine the availability of suitable recording units that would meet the following requirements:

1. Be compact.

2. Have a large memory bank.

3. Be capable of long periods of unattended operation.

4. Be compatible with automatic data processing equipment.

5. Be able to distinguish clearly between each shock input.

6. Be able to distinguish between positive and negative shock inputs.

7. Have a time code.

The study showed that no commercial recorders were available and work was begun to develop a recorder to measure five parameters:

1. Shock (Drop Height).

Venetos (1) has indicated that the greatest damage to a container is likely to occur when the container is dropped during a handling operation. Therefore, the packaging engineer must have available an expression of the magnitude of the shocks incurred by the container. It was determined that the measurement of velocity would be the most useful. Knowing the velocity, the impact energy which protective packaging must absorb can be calculated. Also, velocity can readily be converted to an equivalent drop height ($V = \sqrt{2gh}$) which can be directly related to many container testing procedures based on the free-fall impacting of containers.

2. Temperature.

While there is much data on the climatic conditions in various parts of the

world, the actual temperature in the interior of the package is unknown.

3. Humidity.

As in the case of temperature, the actual humidity in the interior of the package is unknown.

4. Static Load.

The static load that a container is subjected to, must be measured in order to insure that container will be designed to withstand these compressive loads.

5. Dynamic Load.

The forces acting upon a container, when it is subjected to a shock from another container being dropped on it or when it impacts against the wall of a truck or train, are a determining factor in the life of the container. This is the least available type of data required by the designer.

A basic magnetic tape recording unit along with transducers to measure velocity, temperature and humidity was developed. Further work resulted in the development of a static load transducer system and a dynamic load transducer system. As a result of the work accomplished to date there are available three types of recorder systems utilizing the same basic tape recording unit. They are:

1. Shock-Velocity (Drop-Height) Recorder.

This will record only the peak velocity independent of drop surface from three mutually perpendicular planes. This recorder is shock actuated, i.e., the signal is recorded when the shock occurs.

2. Combination Recorder.

This will record temperature in $^{o}F.$, humidity in percent relative humidity, and static load in pounds. It is time actuated a reading being taken every hour.

3. Dynamic Load Recorder.

This will record the peak dynamic superimposed loads in pounds that containers experience when subjected to impacts by other containers or pallet loads subjected to impacts by other pallet loads. The results will reflect the effect of both mass and impact surface.

The data stored in the magnetic tape is retrieved using a data retrieval and processing system. This system converts the velocity analogs to equivalent velocity showing both magnitude and direction. The vectors are combined electronically to give a resultant drop height expressed in inches. The temperature and humidity are expressed in $^{o}F.$ and percent relative humidity, respectively, and plotted graphically with respect to time by a two-coordinate plotter. The static & dynamic superimposed loads are expressed in force (pounds) and the information obtained from all recorders is related to time.

After retrieval the information collected will be statistically analyzed to provide quantitative data for use in the design of containers and testing procedures. Eventually the data will be consolidated in table form. From the statistical tables developed the engineer can predict, for the confidence level desired, how many times the package will be impacted, from what height, the temperature and humidity extremes expected and the compressive strength desired. Based on these predictions, criteria can be established for use in laboratory free-fall testing methods, conditioning rooms, and compression machines.

BASIC RECORDER UNIT

The basic recording unit (Figure 1) meets all the design parameters previously outlined. It consists basically of:

1. Spring-loaded magnetic tape supply and take up reels.

2. A four-channel in-line tape recording head.

3. A rotary stepping motor to advance the tape 1/16th of an inch for each data input.

4. A 45-volt D.C. power supply.

5. Solid-state circuitry to provide the proper electrical triggering impulses for advancing the stepping motor.

It is a small self-contained unit (6-3/4 x 8 x 9 inches) weighing approximately 10 pounds that will record up to 16,000 events on magnetic tape while operating unattended in the field for periods of up to five months. The recording unit is shock mounted within six 1-inch-thick polyurethane foam pads and contains a small 45-volt D.C. power supply. Although analytical and experimental studies indicate that both the battery and shock mounting system are adequate under even the extreme conditions, it is desirable, wherever possible, to use a larger capacity battery as well as additional cushioning pads.

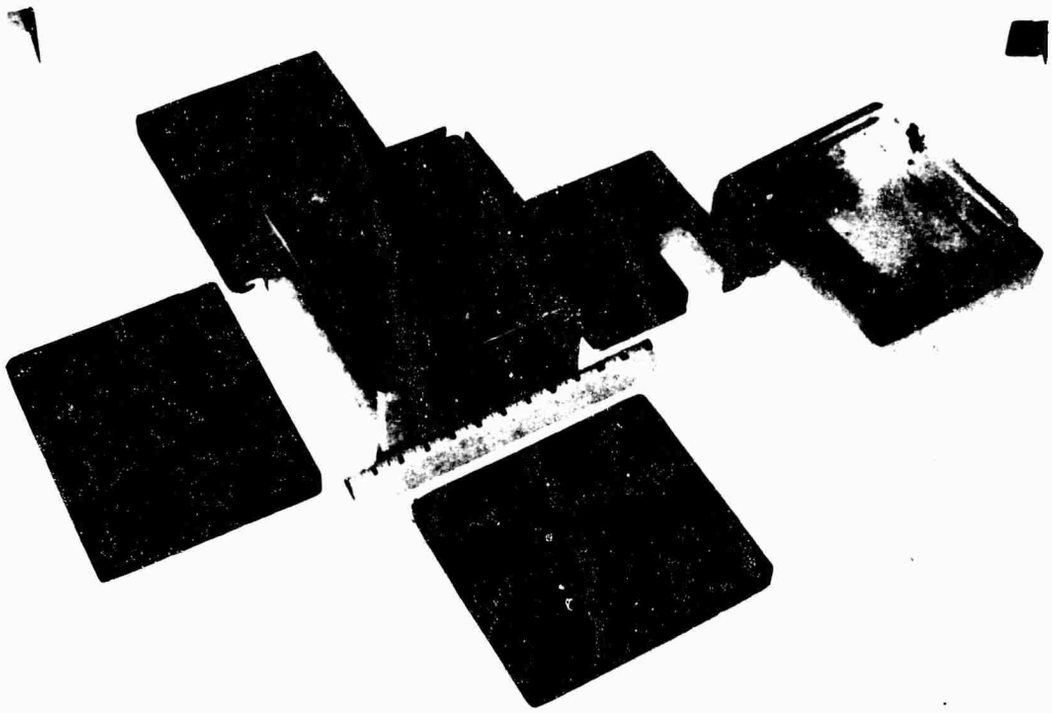

Figure 1. Basic Recording Unit

A timing circuit is incorporated into the recorder to actuate the advancing electronics at either one hour or six hour intervals. A Bulova Accutron timer closes a switch at the predetermined time causing a pulse to be fed to the recording head and recorded on the magnetic tape as a timing mark. This pulse also energizes the digimotor which advances the magnetic tape 1/16th of an inch. The recording of parameters can either be time actuated, as in the case of the combination recorder, or force actuated. In the latter case, in addition to the time marks, the pulses generated by the measuring transducer are recorded. These pulses after being recorded on magnetic tape actuate the advancing electronics without generating a time pulse, thus allowing the analyzer to determine the approximate time the event took place.

The recording process is unique in that, unlike conventional recorders, the recording is done while the tape is stationary. As a result there is minimal constant drain across the battery allowing the recorder to be used for prolonged periods of time with its small, lightweight, power supply. There was no information available on characteristics of recording on tape while stationary. The process was developed in-house. Laboratory tests showed that by using high quality instrumentation, tape inputs of from 50 millivolts D.C. to 260 millivolts D.C. (Figure 2) could be recorded while still remaining in the linear portion of the tape. By electronically conditioning the signal from the transducer to be compatible with the linear portion of the tape, the desired range of values can be recorded with the greatest accuracy.

When the basic recorder is married to a set of transducers with conditioning electronics, it assumes the identity of the parameter(s) being measured. Work on three types of recorders have been completed.

1. Shock-Velocity (Drop-Height) Recorder.

The theoretical design and development of the velocity (drop-height) transducer (Figure 3) was previously discussed by Venetos (1) and will not be repeated here. The transducer consists of a teflon-coated permanent Alnico-V magnet, spring mounted within an aluminum tube and housed in a low permeability sleeve to prevent stray magnetic fields from affecting the signal output. The helical compression spring is fabricated from non-magnetic monel wire. The entire system has a natural frequency of 10 Hz. The transducer is 1-1/16 inches in diameter and 7 inches long, weighs 1 pound and is capable of measuring drop heights from 3 to 48 inches and half sine shock pulses of up to 30 milliseconds (Figure 4).

Six of these transducers, along with conditioning electronics, are joined to the basic recorder to form the shock-velocity (drop-height) recorder. On impact, the signal generated by the transducer is fed through an actuating switch circuit which, if the signal exceeds that produced by a 3-inch drop, is turned on until the maximum signal is produced and recorded. The threshold level is set at 3 inches to prevent recording of low level impacts of constant frequencies such as those common to rail or truck transportation. This allows greater usage of the tape for recording meaningful data. Activation of the switch circuit causes a series of transistors to be biased into conduction. This provides a path for the power supply to discharge through the digimotor which is actuated and advances the tape. Another electronic switch, which blocks all secondary signals to the recording head for a period of two seconds, is set into operation by the current pulse associated with the operation of the digimotor. This pulse causes a series of transistors connected in parallel between the transducer coil and recording head, to conduct current which effectively shorts or grounds all secondary signals before they reach the recording head (see Figure 5). In this way the secondary signals caused by oscillation of the magnet after impact as well as those caused by rolling or toppling of the container have no effect on the recorded signal.

Using this method, positive and negative signals are recorded on three channels, one for each axis. The fourth channel is used to record a timing pulse either once each hour or once every six hours.

2. Combination Recorder.

The combination recorder contains circuitry and transducers to record temperature, humidity and static load. This recorder unlike the shock-velocity (drop-height) recorder, is time actuated, a reading being taken every hour. The time pulse is fed to the input of a uni-vibrator as shown in Figure 6. The output of a uni-vibrator appears as a 100-millisecond 12-volt rectangular pulse, which is used to operate both the temperature and humidity electronics as well as to actuate the static load power supply module. Since the uni-vibrator is normally off, the 12-volt power supply experiences little current drain. When a positive input pulse is fed to the uni-vibrator it produces a rectangular pulse whose duration is dependent upon an

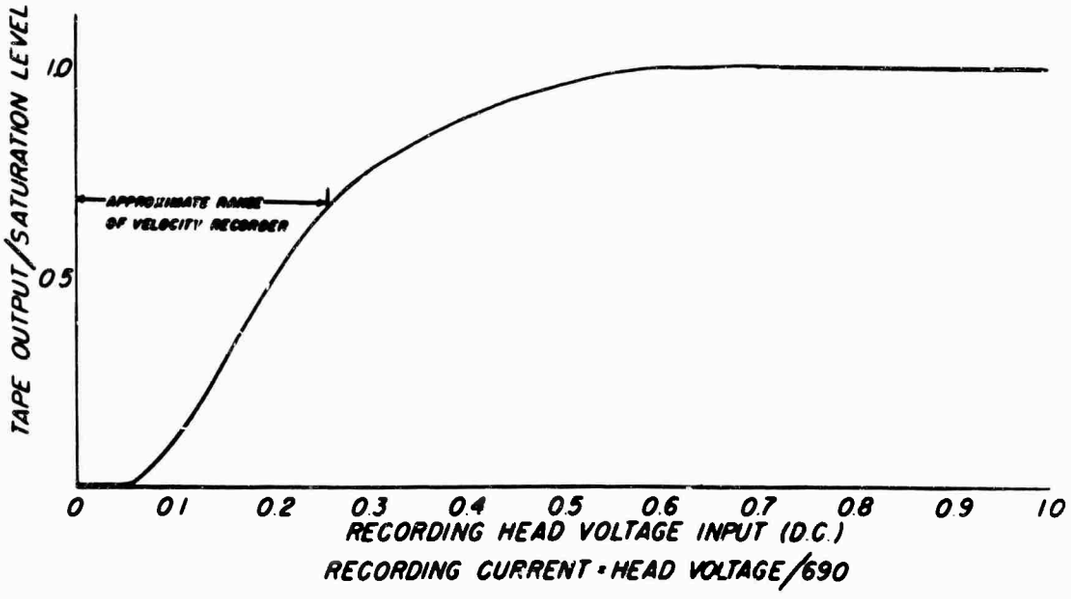

Figure 2. Nortronics BQQ3K Recording Head
Ampex Instrumentation Tape No. 748

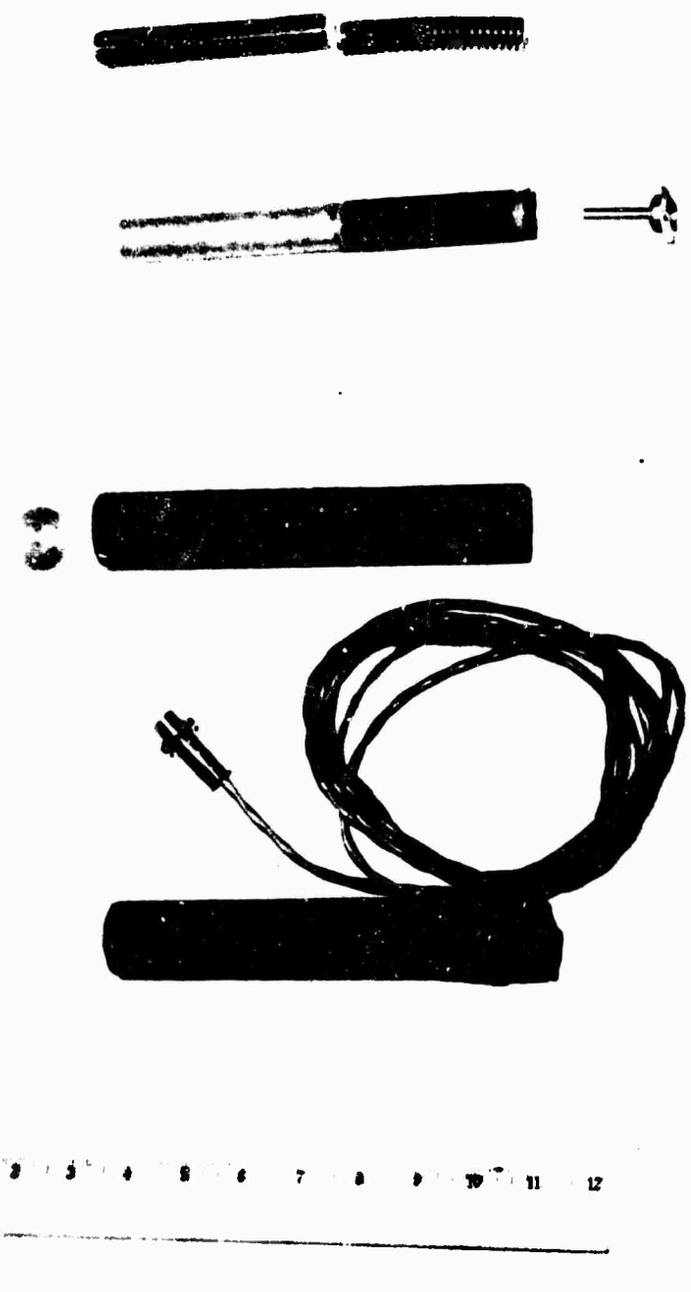

Figure 3. Velocity (Drop-Height) Transducer

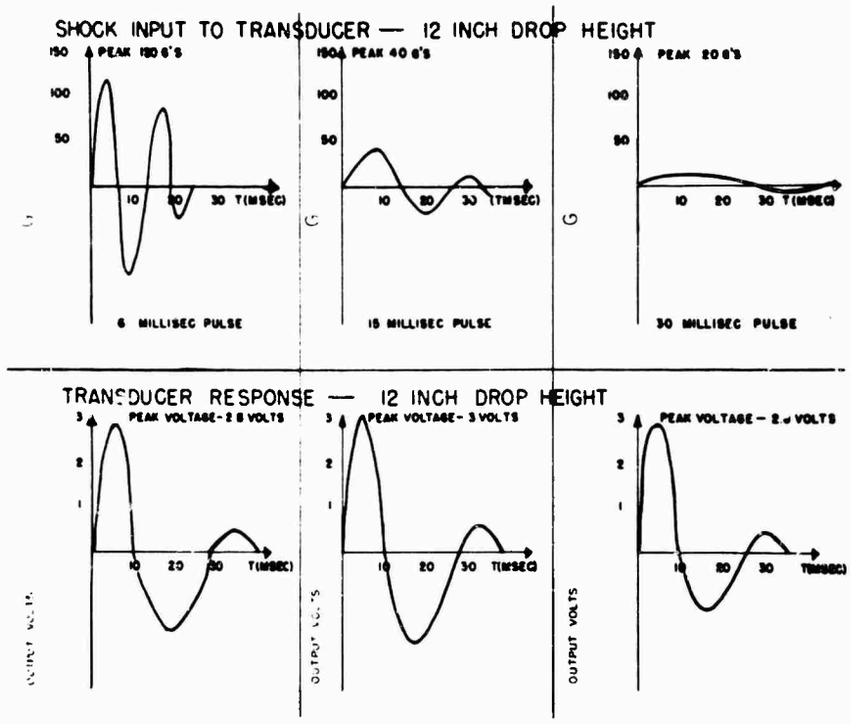

Figure 4

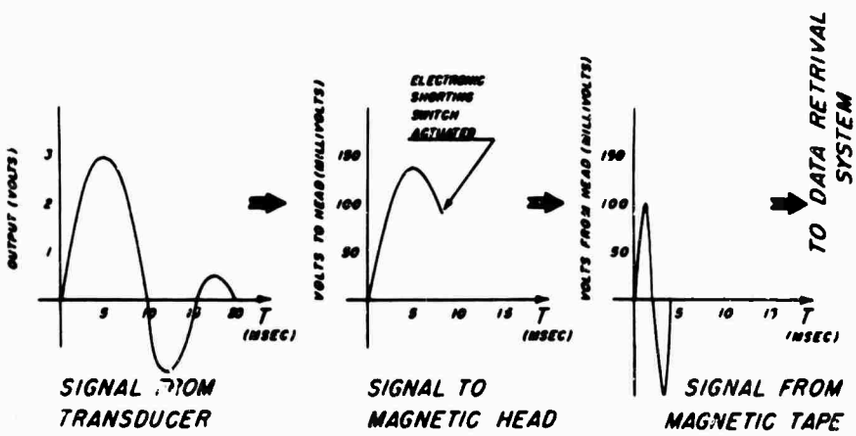

Figure 5. Waveshapes of Typical Velocity Signal During Acquisition, Recording and Playback

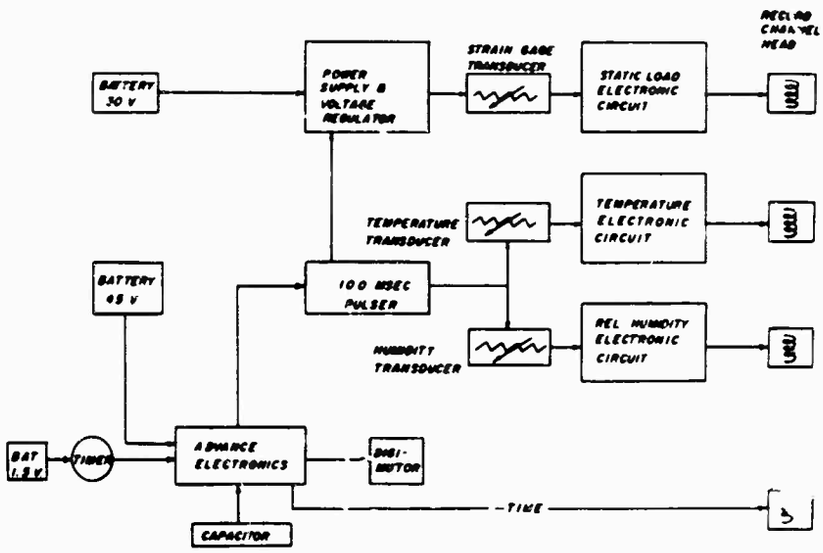

Figure 6. Block Diagram - Combination Recorder

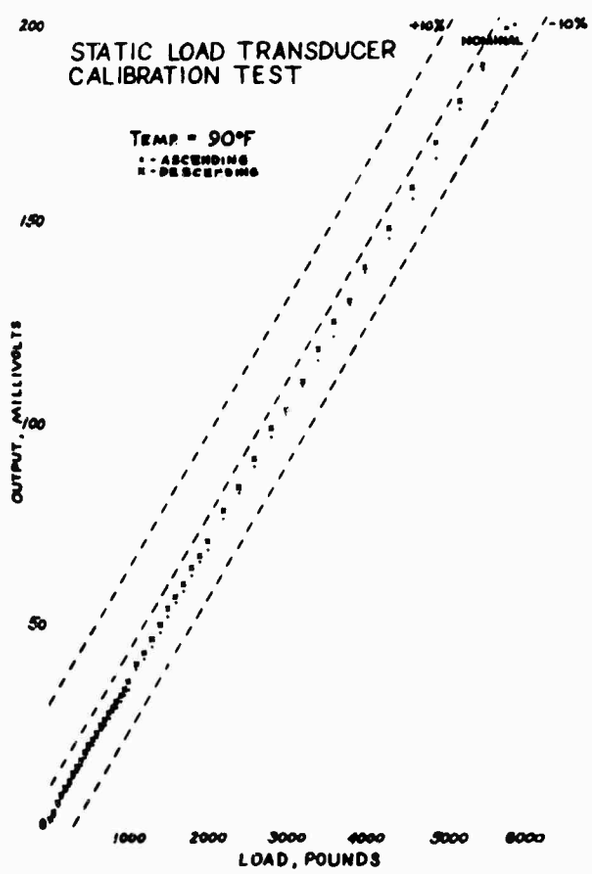

Figure 7

internal RC time constant and whose amplitude depends upon the operating potential. The output of the uni-vibrator is fed to the temperature sensor which consists of a voltage regulator and a bridge circuit and to the humidity transducer consisting of a voltage regulator and an amplifier. The bridge circuit of the temperature sensor contains two temperature dependent thermistors and two equivalent calibration resistors. The output of the amplifier in the humidity sensor, is dependent upon the input bias which is a function of the electro-humidity transducer. The static load power supply modules, activated by the pulse from the uni-vibrator, supplies pulse excitation to the static load cell bridge whose output is proportional to the load being measured. This output is then amplified, converted to a D.C. level and fed to the recording head. Using these transducers the combination recorder is capable of measuring temperature from -50°F. to +150°F., humidity from 10% R.H. to 90% R.H. and static loads from 0 to 6000 pounds. A calibration curve for the static load system is presented in Figure 7.

3. Dynamic Load Recorder.

The dynamic load recorder consists of the basic recording unit married to three sets of dynamic load transducers mounted in three mutually perpendicular planes. The operation of this recorder is similar to the static load portion of the combination recorder except that it is force actuated. The transducers, each consisting of four load cells connected in series, can be used to measure both static and dynamic loads.

DATA RETRIEVAL SYSTEM

The tapes containing data are processed using a data retrieval system (Figure 8). The data recorded is in the form of pulses whose amplitude and polarity are proportional to the parameter being measured. The system accepts data from the four parallel data channels, three containing analog data and the fourth containing timing information. Each analog data point consists of either a positive leading pulse or negative leading pulse in which the peak amplitude is proportional to some physical quantity. The amplitude and polarity of the leading data pulse is recognized, measured and recorded by the system. A fourth analog data channel is generated in the system by combining the velocity vectors from the three velocity channels and computing the equivalent impact height. At least one of the four input channels from the tape must contain information before the system will generate a read command.

The system consists of a control panel, a tape playback unit, a programmer, an analog to digital converter, a high-speed electro-optical printer, a two-pen recorder, and power supply racks. With the exception of the programmer and the control panel, all the equipment is commercially available. The programmer serves to interface and control the various equipment and consists of commercially available plug-in digital models. Some special circuitry used in this unit for signal conditioning and control are built on plug-in boards similar to the purchased logic plug-in boards.

Using this system, the tape is played back at 1-7/8 ips and the pulses fed to the peak memory drivers (Figure 9). The initial print signal is then fed to the high-speed optical printer initiating a line of print. Simultaneously, the peak signal amplitude is stored by the peak memory, scaled to engineering units by the output amplifiers, and fed to the analog to digital converter in proper sequence as determined by feedback from the electro-optical printer. When the retrieval system is used for the velocity mode, the signal output from the peak memory is also fed through a set of squares to summing amplifiers and then to the multiplex sequencer. Specifications for the system are as follows:

1. Three Modes of Operation:

   a. Velocity.

   b. Combination (Temperature, Humidity and Static Load).

   c. Dynamic Load.

2. Logging rate-30 lines/sec.

3. Input rate up to 150 data pulses/sec.

4. Time to retrieve and process six months of data (57,000 data pulses maximum) less than 10 minutes.

5. System Accuracy - ±1%, full scale.

6. Stability-Drift from Calibration -
   0.05%/day
   0.01%/°C.

STATUS

Development work on the shock (drop-height) recorder and combination recorder has been completed. The shock recorder is estimated to cost less than $2500 each. The dynamic load recorder is 90% complete.

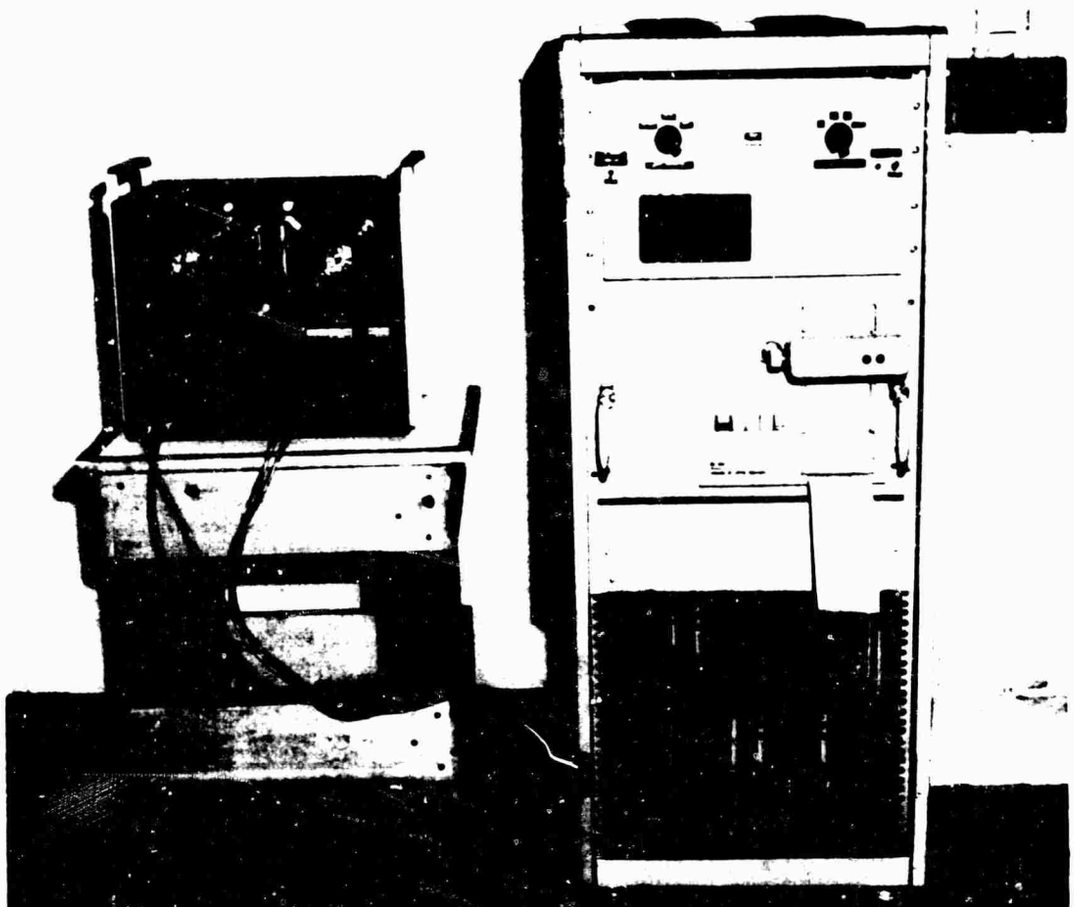

Figure 8. Data Retrieval System

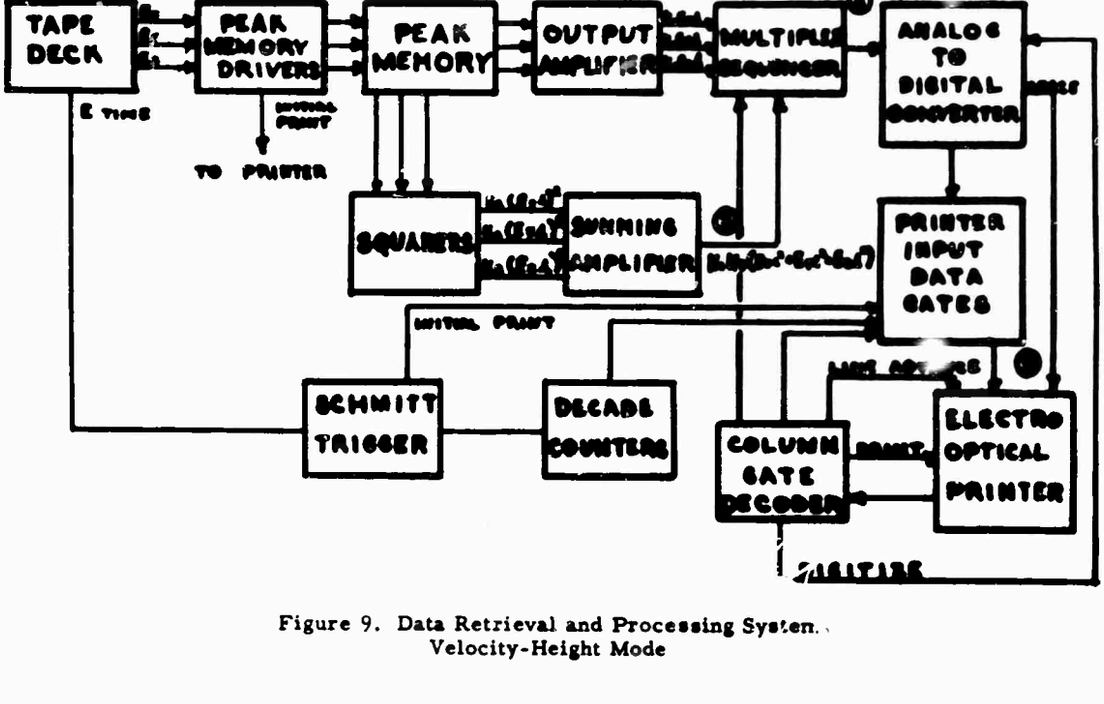

Figure 9. Data Retrieval and Processing System. Velocity-Height Mode

Work on an acceleration recorder is continuing at the Natick Laboratories. The recorder will measure and record the deceleration forces, in gravitational units, that packaged items received during transportation and storage.

LIMITED TESTS

A limited field test shipment from Natick Laboratories to Fort Lee, Virginia, with an intermediate stop at Tobyhanna Ordnance Depot was made using the 12 shock (drop-height) recorders. The test shipment consisted in part of 512 No. 10 can size containers each of imitation maple syrup,(gross weight 60 pounds), dried dehydrated potatoes, (gross weight 21 pounds), and peas, (gross weight 47 pounds). In addition 20 unitized loads, 40 x 48 x 54-1/2 inches, (gross weight 1840 pounds), were also included in the shipment. Nine individual shipping cases were instrumented with the shock recorders, three each weighted to simulate the cases of imitation maple syrup, dried dehydrated potatoes and peas. Three of the unit loads were also instrumented with recorders.

Analysis of the data received indicated that the intensity and frequency of occurrence of handling shocks may be far less than is commonly assumed. Test data also indicated that palletization of supply items is effective in reducing the shock hazards which containers experience in shipment. The average drop-height was found to be 14 inches with a maximum of 28 inches. The containers were subjected to 18 handlings apiece and were subjected to two to three impacts each. Some minor deficiencies were noted during the test. Most notable was a high quiescent current drain which decreased battery life considerably. This drain was traced to the activating switch which has been redesigned to reduce this drain tenfold.

FUTURE PLANS

At present, the most effective method of using the various recorders has not been determined. Test shipments are not only costly and time consuming, but probably do not give a true indication as to what is actually happening in the field. The largest amount of significant information could be obtained in the shortest period of time by placing the recorders in actual shipments. It is planned to establish a Data Gathering Program, with participation by other Government Agencies as well as industry.

In concept, participants would include recorders in shipments made by them, and furnish the resulting magnetic tapes together with other pertinent information regarding the shipments to the Natick Laboratories. The tapes would then be processed and a copy of the print-out in digital form furnished to the shipper. Recorders would be acquired by the participants at their own expense using manufacturing data furnished by the Government or by loan of Government-owned recorders to the extent available. In this manner, a considerable amount of data would be acquired in a relatively short period.

REFERENCE

(1) M. A. Venetos, "Development of Velocity Shock Recorder for Measurement of Shipping Environments", The Shock and Vibration Bulletin 36, Part 6, pp. 173, Feb. 1967.

This paper reports research undertaken at the U. S. Army Natick (Mass) Laboratories and has been assigned No. TP 543 in the series of papers approved for publication. The findings in this report are not to be construed as an official Department of the Army position.

NORMAL AND ABNORMAL DYNAMIC ENVIRONMENTS ENCOUNTERED IN TRUCK TRANSPORTATION

J. T. Foley
Sandia Laboratories
Albuquerque, New Mexico

Dynamic input to cargo on a 2-1/2-ton flatbed truck was measured in both normal and abnormal environments. The load consisted of a distributed-mass dummy mounted on an isolated pallet. Instrumentation consisted of the ELI 31 portable environmental sampler used in conjunction with piezoelectric transducers located ahead of and behind the truck/load interface. Vibran and Spectra are the data reduction formats selected to portray the events. Data taken at the "input-to-cargo interface" during the tests were categorized and evaluated by the Sandia Laboratories Environmental Criteria Group.

INTRODUCTION

Research into the frequency of occurrence of situations encountered in truck transportation indicated that certain incidents may occur that border on "accident" situations. These situations, producing transient, high-amplitude accelerations, may be a prime contributor to catastrophic failures of rigidly tied-down cargo or fragile structures mounted on mitigating pallets.

This study exemplifies the application of some approaches to environmental measurements, data reduction, and methods of interpretation which have been developed by the Environmental Criteria Group at Sandia Laboratories over the past nine years [1, 2, 3]. Special research-type tests have been devised to supplement a continual search for environmental data published in reports, papers, and articles [2, 4, 5, 6, 7]. The testing efforts relate environmental intensities and durations to events which may take place during the expected use of a product and include presentation of data in a manner which is useful to design, development, test, and reliability engineers [1, 2, 8].

This work was supported by the United States Atomic Energy Commission.

TEST PROCEDURES

In this series of tests, a 2-1/2-ton flatbed truck was loaded with cargo which consisted of a distributed-mass dummy mounted on an isolated pallet (Figs. 1, 2, and 3). Instrumentation consisted of the ELI 31 portable environmental sampler (Fig. 4) [9] used in conjunction with piezoelectric transducers located ahead of and behind the truck/load interface on main numbers of the truck bed.

Fig. 1 - Truck used in tests

Fig. 2 - Load in truck tests

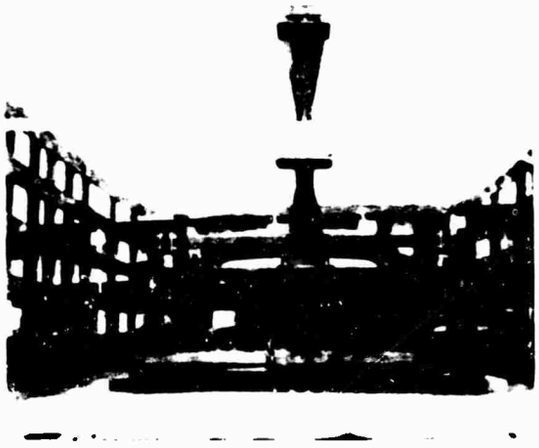

Fig. 3 - Load in truck tests

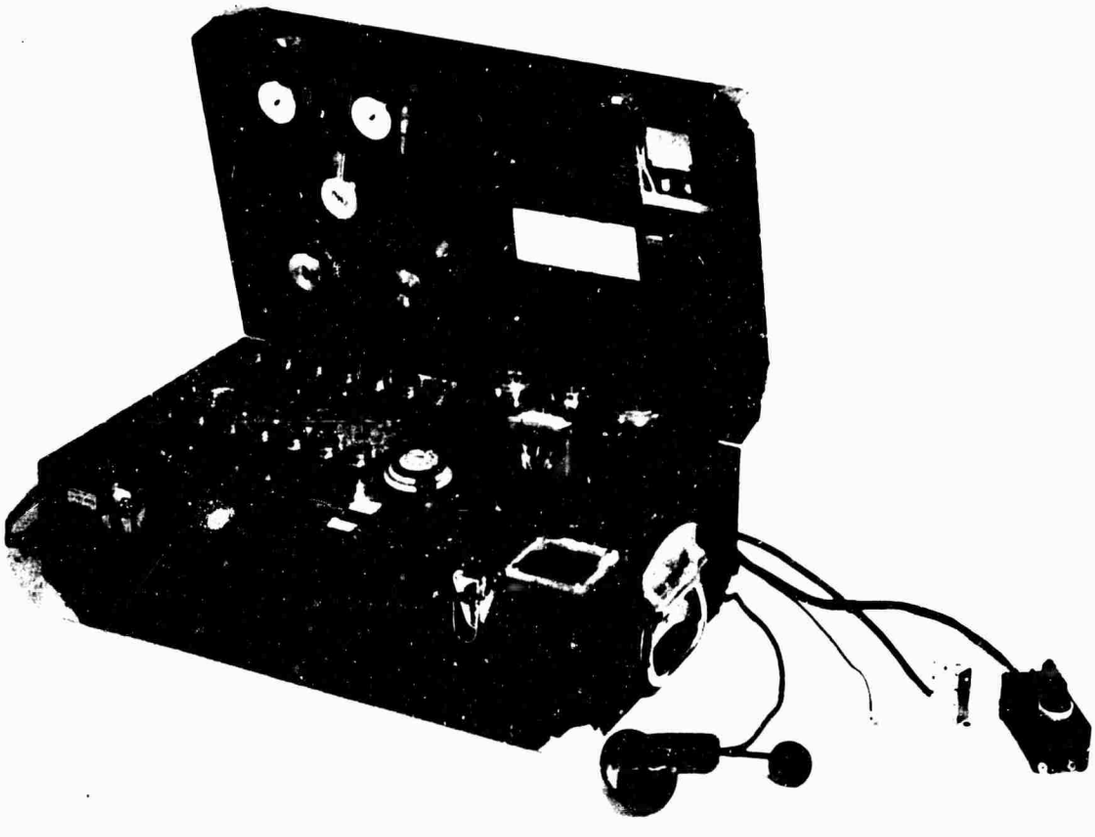

Fig. 4 - ELI 31 portable environmental sampler

The general procedure was to drive over the route chosen, isolate certain conditions which might produce unique dynamic environments, and sample the events. The route started in Amarillo, Texas, and continued west to the Texas/New Mexico border on U.S. 66 and Interstate 40. Events sampled along this route which were considered normal environments were:

1. Backing up to loading dock across RR tracks (Fig. 5). (Vibran)
2. Driving to weighing station over a series of RR tracks. (Vibran and Spectra)
3. Going into a dip at 15 mph. (Vibran)
4. Driving from a low, level road to a raised road. (Vibran)
5. Driving onto bad overpass at 50-55 mph. (Vibran)
6. Driving on heavily patched asphalt highway at 50 mph. (Vibran)
7. Driving on access road parallel to interstate highway. (Vibran)
8. Driving on smooth blacktop, four-lane interstate highway at 50, 55, and 35 mph. (Vibran)
9. Driving in paved construction zone at 45 and 55 mph. (Vibran)
10. Driving on rough blacktop at 60 mph. (Vibran)

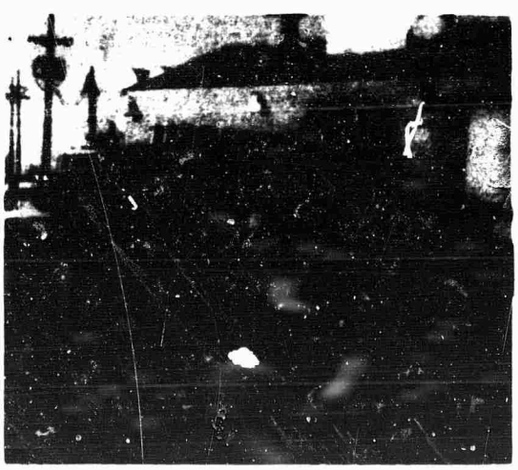

Fig. 5 - Loading dock and railroad track employed in tests

TABLE 1

Truck Test Instrumentation Directory
Calibrate Values on Data Tape

ELI 31 Channel No.	Location in Test
1	V - Truck bed, aft of pallet on ℄
2	L - Truck bed, aft of pallet on ℄
3	V - Truck bed, fwd of pallet on ℄
4	L - Truck bed, fwd of pallet on ℄
5	T - Truck bed, fwd of pallet on ℄
6	L - Left rear, load mount
7	V - Left rear, load mount
8	T - Right front, load mount
9	V - Right front, load mount
10	L - Top of dummy load
11	T - Top of dummy load
12	V - Top of dummy load
13	480-cps servo time base
14	Voice channel

V = vertical axis
L = longitudinal axis
T = transverse axis

Instruments:
ELI 31 recorder
Dictaphone
Citizen's band transceivers

Samples taken in a second series were of abnormal situations which might occur along the route and which could produce severe environmental inputs. These were as follows:

1. Colliding with loading dock. (Spectra)
2. Driving over RR tracks at high speed, 45 and 50 mph. (Spectra)
3. Driving with two wheels on the shoulder at 45 mph. (Vibran)
4. Driving completely on the shoulder at 45 mph. (Vibran)
5. Driving off the road in desert brush (Fig. 6). (Vibran)
6. Driving into a dip at 50 mph. (Vibran)
7. Driving onto the median of an interstate highway (turning around). (Vibran)
8. Hitting pot holes in a truck stop at 45 to 50 mph. (Spectra)
9. Driving on a dirt road at 45 mph. (Vibran)
10. Running over a cattle guard at 45 mph (Fig. 7). (Spectra)

Fig. 6 - Dirt road and desert brush in area where tests were conducted

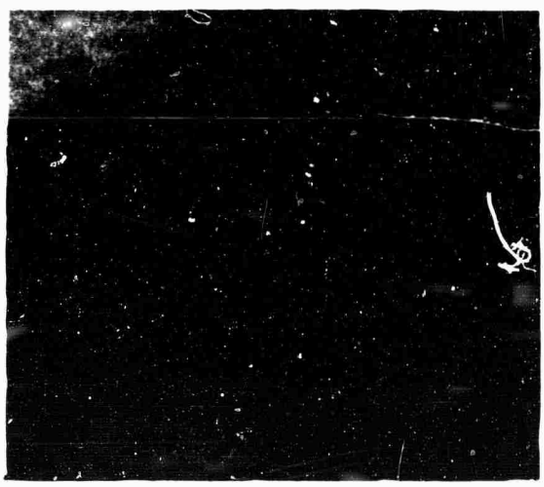

Fig. 7 - Typical cattle guard over which environments were sampled

DATA REDUCTION

The descriptive terms, Vibran (vibration analysis) and Spectra (response spectra of single-degree-of-freedom systems), indicate the data reduction format selected to portray the event [2, 3, 4]. Figure 8 is an example of the Vibran data format. Spectra data format is illustrated in Figs. 10, 12, 14, 16, and 18.

DATA EVALUATION - NORMAL ENVIRONMENTS

Long-Duration Phenomena -- Program Vidar (Vibran data reduction [2]) was utilized to analyze the normal environments of long duration. The following functions were performed:

1. The vertical axis was selected as being the axis in which maximum acceleration levels were detected.
2. The Vibran data from the two truck-bed vertical pickup locations were combined into a composite acceleration density description of the dynamic environment for each of the normal events sampled.
3. A tabulation of frequency of occurrence of road types [2] was used as a guide to obtain weighting factors for each of the ten events. These weighting factors were then applied in the production of a composite acceleration probability density description of the environment produced in the vertical axis at the truck/load interface. Table 2 gives the resultant acceleration probability description of a trip in which these ten road types would be encountered. Table 3 lists the weighting factors that were applied to each road type when generating the composite environment description.

Transient Phenomena -- One normal event, considered to be sufficiently transient to warrant analysis in terms of shock spectra, was the crossing of railroad tracks at slow speed. Figure 9 presents the vertical g-time history of this event; Figure 10 presents the resultant shock spectra, with the responding single-degree-of-freedom systems assumed to have critical damping ratios of 0, 0.03, and 0.10.

In general, spectra depict the response transient truck transport environments taken at the payload/truck-bed interface are interpreted by the Environmental Criteria Group as follows:

1. Shock spectra picture the response severity on cargo.
2. The 0.03 damping spectrum is an estimate of the response severity produced on nonisolated cargo systems.
3. The 0.10 damping spectrum is an estimate of the response severity produced on isolated or mitigated cargo systems.

TABLE 2

Composite of All Normal Conditions
(Vertical axis, forward and aft locations)

PROBABILITY OF OCCURRENCE, PERCENT

0-PEAK ACCELERATION (g)	Frequency CPS 0-5	5-10	10-20	20-30	30-45	45-60	60-87	87-125	125-175	175-250	250-350
3.2											
2.3											
1.65											0.06
1.2			0.01							0.01	0.01
0.86	0.21		0.01							0.50	0.00
0.62	0.86	0.20	0.02						0.02	4.47	0.00
0.45	1.93	0.92	0.19						1.39	11.22	0.21
0.32	2.76	3.67	0.93		0.04		0.04		9.39	13.50	1.50
0.23	7.85	10.14	2.47	1.05	0.87	0.24	0.60	0.19	18.14	12.71	5.97
0.17	9.55	14.38	6.48	3.43	2.83	1.46	3.12	0.90	14.53	8.67	9.98
0.12	13.86	19.63	12.12	8.98	7.28	4.63	7.47	5.25	13.33	8.83	14.72
0.10	62.99	51.03	77.76	86.54	88.97	91.67	88.77	93.65	43.19	40.10	67.52

No. of Peaks Counted

Note: Acceleration distributions less than 0.01% are not reported.

Total No. of Peaks Counted: 273,995

TABLE 3

Normal Conditions
Frequency of Occurrence

Weight applied to road types for deriving composite description of environment

	Event	Weight
1.	Backing up to dock	1
2.	Crossing railroad tracks	8
3.	Dip	2
4.	Low. level road to high. level road	2
5.	Overpass	1
6.	Asphalt road at 50 mph	10
7.	Access road	1.5
8.	Four-lane highway	1.5
9.	Construction zone	1.0
10.	Blacktop at 60 mph	10

ACCELERATION DISTRIBUTION, PERCENT

0-PEAK ACCELERATION (g)	0-5	5-10	10-20	20-30	30-45	45-60	60-87	87-125	125-175	175-250	250-350
3.2	5.89										
2.3	0.00										
1.65	2.94			Driving off road in desert brush.							
1.2	0.00										
0.86	0.00										
0.62	0.00										
0.45	0.00	1.36									
0.32	5.93	9.44					0.52				
0.23	14.68	16.19					10.53		0.42	0.60	0.70
0.17	35.29	24.34	1.76	0.78	0.13		4.69		[illegible]1	5.95	0.00
0.12	14.68	16.20	11.85	3.01	1.92		0.13	0.10		15.45	0.85
0.10	20.61	32.46	86.39	96.27	97.88	99.90	84.05	99.85	87.71	77.25	99.15
Frequency CPS	0-5	5-10	10-20	20-30	30-45	45-60	60-87	87-125	125-175	175-250	250-350
No. of Peaks Counted	34	74	227	401	622	837	769	1701	2321	3270	4770

Total No. of Peaks Counted: 15,026

Fig. 8 - Example of Vibran format

4. The 0.0 spectrum is an estimate of the upper limit of response severity which may be achieved in the first application of a series of pulses of the type from which spectra were obtained regardless of the damping which may be present in the system.
5. In specific evaluations, cargo responses greater than those predicted for 0.0 damping indicate that it is questionable whether the system under consideration approached a single-degree-of-freedom system.

The shock spectra shown in Figure 10 are those derived for the pickup location at the rear location on the truck bed. These spectra envelop the spectra obtained at the forward location on the truck bed and are, therefore, considered to represent the greatest vertical axis response severity relative to location of cargo on the truck bed.

DATA EVALUATION - ABNORMAL ENVIRONMENTS

Long-Duration Phenomena -- The following events were considered to occur over a period of time which precluded their interpretation as transient phenomena:

1. Driving with two wheels on the shoulder at 45 mph.
2. Driving completely on the shoulder at 45 mph.
3. Driving off the road in desert brush.
4. Driving into a dip at 50 mph.
5. Turning around on the median of a four-lane highway.
6. Driving on a dirt road at 45 mph.

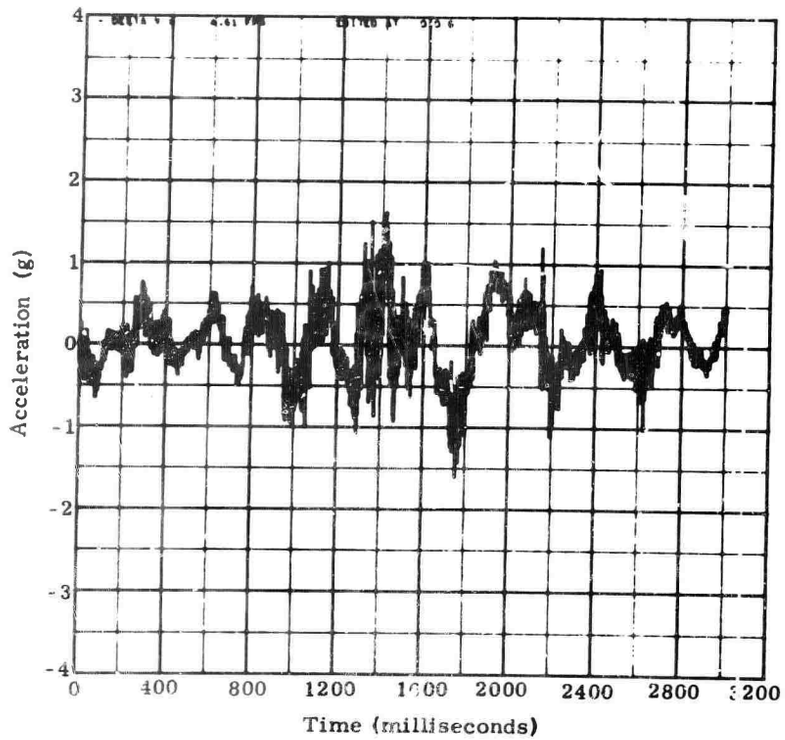

Fig. 9 - Driving across railroad tracks at stockyards - vertical, aft on truck bed (Channel 1)

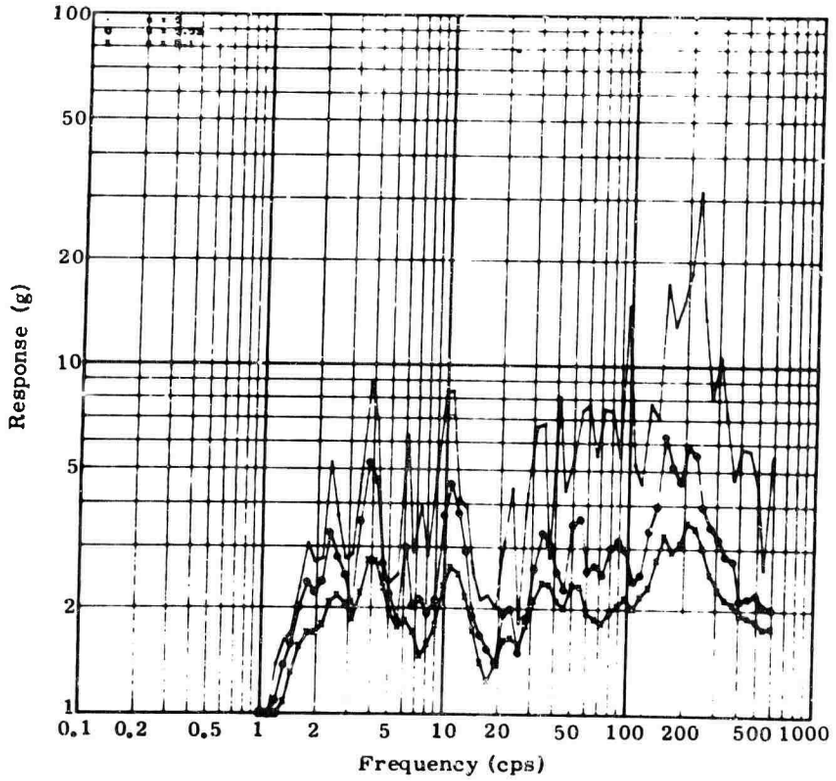

Fig. 10 - Driving across railroad tracks at stockyards - vertical, aft on truck bed (Channel 1)

Program Vibrair was utilized to analyze these events in the following manner:

1. Vibrair reductions of the vertical axis pickup locations were combined to provide a description of the "input-to-load environment" for each event.
2. A probability description was derived of the environment that would be experienced if all these events occurred on a trip where each event was considered equally likely to occur. Table 4 provides this description.

TABLE 4

Composite of All Abnormal Conditions
(Vertical axis, forward and aft locations)

PROBABILITY OF OCCURRENCE, PERCENT

0-PEAK ACCELERATION (g)	Frequency CPS 0-5	5-10	10-20	20-30	30-45	45-60	60-87	87-125	125-175	175-250	250-350
3.2	*										
2.3											
1.85	*										
1.2											
0.86										0.05	
0.62										0.84	
0.45		1.83							0.41	0.06	
0.32	1.90	3.61	0.92	0.76	0.14			0.05	3.71	18.68	
0.23	16.67	16.41	8.60	2.52	0.94	0.37	2.27	0.97	15.16	23.10	1.59
0.17	15.13	24.37	17.13	8.97	8.02	5.06	5.94	1.39	23.40	16.97	8.41
0.12	15.25	16.33	23.82	21.75	24.54	12.96	16.22	9.86	23.03	13.15	19.88
0.10	51.55	37.29	44.57	66.00	66.37	81.71	77.62	86.72	34.20	20.43	70.12

* Net acceleration probability distributions less than 0.01% are not reported.

Total No. of Peaks Counted: 93,170

Transient Phenomena -- Four events in the abnormal category evaluated as transient phenomena were (1) collision with loading docks, (2) crossing railroad tracks at high speed, (3) crossing a cattle guard at high and low speeds, and (4) hitting pot holes at high speed.

1. Collision With Loading Dock

Collision with a loading dock has a characteristic which separates this event from other truck transport phenomena evaluated in these tests. The longitudinal, not the vertical, axis produces the greatest response severity. Figure 11 shows the g-time history of this event, and Fig. 12 shows the derived shock spectra from a truck-bed location.

2. Crossing Railroad Tracks at High Speeds

Figures 13 and 14 show the g-time history and spectra obtained at a cross speed of 45 mph. As in other environmental events of this nature, shocks at the aft location on the truck bed are the most severe, and the vertical axis is, again, the "governing" axis.

Response severity during crossings of railroad tracks, however, may not be consistent for all possible cargo systems. A comparison with shock spectra obtained when crossing tracks slowly from a stop (Figs. 9 and 10) indicates that low-speed crossings may have a greater response severity for low natural-frequency cargo systems and that high-speed crossings have a greater response severity for high natural-frequency cargo systems.

The g-time histories of railroad crossings indicate that the characteristic environment is one of repetitive shock. For this reason, it would appear that the environment would be represented best by (1) the 0 damping spectrum followed by (2) either the 0.03 or 0.10 damping spectrum, depending upon whether a mitigated or nonmitigated cargo system is being evaluated.

3. Crossing a Cattle Guard at High and Low Speeds

Figures 14 and 15 present the g-time histories and spectra obtained during cattle-guard crossings from the rearward (vertical) truck-bed location. Both the time histories and spectra indicate a remarkable similarity to railroad crossings. As a result of the comparison, our present interpretation is that this environment is not unique and that its potential effects on cargo are the same as those effects produced in crossing railroad tracks.

4. Hitting Pot Holes at High Speed

The pot holes encountered in this test were in the unpaved parking area of a truck stop. They consisted of depressions caused by trucks standing when the surface was wet, wheel spin, and ruts formed under braking conditions, as well as ridged ground irregularities produced by general wind and water action. For a considerable distance leading to this area, the paved highway was very smooth blacktop, straight and level, with a posted 60-mph speed limit. This situation made it possible for a vehicle to approach a truck stop at a high rate of speed and turn into an abrupt collection of irregularities with little or no reduction in its highway velocity. A nominal velocity of 45 mph was chosen for sampling this event.

During this event, the ELI 31 recording system (weight, 90 pounds), which was resting on a foam plastic pad, separated from the pad and came to rest on the truck floor, moving a distance of about 3 feet in the plane of the truck bed. Vertical height traversed by the recorder was estimated to be of the order of 2 to 4 inches. This vertical travel estimate was inferred from passenger response in the truck cab.

Figures 17 and 18 present the g-time history and spectra obtained during this event. Again, the vertical axis and the aft location on the truck bed produced the governing severity of response.

A comparison of response severity for this event with all other events sampled in these tests indicates that pot holes and bumps are potentially the most severe transient vertical environment that cargo will encounter in truck transport.

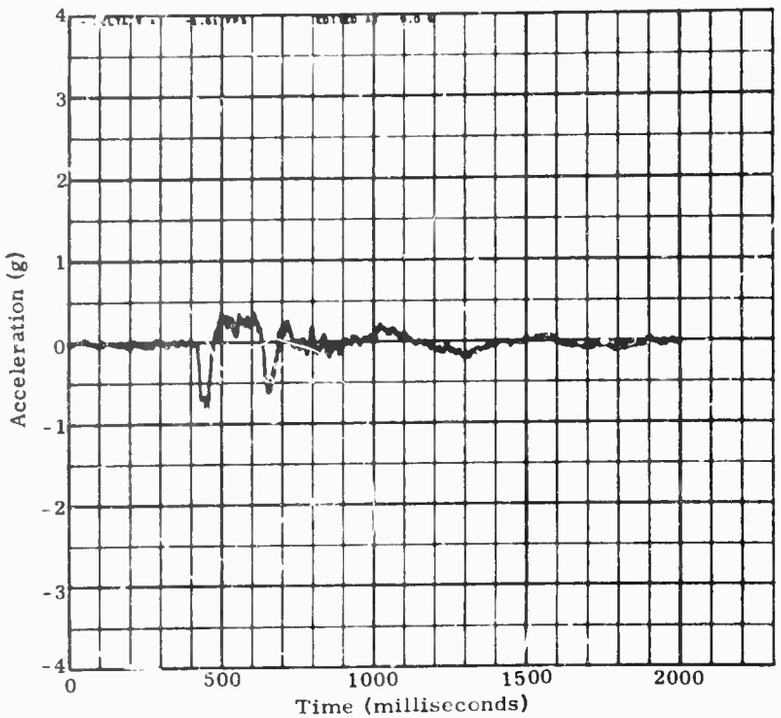

Fig. 11 - Backing into loading dock - longitudinal, forward on truck bed (Channel 4)

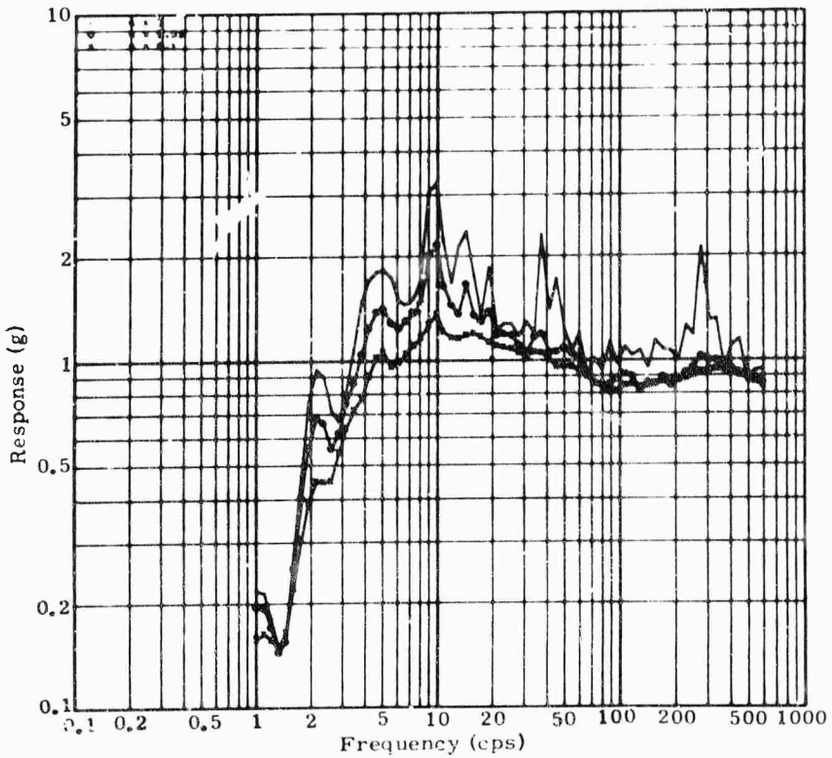

Fig. 12 - Backing into loading dock - longitudinal, forward on truck bed (Channel 4)

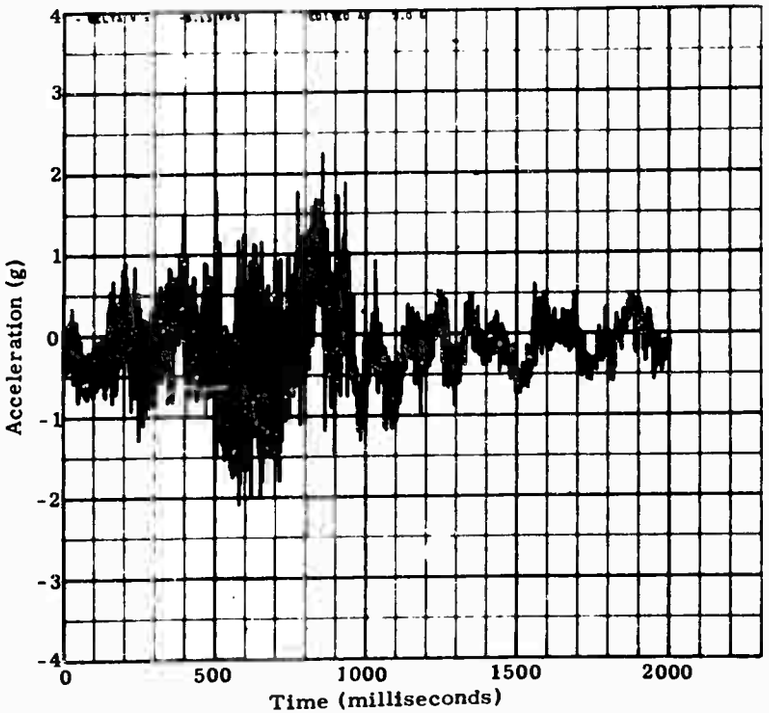

Fig. 13 - Driving across railroad tracks at 45 mph - vertical, aft on truck bed (Channel 1)

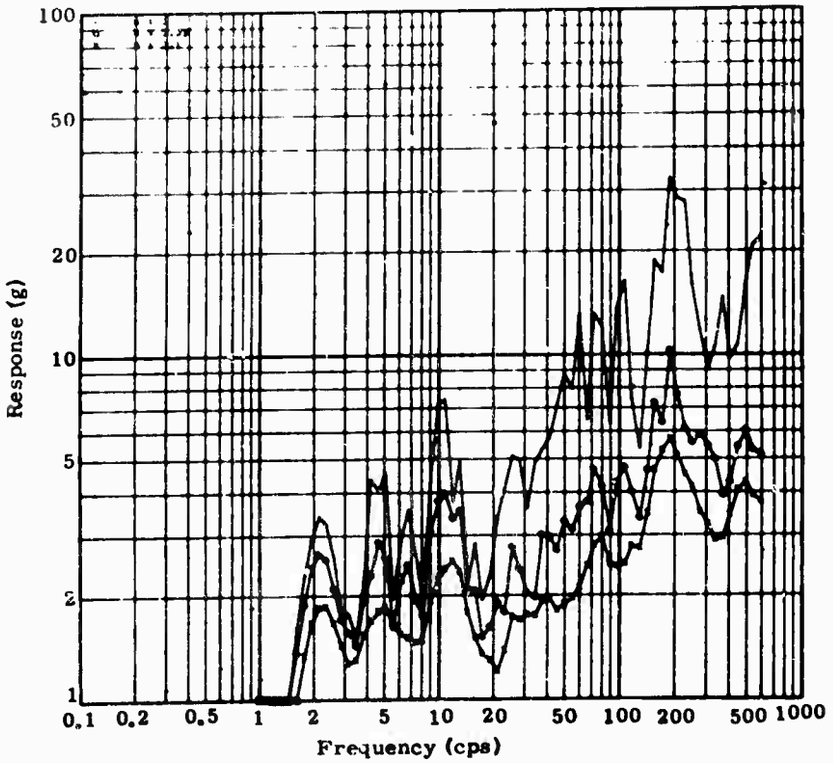

Fig. 14 - Driving across railroad tracks at 45 mph - vertical, aft on truck bed (Channel 1)

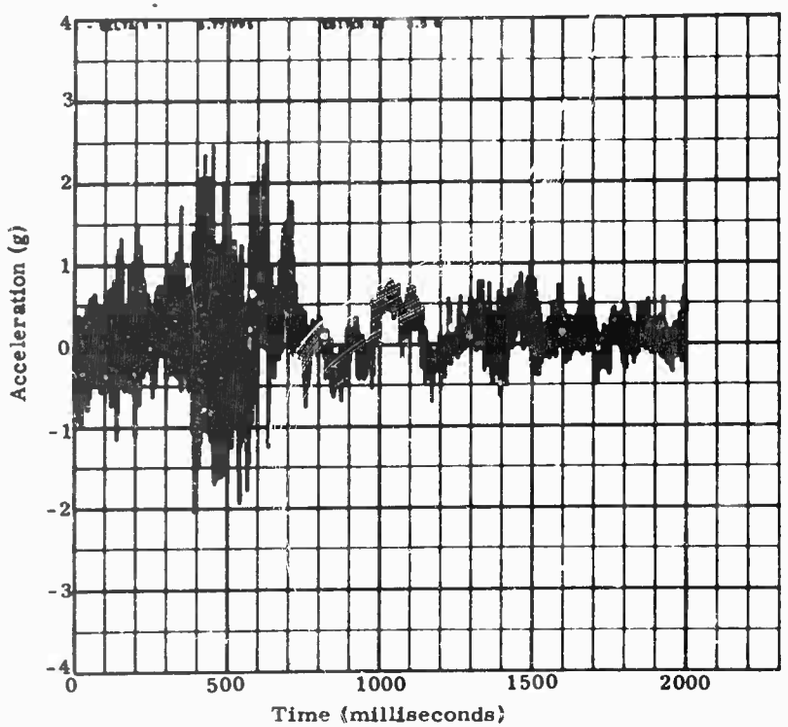

Fig. 15 - Driving across cattle guard at 45 mph - vertical, aft on truck bed (Channel 1)

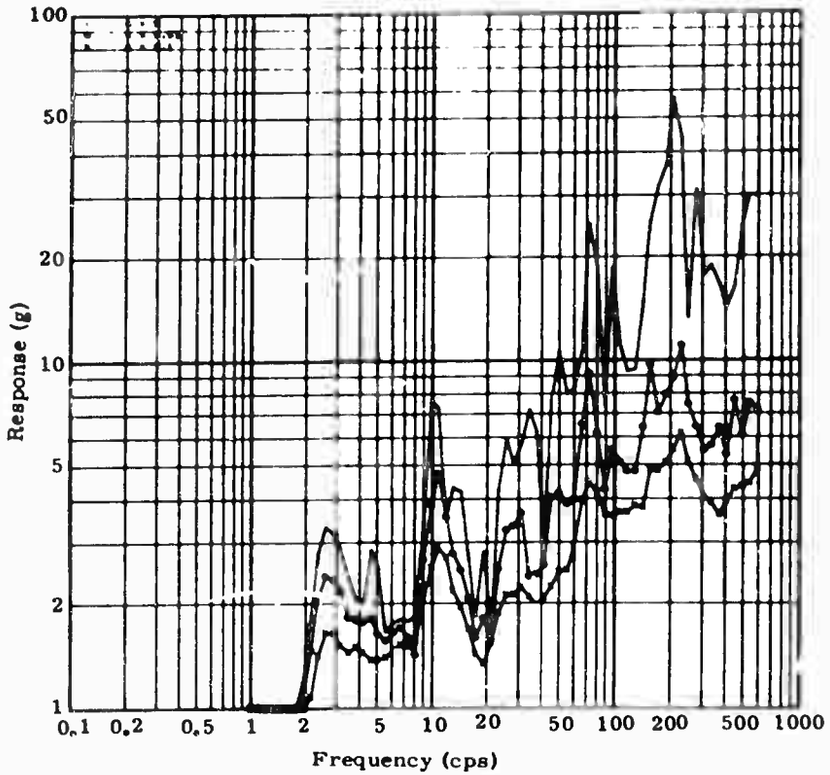

Fig. 16 - Driving across cattle guard at 45 mph - vertical, aft on truck bed (Channel 1)

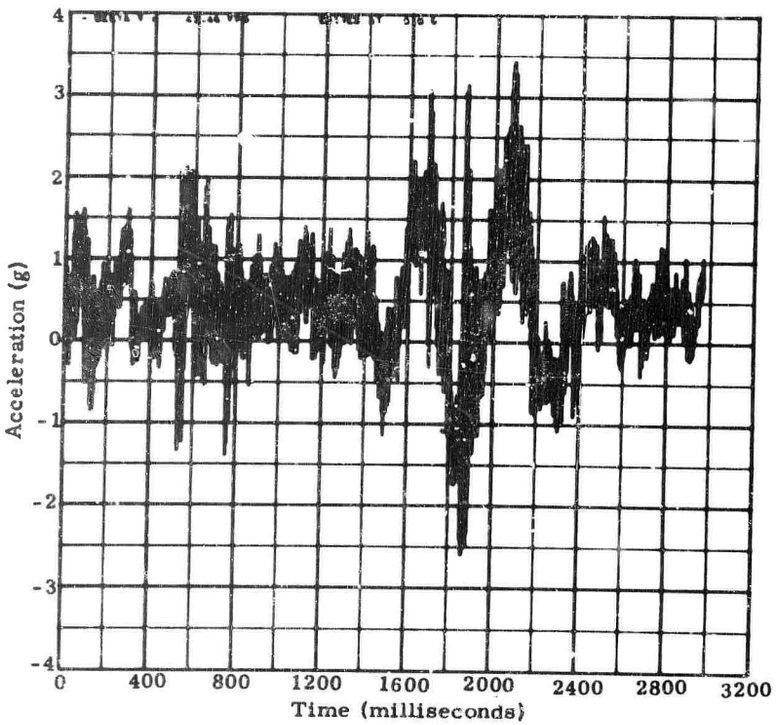

Fig. 17 - Driving across pot holes at truck stop - vertical, aft on truck bed (Channel 1)

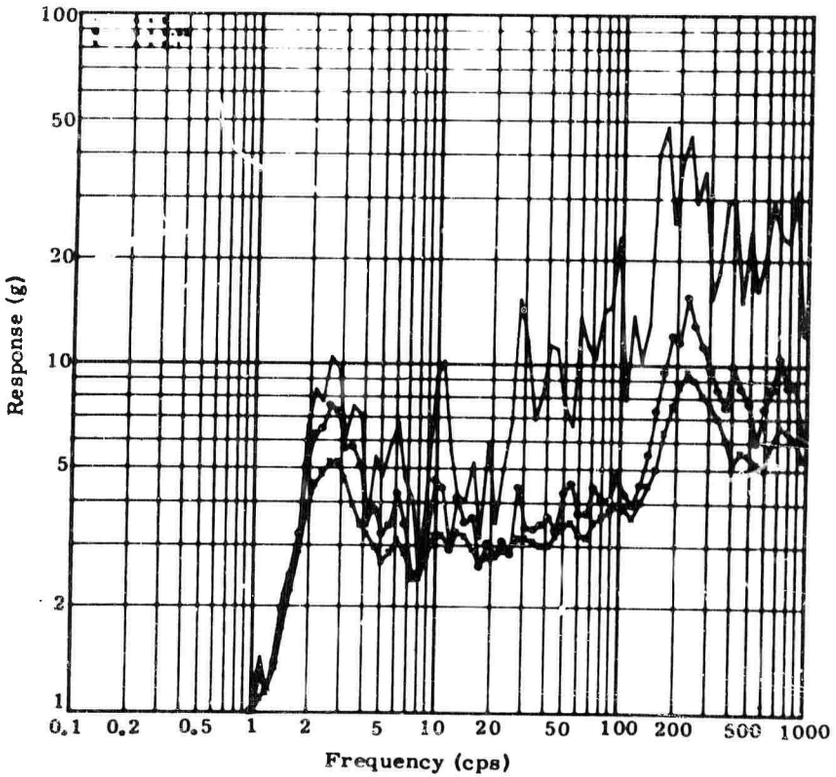

Fig. 18 - Driving across pot holes at truck stop - vertical, aft on truck bed (Channel 1)

EVALUATION SUMMARY

Data sampling performed during these tests appears to have accomplished the following:

1. Our data bank store of environmental descriptions of the dynamic inputs to cargo during normal over-the-road operations was extended to include data in the flatbed-truck category.
2. Certain near-accident events were measured which, to our knowledge, have not been discribed previously in quantitative terms which relate to potential effects on cargo.
3. Location of cargo on the truck bed has an effect on the severity of vertical inputs to cargo, with cargo located over or near the rear wheels getting the roughest ride.
4. Location of cargo on the truck bed appears to have little, if any, effect on longitudinal shocks that may be imposed on the cargo.
5. Speed appears to produce differing response severities on cargo. Low speeds have greater effect on low natural-frequency cargo; high speeds have greater effect on high natural-frequency cargo.
6. Except for off-road operation in bumpy terrain, it appears that long-duration phenomena encountered in normal situations are more severe than the long-duration phenomena encountered in what we considered to be unusual events in this test.
7. These evaluations of transient phenomena have led us to postulate a ranking of these transient phenomena in terms of response severity. The results indicate that pot holes or bumps produce the most severe vertical axis environment, and collisions with objects such as loading docks produce the most severe longitudinal environment.
8. Some events are not unique in the dynamic sense, as exemplified by the similarity of environment encountered on railroad tracks and cattle guards.

FUTURE EXPERIMENTS

The data obtained in these investigations consisted exclusively of acceleration amplitudes. To maximize interpretation and application of these data, we plan to obtain apparent weight measurements using either the actual truck and load upon which these acceleration measurements were obtained or a similar truck with the same load rating and configuration. Of particular interest in this respect would be apparent weight measurements in the 0-to-10-cps region [10], since it is in this frequency range that, on other types of trucks, the greatest input energies have been detected.

REFERENCES

1. M. B. Gens, "The Environmental Operations Analysis Function," published in IES 1967 Proceedings, pp 29-38.
2. J. T. Foley, "An Environmental Research Study," paper presented at 1967 IES Symposium, April 1967, published in IES 1967 Proceedings, pp. 363-373.
3. W. B. Murfin, "Automated Digital Shock Data Reduction System," paper presented in February 1967 and published in Part 6, Shock and Vibration Bulletin, #36, pp. 21-36.
4. J. T. Foley, "Preliminary Analysis of Data Obtained in the Joint Army/AEC/Sandia Test of Truck Transport Environment," paper presented February 1966 and published in Part 5 of Shock and Vibration Bulletin #35, pp. 57-70.
5. R. A. Harley, "Impromptu Vibration Data Acquisition with the ELI 31 Recorder," 1967 IES Proceedings.
6. R. A. Harley, "Automatic Temperature-Time Data Acquisition in Transportation Environments," 1968 IES Proceedings, pp 263-268.
7. M. B. Gens, "A Preliminary Observation of the Dynamic Environment of Helicopters," 1968 IES Proceedings, pp 423-432.
8. W. B. Murfin, "Dual Specifications in Vibration Testing," paper presented at 38th DOD Shock and Vibration Symposium; to be published in Shock and Vibration Bulletin.
9. F. R. Gustke, "Portable Environmental Sampler," paper presented at 1967 IES Symposium, April 67; published in IES 1967 Proceedings, pp 155-160.
10. J. T. Foley, "The Environment Experienced by Cargo on a Flat Bed Tractor-Trailer Combination" SC-RR-66-677, December 1966.

DISCUSSION

Mr. Renius (Army Tank Automotive Command): Can you tell me what truck you used and why you used that truck? If you used more than one, was there any variation noted between trucks?

Mr. Foley: First of all, the truck that we used for this test was used because it was available. In this particular situation it was a piggy-back test for us. The truck and everything else was furnished by another organization. Actually, it turned out that we had two hours notice to take measurements on this truck, so we took the opportunity. We are also interested in trying to measure the variation from one truck to the next. The next time we get a crack at it we will do it. We just have not gotten around to it yet.

Mr. Childs (SRDE): Were these trucks fully laden or light?

Mr. Foley: The load was relatively light.

Mr. Childs: So the springs would be out of action?

Mr. Foley: Yes. Another point, with regard to your paper, is that the load was all tied down, not loose.

Mr. Childs: So you are actually measuring the shock on the truck, not on the package.

Mr. Foley: That is right. We measured the input to the cargo and only thru the use of shock spectra inferring what this produces in the way of response.

Mr. Christo (Naval Underwater Weapons Research and Engineering Station): With respect to laboratory tests, what would be the best test to simulate truck transportation?

Mr. Foley: There is a reference concerning our views on this at the end of the paper. There is another reference on how to apply this sort of data to derivation of tests. Very roughly, I would say that you need three different types of tests. You need: a low level random vibration test, a repetitive shock test superimposed on a random background, and a very low frequency test - load applications which are very close to static equivalent loads. I think it has to be done in three steps to cover all the parameters.

Mr. Griffith (Bendix Missiles Systems Division): I am rather surprised at the levels of the normal events compared with the abnormal. Have you drawn any conclusions as to whether or not these may have been higher in the normal because of the light load?

Mr. Foley: This is entirely possible. What we would like to do on things like this, though we did not have the opportunity here, is to run a range of loads.

Mr. Griffith: You pointed out that you are using primarily piezoelectric accelerometers. You had some frequencies that were extremely low. How did you obtain these?

Mr. Foley: The system utilized with the accelerometers is essentially a charge amplifier which we feel is good to 2 or 3 hertz. The plot is wrong when it says 0 to 2-1/2 hertz. There is really no zero frequency there. I would have preferred to use piezoresistive types but the short notice for the test prevented this.

DEVELOPMENT OF A RAILROAD ROUGHNESS INDEXING AND SIMULATION PROCEDURE

L. J. Pursifull and B. E. Prothro
U.S. Army Transportation Engineering Agency
Military Traffic Management and Terminal Service
Fort Eustis, Virginia

In order to simulate rail vehicle performance on an analog computer to study shock and vibration characteristics of various rail and cargo configurations, it is necessary to provide an input representing the roughness characteristic of the rail surface. This paper describes a study of methods for measuring and simulating rail surface roughness which resulted in a recommendation to use a white noise generator to provide the required inputs. Measured accelerations on cargo were found to approximate the characteristics of white noise. The measured acceleration values were correlated with descriptive adjectives good, fair, rough, etc., and were further correlated with causative displacement inputs to the railcar springs. A plan for measuring rail surface condition using an accelerometer at the base of the truck springs is described.

The U.S. Army Transportation Engineering Agency (USATEA), Military Traffic Management and Terminal Service, Fort Eustis, Virginia, is concerned with the effects of the transportation environment on military cargoes. One of the Agency's interests is to find better ways of predicting the characteristics and effects of shock and vibration that may be encountered in the land, air, or water modes of transport. The Agency uses an analog computer to simulate vehicle performance with various load configurations, but in order to do this, sufficient information about the vehicle must be known to write the equations of motion. In addition, it is necessary to be able to specify the right-of-way variations that cause a vibratory response and to simulate these variations for input to the computer. Frequently, the most difficult part of the problem is to find a method for introducing the right-of-way characteristics.

This paper deals with only one mode, the rail mode, and describes the approach being taken to develop an index for classification of rail surface roughness, a method for simulation of the rail surface roughness for input to an analog computer, and a method for measurement of the rail surface roughness. Some of the work is still in progress, and further proof-testing in the field is planned to verify the soundness of the Agency's methods. It is anticipated that the approach presented in this paper will stimulate further thought and research on the subject.

This study is limited to consideration of the vertical displacements of the surface profile of a railroad track. The track has other defined characteristics, such as warp, gage, superelevation, cross level, and alignment, which may contribute to the shock and vibration environment, but the key factor to which the railcar suspension system responds is vertical surface roughness. It is also one of the most troublesome factors in track maintenance.

At present, no common agreement exists as to how the surface roughness should be described. In conversations, such adjectives as smooth, rough, good, bad, etc., are used, based on subjective impressions; but these terms have no meaning to a computer unless they are defined with qualitative values. That is the purpose of the railroad roughness index: to assign measurable qualitative limits to the descriptive adjectives customarily used so that the environment can be accurately expressed

and so that one of the causes of confusion and misunderstanding can be reduced or eliminated when a vehicle simulation requirement is described.

First, the possibility was studied of actually measuring and recording on magnetic tape the surface profile variations of large samples of track throughout the United States, the thought being that conclusions might be drawn as to the appropriate displacement levels to be included in each roughness classification. It seemed to be a straightforward approach because there are track-condition measuring cars on the market which could be adapted to produce magnetic tape records. The railroads use these cars to obtain data for scheduling track maintenance. However, the cars that were offered did not produce a precise record of the actual profile because they use a mechanical linkage to establish a base of reference. No completely satisfactory way has been found to maintain this reference linkage steady in the horizontal plane and unaffected by the track variations. Fig. 1 shows a simplified illustration of this basic measurement problem.

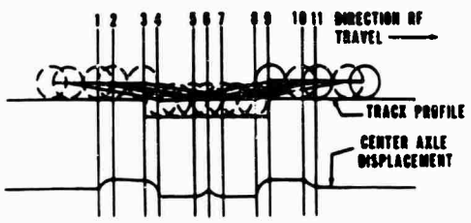

Fig. 1 - Center-axle displacement pattern when a three-axle truck traverses a depressed rail

Typically, a three-wheeled truck is used in which the two outboard wheels are unsprung. The center wheel is allowed 1 degree of freedom with respect to the rigid link connecting the two outboard wheels. The variations in displacement of the center wheel with respect to the connecting link are transmitted mechanically or electrically to a recording device, usually a strip chart recorder, although there is no reason why, with use of the proper transducers, the variations could not be recorded on magnetic tape.

Unfortunately, when the truck proceeds over a track profile variation, as shown in Fig. 1, both the reference base (that is, the connecting link) and the center wheel are displaced in the vertical plane, causing inaccuracies in the recorded profile measurement.

Furthermore, there would be tremendous coordination and scheduling problems involved in attempting to operate track-measuring cars over private rail lines in the United States, and it would take more resources than this Agency could muster to cover adequately the 200,000-plus miles of track in this country. Faced with this situation, USATEA turned to the statistical sampling approach which is described in this paper, and which, for the present, is more practical.

The data available for this undertaking existed in summary form in reports that had been prepared by USATEA in connection with certain monitoring and criteria projects. One report was particularly useful because suitable information was available on spring rates, moments of inertia, etc., for computing vehicle response.

Fig. 2 shows a shipment by railcars of nuclear power plant material on which acceleration measurements were recorded during a trip from Portsmouth, Virginia, to Dunbarton, South Carolina. The monitoring personnel rode in a caboose and provided a record of their subjective impressions as to the relative roughness of different portions of the railroad traversed during the movement. The descriptions furnished by the personnel were supported by the recorded acceleration data. For example, the run between Portsmouth, Virginia, and Rocky

Fig. 2 - Railcars loaded with nuclear casks

Mount, North Carolina, was described as "definitely rough". It had been so rough that sleep was practically impossible. Conversely, the run from Augusta, Georgia, to Dunbarton, South Carolina, was described as "smooth". The report showed that the maximum acceleration recorded on the "rough" Portsmouth to Rocky Mount run was 0.9g at 3 hertz, and the maximum acceleration on the "smooth" Augusta to Dunbarton run was 0.4g at 3 hertz. Therefore, a correlation of the abstract terms "good" and "rough" with corresponding measurable parameters is established. This correlation can be used as a starting point for development of a rail roughness index.

Next, it is necessary to determine whether the accelerations are truly random. If so, the possibility of simulating the roughness with a random noise generator is quite obvious. The evidence affirming this comes from two sources: one is the cumulative distribution of peak accelerations recorded during a rail trip at a constant speed, and the other is a plot of peak accelerations versus frequency contained in Army Technical Bulletin 55-100, Transportability Criteria - Shock and Vibration. (1)

Fig. 3 shows the cumulative distribution of peak accelerations recorded during a 65-mile-per-hour run between Rocky Mount, North Carolina, and Florence, South Carolina. This curve looked enough like a random distribution to encourage further investigation.

To determine better the degree of randomness, the cumulative distribution was divided into 0.1g elements which were used to plot a probability density distribution. A normalized amplitude density curve having the same standard deviation as the data was superimposed for comparison. Fig. 4 shows this comparison.

It is apparent that there is a strong family resemblance. Certainly the plotted data do not ideally conform to a Gaussian distribution which would be characteristic of white noise. Even though distribution is skewed, it does not have the characteristic dips which would indicate cycling.

One possible explanation for the skewing is unequal sampling. For example, skewing would occur if two Gaussian distributions having unequal amplitudes were added. More research is needed in this area to develop a reliable sampling technique.

To illustrate, Fig. 5 shows the route followed during the 65-mile-per-hour run. The trip totaled 173.1 miles between Rocky Mount and Florence. Note, however, that there is a 74.2-mile section between Wilson and Fayetteville which would not normally be traversed by trains coming from the north or south to Wilmington, a busy seaport. It seems reasonable to expect, therefore, that this section which did not receive as much wear and tear might be smoother than the 16.1-mile section from Rocky Mount to Wilson and the 82.8-mile section from Fayetteville to Florence. Such a difference in the samples would account for skewing in the same direction as that noted in the probability density graph, and it points out the

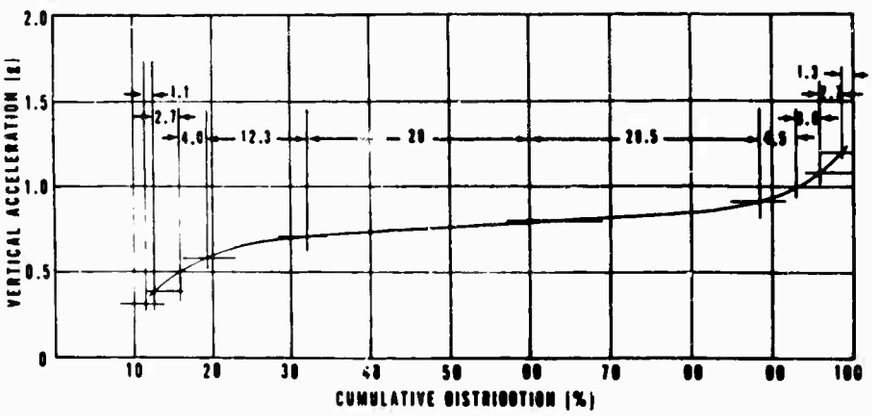

Fig. 3 - Cumulative distribution of peak accelerations recorded during a 65-mph run

(1) TB 500-100, Transportability Criteria - Shock and Vibration, Department of the Army, Washington, D.C., 17 April 1964.

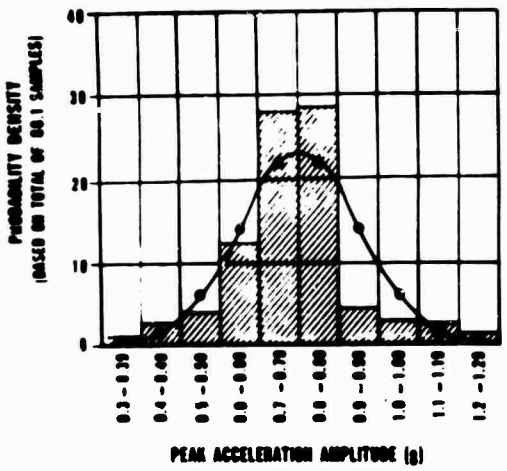

Fig. 4 - Density of peak accelerations with normalized density curve superimposed

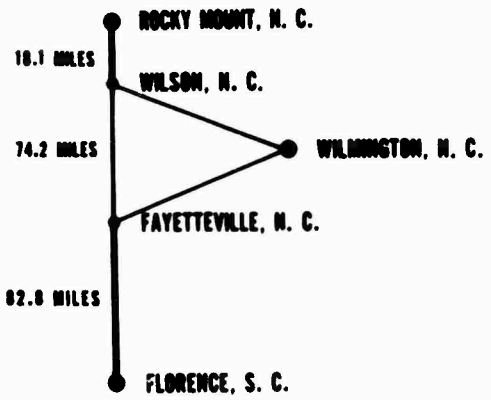

Fig. 5 - Route of 65-mph run

necessity for careful sampling in evaluating and classifying track condition.

The second source of information for determining randomness, TB 55-100, contains a curve of maximum acceleration versus frequency describing the rail environment. This curve represents maximum values recorded during a large number of studies (see Fig. 6). In this perspective, the curve can be considered to represent the characteristics of a statistical sample from an ensemble of systems. Note that the curve is flat out to about 170 hertz. Again, by definition, a flat spectrum is characteristic of white noise and will yield a constant power spectral density, which can be computed using the following equation:

$$\text{Power spectral density} = \frac{g^2}{\Delta f}$$

where

$$g = \sqrt{\Sigma \left(\frac{A}{\sqrt{2}}\right)^2}$$

A = maximum amplitude of acceleration for each frequency in the bandwidth

For white noise, all frequency amplitudes are equal. Therefore, in the case under consideration,

$$g^2 = (17\text{-}. \left(\frac{A^2}{2}\right)$$

and

$$\text{PSD} = \frac{170\ \frac{(4,8)^2}{2}}{170} = 11.52\ (\text{ft/sec}^2)^2,$$

which is independent of frequency.

This indicates, then, that the output of a white noise generator can be used to simulate transportation shocks. The only requirements are that the power spectral density be flat over the frequency range of interest and that the output level be adjustable to meet the voltage scaling requirement of the particular computer program. The voltage scaling would be accomplished with an intermediate amplifier, if necessary.

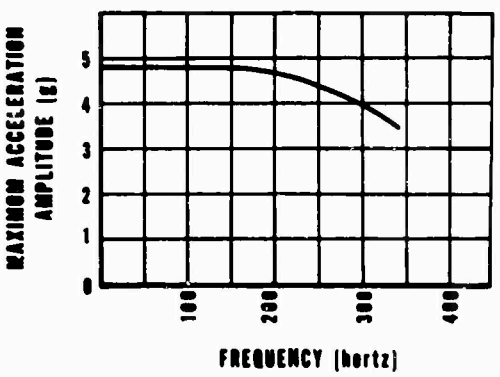

Fig. 6 - Maximum recorded vertical vibration amplitudes versus frequency for rail transport mode

Fig. 7 illustrates the factors affecting the motion of the cargo platform.

Up to this point, the discussion has concerned accelerations that were measured on the cargo. What USATEA is trying to develop,

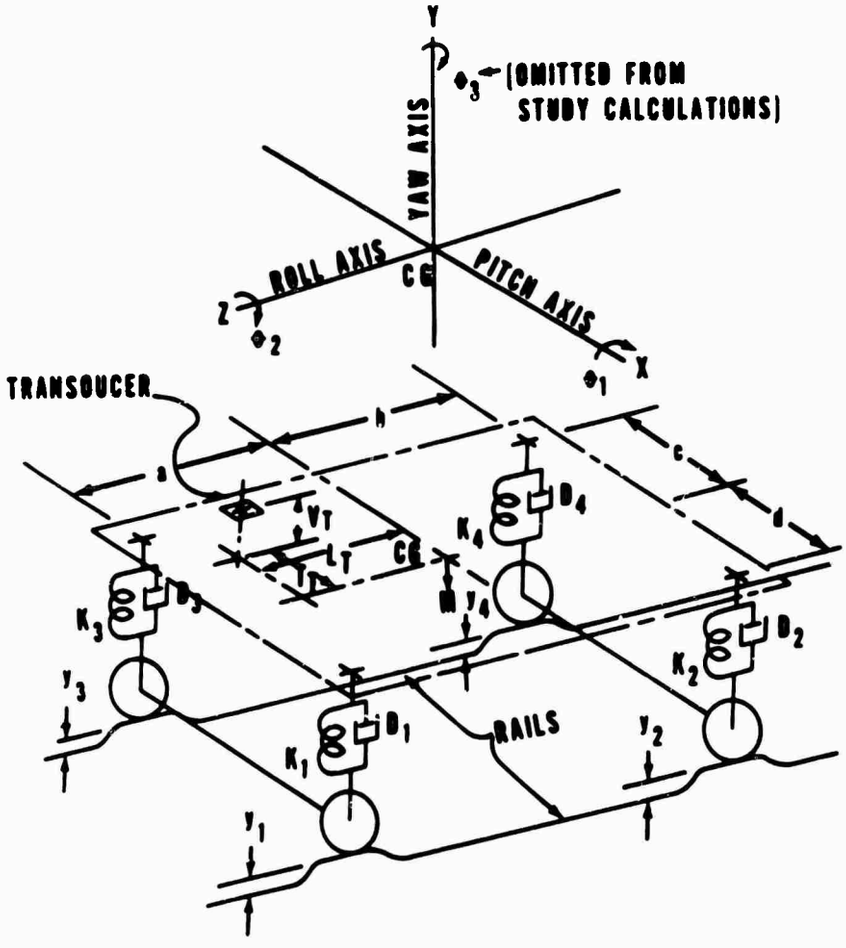

Fig. 7 - Diagram showing railcar motion

however, is an index of rail surface roughness. The next step, therefore, is to relate the measured accelerations on the cargo to the causative variations in the right-of-way. This is accomplished by determining the displacement at the base of the springs that caused the transducer response. This, in effect, rules out flat wheels, eccentric bearings, etc., and assumes that displacements y_1, y_2, y_3, and y_4 are the causative variations.

The causative displacement was determined by simulating the railcar used on the Rocky Mount to Florence run, then varying the amplitude and frequency of the inputs y_1, y_2, y_3, and y_4, until outputs were obtained which corresponded to those measured by the transducer on the cargo.

In Fig. 7, K_1, K_2, K_3, and K_4 are the spring constants; D_1, D_2, D_3, and D_4 are the damping coefficients; a and b are the longitudinal distances from the pitch axis (that is, the X axis) to the respective spring centers; c and d are the transverse distances from the roll axis (that is, the Z axis) to the respective spring centers; L_T and T_T are the longitudinal and transverse distances between the transducer centroid and the pitch and roll axes respectively; and V_T is the vertical distance between the transducer centroid and the horizontal plane through the center of gravity of the vehicle; and M is the unsprung mass.

The three simultaneous equations of motion were written by summing forces in the vertical direction and moments about the X axis and Z axis. The general form of the equations is quite lengthy, but several simplifications were possible in this case.

Fig. 8 shows the diagrammatic side and plan views of the loaded car. Note that it is symmetrically loaded. Therefore, the longitudinal and transverse locations of the spring centers with respect to the center of gravity are equal; that is, distance a is equal to distance b, and distance c is equal to distance d. The spring constants are all equal; that is K_1, K_2, K_3, and K_4 are equal. Furthermore, it was found that damping could be neglected, thus letting D_1, D_2, D_3, and D_4 equal 0. This process was a safe one for the purpose of developing the index because the ultimate result would be a more severe displacement value for a given roughness description than would have been the case if damping were employed. Since the actual value of the damping coefficient was unknown, this simplification was considered prudent.

Following are the three simplified equations of motion, and a fourth equation relating the motion of the transducer to the motion of the center of gravity:

$$\ddot{Y} = -\frac{K}{M}(4Y - y_1 - y_2 - y_3 - y_4) \qquad (1)$$

$$\ddot{\theta}_1 = \frac{Ka}{Mr_1^2}(y_1 - y_2 + y_3 - y_4 - 4a\theta_1) \qquad (2)$$

$$\ddot{\theta}_2 = \frac{Kc}{Mr_2^2}(-y_1 - y_2 + y_3 + y_4 - 4c\theta_2) \qquad (3)$$

$$\ddot{Y}_T = \ddot{Y} + \ddot{\theta}_1\sqrt{(L_T)^2 + (V_T)^2} + (\dot{\theta}_2)^2 (V_T) \qquad (4)$$

In the equations, y is vertical displacement of the center of gravity, and $\ddot{Y}$ is vertical acceleration in feet per second squared; $\ddot{\theta}_1$ is angular acceleration in pitch in radians per second squared, and r_1 is radius of gyration about the pitch axis. $\ddot{\theta}_2$ is angular acceleration in roll, and r_2 is the radius of gyration about the roll axis.

In equation 4, note that $\ddot{Y}$ is the vertical acceleration of the center of gravity, and $\ddot{Y}_T$ is the vertical acceleration of the transducer. The computer programming for these equations is straightforward.

Fig. 9 is a block diagram illustrating the method used to simulate the track roughness input.

Since the rail joints on opposite sides of the track are staggered, a compensation was made in the simulation by shifting the inputs on one side of the railcar 90 degrees with respect to the inputs on the other side. This was accomplished by using a sine generator for the two inputs on one side of the car and a cosine generator for the two inputs on the other side.

In addition, the delay between the time the front truck crosses a surface bump at 65 miles per hour and the time the rear truck crosses

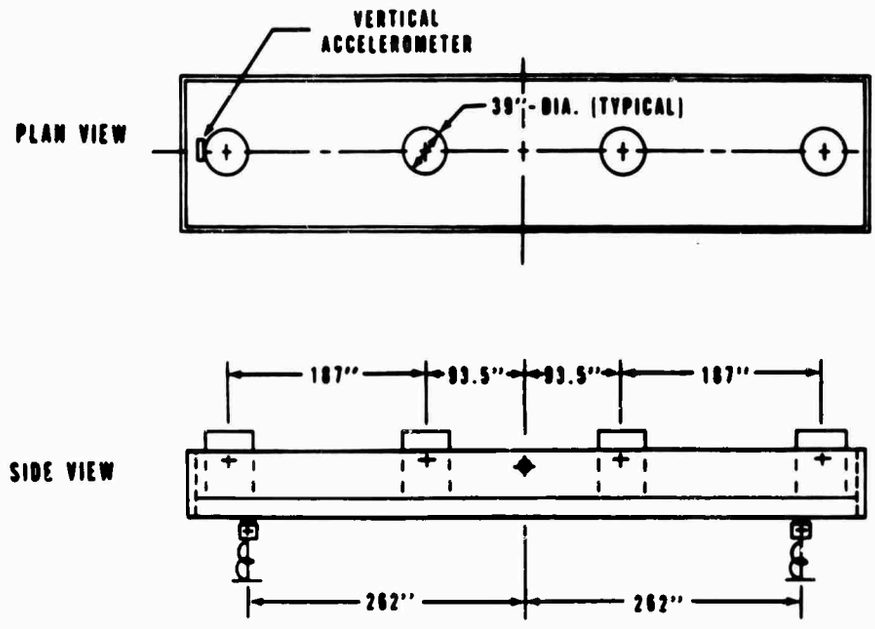

Fig. 8 - Loaded arrangement of instrumented railcar

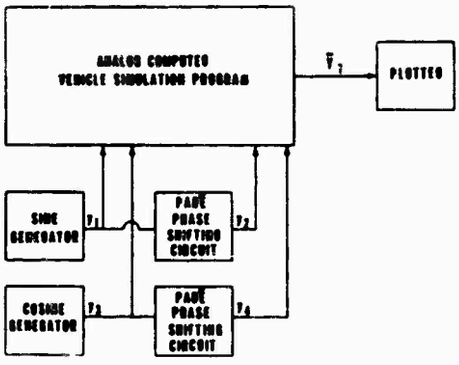

Fig. 9 - Block diagram for programming vehicle simulation

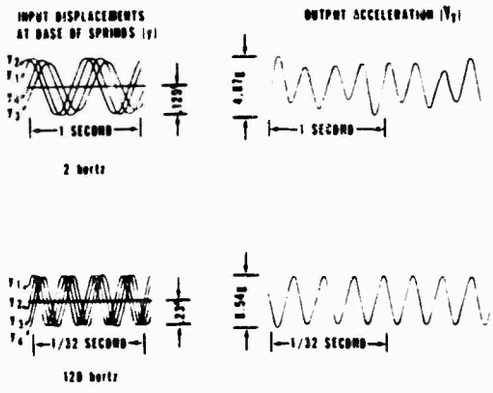

Fig. 10 - 2 and 128 hertz inputs with corresponding outputs from railcar simulation

the same bump can be represented by a phase shift. This is possible because the inputs and responses are steady state. This is expressed by the following equation:

$$\text{Phase shift (in cycles)} = \frac{(a+b)}{S} \times f$$

where

(a+b) = wheelbase in feet
S = speed of railcar in ft/sec
f = frequency

A first-order Padé approximation circuit (described in Electronic Associates, Inc., Handbook of Analog Computation[2]) was used to introduce the phase shifts.

A series of 18 runs with different amplitude sinusoidal inputs was made at each of 8 octave intervals between 2 and 256 hertz. Fig. 10 shows traces of the inputs and corresponding outputs at the highest and lowest frequencies studied. The input curves are calibrated in terms of displacement in feet, and the output curves are given in g's.

Fig. 11 shows the family of curves of maximum displacement amplitude at input versus maximum acceleration at the transducer location resulting from the series of computer runs.

Since the slopes of these curves are constant, a simple transfer function is obtained by plotting the ratio of output to input versus frequency.

Fig. 12 is a graph of the transfer coefficient versus frequency. The spike in the graph occurs at 4 hertz, which is the natural frequency of bounce of the railcar.

It was found that the dwell time to reach peak acceleration at 4 cycles per second is approximately 1.1 seconds. Dwell times of several cycles were required also with inputs of 8 and 16 cycles before the maximum vehicle response was experienced. Since such dwell times are extremely unlikely to occur in actual operations, and because the graph is remarkably flat except at the natural bounce frequency, it was considered reasonable to use the mean value of the transfer coefficient to convert the measured accelerations previously associated with descriptions of ride quality to maximum displacement at the base of the truck springs. As seen on the graph, the mean value of the transfer coefficient is 24g's per foot.

Fig. 13 shows the resulting rail performance index in which are listed five classifications of surface roughness ranging from good to extreme, with corresponding computed values of spring displacement ranging from 0 to 0.2 foot. The values of peak accelerations identified at the end of the loaded test car are shown for comparison with field experience.

Fig. 14 shows a diagram of the instrumentation presently being developed for further studies of the character of surface roughness. An accelerometer is mounted at the base of the springs on one axle of a standard railcar. A resilient mount will be used to eliminate high frequency hash, and the outputs of the accelerometers will be doubly intergrated to provide displacement. Simultaneously, vertical

[2] Electronic Associates, Inc., Handbook of Analog Computation, Princeton, N.J., 1967.

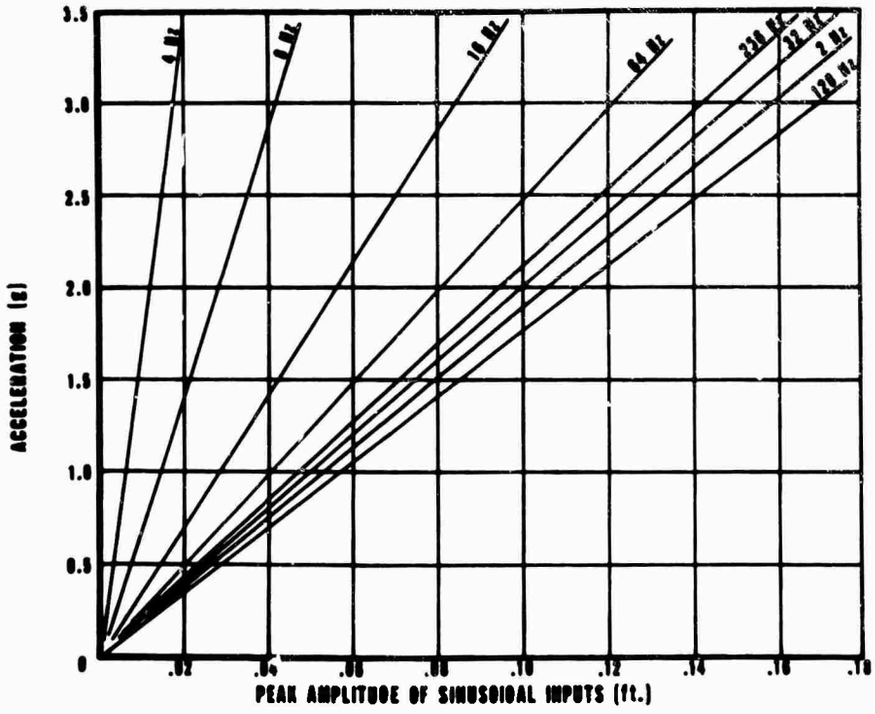

Fig. 11 - Computed maximum vertical acceleration at transducer for various input frequencies and amplitudes

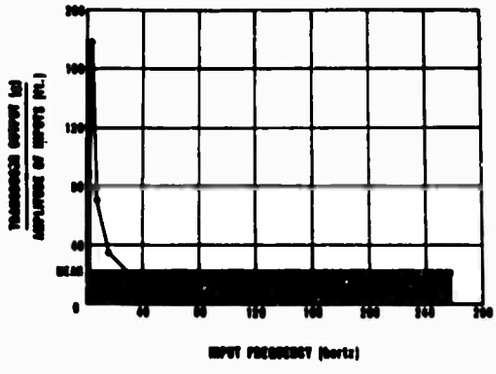

Fig. 12 - Surface roughness transfer coefficient versus input frequency

DESCRIPTIVE ADJECTIVE	RANGE OF PEAK ACCELERATIONS AT END OF INSTRUMENTED CAR (g)	COMPUTED VERT. DISPLACEMENT AT RANGE OF SPEEDS (ft.)
[illegible]	0 - 0.5	0 - .001
[illegible]	0.5 - 1.0	.001 - .002
[illegible]	1.0 - 1.5	.002 - .050
[illegible]	1.5 - 3.0	.003 - .125
[illegible]	3.0 - 6.0	.125 ↑

Fig. 13 - Rail surface roughness index

acceleration at the center of gravity of the vehicle is recorded for comparison with the output of the axle accelerometers. Once a satisfactory level of confidence in the output of the axle accelerometers is achieved, repeatable measurements of surface roughness practically unaffected by variations in the rail car suspensions will be possible.

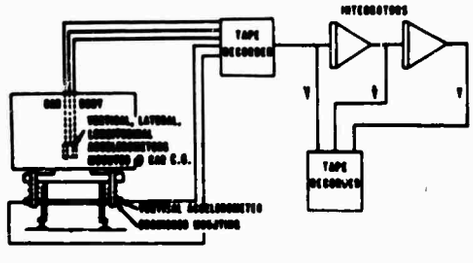

Fig. 14 - Diagram of instrumentation for measurement of rail surface roughness

DISCUSSION

Mr. Sonnemann (Sikorsky Aircraft): We have just completed, as you may know, a fairly extensive work on rail vehicles in connection with our high speed train project. I wanted to comment just briefly on some of our findings because they do not seem to be in complete agreement with what you stated. We have taken some measurements at the wheel-axle interface in order to determine the rail input due to the discontinuities at the joints. Frequently, we have found that we get shocks as high as 20 g and sometimes as high as 50 g. These loads are then rapidly attenuated through the suspension system. Recognizing that it is a passenger vehicle that we are working on compared to the freight car that you were talking about, people's comments as far as a poor ride is concerned would involve levels like 1/2 g. If we exceeded 1/2 g, which we seldom did, people would think the ride was terrible. We have further found that the non-gaussian distribution on which you commented is attributable to two factors. One is the poor conditions of curves on the railroad, and the other is the frequency that grade crossings occur. We have seen that the grade crossings will skew the distributions of g-levels a great deal, because it is at this time that the abnormal inputs occur. These become a factor in the skewing. In the light of our own work, I wonder whether your approach can really be representative of rail roughness, because of its nigh dependence on the suspension system. Have you thought about that aspect of it?

Mr. Prothro: We have thought about it. We are aware of the work that you people are doing and we have had the good fortune of being invited to ride your car next week. We plan to do so. One of the things I referred to was the need to develop better sampling techniques. I think this may be reflected in your finding about the distribution being skewed by traversing grade crossings. Perhaps the work you have done will be sufficient, but we had hoped to stimulate research in this. I did not know that you had made this discovery.

Mr. Hanks (NASA, Langley): I was wondering about your indexing procedures including surface irregularities that are much greater in wavelength than the length of the car. It appears in rough calculation that your wavelengths are the approximate length of the car. If your train speeded up to, say, 120 miles per hour then you would not have any idea whether you would encounter this 4 cycle per second roughness or not.

Mr. Prothro: The 4 cycle roughness was the natural bounce frequency of the car, but the wavelength or the phase shift that we introduced was based on a constant speed of 65 miles per hour. We were comparing this with field data that was made on a constant speed run at 65 miles per hour.

Mr. Hanks: But if you had picked up, say, 1/2 cycle responses or 2 cycles responses these may become critical at 120 or 130 miles per hour. Were you measuring below these levels?

Mr. Prothro: Yes. I guess it was not clear in that diagram but we started with inputs of 2 cycles and even below. We just diagrammed those octave intervals starting with 2 cycles. Surprisingly, the responses below that peak range were instantaneous. In other words, we got the sine wave pattern with an equal amplitude, but in the areas where the peak showed up the responses had to build up. It never did go into uncontrolled resonance.

Mr. Swanson (MTS Systems): I found this paper extremely interesting because last spring I served as a consultant for British Railways. They are very interested in the same problems. We characterized the loading that you have as a succession of random processes that the car meets in its history. The interesting thing about it is that each of these bursts is a stationary random process in itself and can be applied in the laboratory as a burst from a random noise generator. In fact they have gone ahead and are now putting in a system which supplies a succession of rms levels.

I would just like to comment that since your signal is nice and broad-band, it turns out, from sampling theory, that you can get very fast response of your rms level. If you were to put an rms meter on your signal and also filter out the deterministic very low frequency effects like mean load, then you can monitor rms almost instantaneously. I think that your skewing effects and these objective measurements of intensity would go by the board and you could go straight to a nice stable scale of rms's. You could also check for the stretch that you are going to do on probability plots. You could make sure that the values are stationary and that your rms's and constant over that stretch.

Mr. Prothro: I want to point out that our problems occur because someone asks a question. What happens if this thing goes over a rough road? What happens if it goes over a fairly smooth road? We are trying to put a handle on that description.

AN APPROXIMATE METHOD OF DYNAMIC ANALYSIS FOR MISSILE CONTAINER SYSTEMS

Mario Paz, Associate Professor
University of Louisville, Louisville, Kentucky

and

Ergin Citipitioglu,* Associate Professor
University of Louisville, Louisville, Kentucky

*Present Address: University of Cincinnati, Cincinnati, Ohio

An approximate method of dynamic analysis is presented for missile containers which use elastomeric shock mounts. The missile and its mounting frame are treated as a single rigid body supported by springs and dashpots representing the shock mounts. A parabolic spring rate function is assumed to approximate the frequency dependent dynamic properties of the mounts in the mathematical model. The results obtained by this method of analysis are compared with experimental results for the "Walleye" missile container system.

INTRODUCTION

One of the common methods of protecting missiles from shock and vibration during transportation is to mount the missile carrying cradle (usually a rigid frame) to the container by elastomer type of shock mounts. For approximate dynamic analysis of this type of missile container, elastomer shock mounts can be idealized by spring and damper systems in three principal directions. The missile together with the cradle can be treated as a rigid body, thus the whole

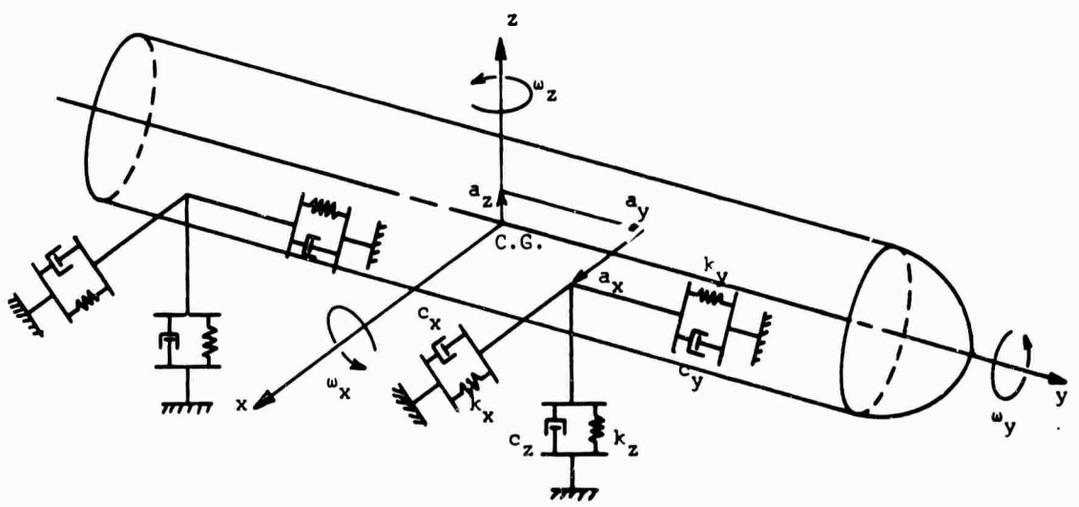

FIGURE 1. RESILIENTLY MOUNTED MISSILE

system may be represented by the mathematical model as shown in Fig. 1.

Dynamic properties of the springs and dampers replacing elastomer shock mounts are frequency and temperature dependent and can be determined by appropriate experiments [1]. The equations of motion for a rigid body supported by arbitrary springs and dampers having constant dynamic properties are derived in the literature [2,3]. In the case of elastomer shock mounts, it is necessary to include frequency dependence of spring rates in the derivation. An approximate method of dynamic analysis in which the spring rates in the principal directions are assumed to be parabolic functions of frequency, is presented. This method has a definite advantage of taking frequency dependence of dynamic properties of elastomer shock mounts into account without introducing complications in the analysis. Expressions are derived for natural frequencies and for transmissibilities of the system. The shock analysis is also presented for determination of the accelerations induced on the missile when the container is subjected to shocks such as the "flat-face free fall test". The results obtained by the method of analysis presented are compared with the experimental results for the "Walleye" missile container.

PROPERTIES OF SHOCK MOUNTS

Elastomer shock mounts can be idealized by springs and dampers in the three principal directions. One of the principal directions represents tension or compression mode and the other two are the shear modes. It should be noted that for cylindrical type of shock mounts, shear modes in two directions are identical.

The results [1] obtained from experiments indicate that frequency-spring rate relations in principal directions (x,y,z) at a given temperature can be expressed as

$$k_i = A_i + B_i \omega^2 \quad (i = x,y,z) \qquad (1)$$

where A_i and B_i are constants obtained from experiments and ω is the frequency. In Eq. (1), spring rates in the principal directions are denoted by k_i for a band of frequency. Depending on the experimental curves, the range of frequency can be divided into several bands of frequency and for each band Eq. (1) is evaluated. Then the analysis is performed for each band. Similar procedure should be followed for dynamic analysis at different temperatures by evaluating k_i at each temperature.

EQUATIONS OF MOTION

For support displacements the dynamic analysis is developed by considering the missile together with the supporting frame (cradle) to be a rigid body with one longitudinal plane of symmetry (yz plane). The mathematical model considered for the analysis is shown in Fig. 1. The resilient shock mounts are assumed to have principal axes parallel to the principal axes (x,y,z) of the missile. The position of any shock mount is given by a_x, a_y, a_z coordinates and the spring rates in x,y,z directions are denoted by k_x, k_y, k_z. The viscous damping coefficients of a resilient mount are indicated by c_x, c_y, c_z in x,y,z directions respectively.

By neglecting the damping, differential equations of motion for the rigid body shown in Fig. 1 can be written for displacements of the support as

$$I_x\ddot{\alpha} - \sum k_y a_z (y_c - u_y) + \sum k_z a_y (z_c - u_z) + \sum (k_y a_z^2 + k_z a_y^2)\alpha = 0 \qquad (2)$$

$$m\ddot{y}_c + \sum k_y (y_c - u_y) - \sum k_y a_z \alpha = 0 \qquad (3)$$

$$m\ddot{z}_c + \sum k_z (z_c - u_z) + \sum k_z a_y \alpha = 0 \qquad (4)$$

$$m\ddot{x}_c + \sum k_x (x_c - u_x) + \sum k_x a_z \beta - \sum k_x a_y \gamma = 0 \qquad (5)$$

$$I_y\ddot{\beta} + \sum k_x a_z (x_c - u_x) + \sum (k_x a_z^2 + k_z a_x^2)\beta - \sum k_x a_y a_z \gamma = 0 \qquad (6)$$

$$I_z\ddot{\gamma} - \sum k_x a_y (x_c - u_x) + \sum (k_x a_y^2 + k_y a_x^2)\gamma - \sum k_x a_y a_z \beta = 0 \qquad (7)$$

where

m = mass of the rigid body

I_x, I_y, I_z = Principal moments of inertia of the rigid body

x_c, y_c, z_c = Displacement components of the mass center in x,y,z directions

α, β, γ = Angular displacements about x,y,z axes

u_x, u_y, u_z = Components of the displacement of the support in x,y,z directions.

Considerable simplification in equations can be accomplished if the shock-mounts are located at points so that the vertical resulting resilient effect passes through the center of mass of the rigid body. This condition will make

$$\sum k_z a_y = 0, \quad \sum k_x a_y = 0, \text{ and also}$$

$$\sum k_x a_y a_z = 0$$

if all of the shock-mounts are located in a horizontal plane having the same value for the coordinate a_z. Other arrangements satisfying the latter condition are possible.

For a harmonic motion of the support having amplitudes U_x, U_y, U_z, the solution of simplified form of Eqs. (2) through (7) is obtained as

$$(\sum k_y a_z^2 + \sum k_z a_y^2 - I_x\omega^2)\alpha - \sum k_y a_z y_c = -\sum k_y a_z U_y \tag{8}$$

$$-\sum k_y a_z \alpha + (\sum k_y - m\omega^2) y_c = k_y U_y \tag{9}$$

$$(\sum k_z - m\omega^2) z_c = \sum k_z U_z \tag{10}$$

and

$$(\sum k_x - m\omega^2) x_c + \sum k_x a_z \beta = k_x U_x \tag{11}$$

$$\sum k_x a_z x_c + [\sum k_x a_z^2 + \sum k_z a_x^2 - I_y\omega^2]\beta = \sum k_x a_z U_x \tag{12}$$

$$(\sum k_x a_y^2 + \sum k_y a_x^2 - I_z\omega^2)\gamma = 0 \tag{13}$$

where ω is the frequency of the motion.

NATURAL FREQUENCIES

Noting that Eqs. (8) and (9) and Eqs. (11) and (12) constitute two independent sets and Eqs. (10) and (13) are uncoupled, the six natural frequencies can be determined by solving the following equations which are obtained by equating to zero the determinants of the coefficients.

$$\sum k_z - m\omega^2 = 0 \tag{14}$$

$$(\sum k_y a_z^2 + \sum k_z a_y^2 - I_x\omega^2)(\sum k_y - m\omega^2) - (\sum k_y a_z)^2 = 0 \tag{15}$$

$$\sum k_x a_y^2 + \sum k_y a_x^2 - I_z\omega^2 = 0 \tag{16}$$

$$(\sum k_x - m\omega^2)(\sum k_x a_z^2 + \sum k_z a_x^2 - I_y\omega^2) - (\sum k_x a_z)^2 = 0 \tag{17}$$

Substituting the expressions for the spring rates given by Eq. (1) into Eqs. (14) through (17), the natural frequencies are obtained as

$$\omega_1 = \sqrt{\frac{C_2 + \sqrt{C_2^2 - 4C_1C_3}}{2C_1}} \tag{18}$$

$$\omega_2 = \sqrt{\frac{C_2 - \sqrt{C_2^2 - 4C_1C_3}}{2C_1}} \tag{19}$$

$$\omega_3 = \sqrt{\frac{\sum A_z}{m - \sum B_z}} \tag{20}$$

$$\omega_4 = \sqrt{\frac{D_2 + \sqrt{D_2^2 - 4D_1D_3}}{2D_1}} \tag{21}$$

$$\omega_5 = \sqrt{\frac{D_2 - \sqrt{D_2^2 - 4D_1D_3}}{2D_1}} \tag{22}$$

$$\omega_6 = \sqrt{\frac{\sum A_x a_y^2 + \sum A_y a_x^2}{I_z - \sum B_x a_y^2 - \sum B_y a_x^2}} \tag{23}$$

where

$$C_1 = (\sum B_y a_z^2 + \sum B_z a_y^2 - I_x)(\sum B_y - m) - (\sum B_y a_z)^2$$

$$C_2 = (I_x - \sum B_y a_z^2 - \sum B_z a_y^2)\sum A_y + (m - \sum B_y)(\sum A_y a_z^2 + \sum A_z a_y^2) + 2(\sum A_y a_z)(\sum B_y a_z)$$

$$C_3 = (\sum A_y a_z^2 + \sum A_z a_y^2)\sum A_y - (\sum A_y a_z)^2$$

$$D_1 = (\sum B_x - m)(\sum B_x a_z^2 + \sum B_z a_x^2 - I_y) - (\sum B_x a_z)^2$$

$$D_2=(I_y-\sum B_x a_z^2-\sum B_z a_x^2)\sum A_x$$
$$+(m-\sum B_x)(\sum A_x a_z^2+\sum A_z a_x^2)$$
$$+2(\sum A_x a_z)(\sum B_x a_z)$$
$$D_3=(\sum A_x)(\sum A_x a_z^2+\sum A_z a_x^2)-(\sum A_x a_z)^2$$

TRANSMISSIBILITIES

Damping can easily be introduced in Eqs. (9) through (13) by substituting $k_i+j\omega c_i$ for k_i where j is imaginary unit and subscript i indicates x, y, and z. Then, after introducing damping, the transmissibilities are obtained for a forced frequency Ω by solving Eqs. (8) through (13) as

$$\frac{x_c}{U_x}=\left[\frac{[k_xA_5-\Omega^2\sum c_xA_6-(\sum k_xa_z)^2+\Omega^2(\sum c_xa_z)^2]^2+[\sum k_x\Omega A_6+\Omega A_5\sum c_x-2\Omega(\sum k_xa_z)(\sum c_xa_z)]^2}{[A_4A_5-\Omega^2\sum c_xA_6-(\sum k_xa_z)^2+\Omega^2(\sum c_xa_z)^2]^2+[A_4\Omega A_6+\Omega A_5\sum c_x-2\Omega(\sum k_xa_z)(\sum c_xa_z)]^2}\right]^{1/2} \quad (24)$$

$$\frac{y_c}{U_y}=\left[\frac{[A_1\sum k_y-\Omega^2A_2\sum c_y-(\sum k_ya_z)^2+\Omega^2(\sum c_ya_z)^2]^2+[A_1\Omega\sum c_y+A_2\sum k_y\Omega-2\Omega(\sum k_ya_z)(\sum c_ya_z)]^2}{[A_1A_3-\Omega^2A_2\sum c_y-(\sum k_ya_z)^2+\Omega^2(\sum c_ya_z)^2]^2+[A_1\Omega\sum c_y+A_2A_3\Omega-2\Omega(\sum k_ya_z)(\sum c_ya_z)]^2}\right]^{1/2} \quad (25)$$

$$\frac{z_c}{U_z}=\left[\frac{(\sum k_z)^2+\Omega^2(\sum c_z)^2}{(\sum k_y-m\Omega^2)^2+\Omega^2(\sum c_z)^2}\right]^{1/2} \quad (26)$$

where

$$A_1=\sum k_ya_z^2+\sum k_za_y^2-I_x\Omega^2$$
$$A_2=\sum c_ya_z^2+\sum c_za_y^2$$
$$A_3=\sum k_y-m\Omega^2$$
$$A_4=\sum k_x-m\Omega^2$$
$$A_5=\sum k_xa_z^2+\sum k_za_x^2-I_y\Omega^2$$
$$A_6=\sum c_xa_z^2+\sum c_za_x^2$$

SHOCK ANALYSIS

Specifications [4] for missile mounting limit the acceleration of the missiles when the system is subjected to stipulated shocks. Dynamically, a shock is an impulsive force acting in a short duration of time compared to the natural period of the system. Impulse results in an instantaneous change of velocity, after which the system starts a motion characterized by free vibrations. Therefore, shock tests may be simulated analytically by free vibrations of the missile with an initial velocity due to stipulated conditions. Analytical studies [2] indicate that the effect of damping in the maximum acceleration resulting from shock is relatively small, therefore it is neglected in the following analysis.

The differential equations of motion (Eqs. (2) through (7)) are solved for an arbitrary initial velocity by making u_x, u_y, u_z equal to zero. The resulting expressions for the angular motion of the rigid body and for the linear displacements of the mass center are given by Eqs. (27) through (32).

$$\alpha=c_1\sin\omega_1t+c_2\sin\omega_2t \quad (27)$$
$$y_c=R_1c_1\sin\omega_1t+R_2c_2\sin\omega_2t \quad (28)$$
$$z_c=c_3\sin\omega_3t \quad (29)$$
$$x_c=c_4\sin\omega_4t+c_5\sin\omega_5t \quad (30)$$
$$\beta=R_3c_4\sin\omega_4t+R_4c_5\sin\omega_5t \quad (31)$$
$$\gamma=c_6\sin\omega_6t \quad (32)$$

where

$$c_1=\frac{R_2\dot{\alpha}_o-\dot{y}_o}{\omega_1(R_2-R_1)},\quad c_2=\frac{\dot{y}_o-R_1\dot{\alpha}_o}{\omega_2(R_2-R_1)}$$

$$c_3 = \frac{\dot{z}_o}{\omega_3} \quad , \quad c_4 = \frac{R_3\dot{z}_o - \dot{\beta}_o}{\omega_4(R_4-R_3)}$$

$$c_5 = \frac{\dot{\beta}_o - R_3 x_o}{\omega_5(R_4-R_3)} \quad , \quad c_6 = \frac{\dot{\gamma}_o}{\omega_6}$$

$$R_1 = \frac{\sum k_y a_z^2 + \sum k_z a_y^2 - I_x\omega_1^2}{\sum k_y a_z}$$

$$R_2 = \frac{\sum k_y a_z^2 + \sum k_z a_y^2 - I_x\omega_2^2}{\sum k_y a_z}$$

$$R_3 = \frac{\sum k_x - m\omega_4^2}{\sum k_x a_z} \quad , \quad R_4 = \frac{\sum k_x - m\omega_5^2}{\sum k_x a_z}$$

and

$\dot{\alpha}_o, \dot{\beta}_o, \dot{\gamma}_o$ = Initial angular velocity of the rigid body about x,y,z axes.

$\dot{x}_o, \dot{y}_o, \dot{z}_o$ = Initial linear velocity in x,y,z directions of the mass center.

$\omega_1, \omega_2, \omega_3, \omega_4, \omega_5, \omega_6$ = Natural frequencies from Eqs. (18) through (23).

By differentiating Eqs. (27) through (32) with respect to time twice, the expressions for angular acceleration of the rigid body and for the linear accelerations of the mass center are obtained as

$$\ddot{\alpha} = -c_1\omega_1^2 \sin\omega_1 t - c_2\omega_2^2 \sin\omega_2 t \qquad (33)$$

$$\ddot{y}_c = -R_1 c_1\omega_1^2 \sin\omega_1 t - R_2 c_2\omega_2^2 \sin\omega_2 t \qquad (34)$$

$$\ddot{z}_c = -c_3\omega_3^2 \sin\omega_3 t \qquad (35)$$

$$\ddot{x}_c = -c_4\omega_4^2 \sin\omega_4 t - c_5\omega_5^2 \sin\omega_5 t \qquad (36)$$

$$\ddot{\beta} = -R_3 c_4\omega_4^2 \sin\omega_4 t - c_5 R_4\omega_5^2 \sin\omega_5 t \qquad (37)$$

$$\ddot{\gamma} = -c_6\omega_6^2 \sin\omega_6 t \ . \qquad (38)$$

It should be noted that Eqs. (27) through (38) are approximate due to the fact that spring rates are frequency dependent. If the change in spring rates corresponding to natural frequencies ω_1, ω_2, or ω_4, ω_5 is relatively large, the error may become unacceptable.

Now, the procedure for shock analysis can be outlined as follows:

1. Determine the components of the initial velocity from the shock test under consideration. (This step is discussed in Ref. [1])

2. Compute the coefficients for Eqs. (27) through (38).

3. Since the expressions obtained in step 2 are for the mass center, maximum linear accelerations can be computed by evaluating the accelerations at various points of the missile.

APPROXIMATE DYNAMIC ANALYSIS FOR "WALLEYE" MISSILE CONTAINER

A schematic diagram of the "Walleye" missile container system is shown in Fig. 2. The locations of the mass center (c.g) and shock mounts are indicated along with other pertinent dimensions. Data regarding the missile and container were provided by U.S. Naval Ordnance Station, Louisville, Kentucky.

NUMERICAL DATA

Mass Moment of Inertias (slug-ft^2)

$I_x = 233.0$; $I_y = 7.80$; $I_z = 233.0$

Weight of the Missile and Cradle (lbs.)

Weight of the missile	$W = 1100$
Approximate weight of cradle	$W_c = 100$
Total weight mounted	$W_m = 1200$

PROPERTIES OF SHOCK MOUNTS

Lord Company type J-5682 shock mounts were used. Experimental property values at ambient temperature as given in the appendix of Ref. [1] are:

Spring Rates (lb/in)

For compression $k_x = 3065.48 + 0.0368\omega^2$

For shear $k_y = k_z = 789 + 0.068\omega^2$

where ω is frequency in radians/sec.

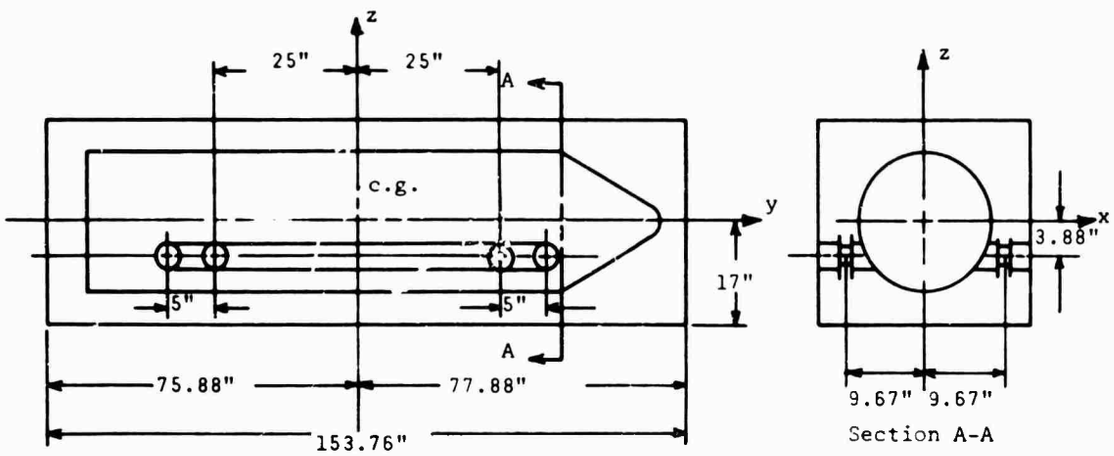

FIGURE 2. SCHEMATIC DIAGRAM OF WALLEYE MISSILE CONTAINER SYSTEM

TABLE 1. COMPARISON OF EXPERIMENTAL AND COMPUTED RESULTS

Direction	NATURAL FREQUENCY (rad/sec)		TRANSMISSIBILITY	
	Experimental	Computed	Experimental*	Computed**
y-α	47.0	47.26	3.7	2.17
y-α	50.0	48.10	3.7	2.16
z	44.0	49.64	4.2	2.34
x-β	***	65.37	***	1.88
x-β	***	180.60	8.9	***

*Maximum transmissibility.

**Maximum transmissibility at the mass center.

***Value is not available.

Numerical work for the dynamic analysis is presented in Ref. [1] in detail. Table 1 shows the analytical and available experimental results.

CONCLUSIONS

An approximate method of dynamic analysis for missile container systems is presented. It is shown that tests required by specifications can be simulated analytically by using the dynamic properties of elastomer shock mounts obtained from experiments. The application of the method during the design stage can result in better and economical missile mounting. Also, a digital computer program can be developed to optimize the missile container systems by using the method in an iteration cycle.

ACKNOWLEDGEMENTS

The cooperation and help of the staff of engineering department of the

U.S. Naval Ordnance Station, Louisville, Kentucky and of Dr. I.W. Tucker, Director of University of Louisville Institute of Industrial Research is acknowledged.

REFERENCES

1. Paz, M. and Citipitioglu, E., "Manual for Missile Mounting" Report, prepared for Naval Ordnance Station, Louisville, Kentucky, Dec. 1966.

2. Harris, C.M. and Crede, C.E. (Editors), Shock and Vibration Handbook, Vol 1, 2, 3, McGraw-Hill, New York, 1961.

3. Meriam, J.L., Dynamics, John Wiley and Sons, Inc., New York, 1966.

4. "Design and Test of Packaging, Packing, Shipping and Handling Equipment for Weapon System Components", Bureau of Naval Weapons, Department of Navy, WR11, July 1963.

DISCUSSION

Mr. Seely (Naval Ordnance Station, Forest Park, Ill.): You showed a slide showing a natural frequency of about 47 Hertz for your container. It may interest you to know that I have just tested a Walleye container and the natural frequency came out to somewhere between 9 and 11 Hertz. The transmissibility ran about 5.

Mr. Citipitioglu: This is radians per second here.

Mr. Seely: That does make a difference.

Mr. Linton (Naval Weapons Station, Seal Beach): We do vibration and shock testing of containers of various sorts up to perhaps 16 feet long weighing a couple of thousand pounds. On the vibration tests we are asked to find the resonant frequency and dwell there. We often find no definable resonance. Perhaps more particularly, they seem to resonate at any frequency up and down the line. This leaves the thought that the larger containers do not seem to have the spring mass system as precisely defined as your analysis indicates for your Walleye container. In trying to do a valid test, it is often difficult to find these resonant frequencies due to the resonances in the container. These are long flimsy containers that shake like a bowl full of jelly at any frequency.

Mr. Citipitioglu: We have not tested the Walleye container. We only used the test results which were available to us. From the mathematical analysis under the assumptions that we have, it is clear that we must have some kind of natural frequency. For the kind of missile containers you are talking about I am not sure what the range of the frequency will be.

Mr. Griffith (Bendix Missiles System Div.): We have designed and built containers for one of the Navy's larger complete weapons system. We also did some testing for the Naval Ordnance Plant at Louisville on a container which I think was for the Walleye. Contrary to what the gentlemen from Seal Beach just said, we have never experienced any problem in determining the resonance of the container suspension system. Our particular weapon has a spring damper system. At resonance we found out we could burn out the dampers very easily because of the motion in there. I think the Walleye container that we tested had some resonances which had transmissibilities around 11 or 12. This is a pretty solid resonance and you should find it easily.

Mr. Citipitioglu: I am familiar with the type of missile container that has dampers on it, but the type on which we worked was strictly mounted by elastomer shock mounts. We did not make any study of the type that you mention.

Mr. Matthews (Naval Missile Center): I tested a shipping container many years ago and found that there are occasions when you can find a resonance and other occasions when you cannot. It depends on what the cushioning material is. If it is linear, of course, you will find a resonance, but many of these things have elastomers and if you study the stress strain curves you will find them very nonlinear. Now if you try to test these to a specification that says find the resonance and dwell there for an hour, then increase the level of your input and dwell there for an hour you will find that you will have a different "resonance." Also, you will find that the resonance will shift as you dwell there because the temperature affects the nonlinear behavior. I really think that the concept of a resonance and a dwell for these nonlinear cushions has to be looked at very carefully.

SIMULATED MECHANICAL IMPACT TEST EQUIPMENT

D. R. Agnew
Naval Air Development Center
Johnsville, Warminster, Pennsylvania

A unique test method has been developed to determine the structural integrity of unit shipping containers for "A"-size stores when subjected to lateral impacts. To facilitate reproducibility of test, control of impact and ease of handling in the performance of this test method, the Simulated Mechanical Impact Test Equipment (SMITE) was designed, developed and found to be satisfactory and practical.

INTRODUCTION

A unique test method has been developed to determine the structural integrity of unit shipping containers for Navy stores when subjected to lateral impacts. To facilitate reproducibility of test, control of impact and ease of handling in the performance of this test method, the Simulated Mechanical Impact Test Equipment was designed, developed and found to be a satisfactory and practical test facility.

The need for such an apparatus became apparent about two years ago when damage reports were submitted to the Aero Materials Department indicating that unit shipping containers used for the packaging of Navy "A"-size stores were unsatisfactory. Investigations of these reports disclosed that the current plastic shipping containers flex under impact and allow the "A"-size stores to be dented without any visible damage to the shipping container. These "A"-size stores are basically rugged electronic hardware which can take high "G" forces but once the thin outer aluminum skin is dented, there is a high probability of a malfunction in performance due to the internal electronic components becoming damaged or "hung-up" and not being properly deployed for operation.

Further examinations of these damage reports revealed that after a 700-mile trip by commercial carrier, the electronic hardware experienced typical damage as depicted in Figure 1. This damaged hardware was reported as inoperable.

In simulating the type of damage reported, the unit containers with hardware were banded four together as prepared for shipment and subjected to the various types of impacts e.g., the tipover onto a pallet, impact onto a loading platform and impact onto a truck bed. In all instances, the impact tests were difficult to accomplish due to the bulk of the pack, weight of the pack and the variance in the human factor. By this variance in human factor, it is meant that in simulating hefting of the pack onto a truck bed or loading platform, it was found that the size and physical condition of the person performing the test were contributing factors in the outcome of the tests. Between the types of impact tests attempted, the tipover onto a pallet (Figure 2) was the easiest to perform and just as severe as the others.

Though the tipover test was the least difficult to perform, problems were still encountered:

1. The test pack as prepared for shipment can weigh up to 125 lbs. and thus requiring at least two test mechanics to perform the tests.

2. The actual tipping over of a pack this size is an unwieldy process and very often more than one specimen may be damaged in the drop test, or multiple test drops may have to be performed to insure reproducibility of results.

To eliminate these difficulties, it was attempted to:

1. Reduce the test personnel to one by applying the force of impact of a shipping pack tipover to a single container sample and thus reducing the specimen weight to be handled.

2. Position the container as depicted in

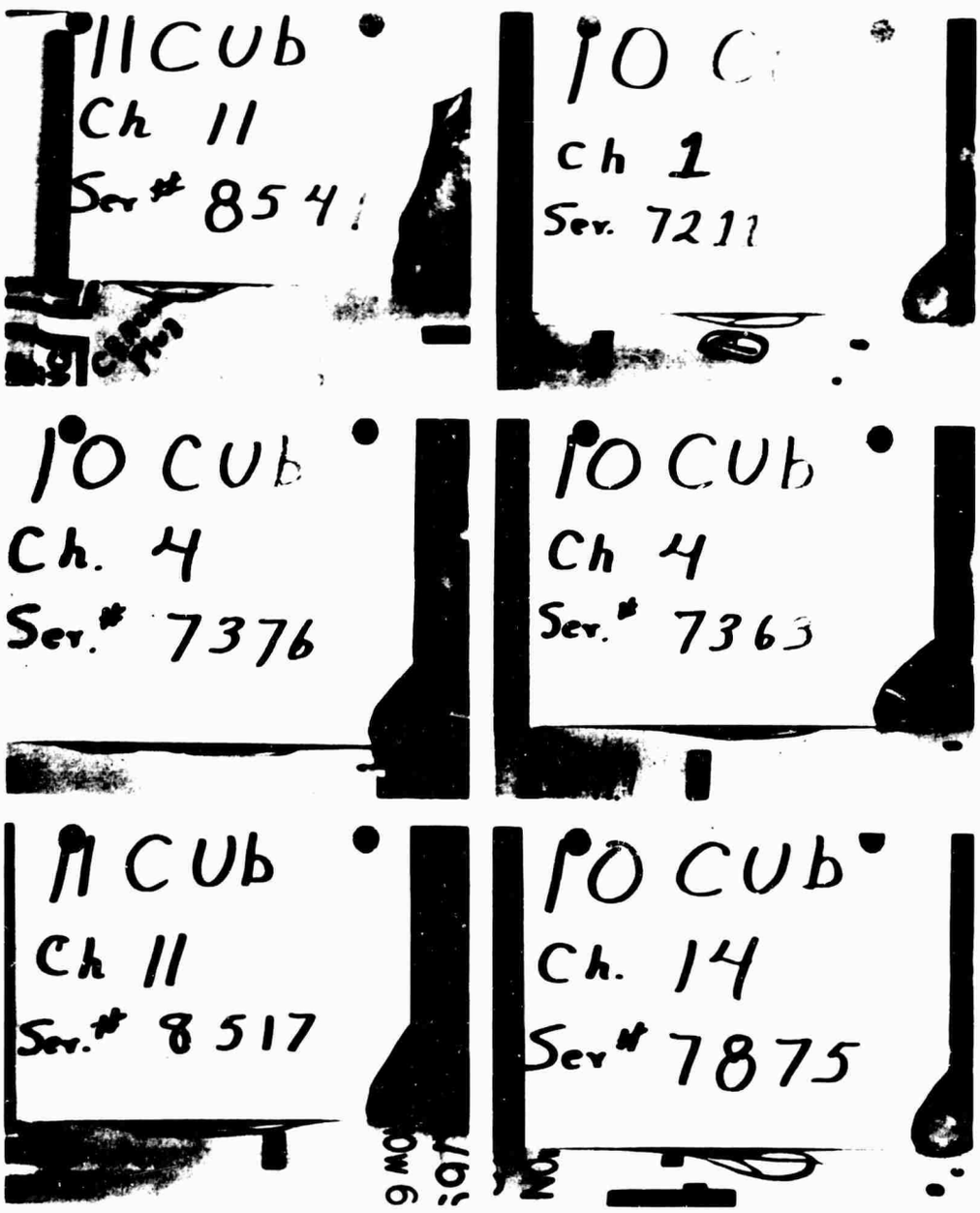

FIGURE 1 - IN-TRANSIT DAMAGE

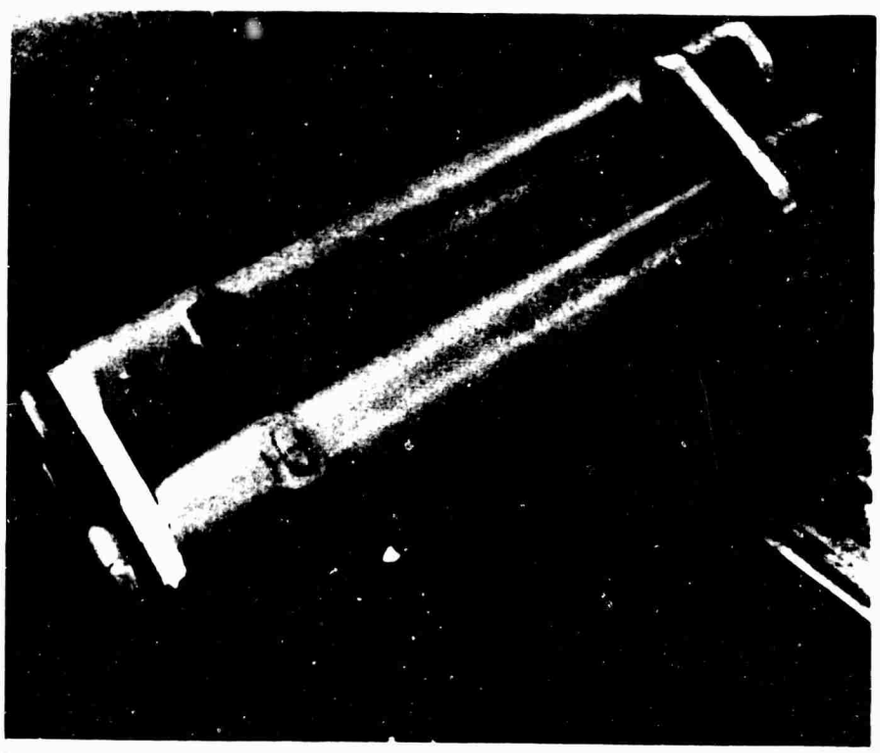

FIGURE 2 - TIPOVER IMPACT ONTO A PALLET

Figure 3 and allow the equivalent tipover impact force of a shipping pack to fall vertically onto the container sample.

3. Achieve optimum control of the test procedure by mechanizing all the dynamic parameters of the test method.

The solution to all these difficulties resulted in the design and development of the Simulated Mechanical Impact Test Equipment, Figures 4 and 5, which produces damage equivalent to a shipping pack tipping over, represented by a single unit container, Figure 6.

In determining the test method parameters and designing the SMITE, it was necessary to conduct the extensive mathematical study that follows:

A derivation relating the rotational parameters of a two-container pack tipping tandem onto a pallet edge to the vertical parameters necessary to give equivalent motion and force during a free-fall drop is presented.

1. The moment of inertia of a right circular cylinder (length = R, radius = r and Mass = M) shall be calculated with respect to its geometric and gravity centers which are one and the same in this case. This cylinder is to be representative of a unit shipping container for Size "A" stores. Moment of inertia of a solid circular cylinder about an axis through the center of gravity and perpendicular to the axis of the cylinder is:

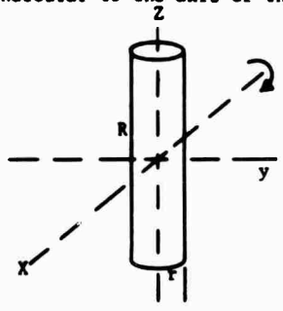

$$I = M\left(\frac{r^2}{4} + \frac{R^2}{12}\right)$$

Explanation: Moment of inertia with respect to the perpendicular plane is Ixy + Ixz = Ix

$Ixy = \frac{1}{2}Mr^2$, r = radius

$Ixz = \frac{1}{3}ML^2$, L = length (R) but at C.G. $\frac{L}{2} = \frac{R}{2}$

$$\therefore Ix = \tfrac{1}{2}Mr^2 + \frac{1}{3}ML^2 = \tfrac{1}{2}Mr^2 + \frac{1}{12}MR^2$$

2. This previous equation (Ix) suggests the shipping container rotates around its center of gravity like a pin wheel, which is not indicative of a tipping-over process. The pivot point for the tipover is contained in the bottom of the upright container and, therefore, I (Ix_1) in the base of the container must be found.

Now consider I of an axis (x_1) in the base of the cylinder and parallel to the axis (x) through the C.G. which was used in the calculation of Ix as described above.

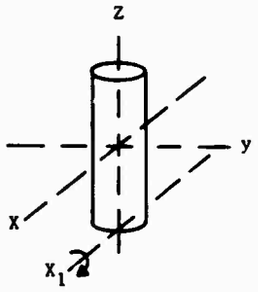

Parallel-axis theorem for masses:

$$I = \bar{I} + Md^2; \text{ but } d = \frac{R}{2}$$

$$Ix_1 = Ix + M\frac{R^2}{4}$$

$$Ix_1 = M\left(\frac{r^2}{4} + \frac{R^2}{12}\right) + \frac{MR^2}{4}$$

$$Ix_1 = M\left(\frac{r^2}{4} + \frac{R^2}{3}\right)$$

3. Again, this last equation (Ix_1) is not wholly indicative of a shipping pack tipping. In actuality, the effective impact is that of a two-unit container, in tandem, striking a pallet edge while pivoting about a point (P) in the base. Therefore, the moment (Ip) of two-unit containers rotating about a point (P) must be found.

Now consider two cylinders placed together:

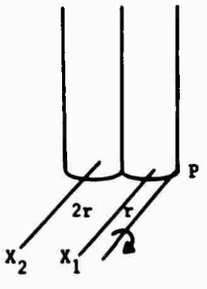

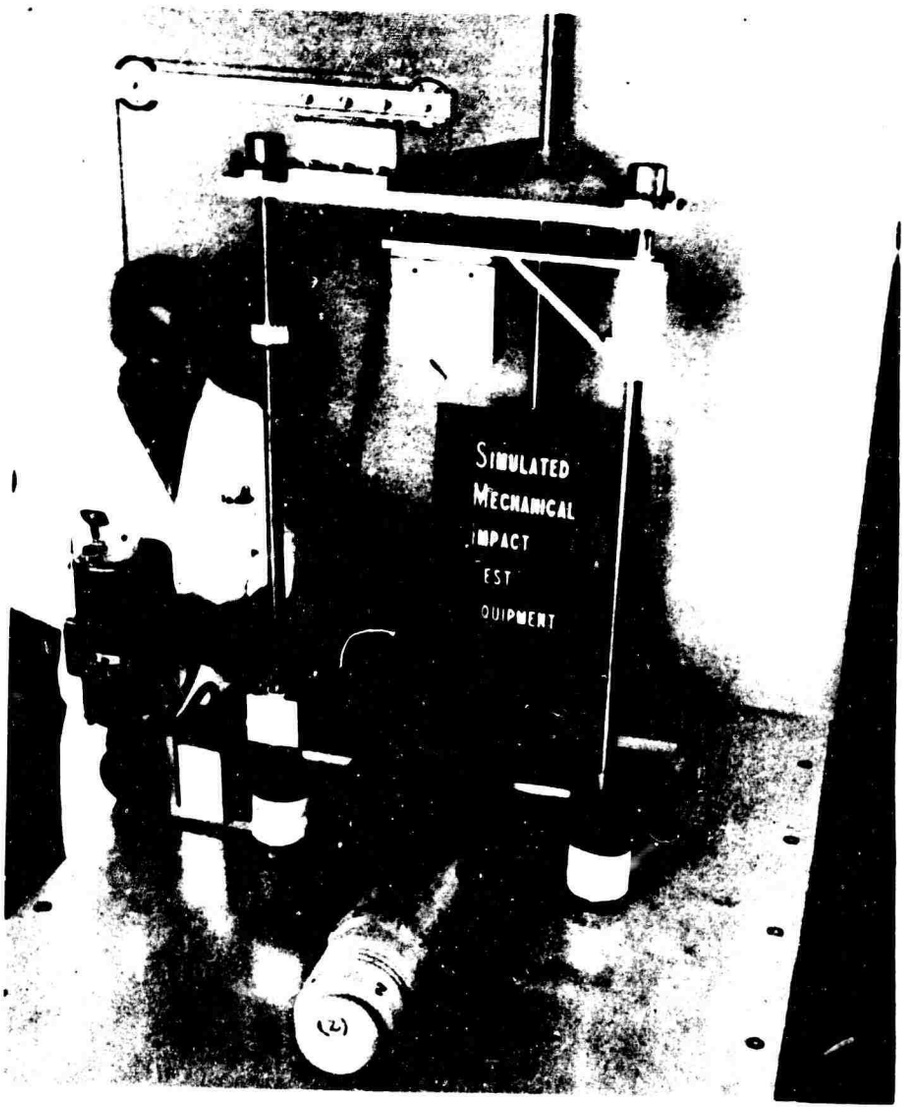

FIGURE 3 - SIMULATED MECHANICAL IMPACT TEST EQUIPMENT

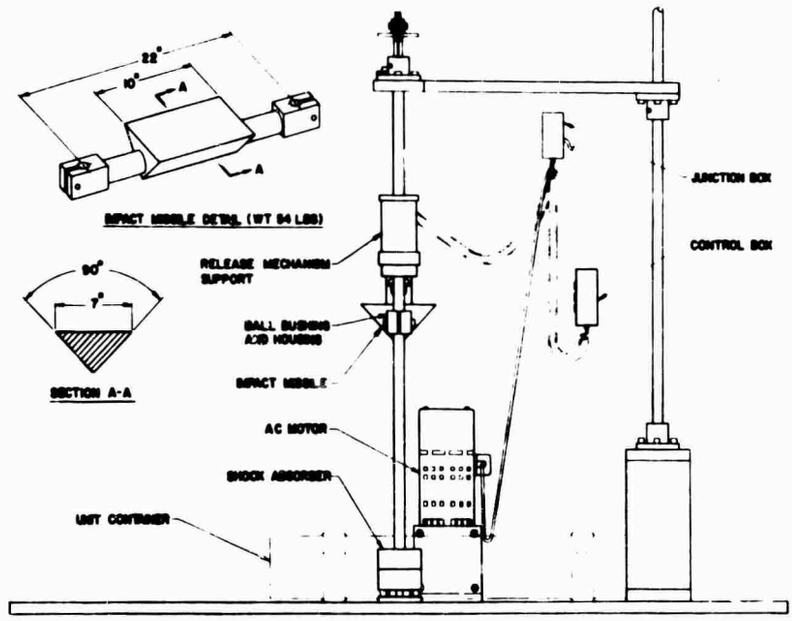

FIGURE 4 - SIMULATED MECHANICAL IMPACT TEST EQUIPMENT

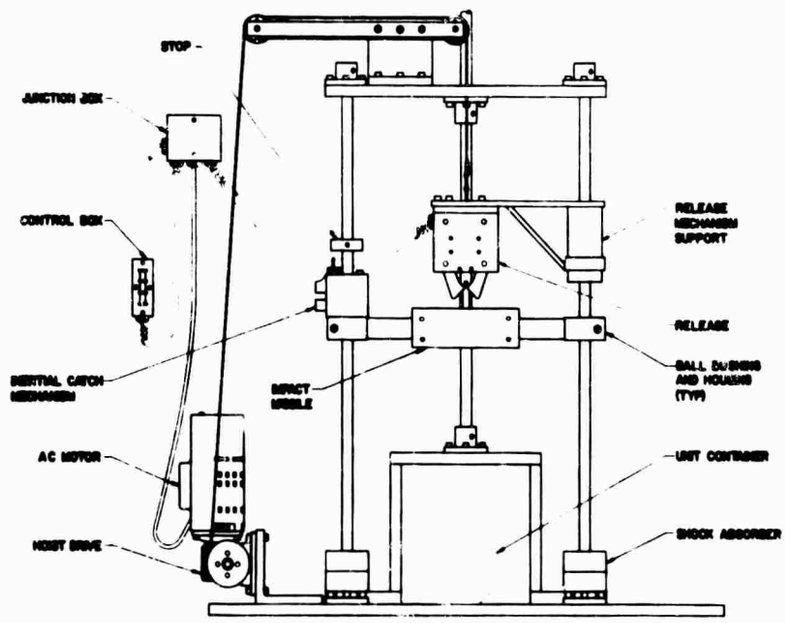

FIGURE 5 - SIMULATED MECHANICAL IMPACT TEST EQUIPMENT

FIGURE 6 - EQUIPMENT REMOVED FROM TEST CONTAINERS
A. FOUR-PACK TIPOVER ONTO PALLET
B. SMITE

Again, parallel-axis theorem for masses:

$$Ip = Ix_1 + Md_1^2 + Ix_2 + Md_2^2$$

$$d_1 = r;\ d_2 = 3r$$

$$Ix_1 = Ix_2 = \bar{I}$$

$$Ip = M\left(\frac{r^2}{4} + \frac{R^2}{3}\right) + Mr^2 + M\left(\frac{r^2}{4} + \frac{R^2}{3}\right) + 9\,Mr^2$$

$$Ip = \frac{2}{3}MR^2 + \frac{21}{2}Mr^2$$

4. Solving for Ip gives the means for relating linear velocity to angular velocity ($v = r\frac{d\theta}{dt}$). In the following, it will be proved that for a shipping pack, this relation will hold; and since the pack is a rigid system, will hold for any point in the system.

Determination of angular velocity and linear velocity:

By definition:

$$\text{Angular acceleration} = \frac{d^2\theta}{dt^2}$$

$$\text{Angular velocity} = \frac{d\theta}{dt}$$

$$\text{Linear velocity} = r\frac{d\theta}{dt}$$

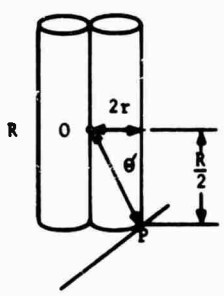

Two pack system in vertical position.

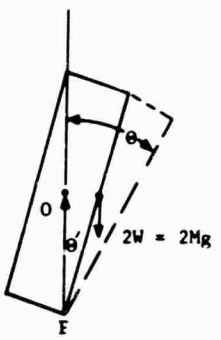

Two containers lumped into a single system and positioned for tipover.

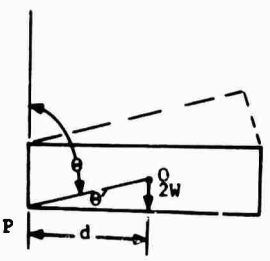

Two containers at impact after tipover.

θ' = the angle the vertical containers must be rotated to the right (clockwise) before free fall tipover takes place.

The $\tan \theta' = \frac{2r}{\frac{R}{2}}$ and $\theta' = \arctan \frac{4r}{R}$

PO = length from point (P) to the center of mass, O.

$$PO = \sqrt{\left(\frac{R}{2}\right)^2 + (2r)^2}$$

θ = the max angle P.O. will rotate during a free fall tipover.

$\theta = 90^\circ - \theta'$

T = torque of the mass center

$T = F \cdot d = 2Mg \cdot d$

W = Weight of one container

d = moment arm of the torque = $\sqrt{(\frac{R}{2})^2 + (2r)^2} \cdot \text{Sin } \theta$

The algebraic sum of the moments about P is

$$\sum Tp = Ip \frac{d^2\theta}{dt^2}$$

and $T = F \cdot d = 2Mg \sqrt{(\frac{R}{2})^2 + (2r)^2} \cdot \text{Sin } \theta$

$$\therefore \sum Tp = 2Mg \sqrt{(\frac{R}{2})^2 + (2r)^2} \cdot \text{Sin } \theta =$$

$$(\frac{2}{3} MR^2 + \frac{21}{2} Mr^2) \frac{d^2\theta}{dt^2}$$

$$\frac{d^2\theta}{dt^2} = \frac{2Mg \sqrt{(\frac{R}{2})^2 + (2r)^2}}{M (\frac{2}{3} R^2 + \frac{21}{2} r^2)} \cdot \text{Sin } \theta$$

and $\frac{d^2\theta}{dt^2} = \frac{d (\frac{d\theta}{dt})}{dt} = \frac{d (\frac{d\theta}{dt})}{dt} \cdot \frac{d\theta}{d\theta}$

$$= \frac{d\theta}{dt} \cdot d (\frac{d\theta}{dt}) \cdot \frac{1}{d\theta} = \frac{2g \sqrt{(\frac{R}{2})^2 + (2r)^2}}{(\frac{2}{3} R^2 + \frac{21}{2} r^2)} \cdot \text{Sin } \theta$$

$$= \frac{d\theta}{dt} \cdot d (\frac{d\theta}{dt}) = \frac{2g \sqrt{(\frac{R}{2})^2 + (2r)^2}}{(\frac{2}{3} R^2 + \frac{21}{2} r^2)} \cdot \text{Sin } \theta \; d\theta$$

Intergrating:

$$\int \frac{d\theta}{dt} \cdot d (\frac{d\theta}{dt}) = \int \frac{2g \sqrt{(\frac{R}{2})^2 + (2r)^2}}{(\frac{2}{3} R^2 + \frac{21}{2} r^2)} \cdot \text{Sin } \theta \; d\theta$$

$$\frac{1}{2} (\frac{d\theta}{dt})^2 = - \frac{2g \sqrt{(\frac{R}{2})^2 + (2r)^2}}{(\frac{2}{3} R^2 + \frac{21}{2} r^2)} \cdot \text{Cos } \theta + C$$

when $\theta = 0$, the equation becomes

$$0 = - \frac{2g \sqrt{(\frac{R}{2})^2 + (2r)^2}}{(\frac{2}{3} R^2 + \frac{21}{2} r^2)} \cdot \text{Cos } \theta + C$$

And C (Constant of Intergration) =

$$\frac{2g \sqrt{(\frac{R}{2})^2 + (2r)^2}}{(\frac{2}{3} R^2 + \frac{21}{2} r^2)} \cdot 1$$

$$\therefore \frac{1}{2} (\frac{d\theta}{dt})^2 = \frac{2g \sqrt{(\frac{R}{2})^2 + (2r)^2}}{(\frac{2}{3} R^2 + \frac{21}{2} r^2)} \cdot (1 - \text{Cos } \theta)$$

$$\frac{d\theta}{dt} = \left[\frac{4g \sqrt{(\frac{R}{2})^2 + (2r)^2}}{(\frac{2}{3} R^2 + \frac{21}{2} r^2)} \cdot (1 - \text{Cos } \theta) \right]^{\frac{1}{2}}$$

$\frac{d\theta}{dt}$ = angular velocity

and v = linear velocity = $r \frac{d\theta}{dt}$

5. Since it has been established that $v = r \frac{d\theta}{dt}$, a look at what happens to a rigid system in rotation impact is in order.

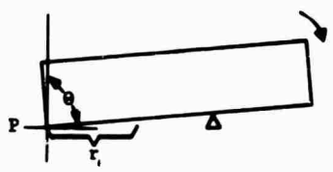

If r is measured from the point (P) of rotation, θ is any angle in the arc of rotation and $\frac{d\theta}{dt}$ is angular velocity (which is constant throughout the system at any particular angle θ), then it can be said that the system upon impact will continue to rotate about all impact points except where the moments of momentum in the clockwise direction equal the moments of momentum in the counterclockwise direction, i.e., the point of impact where none of the motion of the system goes into rotation but where all forces are concentrated (max. transfer of energy). To find this point, consider:

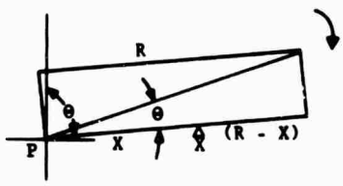

Point X is to be the impact point of max. transfer of energy and, therefore, no new rotation is caused (X is measured along the container wall). Forces to the right of the impact point will tend to cause a clockwise motion and forces to the left will tend to cause counterclockwise motion. Therefore, the effective mass in the counterclockwise direction would be $\frac{X}{R} \cdot 2M$, (2M being the mass of two unit containers in tandem) which acts at a center of mass of $r_1' = \frac{X}{2}$ from the impact point and with $v' = r_1' \frac{d\theta}{dt}$ (r_1', measured from P, equals $\frac{X}{2}$); the solution for the moment of momentum in the counterclockwise direction is:

$$m'v'r_1' = \left(\frac{X}{R}(2M)\right) \cdot \left(\frac{X}{2}\frac{d\theta}{dt}\right) \cdot \left(\frac{X}{2}\right)$$

$$= \frac{M}{2R} \cdot \frac{d\theta}{dt} \cdot X^3$$

The effective mass in the clockwise direction would be $\frac{R - X}{R} \cdot 2M$ which acts at a center of mass $r_1'' = \frac{R - X}{2}$ from the impact point and with $v'' = r_1'' \frac{d\theta}{dt}$ (r_1'' measured from p equals $\frac{R + X}{2}$); the solution for the moment of momentum in the clockwise direction is:

$$m''v''r_1'' = \left(\frac{R - X}{2}(2M)\right) \cdot \left(\frac{R + X}{2}\frac{d\theta}{dt}\right) \cdot \left(\frac{R - X}{2}\right)$$

$$= \frac{M}{2R} \cdot \frac{d\theta}{dt} (R + X)(R - X)^2$$

As previously stated when the moment of momentum in the clockwise direction equals the moment of momentum in the counterclockwise, none of the motion of the system goes into rotation but is concentrated at the impact point; therefore,

$$m'v'r_1' = m''v''r_1''$$

$$\frac{M}{2R} \cdot \frac{d\theta}{dt} \cdot X^3 = \frac{M}{2R} \cdot \frac{d\theta}{dt} \cdot (R + X)(R - X)^2$$

expanding

$$X^3 = (R + X)(R - X)^2$$

$$X^3 = XR^2 - 2X^2R + X^3 + RX^2 + R^3 - 2XR^2$$

$$X^3 = R^3 - X^2R - XR^2 + X^3$$

$$0 = R^3 - X^2R - XR^2$$

$$0 = -R(X^2 + XR - R^2)$$

Solving for X gives a positive root at 0.62 R.

Then it can be stated that the point of maximum transfer of energy on impact and the point where none of the motion of the system goes into rotation on impact is 0.62 the length of the container (0.62R).

6. Now equating linear momentums to angular momentum

$$2MV \text{ (linear)} = 2Mr\frac{d\theta}{dt} \text{ (angular)}$$

$$\text{from (4) } \frac{d\theta}{dt} = \left[\frac{4g\sqrt{\left(\frac{R}{2}\right)^2 + (2r)^2}}{\frac{2}{3}R^2 + \frac{21}{2}r^2} \cdot (1 - \cos\theta)\right]^{\frac{1}{2}}$$

from (5) r = 0.62R

$$\therefore 2MV = 2M(0.62R)\left[\frac{4g\sqrt{\left(\frac{R}{2}\right)^2 + (2r)^2}}{\frac{2}{3}R^2 + \frac{21}{2}r^2} \cdot (1 - \cos\theta)\right]^{\frac{1}{2}}$$

which is the effective momentum at the maximum transfer of energy at point of impact for a two container system tipping over in tandem.

Again, equating linear momentum to angular

$$M_1V = 2M_2r\frac{d\theta}{dt}$$

$$M_1 \cdot \sqrt{2gs} = 2M_2(0.62R)$$

$$\left[\frac{4g\sqrt{\left(\frac{R}{2}\right)^2 + (2r)^2}}{\frac{2}{3}R^2 + \frac{21}{2}r^2} \cdot (1 - \cos\theta)\right]^{\frac{1}{2}}$$

and $M = \frac{W}{g}$

7. From (6), it can be said the vertical parameters necessary to give equivalent motion and force during a free fall drop are now equated to the rotational parameters of a two container pack tipping tandem onto a pallet edge 5" high.

$$M_1V = 2M_2r\frac{d\theta}{dt}$$

$$\frac{W_1}{g} \cdot \sqrt{2gs} = 2\frac{W_2}{g}(0.62R)$$

$$\left[\frac{4g\sqrt{\left(\frac{R}{2}\right)^2 + (2r)^2}}{\frac{2}{3}R^2 + \frac{21}{2}r^2} \cdot (1 - \cos\theta)\right]^{\frac{1}{2}}$$

W_1 = Weight of free falling body

W_2 = Weight of unit tipping over plus weight of container

g = Acceleration due to gravity

R = Length of pack

r = radius or half the width of a unit container

$$O = 90° - \arctan \frac{4r}{R} - \arcsin \frac{5}{.62R}$$

From this equation, a solution for S can be found, which is the distance the impact missile of the SMITE should be dropped onto the unit container to simulate the most severe rough handling environment that this particular type of shipping container will experience.

Currently, the SMITE is required by specification MIL-S-23665 as one of the major procedures for preproduction testing of unit shipping containers covered by that specification.

So far, this presentation has dealt with more or less a specific packaging problem whereas it is becoming more evident that many packaging systems are being damaged by the same types of impacts as described here. Further, it has been observed that shipping containers have received other types of lateral impacts whether from fork lifts, containers banging into one another, ramming into projections from main structures in storage areas or general rough handling in transit. So accordingly, consideration is being given to an evaluation of the types of impacts containers receive during shipment, storage and handling and subsequent modification of the SMITE to accomplish a variety of controlled reproducible test methods. For example, damage caused by a fork lift could be reproduced by changing the configuration of the impact missile of the SMITE to represent fork lift tines and by establishing the speed of a fork lift, the distance the impact missile must be dropped to simulate the effect of a fork lift ramming a pallet load of containers can be calculated. Thus, a laboratory test can be performed with the SMITE so that the effect of a fork lift ramming a large pallet load can be predicted.

In summary, it is to be noted that a test apparatus and procedure have been developed to simulate a most severe shock impact that shipping containers experience during the transportation and storage environment. This test method was developed after an evaluation of damage reports revealed that certain Navy electronic gear, especially those with a long narrow configuration, were being received at the destination point in an inoperable condition. The evaluation also revealed that the containers housing this gear were being impacted onto loading platforms or truck beds or tipping over onto pallets or other such protrusions or being rammed by fork lifts. Though the specifications governing the aforementioned type of electronic equipment are specific about the packaging of these items, it became evident that there was a need for an additional requirement which would insure the structural integrity of shipping containers when subjected to these lateral impacts. Through extensive mathematical analyses and laboratory tests, the velocity and force parameters of the impacts described were equated to a vertical drop test. The equipment to accomplish this vertical drop test is the Simulated Mechanical Impact Test Equipment, Figures 3, 4 and 5.

When employing the Simulated Mechanical Impact Test Equipment for laboratory evaluations, it has been found that:

(1) Correlation between actual rough handling environments and laboratory tests is excellent.

(2) Reproducibility of test results is readily achieved.

(3) The actual weight and size of the test load can be reduced to an easily handled container specimen, i.e. if a shipping container houses 2,4,6-----12, 24 etc. unit containers, in general, the weight and size of the test specimen in proportion would be the reciprocal of the number of unit containers housed in the shipping pack.

(4) Due to the reduced specimen size and weight, only one test mechanic is required to perform tests.

(5) The effects of rough handling environments on large shipping loads can be predicted from easily performed laboratory tests.

(6) For the reasons stated in (1) through (4), considerable time savings are realized.

With the ever-increasing sophistication to general types of equipment and the advanced technology being employed in the field of specialized systems, it is the objective of the Aero Materials Department to exert equivalent effort to insure that these equipment and systems are protected adequately against transportation and storage environments. The SMITE is one step of many steps to be taken in this direction.

ENVIRONMENTAL MEASUREMENTS

SUCCESS AND FAILURE WITH PREDICTION AND SIMULATION OF AIRCRAFT VIBRATION

A. J. Curtis and N. G. Tinling
Hughes Aircraft Company
Culver City, California

A captive flight vibration study program was conducted on a Phoenix missile installed in the open weapons bay of the F-111B aircraft. The program included a prediction of the flight vibration environment followed by a flight measurements program and a laboratory vibration test of the missile.

The vibration environment of the missile was predicted using a statistical method developed by one of the authors (Ref. 1). This method, which makes use of measured data from flight tests of three different installations in high performance aircraft is summarized in sufficient detail to explain the basis of the prediction and analysis of the flight data.

Flight vibrations were measured on missile structure at fifteen locations. The data were evaluated statistically using a digital processing method identical to the process used in the prediction technique. Spectral density data, normalized to dynamic pressure, are presented and comparisons are made to the predicted vibration environment. From these comparisons the areas of valid prediction, i.e., success, and some areas of weakness, i.e., failure, of the method are delineated.

A rather sophisticated method was developed for the laboratory vibration test of the missile in an attempt to simulate the aerodynamically induced flight vibration. The method is explained in detail and the results are compared to the measured flight vibration.

INTRODUCTION

A statistical method for the prediction of the aircraft vibration environment was proposed by the senior author in Ref. 1. This method was used to predict the vibration environment of the PHOENIX missile during captive flight in the weapons bay of the F-111B aircraft with bay doors open. A paper (Ref. 2) to be presented at the 39th Shock and Vibration Symposium by Kiwior, Mandich and Oedy describes the program in which this vibration environment was measured. A paper by Curtis and Herrera (Ref. 3) described the laboratory vibration test method developed to simulate the predicted random vibration environment, using both input and response control.

This paper examines the degree of agreement between the predicted and measured environments and the degree to which the laboratory test simulated the captive flight environment.

PREDICTED VIBRATION ENVIRONMENT

The technique developed to predict the missile captive flight random vibration environment grew out of the following observations. First, the random vibration spectra obtained in a number of different flight measurement programs could generally be described by a broadband, approximately constant acceleration spectral density with one or more relatively narrowband spectral peaks superimposed. While usually consistent for a particular measurement channel, in general, the center frequencies of these narrowband peaks seemed equally likely to occur at any frequency when a large number of different measurements were compared. Conversely, they were unlikely to occur at every frequency simultaneously, as is implicitly assumed when the envelope of a number of spectra is used as a prediction. Second, the vibration magnitude varies with the aircraft flight conditions and is

generally believed to be most strongly dependent on the free stream dynamic pressure, q. Third, there seems to be no basic reason to expect that the vibration, for equivalent flight conditions, in the same general location or zone in different vehicles of the same class should be significantly different.

Therefore, the basic assumption was made that, after appropriate normalization with respect to flight conditions, the random vibration environment within the same general location of all missiles with similar installation characteristics can be described by the same spectrum. This "general" spectrum consists of a broadband spectral density with several narrowband spikes superimposed. The only significant difference between weapon bays, missiles, or between specific locations in the same missile for equivalent flight conditions, will be in the center frequencies of these spikes. It was further assumed that appropriate normalization could be achieved on the basis that the rms acceleration within any relatively narrow bandwidth is directly proportional to the free stream dynamic pressure, q.

The method of obtaining the general spectrum was one of:

a) Collecting all available flight measurement data from various missile installations.

b) Screening, coding and tabulating the data.

c) Normalizing the data with respect to q.

d) Computing mean values, variances, etc., to obtain the most likely spectral density at any desired value of q.

The vibration source data used for the prediction of the Phoenix missile captive flight vibration in early 1964 were derived from measurements made on the GAR-11/F102, GAR-3/F106A, GAR-9/B-58 installations. These source data were put in digital form by tabulating acceleration spectral density values within each of 52 contiguous 10 percent bandwidths (between 20 and 2650 Hz) along with the respective flight conditions, measurement location, and identification numbers.

The data was normalized using the following severity factor, K, which is the slope of a linear rms acceleration-dynamic pressure relationship:

$$K_i = \left\{ W(f_i)\, BW_i \right\}^{1/2} \Big/ q \qquad (1)$$

where

$W(f_i)$ is the observed acceleration spectral density (g^2/Hz) at frequency f_i

BW_i is the bandwidth (Hz) with center frequency f_i

The data were arranged into groups, based on missile axis and location. For each group the following quantities were computed at each center frequency:

1. Mean K_i ($\overline{K}_i$)
2. Maximum K_i
3. Standard deviation of K_i about $\overline{K}_i$, (S_i)
4. $\left[\overline{K}_i + 2.33\, S_i \right]$

The broadband spectral density at a desired value of q is estimated from

$$W_n(f_i) = \left\{ \overline{K}_i\, q_n \right\}^2 \Big/ BW_i$$

while the spectral density of the narrowband peaks may be estimated from:

$$W_n(f_i) = \left\{ (\overline{K}_i + 2.33\, S_i)\, q_n \right\}^2 \Big/ BW_i$$

(includes 98% of Rayleigh distribution)

Comparison of the severity factors between the various groups revealed that there was no significant difference in vibration severity between missile body locations and between missile axes. Therefore the predicted environment for the missile was based on a group composed of all source data.

It should be noted that the F-106A source data contained in this group was modified. A weighting factor of 0.36 was applied to the spectral density values. This was an estimated factor to account for the difference in "filled volume" between the two weapons bays. In addition, this same data was smoothed. That is, prior to statistical evaluation, the data has unfortunately been averaged over bandwidths which were much greater than 10 percent. While not affecting the average severity factors, the standard deviations obtained were unrealistically small in the very low frequency range. Figure 1 shows the predicted broadband and narrowband spectral density computed for a dynamic pressure of 1000 psf. (This value of q is convenient for scaling to any other desired q.)

MEASURED VIBRATION DATA

Flight vibration data was obtained from an instrumented Phoenix missile installed in the weapons bay of the F-111B aircraft. A detailed description of this measurement program is contained in reference 2. Briefly, data from fifteen accelerometers mounted on missile structure, as shown in Figure 2, were recorded during straight and level flight

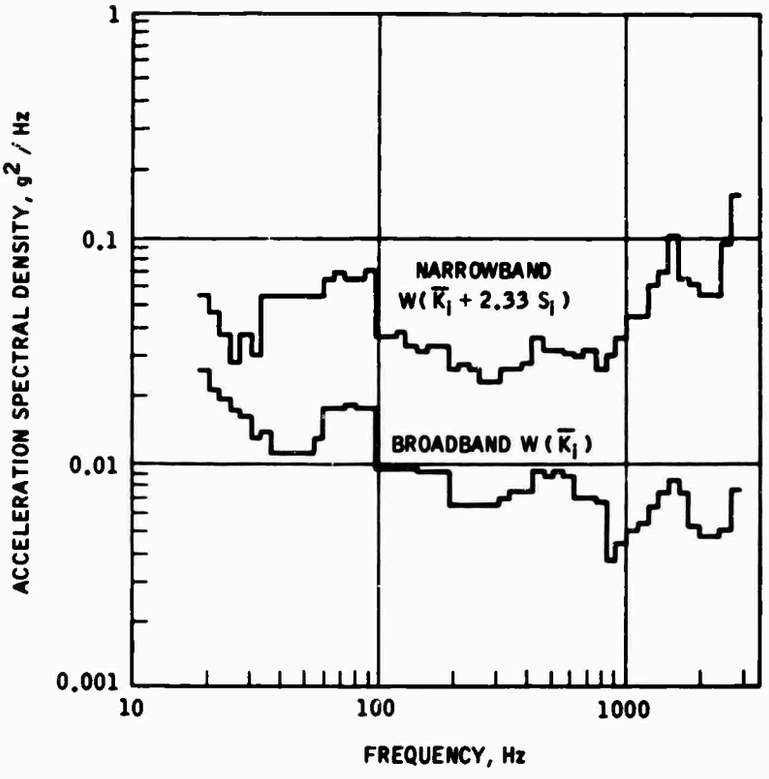

FIGURE 1 Predicted Acceleration Spectral Density for Dynamic Pressure of 1000 psf.

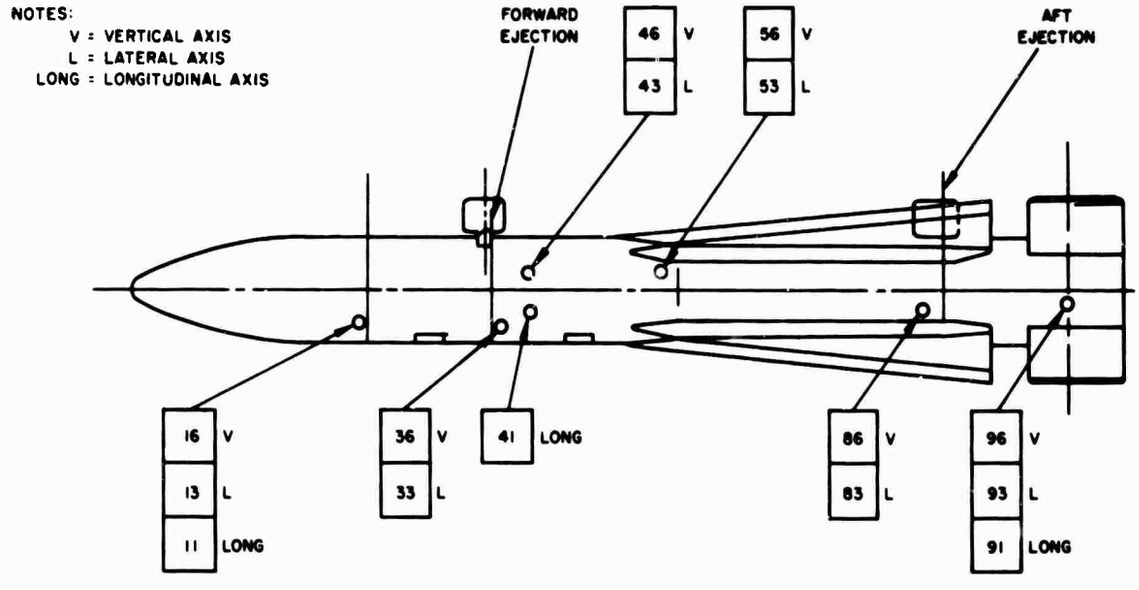

FIGURE 2 Accelerometer Locations, Phoenix Captive Flight Test Missile

with weapon bay doors open. The flight conditions for which data were obtained and the corresponding overall root mean square acceleration of the fifteen accelerometers are tabulated in Table 1.

These flight data were reduced to acceleration spectral density using the HAC developed spectral analysis system described in Ref. 3. Succinctly, the analyzer is a 10% constant bandwidth comb filter system with 52 filters with center frequencies between 20 and 2650 Hz. Because of the limited amount of time that the bay doors were open an integration time of only five seconds was used in the analysis. This integration time gives a BT product of 10.25 for the 20 Hz filter and 1225 for the 2650 Hz filter. These BT products result in mean square errors of 10 and 0.08 percent, respectively.

Arrangement of the flight data in a form suitable for presentation and comparison to the predicted levels was accomplished by a statistical evaluation using a digital processing method identical to the process used in the prediction technique. The data was arranged into 15 basic groups each composed of data from a single accelerometer channel. Additional groups were formed by combining the basic groups. Severity factors, standard deviations, etc., were then computed for these groups using a linear q dependent model. Broadband ($W_n(\bar{K})$) and narrowband ($W_n(\bar{K} + 2.33\ S)$) spectral densities computed for a dynamic pressure of 1000 psf are shown in Figure 3 for the computation group which contains all flight data listed in Table 1.

VALIDITY OF PREDICTED ENVIRONMENT

Before comparing the predicted environment to the measured environment, it is important to examine two basic assumptions. The first is the assumption of a linear q dependent model. The second is the assumption that the vibration magnitude was similar for all locations and directions.

The linear q dependent model used in the

TABLE 1

Flight Conditions and Overall Acceleration Levels

AIRCRAFT PARAMETERS			BROADBAND (19-2780 Hz) RMS ACCELERATION, g RMS														
MACH NO.	DYNAMIC PRESSURE q, LBS/FT^2	ALT, FT	CH 11	CH 13	CH 16	CH 33	CH 36	CH 83	CH 86	CH 91	CH 93	CH 96	CH 41	CH 43	CH 46	CH 55	CH 56
.97	300	37,000	.44	.94	1.09	.78	.80	.83	.89	.62	1.27	1.15	.47	.87	.84	.84	.62
.60	280	17,000	.53	.52	.77	.52	.54	.63	.65	.51	1.07	1.06	.34	.64	.65	.64	.48
.45	280	2,000	.28	.74	.61	.43	.46	.55	.55	.40	.94	.81	.29	.55	.56	.56	.42
.53	420	2,000	.42	1.12	1.00	.80	.82	.95	.96	.69	1.59	1.39	.50	.88	.88	.85	.68
.60	500	2,000	.55	1.41	1.31	1.06	1.10	1.41	1.42	.96	2.16	1.88	.65	1.17	1.15	1.07	.92
.85	560	17,000	—	—	1.71	—	—	1.80	1.99	1.28	—	2.39	—	1.70	—	1.50	—
1.18	590	29,000	.85	1.75	2.09	1.90	1.84	1.92	2.12	1.22	2.56	2.27	1.05	1.91	1.84	1.81	1.55
1.30	540	36,000	1.15	2.06	2.63	2.87	2.78	2.70	2.96	1.66	3.04	3.04	1.74	2.98	2.61	2.54	1.96
.85	560	17,000	.78	1.80	2.83	1.95	1.81	2.04	2.18	1.33	2.69	2.44	1.11	2.05	1.98	1.67	1.51
.95	700	17,000	1.09	2.18	2.89	2.38	2.28	2.59	2.71	1.54	3.28	2.94	1.30	2.38	2.27	2.11	1.66
.78	530	18,000	.74	1.76	1.99	1.74	1.65	1.98	2.14	1.34	2.76	2.60	.95	1.80	1.74	1.53	1.25
.85	740	18,000	1.83	2.37	2.91	2.57	2.45	3.07	3.18	1.80	3.63	3.45	1.45	2.66	2.49	2.34	1.91
.60	500	2,000	—	—	1.30	—	—	1.26	1.30	1.8	—	1.75	—	1.09	—	1.04	—
1.30	758	30,000	1.40	2.78	4.19	4.18	5.87	4.31	4.36	2.10	5.92	3.93	2.48	4.16	3.56	3.99	2.96
.95	700	17,000	—	—	2.53	—	—	2.38	2.57	1.45	—	2.70	—	2.23	—	2.02	—
.85	1000	2,000	1.18	2.47	3.09	2.96	2.89	3.57	3.75	2.14	4.44	4.19	1.59	2.93	2.76	2.66	2.16
.90	1160	2,000	1.45	3.18	5.71	3.54	3.41	4.21	4.27	2.50	5.18	4.82	1.89	3.47	3.23	3.26	2.48
.95	1240	2,000	1.77	3.58	4.82	4.16	5.92	4.60	4.58	2.74	5.58	5.89	2.22	4.02	3.64	3.59	2.87
.65	580	2,000	.69	1.74	1.78	1.43	1.45	1.88	1.90	1.40	2.76	2.63	.82	1.56	1.49	1.47	1.21
.78	680	2,000	.77	1.99	2.01	1.66	1.65	2.07	2.18	1.59	3.00	2.92	.92	1.70	1.70	1.62	1.32
.80	880	2,000	1.11	2.60	5.00	2.61	2.52	5.50	3.61	2.14	4.18	4.87	1.46	2.65	2.52	2.54	2.88
.76	500	10,000	.62	1.52	1.56	1.29	1.29	1.82	1.88	1.07	2.28	2.88	.85	1.45	1.36	1.28	1.12
1.15	1820	17,000	1.88	3.40	5.36	5.88	4.67	5.01	4.85	2.51	4.70	4.72	2.88	5.04	4.17	4.26	5.58
1.15	1020	17,000	1.98	3.52	5.49	5.34	4.99	5.38	5.28	2.84	5.27	5.41	3.19	5.30	4.47	4.37	3.40
1.15	1820	17,000	2.82	3.51	5.75	5.14	4.72	5.85	5.20	2.72	4.89	5.18	3.05	5.03	4.39	4.16	5.24
.70	500	18,000	.68	1.52	1.75	1.28	1.29	1.68	1.80	1.89	2.32	2.87	.79	1.41	1.31	1.23	1.09
1.05	660	22,000	1.15	3.22	3.12	2.55	2.36	2.80	2.87	1.55	3.14	2.91	1.42	2.47	2.14	2.27	1.64
1.05	668	22,000	1.23	2.22	3.43	2.79	2.57	2.96	3.29	1.73	3.36	3.34	1.60	2.80	2.49	2.38	1.85
1.05	668	22,000	1.12	2.14	3.24	2.50	2.36	2.58	2.87	1.55	2.95	2.93	1.41	2.48	2.21	2.18	1.65
1.15	1828	17,000	—	—	6.15	—	—	—	5.24	2.93	—	5.81	—	5.45	—	4.81	—

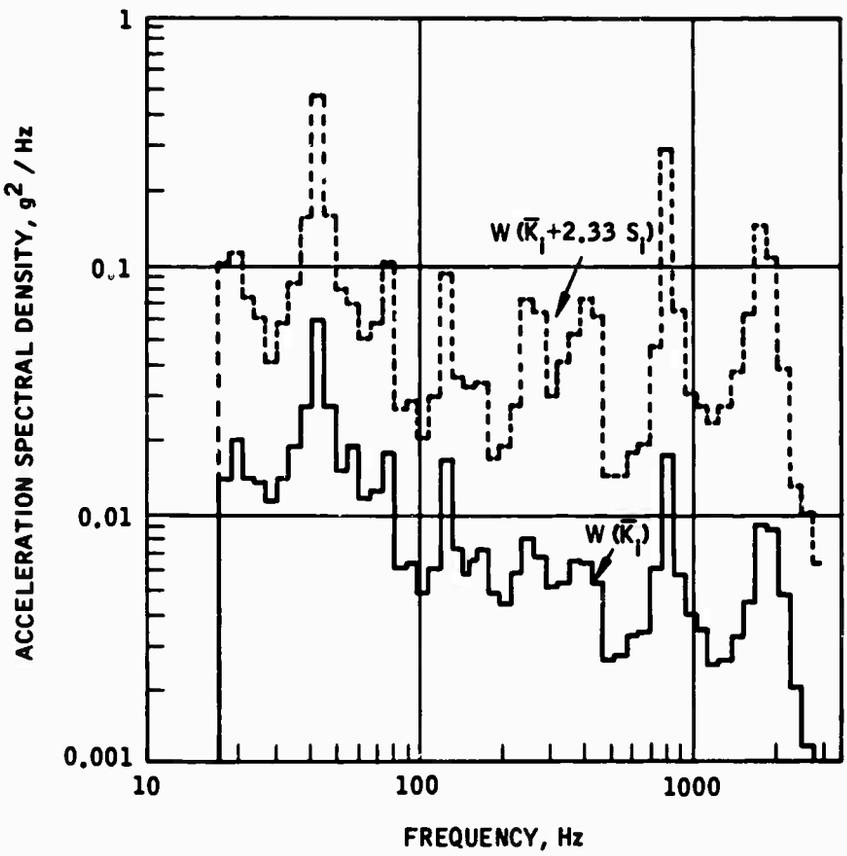

FIGURE 3 Mean and Extreme Acceleration Spectral Densities for Dynamic Pressure of 1000 psf. Computed for Group composed of all Flight Data

statistical evaluation of the flight data implies that the rms acceleration in any bandwidth (for a given accelerometer location) is directly proportional to the dynamic pressure. This assumption was based on observations of data from many previous flight measurements. It implies that the spectrum shape remains constant (i.e., the spectral density will increase everywhere by a decade for a 3.16 factor increase in dynamic pressure).

During the computer evaluation of the Phoenix flight data the following parameters were calculated for each spectrum:

1. Mean frequency ($\bar{F}$) =

$$\frac{\sum_{i=1}^{52} W(f_i) \times BW_i \times f_i}{\sum_{i=1}^{52} W(f_i) \times BW_i}$$

2. Area Moment radius about $\bar{F}(R_o)$ =

$$\left[\frac{\sum_{i=1}^{52} W(f_i) \times BW_i \times f_i^2}{\sum_{i=1}^{52} W(f_i) \times BW_i} - [\bar{F}]^2\right]^{1/2}$$

3. Overall Severity Factor (K_o) = grms/q

At a given location, these parameters should be constant for all flight conditions if the data follows a linear q model. Table 2 lists the values of these parameters with their corresponding flight conditions for the data from accelerometer 33.

It is evident from this table that, for this particular channel, the spectrum shape and overall severity have a definite trend with Mach No. The mean frequency and overall severity factor increases with increasing Mach No. and the radius of gyration about the mean frequency decreases with Mach No. The overall severity factor (K_o) is plotted vs Mach No. for this channel in Figure 4. This figure is typical of all channels and indicates that the overall severity has an increasing trend with Mach No. The deviations from the linear q model in the frequency domain can be studied by examining the parameter S_i/K_i, shown in Figure 5 for the data from accelerometer 36. The values shown on this curve are typical of all channels. It is apparent that there is more spread in the higher frequency region (i.e., the standard deviation over mean severity factor is significantly higher in the

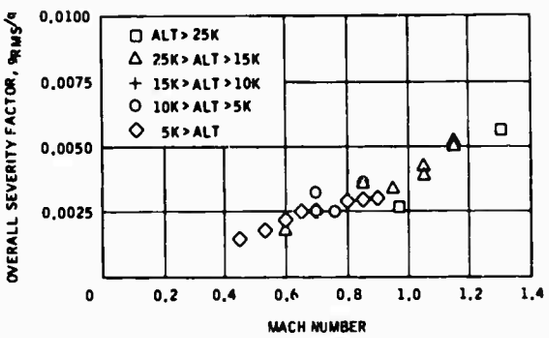

FIGURE 4 Overall Severity Factor Versus Mach No. - Accelerometer No. 33

TABLE 2
Spectrum Characteristics - Channel 33

Mach No.	Altitude Ft	Dynamic Pressure psf	$\bar{F}$ Hz	R_o Hz	K_o
0.45	2000	280	924	738	0.00152
0.53	2000	420	1080	670	0.00190
0.60	2000	500	1087	674	0.00213
0.60	17000	280	939	697	0.00186
0.65	2000	580	1149	653	0.00246
0.70	10000	500	1175	659	0.00256
0.70	2000	680	1189	638	0.00245
0.70	10000	530	1232	606	0.00328
0.76	10000	500	1072	655	0.00257
0.80	2000	880	1225	610	0.00297
0.85	2000	1000	1294	567	0.00296
0.85	10000	740	1282	569	0.00348
0.85	17000	560	1270	569	0.00348
0.90	2000	1160	1305	565	0.00305
0.95	2000	1240	1330	549	0.00336
0.95	17000	700	1302	558	0.00339
0.9	37000	300	1177	633	0.00260
1.05	22000	660	1321	555	0.00382
1.05	22000	660	1334	533	0.00422
1.05	22000	660	1350	534	0.00387
1.15	17000	1020	1395	478	0.00504
1.15	17000	1020	1395	470	0.00524
1.15	17000	1020	1396	473	0.00498
1.30	30000	750	1423	462	0.00558
1.30	36000	540	1401	471	0.00569

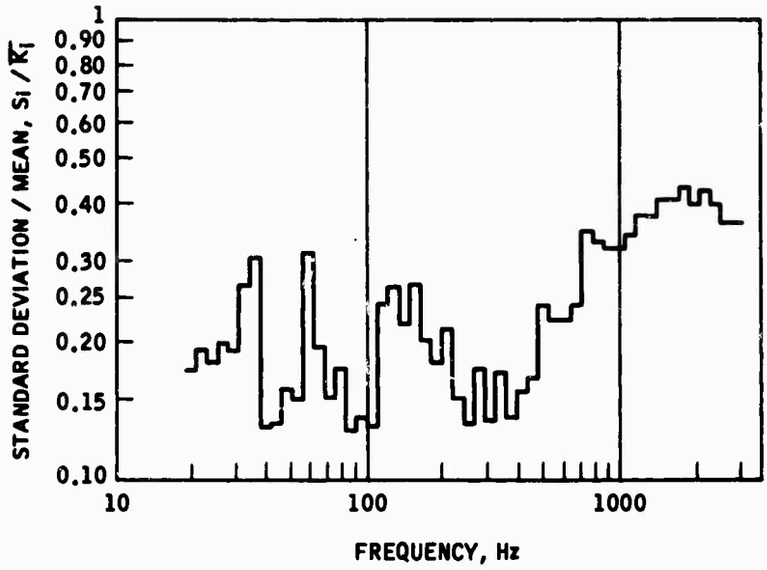

FIGURE 5 Ratio of Standard Deviation of Severity Factor to Mean Severity Factor - Accelerometer 36

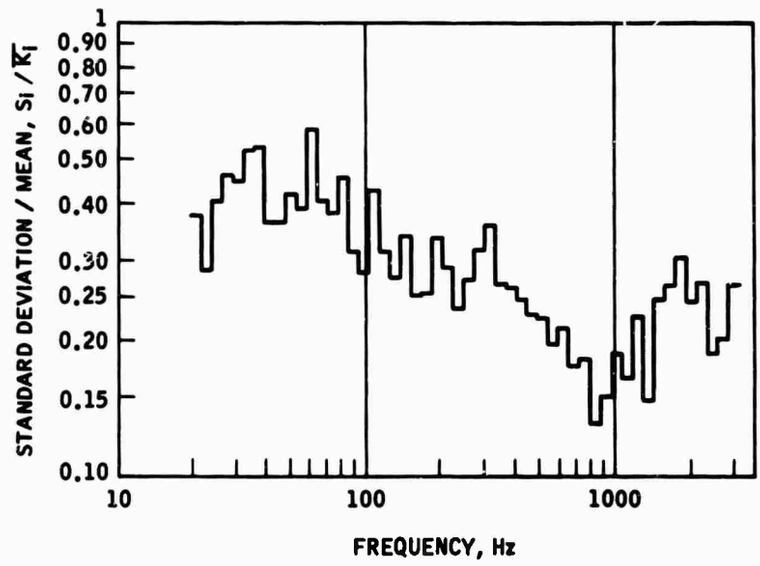

FIGURE 6 Ratio of Standard Deviation of Severity Factor to Mean Severity Factor using Modified Severity Factor (K' = K/M) - Accelerometer 36

upper frequency range). In effect this means that either the model is less satisfactory in the high frequency region or that there are more perturbations (i.e., non-linear effects, etc.) at higher frequencies. From the previous discussion of the data in Table 2, it was noted that the mean frequency of the spectrum increased with increasing Mach No. All this strongly suggests that the high frequency vibration severity is a function of both Mach No. and the dynamic pressure, while the low frequency range is mostly dependent on dynamic pressure alone. To further examine this trend, the data were re-evaluated using the following model for severity factor:

$$K_i' = \left\{ W_i \times BW_i \right\}^{1/2} / q \times M$$

Figure 6 contains a plot of $S_i/\overline{K}_i'$ for the data from accelerometer channel 36. This can be compared to the plot in Figure 5 which is a plot of the same quantities calculated for the linear q dependent model. This comparison shows that the ratio of $S_i/\overline{K}_i$ is greatly affected by the model chosen. In the low frequency region below approximately 400 Hz the linear q dependent model has the lowest ratio of $S_i/\overline{K}_i$. Above approximately 400 Hz the q x M model has the lowest ratio of $S_i/\overline{K}_i$. A final examination of this trend was performed by computing the overall acceleration level below 400 Hz for the data from accelerometer channel 36 using a linear q dependent model. The overall severity factor (K_o) based on the recomputed acceleration levels is plotted vs Mach No. in Figure 7. Note that the trend with Mach No. is insignificant thus indicating a linear q dependent model is valid for this frequency range. In conclusion, the linear q dependent model is satisfactory except in the high frequency (above 400 Hz) range of the spectrum where the severity factor increases with increasing Mach No. At present there has been no investigation of the causes of this Mach No. dependency, which, if present, was not evident in other installations. For the purpose of comparing the measured and predicted environments, the linear q-dependent model is satisfactory since:- 1) the prediction employed a linear model; 2) the model is very accurate for 4 1/2 octaves of the 7 octave bandwidth; 3) the Mach No. effect changes the levels significantly only for high q and high Mach No. conditions for which no data exists; and 4) the difference in standard deviations of severity factors above 400 Hz for the two models (see Figures 5 and 6) is not overwhelming.

During the prediction study, the missile vibration data was evaluated for groups of data from various regions of the missile (i.e., mid, aft, forward and missile axes). However, because no significant differences between regions were found, the Phoenix requirements were based on an evaluation group composed

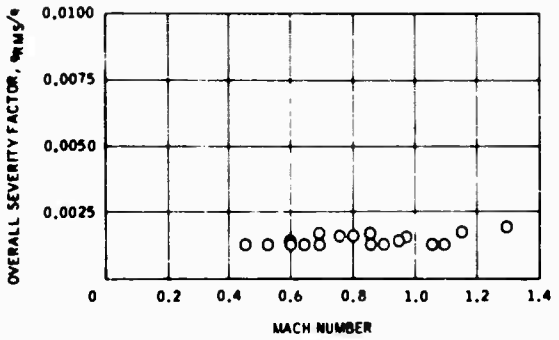

FIGURE 7 Overall Severity Factor (20 - 400 Hz) vs Mach No. Accelerometer 36

of all locations and directions. The flight data was examined for these trends by comparing mean severity factors between various regions and directions. After comparing the various severity factors it was concluded that with the exception of the lateral aft region, which was slightly more severe than any other location, vertical and lateral vibration severity was similar throughout the missile. Longitudinal severity factors were approximately one half the severity factors for the vertical and lateral directions.

A comparison of the predicted environment to the measured environment on an overall or volumetric basis can be made by examining Figures 8 and 9. Figure 8 is a plot of the ratio of mean severity factors vs frequency and Figure 9 is a plot of the ratio of the ratios of standard deviation to mean severity factor vs frequency.

Figure 8, the ratio of mean severity factors, indicates that the predicted severity factor compares very closely with the measured severity factor. The ratio oscillates about a value slightly less than unity. Only two frequencies exceed + 3 db which is unconservative while three clusters of three or four frequencies exceed - 3 db, approaching - 6 db. Considering the customary ± 3 db tolerance used in vibration testing, the difference between predicted and measured values is considered small. The ratio of the ratios of $S/\overline{K}$ indicates that there is more spread in the measured data (i.e., this ratio oscillates about a value greater than unity).

In the very low frequency (below 35 Hz) only the previously smoothed data contributed to the predicted values. Thus unrealistically low $S_i/\overline{K}_i$ (predicted) values influence Figure 9. Above 250 Hz, the previously discussed Mach

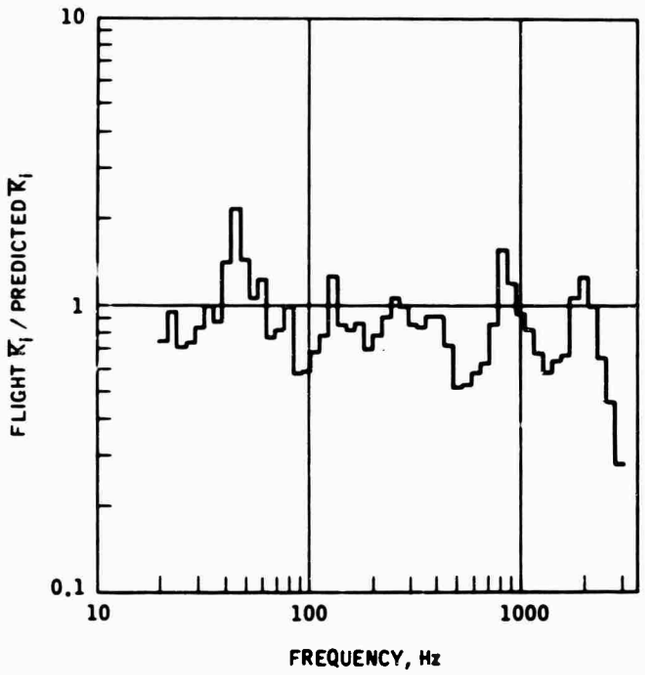

FIGURE 8 Ratio of Mean Severity Factors - All Flight Data/Predicted Values

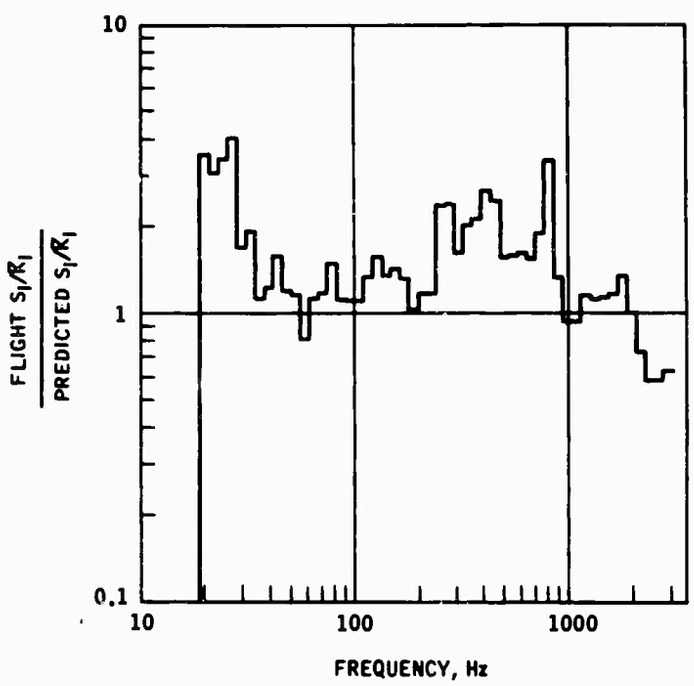

FIGURE 9 Ratio of Ratios of Standard Deviation to Mean Severity Factor - All Flight Data/Predicted Values

No. effect tends to give high $S_i/\bar{K}_i$ values. Even allowing for these factors, it does appear that the variability of severity factor within a missile is as great as the variability between different missile/aircraft installations.

LABORATORY VIBRATION SIMULATION

It is customary to describe the laboratory vibration environment in terms of the specified vibration excitation of a test item. In this case, the degree of laboratory simulation would be assessed in terms of simulation of excitation. However, to be consistent with the prediction technique employed to derive the vibration test parameters, both excitation and response vibration levels are controlled, as described in Ref. 3. Then both excitation and response levels may enter into assessment of the simulation. However, for the missile test, no attempt was made to simulate the excitation in the testing of the missile. During captive flight with bay doors open, the excitation is aerodynamic and occurs over the entire missile surface whereas in the laboratory the excitation is applied to the missile at a single point for any one test. There is, therefore, no simulation of modal excitation. It should be expected that the dynamic relationships between locations in the missile that occur in captive flight will not be duplicated in the laboratory.

Therefore, in the laboratory test, no attempt was made to duplicate the vibration level at particular missile locations. Rather the objective of the method was to produce an "average" or "volumetric" vibration response throughout the missile equivalent in severity to the predicted response. It will be seen that the use of multiple successive excitation points to achieve this objective is crucial. The following method was used in an attempt to simulate this average response.

The missile, suspended by the launcher attachments, was subjected to broadband random vibration. The excitation was successively applied at the forward and aft ejection bulkheads for the vertical and lateral directions and, since it was the only practical location, at the aft end of the missile for the longitudinal direction.

Accelerometers at the excitation locations were controlled to a spectral density based on the predicted mean value ($W_n(\bar{K})$) shown in Figure 1. Other accelerometers were located at a number of locations on missile structure representative of likely locations for flight measurements. The spectral density values at these accelerometers were limited to a value based on the extreme spectral density ($W_n(\bar{K} + 2.33S)$) of Figure 1 by reduction of the excitation in narrow frequency bands which corresponded to frequency bands of maximum response. A detailed description of the implementation of this test method is included in Ref. 3 and will not be repeated here.

To compare the results of the laboratory tests to the measured environment, it was necessary to treat the test data as if it were a set of flight data, all measured at a dynamic pressure equal to the dynamic pressure upon which the test levels were based. For each accelerometer location, a maximum vibration spectrum was computed by enveloping all spectra obtained at that location during the several excitations. These maximum spectra were then normalized with respect to q and equivalent severity factors computed. These data were then formed into comparison groups analogous to those used in evaluating the flight data. Mean values and standard deviations of the severity factor for these groups were computed.

It would perhaps be most natural to compare the test results to the predicted environment in order to assess the degree of simulation achieved. However, the measured environment was now at hand and the major emphasis was to assess the degree to which the test had simulated the measured environment. Since, as discussed earlier, the measured and predicted environments were in good agreement, comparison to the measured environment was satisfactory.

Figures 10 and 11 demonstrate the degree to which the "volumetric" missile response was simulated. Figure 10 is a plot, vs frequency, of the ratio of the mean severity factor from flight data to that from laboratory test with all data included in the groups, similar to Figure 8. Figure 11 is a plot, vs frequency, of the ratio of the ratios of standard deviation to mean severity factor, similar to Figure 9. Close simulation is achieved if these two plots are close to unity across the frequency range although it is probably desirable to have the $\bar{K}$ ratios somewhat less than unity to achieve some conservatism. From Figure 10, it is concluded that the test levels were somewhat deficient above 200 Hz while from Figure 11, it appears that the maximum response spectral density was set at too low a level (relative to the maximum input spectral density) since the $S/\bar{K}$ ratio oscillates about a value greater than unity. However, during the laboratory tests there were only a few frequency bands where excitation was reduced in order to limit the response and these were usually below 200 Hz. Thus it is believed that the major factor in the inadequacy of the test levels above 200 Hz was in fact due to the rapid attenuation with distance from the excitation point. In the higher frequency region, there was very little amplification of the excitation and the extreme response values were not approached. This factor points out the difficulty of simulating aerodynamic

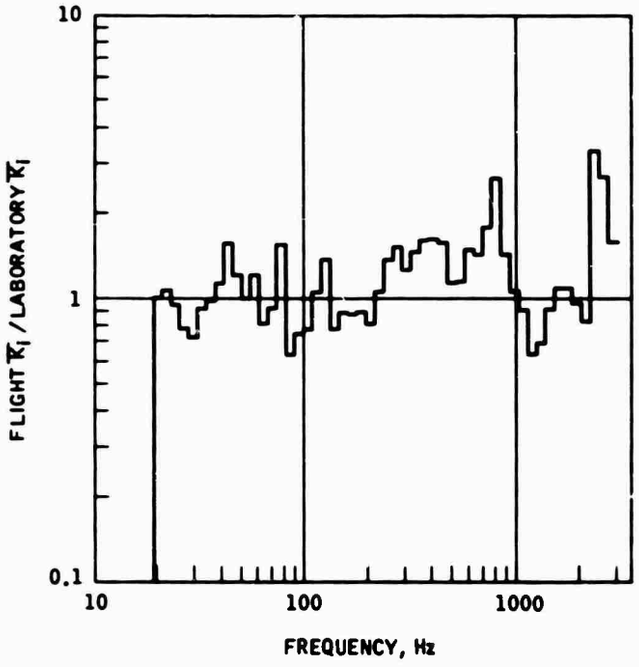

FIGURE 10 Ratios of Mean Severity Factors - All Flight Data/Laboratory Data

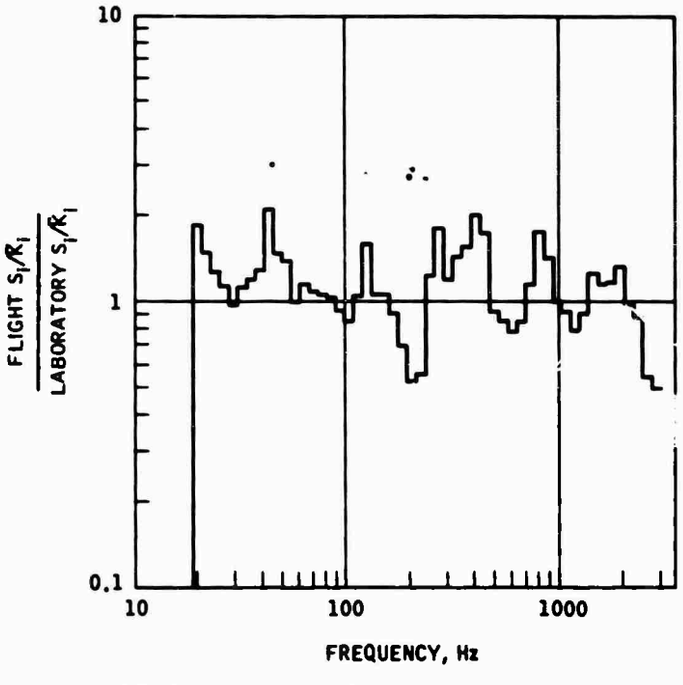

FIGURE 11 Ratio of Ratios of Standard Deviation to Mean Severity Factor - All Flight Data/Laboratory Data

excitation by single point excitation and the need to conduct successive excitation at a number of points.

In spite of these differences, it is believed that Figures 10 and 11 show that the degree of laboratory simulation, judged on the basis of all accelerometer locations, was remarkably good.

The degree of simulation achieved at a particular location is, as should be expected, less satisfactory and highly variable. Figures 12 and 13 present the ratio of $\overline{K}$ from flight data to test data for the forward ejection bulkhead in the lateral and vertical directions respectively. These were excitation points during test. In this case, $\overline{K}$ for the test data is actually the severity factor from the maximum test spectrum for that location. Since the ratio of the maximum to the mean severity factor for the flight data was between 2 and 3, good simulation would be achieved if the $\overline{K}$ ratios in these figures fluctuated between unity and approximately 0.3. Figures 14 and 15 are similar plots for the guidance unit bulkhead in the lateral and vertical directions respectively, which were response control locations during test. The difficulties of simulating an environment in any detail at a number of points is readily apparent from the variations in and between these four figures.

In addition to the previously mentioned difficulty due to attenuation with distance from the excitation, it is now apparent that use of a single accelerometer for input level control also contributed to the degraded simulation. As discussed in Ref. 3, use of a single accelerometer prevents the occurrence of a spectral density value greater than the mean value, at least while excitation is applied at that point. To explore the possible improvement in simulation to be achieved by use of the power average of several accelerometer signals for the test level control, the laboratory test data for vertical excitation at the forward ejection bulkhead was examined. Figure 16 is a plot of the spectral density at the input point and the maximum response spectral density observed at any other location on the missile using the single accelerometer for input level control. Figure 17 is a plot of a computed input spectral density, using the power average of three accelerometer signals and the computed maximum response spectral density which would occur with the computed input, assuming linearity of response. A detailed discussion of the locations, etc, of these maximum response spectra is beyond the scope of this paper. However, the improvement in simulation of the high frequency spectrum above 200 Hz is evident from comparison of these figures.

CONCLUSION

This paper has attemped to describe, within reasonable limitations of time and space, the results of efforts spanning almost five years covering the prediction, the simulation, and finally, the measurement of the captive flight vibration environment of the Phoenix missile. While the title selected (before much of it was written) was perhaps rather strongly worded, the study is believed to illustrate the basic validity of the prediction and test methods described while pointing out some of the limitations which generally face the dynamicist working on this type of problem.

The major conclusions which the authors draw are as follows:

1. On an overall or "volumetric" basis, the prediction technique yielded very satisfactory results.

2. On a similar basis, the simulation technique also yielded satisfactory results.

3. Neither the prediction technique nor the simulation technique should be expected to match the measured environment in much detail. Further the variability observed in the measured environment was such that the likelihood of any technique being able to do so appears quite small.

4. Although it has been rather generally agreed that the linear q-dependent model is a valid one, the discovery of the Mach No. dependence for frequencies in excess of about 400 Hz for this installation was surprising and perhaps significant for future development of prediction techniques.

5. While the test methods employed entail some complexity, the vibration of test objects of significant dimensions and weight, such as the Phoenix missile can only have real significance with respect to the usage environment if: 1) the response of the test object is employed in control of the tests; 2) the excitation is applied at a number of points, either successively or possibly simultaneously; and 3) the excitation is controlled from the power average of several accelerometers.

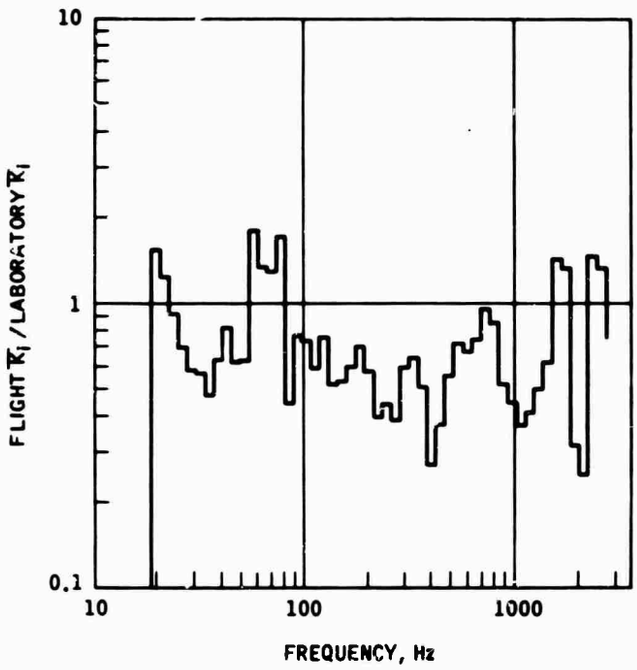

FIGURE 12 Ratio of Mean Severity Factors - Flight Data/Laboratory Data, Forward Ejection Bulkhead Lateral

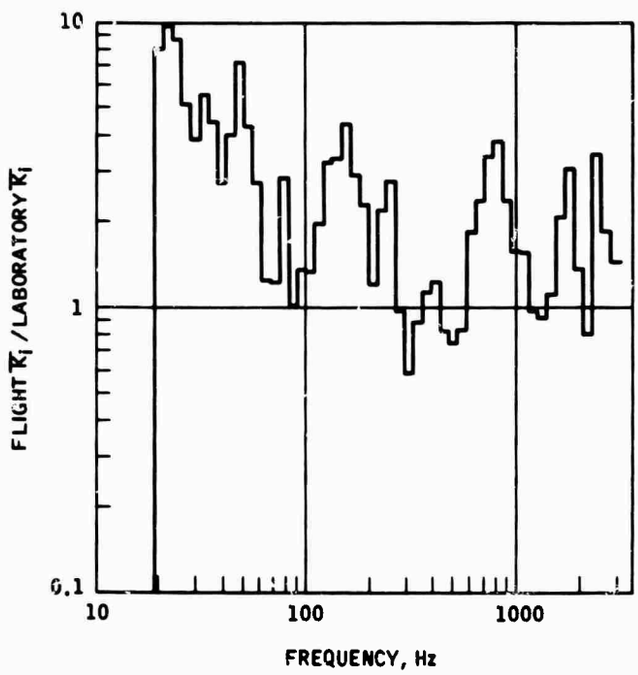

FIGURE 13 Ratio of Mean Severity Factors - Flight Data/Laboratory Data, Forward Ejection Bulkhead Vertical

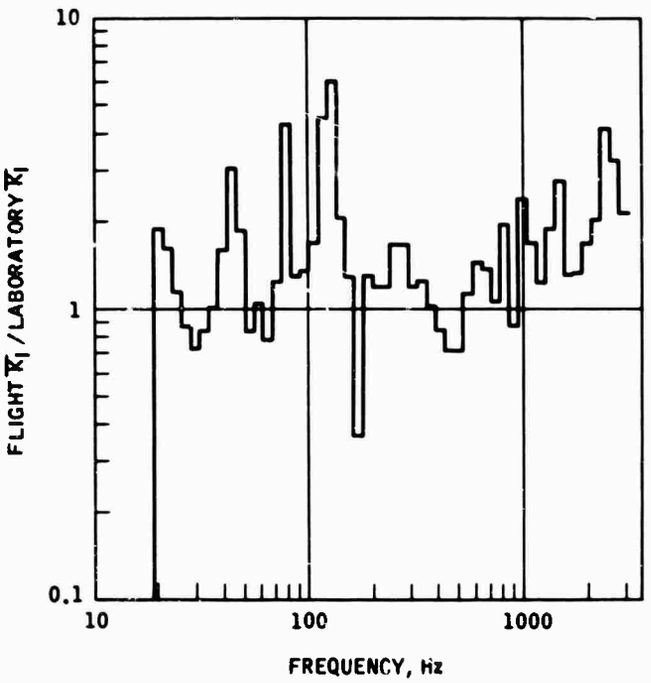

FIGURE 14 Ratio of Mean Severity Factors - Flight Data/Laboratory Data, Guidance Unit Bulkhead Lateral

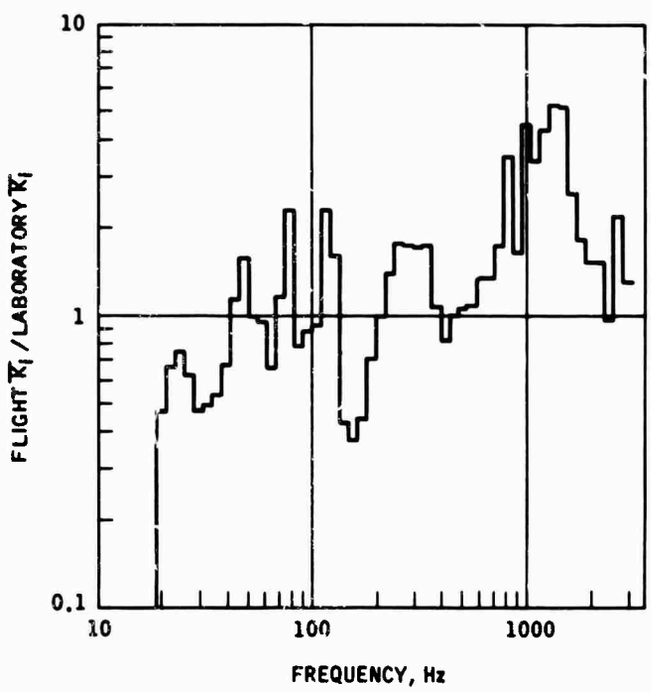

FIGURE 15 Ratio of Mean Severity Factors - Flight Data/Laboratory Data, Guidance Unit Bulkhead Vertical

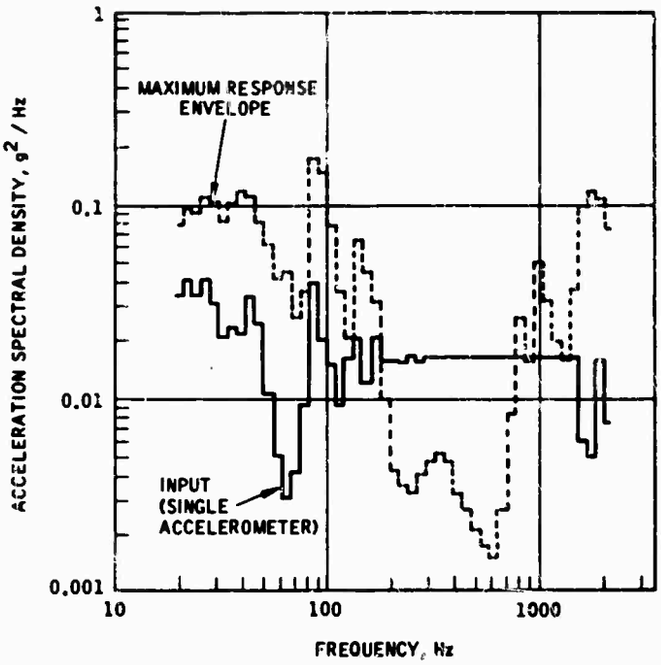

FIGURE 16 Phoenix Missile Assembly Test - Envelope of Maximum Response Acceleration Spectral Density and Input Acceleration Spectral Density when Input is controlled from a single accelerometer.

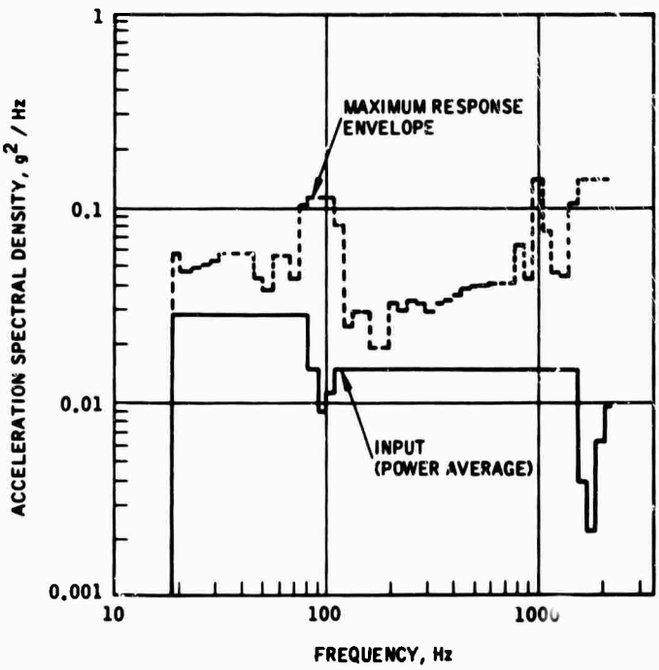

FIGURE 17 Simulated Phoenix Missile Assembly Test - Envelope of Maximum Response Acceleration Spectral Density and Input Acceleration Spectral Density if control had been power-averaged from several accelerometers.

REFERENCES

1. A. J. Curtis, "A Statistical Approach to Prediction of the Aircraft Flight Vibration Environment", Shock and Vibration Bulletin 33 (Part I): 1-13, (1964)

2. T. M. Kiwoir, R. P. Mandich and R. J. Oedy, "PHOENIX Environmental Measurements in F-111B Weapons Bay", Shock and Vibration Bulletin 39. (To be published)

3. A. J. Curtis and J. G. Hererra, "Random Vibration Test Level Control Using Input and Test Item Response Spectra", Shock and Vibration Bulletin 37 (Part 3): 47-60, (1968)

DISCUSSION

Mr. Naylor (Defence Research Establishment, Suffield, Canada): I do not remember your original formula very closely, but I believe the severity was proportional to the dynamic pressure. So it is proportional to Mach number squared. Now you find that this only applied up to 400 Hz. Above this it is proportional to Mach number cubed. I would like to get your views on why this should be. I think maybe it is because up to 400 Hz we have bending effects and beam vibrations in the missile, and above this it goes into panel resonances, and the panel resonances are more susceptible to acoustic excitation. Would this theory have your support?

Mr. Curtis: I really think that the most honest was of answering that question is that we have not really tried to explain this phenomenon that we have found. It seems to be there, we have not had a chance to try to get an explanation. But it does seem to be something that should be incorporated in future efforts in trying to make a prediction. I certainly have no quarrel with the postulate that you just made, but I am not sure that I am qualified to agree with it, either.

PHOENIX ENVIRONMENTAL MEASUREMENTS IN F-111B WEAPONS BAY

T. M. Kiwior
Mechanics Research, Inc.
El Segundo, California

R. P. Mandich and R. J. Oedy
Hughes Aircraft Company, Missile Systems Division
Canoga Park, California

A description of the PHOENIX T-20 Data Acquisition Instrumentation System is given. The PHOENIX T-20/F-111B Bay Environmental Measurements Flight Test Program is discussed. Early unsteady bay pressure predictions and actual measurements are compared and discussed.

INTRODUCTION

A series of experimental captive flight environmental measurement tests of a PHOENIX missile in the weapons bay of an F-111B aircraft was conducted to measure and record vibration, shock, structural response, gross loads, temperature, aerodynamic pressure and acoustic environments. The measurement system consisted of two parts: A tactical missile with sensors and required signal conditioners, multiplex system, onboard tape recorder, and power regulation system substituted for various internal components; and a tactical launcher with flexure devices replacing the launcher ejector mechanisms to measure hook loads and missile gross loads. A total of eighty-six channels of data including aircraft parameters were recorded.

The first portion of the paper describes the flight test program, the hardware and instrumentation, and the performance of the measuring system in field usage. The second portion of the paper describes the fluctuating pressure measurements, the approach used to make early estimates of the severity of the bay unsteady pressures, and the comparison between estimated and measured values.

Captive flight environmental measurement tests of a PHOENIX missile in the weapons bay of an F-111B aircraft were conducted during the period of 30 March to 3 August 1967 to obtain data to verify and/or update the missile load and environmental design requirements. The instrumented missile system consisted of an instrumented missile, instrumented launcher, and a magnetic tape recorder carried within the missile. The program was limited to environmental measurements in the weapons bay without any adjacent stores.

The original captive flight vibration and acoustic pressure environmental design requirements for the PHOENIX missile were determined by grouping, scaling, and extrapolating measured data from various air-to-air missiles flown on other aircraft. The missile and launcher dynamic loads were predicted from the estimations of the bay pressure excitations. The confidence intervals associated with the vibration, fluctuating pressure, and dynamic load predictions were such that experimental verification of the design levels was required.

PHOENIX T-20 MISSILE

The PHOENIX T-20 measurement system was dependent on the mother aircraft for power and recorder command signals only. This was desired to minimize changes to the aircraft to accommodate the missile, and was particularly advantageous since measurements were to be obtained on the wing pylon as well as in the bay.

The missile employed in obtaining the environmental measurements in this test program was designated T-20. In order to provide meaningful measurements of actual conditions, T-20 was designed to be dynamically similar to the tactical missile. It utilized a tactical fuselage, tactical wings and control surfaces, tactical radome, and a tactical (inert) rocket motor. The data acquisition instrumentation was substituted for various internal components, but tactical weight and center of gravity were maintained. Temperature measurements in the bay were made primarily to evaluate temperature effects on the dynamic instrumentation.

The missile instrumentation system consisted of sensors and required signal conditioners, a multiplex system, an onboard tape recorder, a power regulation system, and associated electrical wiring. Special force measuring mechanisms were designed, fabricated, and installed in the bay launcher to mate

the launcher to the PHOENIX missile. A description of the measurement system, transducers, channel frequency responses, locations on the T-20 missile, and multiplex frequency band are presented in the following text. A block diagram of sensor locations is shown in Figure 1.

Accelerometers

The missile was instrumented with 19 crystal accelerometers having a frequency response range from 5 to 2000 Hz, and 4 strain gage accelerometers with a frequency range from 0 to 300 Hz. The transducers were mounted at various missile stations along the longitudinal, lateral and vertical axes.

All accelerometers located in the missile fuselage were calibrated to ±25g pk-pk. Figure 2 shows a front view of the guidance section bulkhead with two strain gage accelerometers and amplifiers and three crystal accelerometers installed. The large steel cylinder in Figure 2 is ballast to maintain c. g. and weight requirements. Figure 3 shows the accelerometer installation at station 59.5 between the armament and guidance sections. The accelerometers at stations 127 and 146 are shown in Figures 4 and 5, respectively. Figure 6 shows the accelerometers at station 82.3 as well as a number of signal conditioning amplifiers.

Acoustic Microphones

Two crystal microphones were mounted flush with the missile fuselage, one at missile station 39 at 6 o'clock and another midway between control surfaces 3 and 4 at 9 o'clock (looking forward). The microphone-amplifier systems were calibrated to measure a maximum of 162 db within a frequency band from 10 to 10,000 Hz. The microphones were later recalibrated to 173 db full scale to avoid clipping occasional peaks anticipated at the more severe environments.

Resistance Thermometers

Temperature sensitive film resistors of a nickel base material were used to detect temperatures. These were electrically connected in a one active arm bridge to produce a full scale signal variation for temperatures from -75°F to +300°F. A typical installation is shown in Figure 7.

Pressure Transducers

Nine strain gage pressure transducers with dc amplifiers were installed on the missile. These were located on the right side, left side, and bottom of the missile near the front, middle, and aft sections of the missile. The transducers employed were the absolute pressure type, calibrated to 25 psia to allow for the altitude effect on pressure. These sensors were capable of measuring quasi-static pressure variations.

Force Measurement Mechanisms

The ejection hook boxes, mounted in the launcher to which the missile hooks normally attach, were replaced with specially designed Force Measurement Mechanisms (FMM). These units were designed specifically for the F-111B bay launcher and pylon. Figure 8 shows a sketch of an assembled FMM while Figure 9 shows an exploded view. Two of these units were required to mate the missile and launcher, one for the forward hooks and one for the aft hooks. A third unit was fabricated and maintained as a spare. The FMM had strain gaged load links arranged to measure 4 forces, right and left vertical, lateral and longitudinal.

Since the PHOENIX aft hooks are designed to transmit no longitudinal load, the aft longitudinal link was not monitored. Thus, seven data signals defined the three missile loads (vertical, lateral, longitudinal) and three moments (roll, pitch, and yaw).

Individual tests were performed on the force measurement mechanisms to calibrate them for measuring missile hook loads. The calibration loads were applied using a special loading fixture both along one axis at a time, and with six load components applied simultaneously. A statistical twenty-five point combined loading schedule was utilized for the combined loadings. Calibration constants were determined using a multiple nonlinear regression digital computer program. The coefficients were subsequently utilized to determine missile hook loads from flight test signals.

Two force measurement mechanisms were then installed in the bay launcher and a combined missile-launcher test performed to calibrate the launcher for missile gross loads and moments. The test consisted of installing the missile on the launcher in a loading fixture, applying combined loads and moments, and measuring the resultant FMM signals. Distributed loads were applied by means of mechanical jacks and whiffle trees. A similar statistical twenty-five point combined loading schedule and the multiple nonlinear regression digital computer program were used to determine calibration constants. The coefficients from this test were utilized to determine missile gross loads and moments from the flight measurements.

Wing and Control Surface Bending Transducers

Forward and aft wing lugs as well as control surface shafts were instrumented with strain gages to sense bending moments. Control surface shafts were also instrumented to sense torsion. Typical wing lug and control surface strain gage installations are shown in Figures 10 and 11, respectively. All of the strain gaged missile components produced approximately ±10 mv full-scale signal for full-scale load. These data channels employed low input level voltage controlled oscillators (VCO)

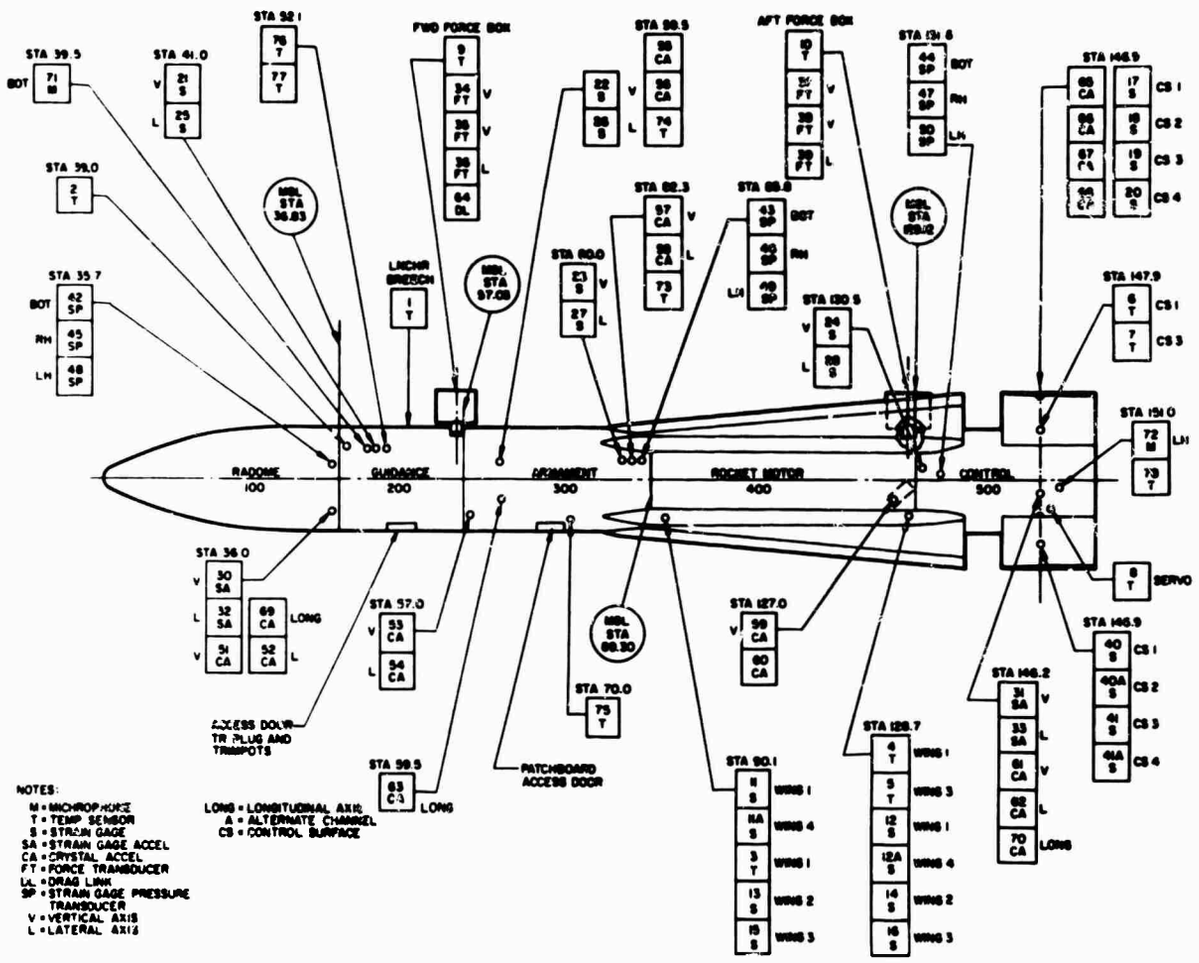

Figure 1 - Sensor locations

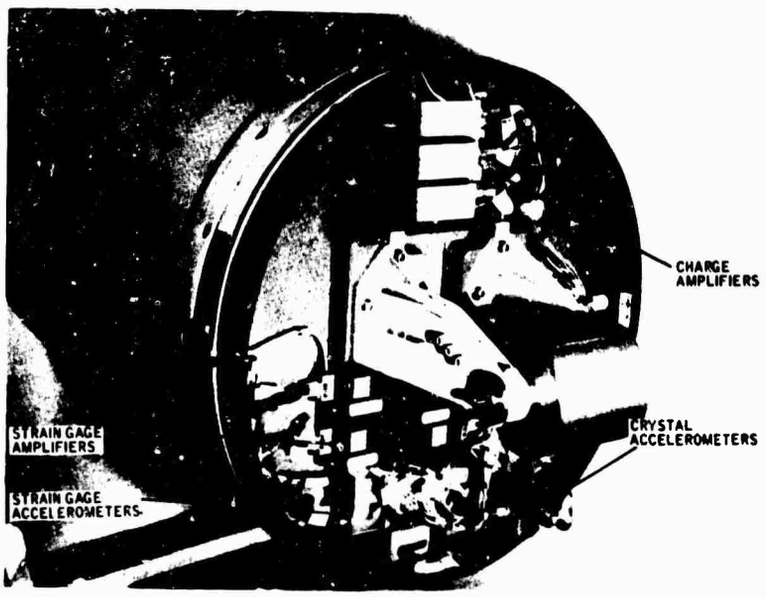

Figure 2 - Guidance section bulkhead

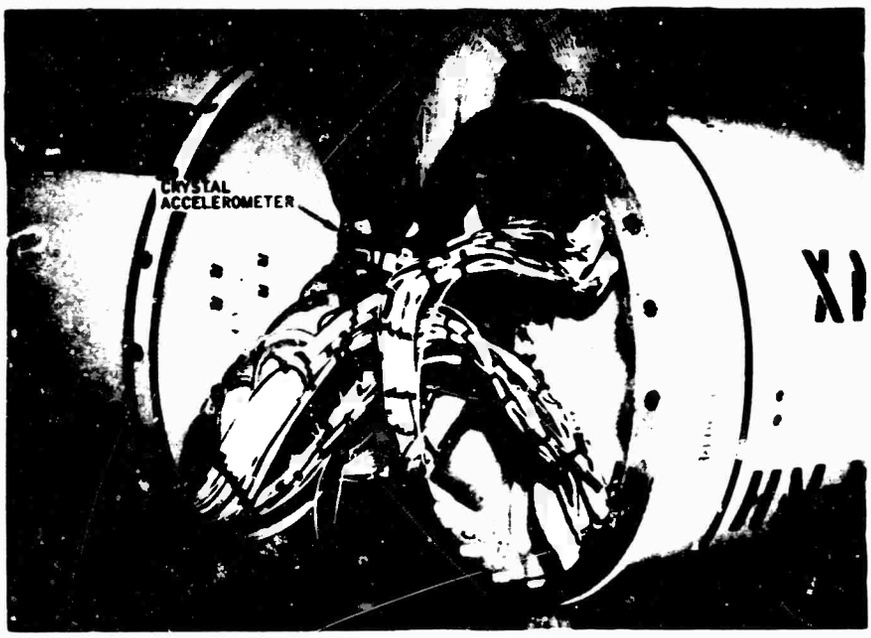

Figure 3 - Instrumentation interconnection between armament section - guidance section

Figure 4 - Accelerometer installation, station 127

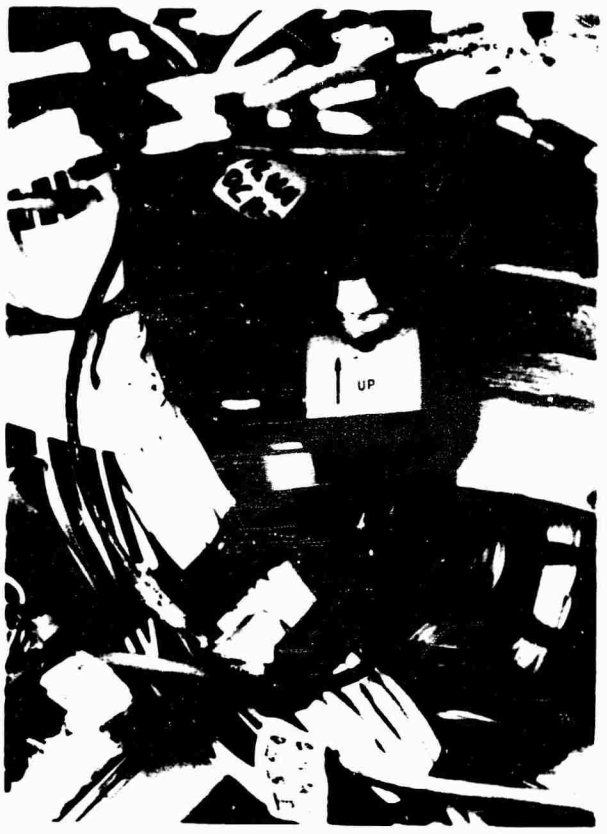

Figure 5 - Accelerometer installation, station 146

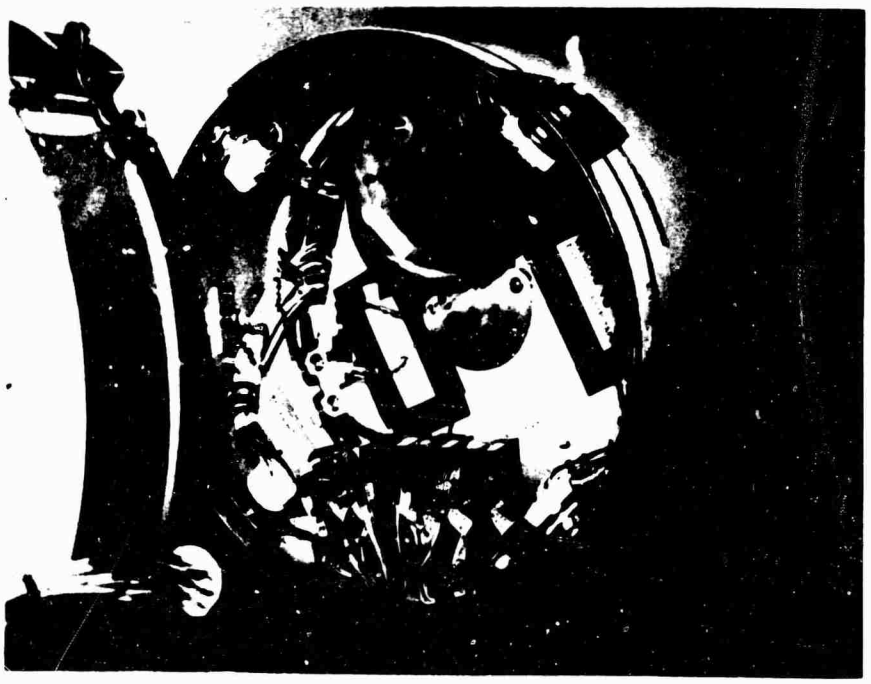

Figure 6 - Aft view of armament section

Figure 7 - Typical resistance thermometer installation

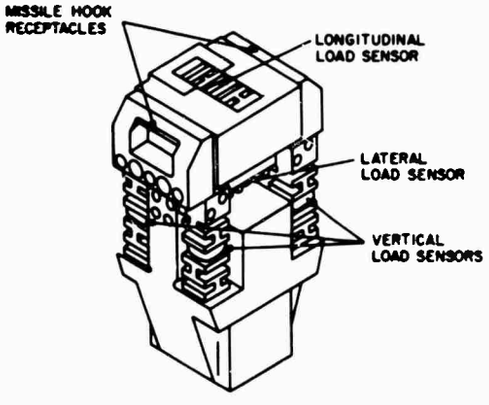

Figure 8. Assembled view, force measurement mechanism

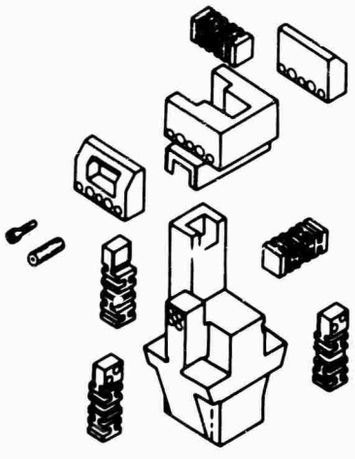

Figure 9 - Exploded view, force measurement mechanism

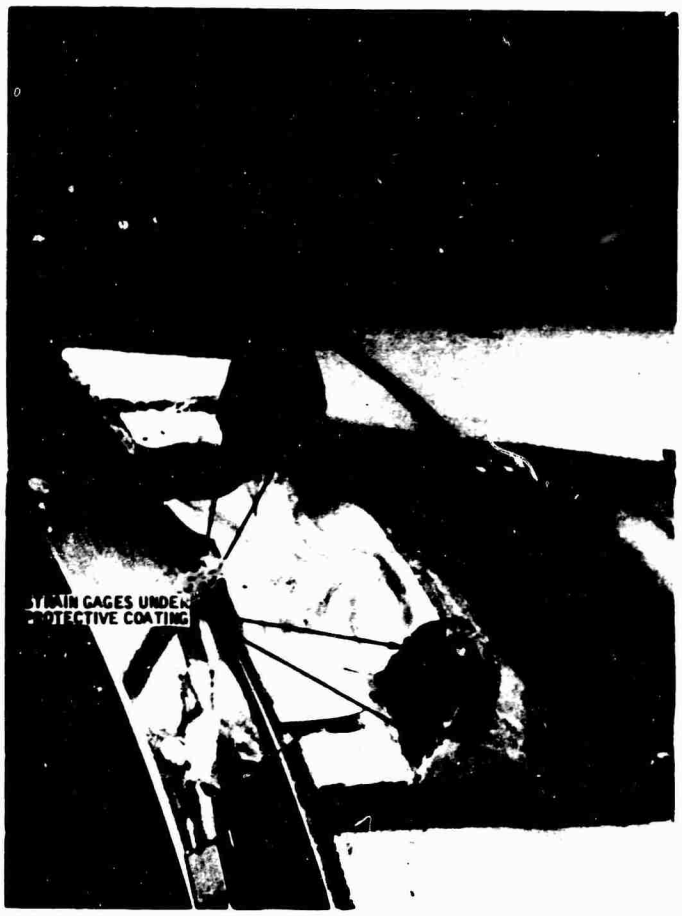

Figure 10 - Wing lug strain gage installation

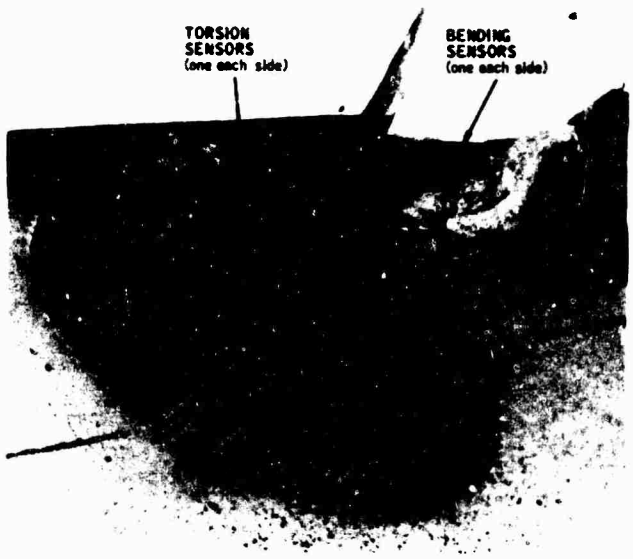

Figure 11 - Typical control surface strain gage installation

in the multiplexer section of the data acquisition system.

Both the wing lug and control surface strain gage transducers were load calibrated. Full-scale load was first applied, and the signal conditioning circuit adjusted for full-scale output. Loads were then applied in increments of 20% of full scale, and the output voltages recorded. A standardization resistor was shunted across one leg of the bridge, and the resulting output was also recorded. The minimum least squares linear fit was determined for each transducer.

Fuselage Bending and Launcher Attach Link Strain Gages

Strain gage transducers were installed on the T-20 fuselage to measure bending. Vertical and lateral sensors were installed at stations 41, 59.5, and 80.

The launcher as mounted in the bay of the F-111B is attached by redundant brackets on the outboard side and pinned by links on the inboard side. These inboard links were equipped with strain gages and calibrated to measure the loads transmitted from the launcher to the bay floor.

MULTIPLEX/DEMULTIPLEX SYSTEMS

Multiplex System

The multiplex system consisted of 84 subcarrier voltage controlled oscillators (VCO), one reference oscillator, 13 mixer amplifiers, one VCO voltage calibrator and a mounting chassis with the necessary interconnecting wiring, connectors, and test points. The multiplex system provided a means of recording 84 channels of data on 12 tracks of a 14-track onboard tape recorder. Each of 12 mixer amplifiers accepted the outputs of seven subcarrier oscillators. The seven subcarrier frequency bands were the same for each of the 12 tracks. The subcarrier voltage controlled oscillators changed the analog data being measured into frequency modulated data. The amplitude of the analog signal became the magnitude of the oscillator frequency, and the frequency of the analog signal became the rate of change of the oscillator frequency. This system of data recording had several advantages. It allowed simultaneous recordings of seven non-overlapping data channels on each tape track and it afforded greater accuracy than direct or analog recording. In addition, frequency modulation permitted recording dc signals which is not possible with direct recording. Data channels with center frequencies of 5.4 kc, 12.5 kc, 20.8 kc, 29.2 kc, 37.5 kc, 64.0 kc and 96.0 kc were employed on each tape track. Figure 12 shows a schematic diagram of a typical track of data made up of seven channels. High level VCO's requiring an input signal of 0-5 volts were used for the amplified channels while low level VCO's requiring ±10 mv input signal were used with the strain gage channels. A 128 kc reference oscillator signal was mixed on each track in order to provide a means of flutter compensation upon playback. An additional mixer amplifier was used at the output of the reference oscillator to ensure adequate isolation between multiplex tracks. A voltage calibrator provided precise calibration voltages simultaneously to all subcarrier oscillators. The calibrator also provided a calibrate command signal to operate the calibrate relays in each of the subcarrier oscillators.

Figures 13 and 14 show the bottom and top view of the Multiplex System/Tape Recorder Assembly on which the majority of the VCO's were mounted. Upon command from either the Ground Checkout Box, or the Aircraft T-20 Control Panel, the input to the VCO's was switched from the sensor signal conditioners to the calibrate relay. A three-level VCO calibration voltage was then sequentially fed to each VCO. In actual system operation, these calibration voltages were automatically recorded on the magnetic tape prior to each data run. The calibration sequence could also be manually stepped from the Ground Checkout Box.

Demultiplex System

The demultiplex system (ground station) was used to convert the frequency modulated (FM) data, which was recorded in the direct mode on the missile tape recorder, back to a usable analog format. It consisted of 4 data discriminators, one reference discriminator, 2 delay lines, 13 channel selectors (filters), 10 output filters, one reference discrimination filter and one reference channel selector. This equipment enabled data to be reduced from any 4 channels on any two tracks of either the even or the odd recorder heads. Tape speed compensation, using the 128 kc reference signal, was an integral part of this system. This tape speed compensation reduced the effect of tape recorder wow and flutter by 30 db.

TAPE RECORDER

The tape recorder and associated record electronics, as shown in Figure 14, was employed. Tracks 4 and 6 were standard FM to give a frequency response of 0-10 kc desired for acoustic data. The remaining 12 tracks employed direct record electronics with a frequency response of 500 cycles to 150 kc. The tape transport system had a capacity of 1200 feet of one inch wide, one mil tape. The machine operated at 30 inches per second providing a total available recording time of 8 minutes. The recorder head configuration was standard IRIG allowing tape playback on any other IRIG tape machine. Although the data on all tracks was frequency modulated, it was recorded in the direct mode, and therefore had to be played back with direct reproduce amplifiers through the demultiplex system.

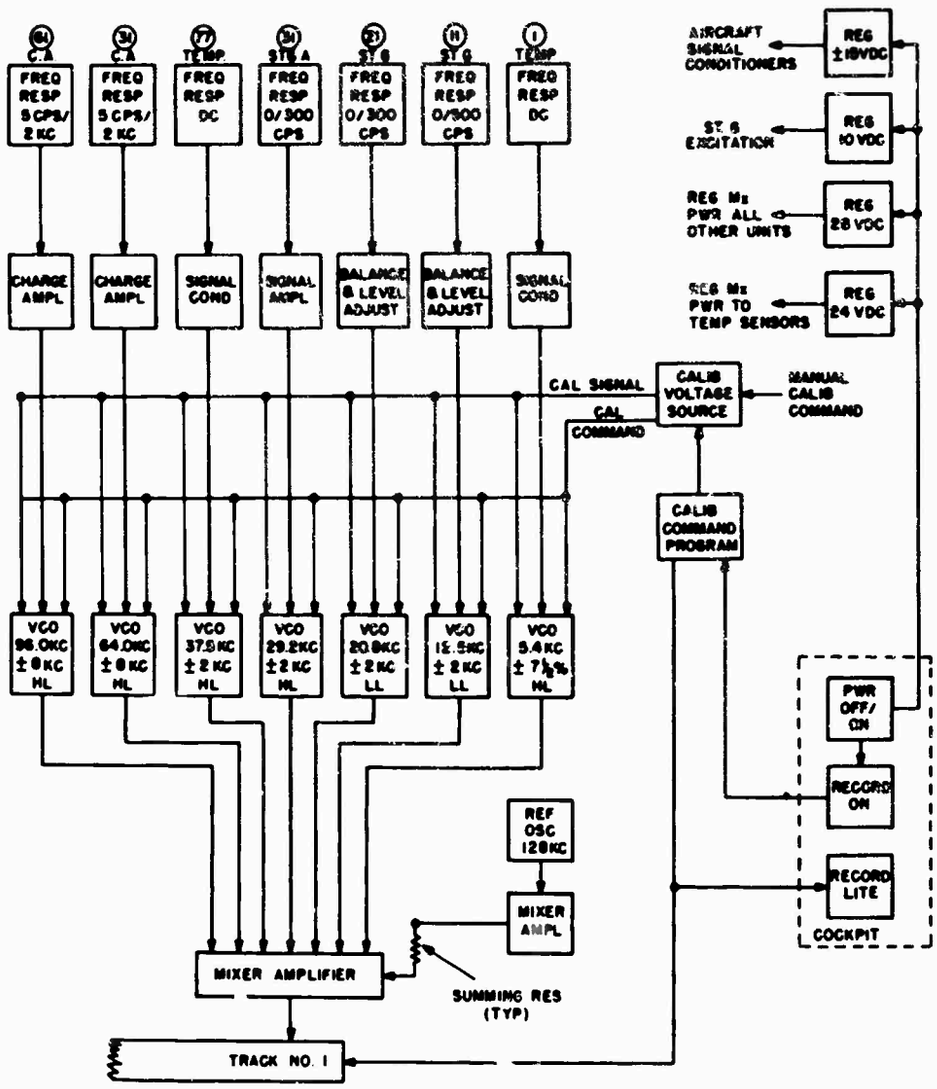

Figure 12 - Instrumentation for a typical data track composed of 7 channels

SPECIAL EQUIPMENT

A T-20 Ground Checkout Box was used to check the operation of the instrumentation sensing devices and signal conditioners. Every channel could be monitored with this unit connected to the missile. Provision was made to supply power to the missile through the checkout box eliminating the need for aircraft power. Resistance-calibration resistors for the strain gage and FMM channels were provided internally and could be switched into the circuit for checking purposes. A precision meter and an oscilloscope were provided for monitoring purposes. In addition, the console provided recorder function control with voice annotation capabilities.

The aircraft T-20 control panel, located in the A/C cockpit, had the functions of power on/off, camera on/off, and recorder on/off. The recorder could be operated either in an automatic 22 sec. mode or in a continuous mode. In the latter mode, the tape recorder would continue until the function switch was returned to the "off" position, or until the 8 minutes of tape was expended, in which case the tape recorder would automatically turn off.

AIRCRAFT PARAMETER INSTRUMENTATION

In addition to the instrumentation already discussed, provision was made to record aircraft altitude, Mach number, vertical load factor, pilot commentary, and IRIG "B" timing signal.

Altitude and Mach Number

Aircraft altitude and Mach number were both available in terms of two of the three voltages of a three phase synchro system. Therefore, two data channels were required for each parameter. The 400 cps synchro voltages were conditioned by an AC/DC converter and scaled to be compatible with the multiplex system voltage controlled oscillator input requirements. In actual operation, Mach number and altitude were both independent variables. Therefore, great care was exercised by the pilot to fly the aircraft at the prescribed conditions.

Vertical Acceleration

Aircraft vertical acceleration was available from aircraft instrumentation as a proportional dc voltage. Signal conditioning was required to make the signal compatible with the multiplex system. Most flight conditions were straight and level; however, for the six symmetrical maneuvers, the data to be analyzed could be accurately located using vertical acceleration as a parameter.

Pilot Commentary and IRIG "B" Timing

Provision for pilot commentary was designed into the data acquisition system. An IRIG "B" time code was recorded in every case to provide an accurate means of channel to channel cross reference.

FLIGHT TEST PROGRAM

The Mach number and altitude for each test point that was flown are shown graphically in Figure 15. Circled points indicate straight and level flight at constant speed. Those points with a number alongside the circle indicate that a maneuver was performed during the data recording period. The flight test parameters (Mach number, altitude dynamic pressure, aircraft angle of attack, maneuver, and wing sweep angle) are listed in Table 1.

The PHOENIX T-20 missile was installed in the starboard side of the F-111B bay as illustrated in Figure 16. Figure 17 shows a side view of the missile in the bay. The adjacent port side of the bay was vacant for all tests.

In performing the bay-flight points at straight and level flight, the pilot brought the aircraft to the specified flight condition, altitude and Mach number, and stabilized at these conditions. When all was ready, the Missile Control Officer (MCO) started the tape recorder to begin recording data. Four seconds after starting the tape recorder, he would open the bay doors. The tape recorder shut off automatically after 22 seconds. On several occasions, the manual tape recorder mode of operation was used to facilitate the timing of aircraft maneuvers with the bay doors opening sequence.

Motion picture coverage was provided to show the motion of the fuselage, wings and control surfaces during flight. The camera was mounted in the forward end of the bay slightly to the port side of center and looked almost axially aft along the length of the missile and bay. The camera was started by the MCO a few seconds before the bay doors opened and shut off at approximately the same time the doors were closed.

A preflight and postflight checkout of each channel was conducted using the Ground Checkout Box. Immediately after each flight, time-history plots for all channels were carefully inspected for indications of data system malfunctions or data clipping, and to ensure that unexpected, excessive missile/launcher loads were not occurring. This data reduction and evaluation cycle was performed rapidly to cause minimum delay to succeeding flights. In several instances data channels were rescaled to better match full scale recording levels to actual data.

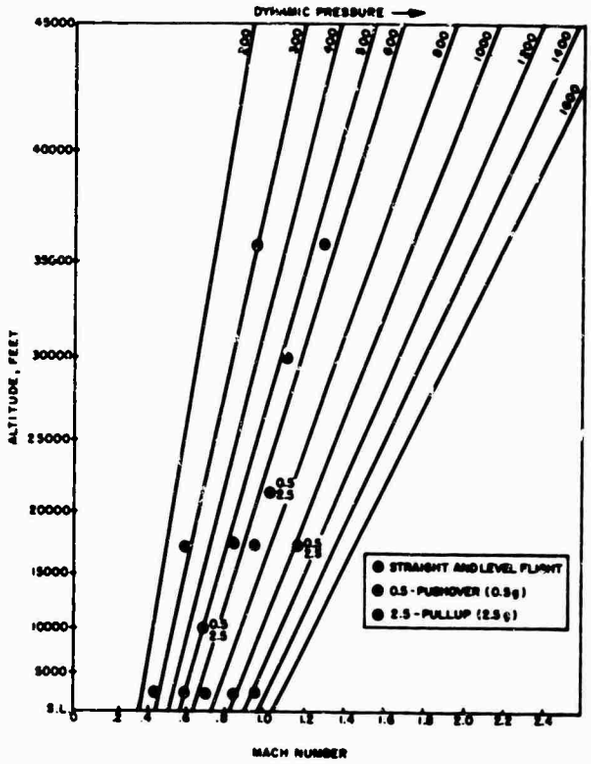

Figure 15 - PHOENIX T-20/F-111B weapons bay data flight points

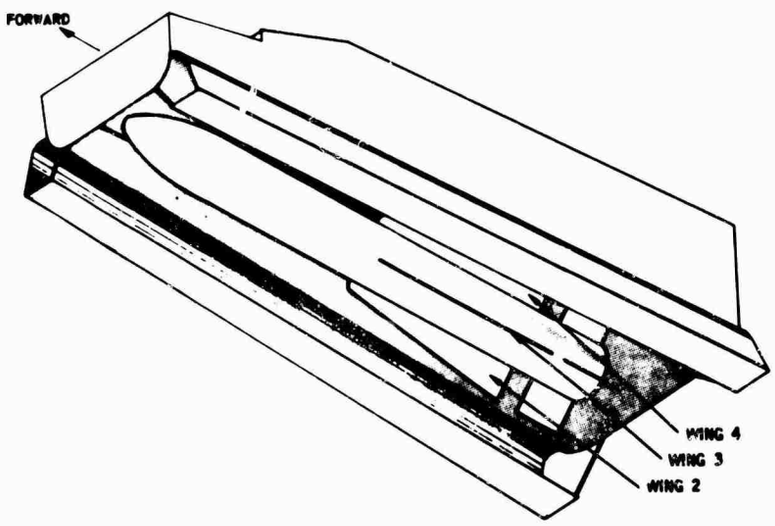

Figure 16 - PHOENIX missile, starboard store position in F-111B bay

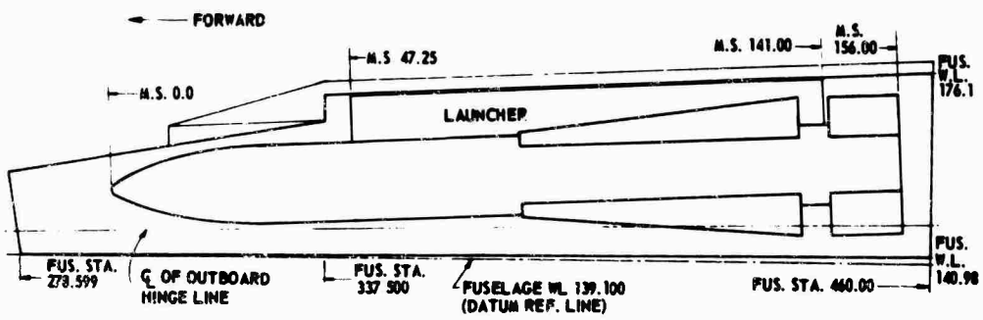

Figure 17 - Side view of T-20 in F-111B bay

Figure 13 - Bottom view of multiplex system/
tape recorder assembly

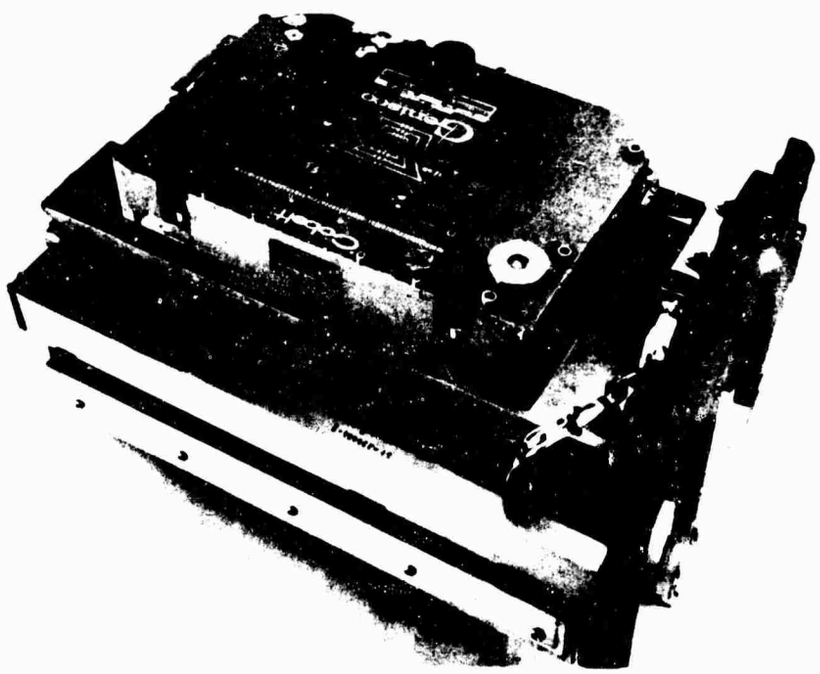

Figure 14 - Top view - multiplex system/
tape recorder assembly

The F-111B bay test flights were flown out of the Hughes Aircraft Culver City, California facility. Chase plane coverage was provided by the Navy facilities at Point Mugu. Missions were flown on the Point Mugu Test Range and the Edwards AFB Supersonic Range. The measurement system performed excellently in field usage resulting in a very successful 90% data retrieval for the entire flight program.

On several occasions throughout the flight test program, various channels of data were lost. However, because of the rigorous post flight checkout and quick look procedures, replacement and repairs could be made before the next flight.

Post Flight Data Reduction and Evaluation

A more detailed data reduction and evaluation phase was performed after all flight tests were completed. For a description of all the measurements, their data reduction and their data evaluation, one is referred to Refs. 1 and 2. Ref. 2, a paper to be presented at the 39th Shock and Vibration Symposium by Curtis and Tinling, examines the degree of agreement between the predicted and measured vibration environments. In this paper the unsteady pressure measurements are presented and compared with those used for structural design.

PHOENIX BAY PRESSURE PREDICTIONS

A particularly difficult problem in the early design of the PHOENIX missile, was the establishment of open door design loads criteria for the missile in the F-111B bay. The criteria were needed to estimate an upper bound on oscillatory loads and vibratory responses in order to size the missile and launcher structures.

Aircraft flight experience with the Falcon series of missile manufactured by Hughes Aircraft Company had shown that a severe vibration environment often exists in a weapons bay when the doors are opened. Visual examination of accelerometer and strain gage traces had shown that bay mounted structures tend to be most highly excited at their lower structural frequencies and to respond with high stress levels. It seemed likely that the forcing frequencies must form a continuum, so that all structures placed in a bay would vibrate.

The engineering significance of the problem is that bay mounted missiles vibrating rapidly at relatively high stress levels, even for the short time the bay doors are open, may undergo a large number of oscillations and thus may accumulate significant fatigue damage. This fatigue environment, together with the peak response loads, tends to be of such significance as to ultimately dictate the final design.

The task of establishing design loads criteria for the PHOENIX missile was made difficult since there were not, either from analyses or by past wind tunnel or flight measurements, sufficient information to accurately estimate either the rms values of the unsteady pressure excitations at locations within the F-111B bay or the power spectral densities and spatial correlations of pressures. Furthermore, there existed so few unsteady pressure data for three-dimensional cavities and bays with missiles that confidence in simulation was low, and this discouraged the initiation of wind tunnel tests to obtain the unsteady pressure data on the PHOENIX/F-111B bay configuration. It was reasoned that if data were collected using small scale models, the applicability of the results to full scale missiles would be questionable. Full-scale flight tests of the missile in bays of other aircraft were considered, but found not feasible since the geometry of the aircraft in the vicinity of the missiles would need major and costly modifications to simulate the local geometry of the F-111B aircraft.

As a result of these problems, it was decided to develop bay dynamic loads criteria for the PHOENIX missile utilizing the empirical-analytical techniques of Ref. 3. It was assumed that the principal source of vibratory loads in the F-111B bay would be the unsteady pressures in the bay. Consequently, design criteria were derived based on analysis of flight test response data for other captive bay missiles, and the analytical establishment of a pressure excitation acting over those missiles which produced responses compatible with their observed measurements.

As noted in Ref. 3, with one piece of response data to match (for example, the rms acceleration at the nose of a missile), one degree of freedom can be allowed in the description of the total fluctuating pressure acting on a missile. Thus, by selecting the spatial correlation of pressures as a fixed shape and by approximating the random pressures by white noise with a high cutoff frequency, an estimate of the fluctuating pressures acting on a captive missile can be derived from a single response measurement. The reference suggested that mathematical models of missiles be analyzed to find the level of the white-noise spectrum.

To establish design loads criteria for the PHOENIX missile in the F-111B bay, strain gage and accelerometer data obtained during captive flight tests of previous HAC bay installed missiles (GAR-11 missile/F-102 aircraft, GAR-3/F-106A, HM-55/J35F and GAR-1D/F-101B) were analyzed to estimate the oscillatory bay pressures. Pressure magnitudes found in the above manner were plotted against dynamic pressure, as shown in Figure 18. Trends with q and bay configuration were investigated before selecting a white-noise pressure spectrum for PHOENIX design.

To this spectrum were then added narrow-band levels at the estimated cavity resonant frequencies. The magnitudes of the narrow-band levels were estimated from the test data in Ref. 4.

Figure 19 shows the oscillatory pressure environment predicted for the PHOENIX in the F-111B bay. For dynamic pressures measured in psf, the level portion of the spectrum had a value in psi^2/Hz equal to $3.78\ (10)^{-10}\ q^2$. Superimposed on this spectrum are shown estimates of the narrow-band spectral levels corresponding to the calculated bay resonant frequencies. The rms oscillatory pressures were predicted to vary linearly with dynamic pressure (q).

The pressure estimates were subsequently used to predict missile and launcher structural loads. The results are documented in Ref. 5. It was of interest, as the flight test program progressed, to compare the structural load and unsteady pressure predictions of the reference with those measurements by T-20.

UNSTEADY PRESSURE DATA REDUCTION

All unsteady PHOENIX T-20 pressure data reduction was performed using special purpose analog instruments which operated directly on the output voltage time history signals from the data recorders. The data were reduced into one or more of three different forms, as follows:

a) RMS values
b) Power spectral density functions
c) Cross correlation functions.

RMS values were used as a rudimentary measure of dynamic severity for general data studies. Power spectra were employed to obtain a spectral decomposition of the data. Cross correlations were computed to provide information needed to check certain critical assumptions in the original dynamic load predictions for the PHOENIX missile.

RMS Value Measurements

The rms pressure values were continuously recorded in real time during the interval when the bay doors were fully open and the data were stationary. This time interval was about 5 seconds long, which was ample for the voltmeter averaging circuit used for data reduction to fully respond to the data signals and produce unbiased rms estimates for the open bay environment. The lower frequency range of the instrumentation cut off at 2 Hz. This means that static levels (represented by a dc signal level) were not included in the measured rms values.

The purpose of measuring rms values for selected data channels was to obtain a rudimentary measure of severity (dispersion) for open bay dynamic data of interest. This measure of severity was needed to study relationships between selected open bay dynamic data (acceleration, pressure, and strain) and pertinent flight parameters (dynamic pressure and Mach number).

Power Spectra-measurements

The power spectra was measured from sample records which were formed into loops and recirculated to provide a continuous input to the analyzer. The sample records were selected during the time interval when the bay doors were fully open and the data were stationary. In most cases, nonstationary effects diminished immediately after the bay doors were fully open, permitting a four second long sample to be used. In a few cases, however, data were recorded during maneuvers which introduced additional nonstationary effects. For these data, sample record lengths were restricted to as short as 2 seconds.

Cross-Correlation Measurements

The purpose of the cross-correlation measurements was to establish the degree of similarity or statistical dependence between the measured unsteady pressures at different stations along the missile, and around the missile at the same station. Comparisons are made at various missile stations separated longitudinally and radially. The correlation coefficient was computed every one thousandth (.001) of a second.

UNSTEADY BAY PRESSURE MEASUREMENTS

The validity of the assumption that the principle cause of vibration during open bay captive flight would be the aerodynamically induced fluctuating pressure field in the bay was readily substantiated by inspection of the data time histories before and after the bay doors were opened. It remained, however, to establish the relationship between the aerodynamically induced pressure field in the open bay and the aircraft flight conditions.

For "clean" or smooth structures moving through ambient air a turbulent aerodynamic boundary layer is produced whose magnitude and spectral characteristics have been fairly well defined by past theoretical and experimental studies. Specifically, the power spectrum for the pressure field, when suitably normalized, can be represented by a simple curve, as illustrated in Figure 20. For the problem at hand, the configuration was that of a missile in an open bay, which is quite different from the idealized case discussed above.

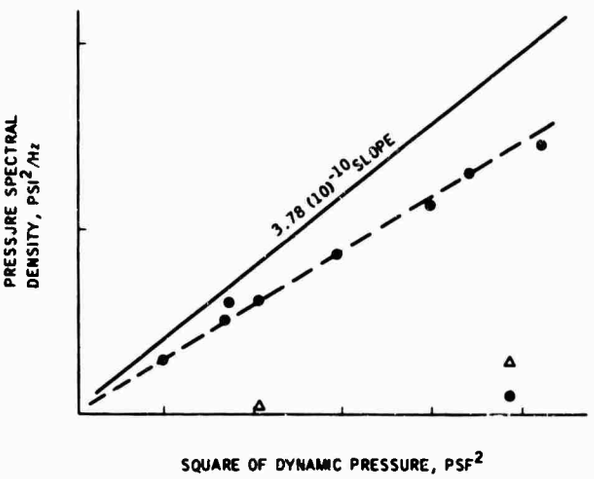

Figure 18 - Bay pressure magnitudes

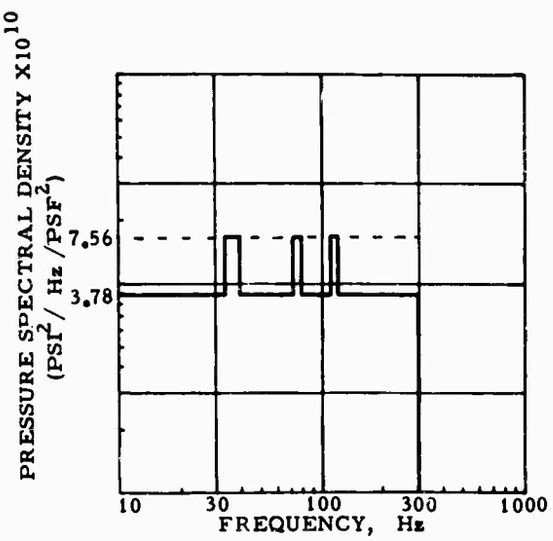

Figure 19 - Bay pressure spectrum predicted for all missile sections

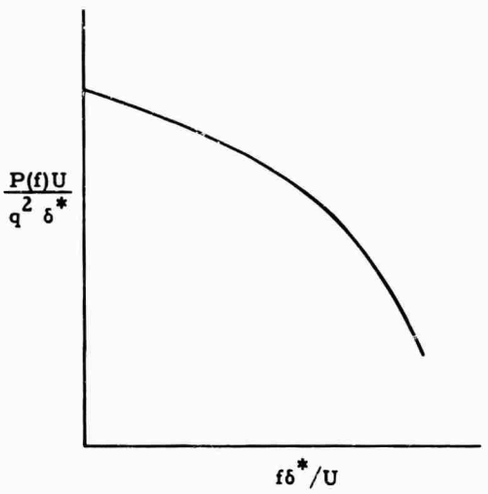

Figure 20 - Idealized pressure spectrum

In particular, the open cavity introduced acoustic resonances.

Inspection of the pressure transducer data revealed the presence of peaks in the pressure power spectra undoubtedly due to cavity resonances. However, the peaks were generally less than three to one. Even allowing for the suppression of the indicated peaks by the bias errors inherent in the data reduction, it was clear that no unstable or strongly coupled cavity resonance occurred.

The next step was to determine if the power spectra for the pressure measurements would collapse to a curve similar to Figure 20 when normalized in a similar way. (In Figure 20, P(f) is pressure spectral density, f is frequency, U is free-stream velocity, q is dynamic pressure, and δ^* is boundary layer thickness.) If so, there would be strong evidence that the measured pressures were due to boundary layer turbulence, or something directly proportional to it.

The difficulty was to choose normalizing factors to apply to the bay data. It was decided to replace the parameters U, q, δ^* by V, q, D (V is aircraft speed, q is dynamic pressure, D is transducer diameter).

The pressure data for all pressure transducer and microphone measurements for straight and level flight conditions were normalized as shown in Figures 21 through 24. In these figures, rms pressure values are shown plotted against dynamic pressure with a regression line fitted to the data. The normalized pressure spectra are presented as a spread where the gray area is the range of the maximum to minimum values observed at each frequency, and the dark line is the approximate mean of the values observed at each frequency (note that the mean is not necessarily the middle of the range). Keeping in mind the random errors introduced during the data reduction, it is seen that the pressure data do scale reasonably well using the variables of boundary layer turbulence. Had the pressure data been due principally to strong modal resonances of the cavity, the spectra would not have collapsed as well as they did.

The pressure data were also investigated for a Mach number dependence. This was done by dividing the rms pressure values by q and plotting the resulting normalized rms values versus Mach number. In some cases, slight trends of rms/q appeared to be present, but the trends were not considered significant compared to the data scatter. A summary table of rms pressure levels is presented in Table 1.

On the basis of the above studies, it is concluded that the pressure field in the bay is due primarily to random boundary layer pressure driving many acoustic modes of the cavity. The amplitude of the measured rms pressure is approximately 10 to 15 db higher than that predicted by flat plate theory, but this can be accounted for by the resonant amplification by the cavity modes.

The pressure spectra for the microphones were generally processed only to 2000 Hz. The data were checked above 2000 Hz, and displayed a characteristic rapid drop off to 10,000 Hz.

Data were also measured for closed aircraft bay doors, but were not processed, however, due to their extremely low magnitudes.

An evaluation of the pressure data was performed using cross-correlation analysis. For the original missile load predictions, it was assumed that the pressure field acting on the missile structure was perfectly correlated (a correlation coefficient of unity at zero time delay) from one point to another. It was of interest to check the validity of this assumption using the actual measured pressure data. Such checks were made by computing the cross-correlation coefficient for the pressure measurements between various selected points. The results are presented in Figures 25 and 26. Definite correlation was exhibited between the pressures at stations 131.62 and 151 on the left side of the missile (a separation of 19.38 inches). The correlation coefficient was 0.35 for one flight and 0.2 for another. In both cases, the correlation peaks occurred at a time delay of about ±3 milliseconds. This means that from 20% to 35% of the excitation power at station 131.62 appeared some 3 milliseconds later at station 151, and vice versa. The correlation peaks are approximately symmetric about zero time delay. The cross-correlation function between the pressures at two points in a turbulent boundary layer on a smooth structure would generally be asymmetric about zero time delay. This implies that, although the boundary layer was the basic source of excitation, the pressure field inside the bay cavity was significantly modified by the acoustic resonant modes of the cavity.

Referring again to Figures 25 and 26, significant correlation was also exhibited between the pressures on the bottom and the right side of the missile at station 35.7 (a separation of 11 inches). The coefficient was about 0.3 with a zero time delay. This indicates that the pressure field was instantaneously correlated at points around the circumference of the missile at any given station, as would be expected.

The other measured cross-correlations were for points separated by 50 inches or more. No significant correlation peaks are indicated. In summary, it appears that the spatial correlation characteristics of the pressure field on the missile diminished with distance to a correlation of about 0.3 at 20 inches separation, and to a negligible correlation coefficient at more than 50 inches separation.

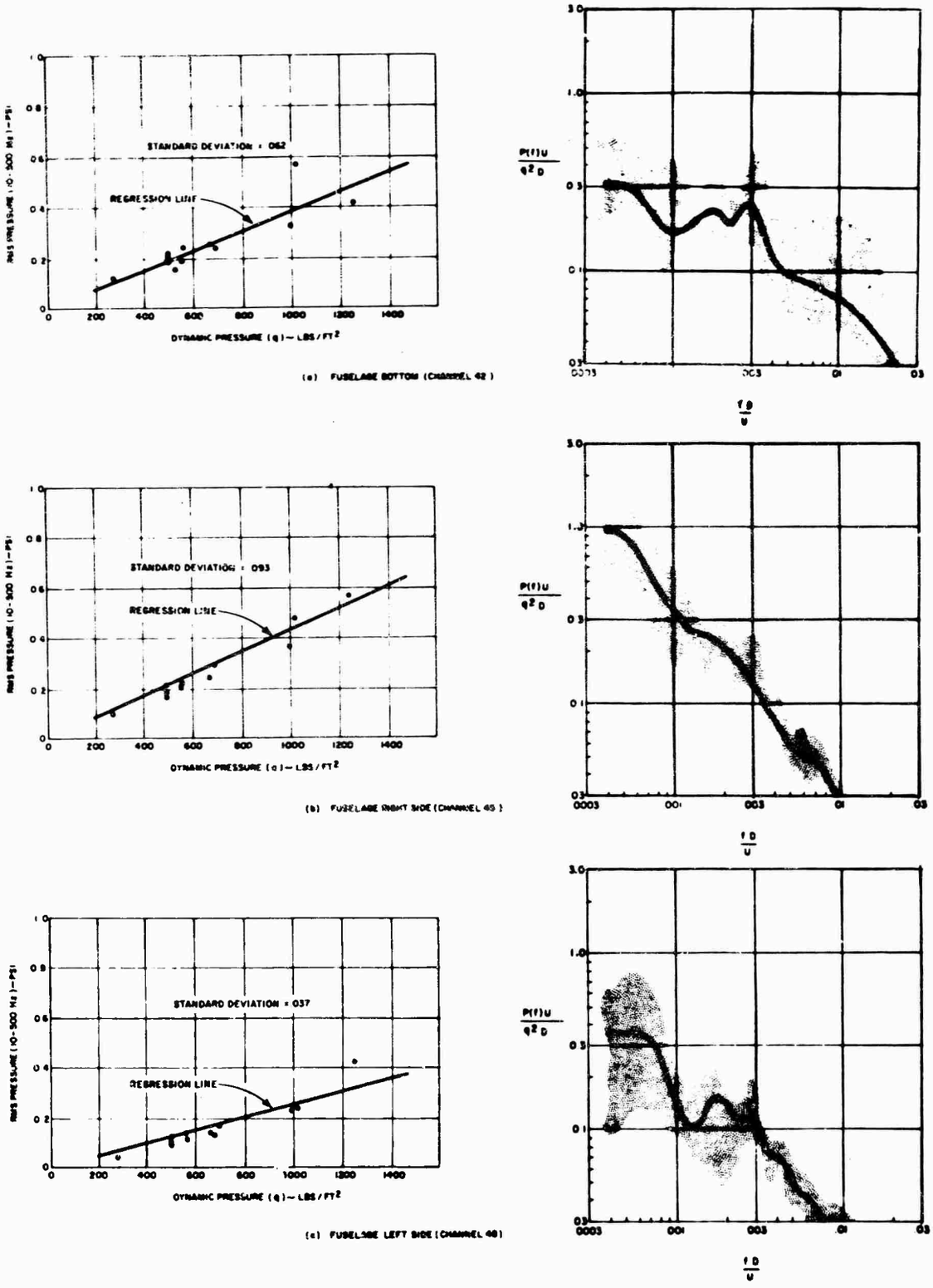

Figure 21 - RMS pressure and nondimensional pressure spectra measured at the fuselage surface at missile station 35.7

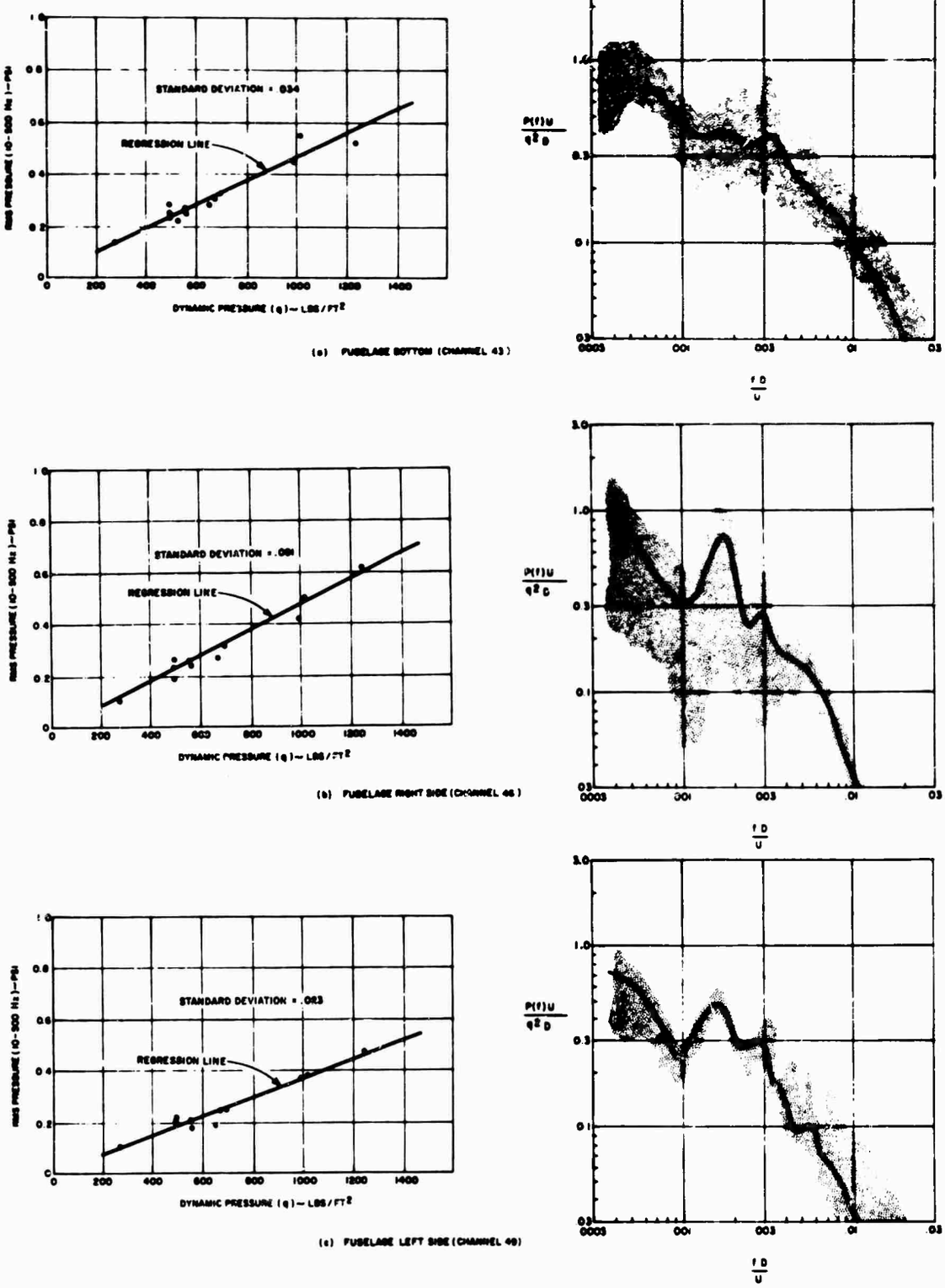

Figure 22 - RMS pressure and nondimensional pressure spectra measured at the fuselage surface at missile station 85.82

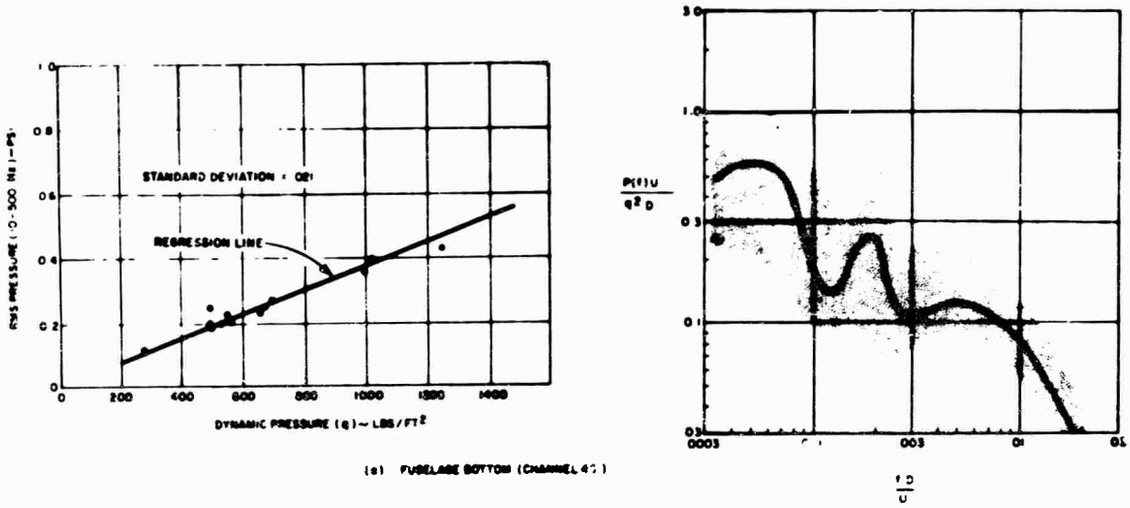

(a) FUSELAGE BOTTOM (CHANNEL 41)

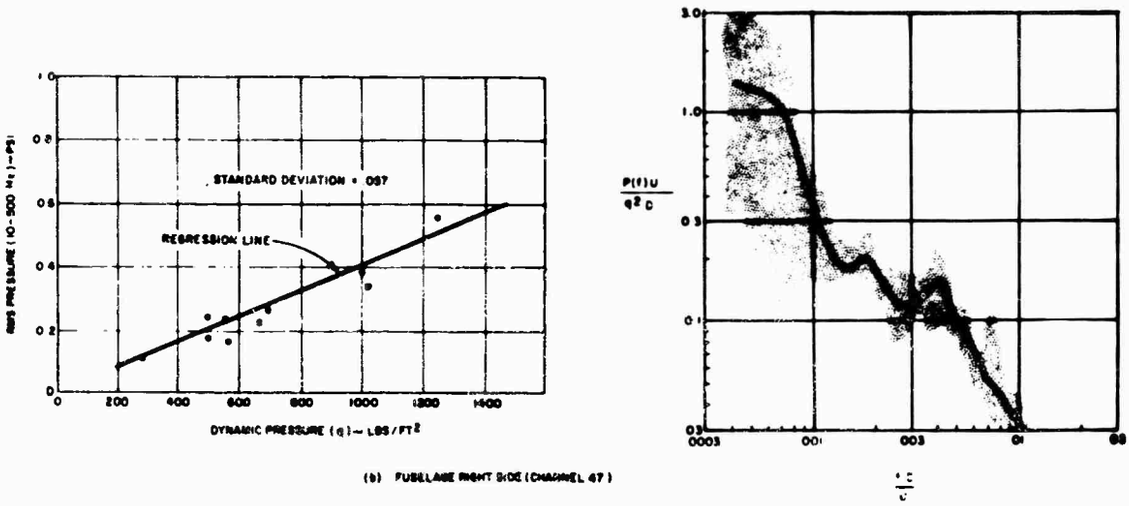

(b) FUSELAGE RIGHT SIDE (CHANNEL 47)

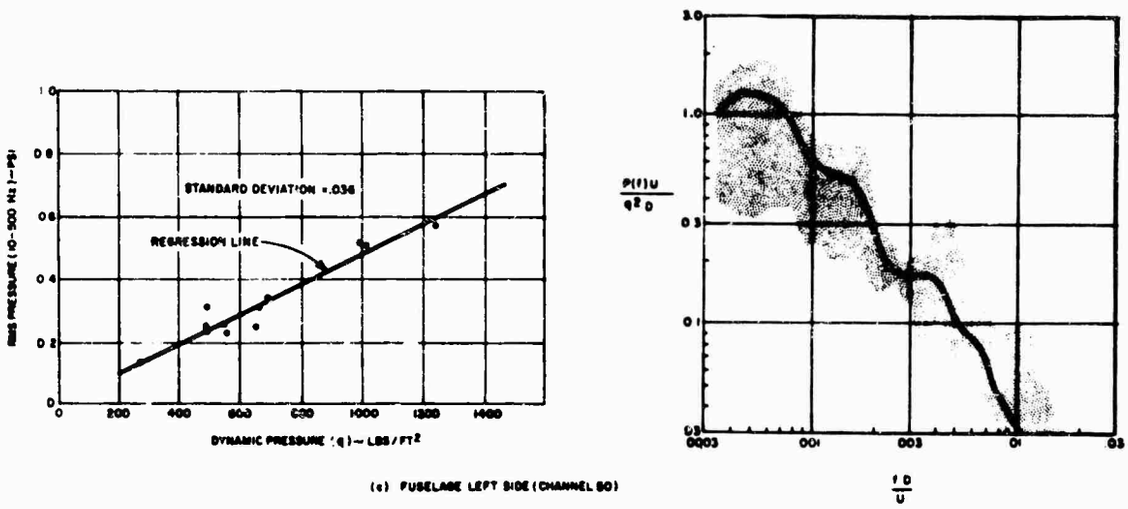

(c) FUSELAGE LEFT SIDE (CHANNEL 60)

Figure 23 - RMS pressure and nondimensional pressure spectra measured at the fuselage surface at missile station 131.62

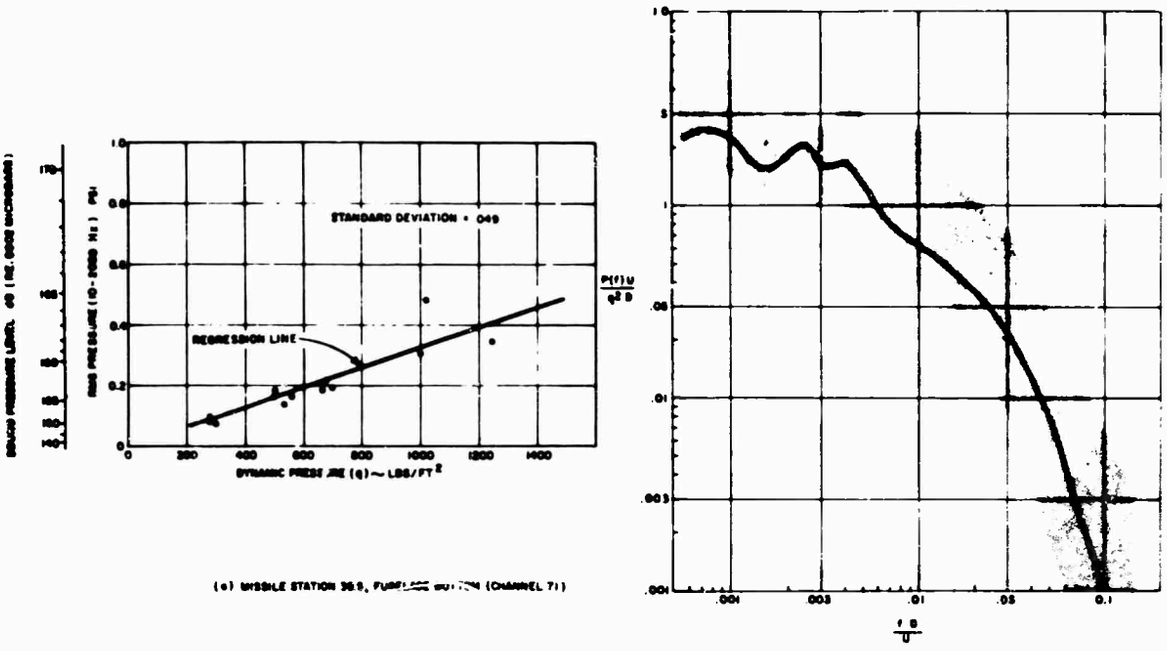

(a) MISSILE STATION 369, FUSELAGE [illegible] (CHANNEL 71)

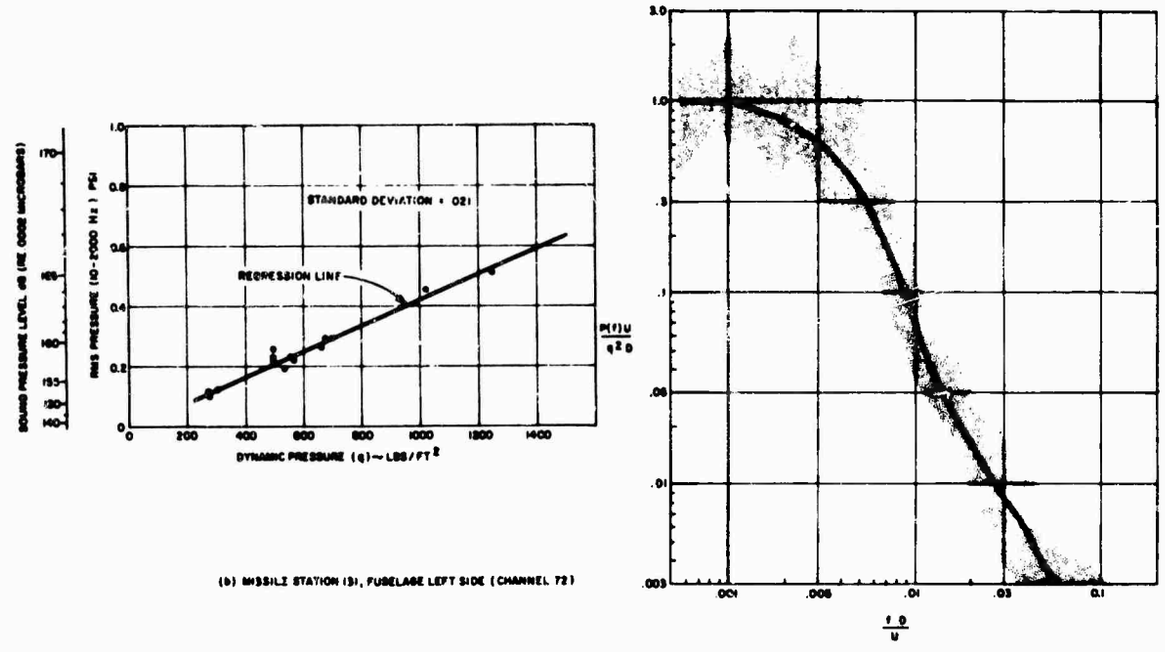

(b) MISSILE STATION 131, FUSELAGE LEFT SIDE (CHANNEL 72)

Figure 24 - RMS pressure and nondimensional pressure spectra for the microphones at the missile fuselage

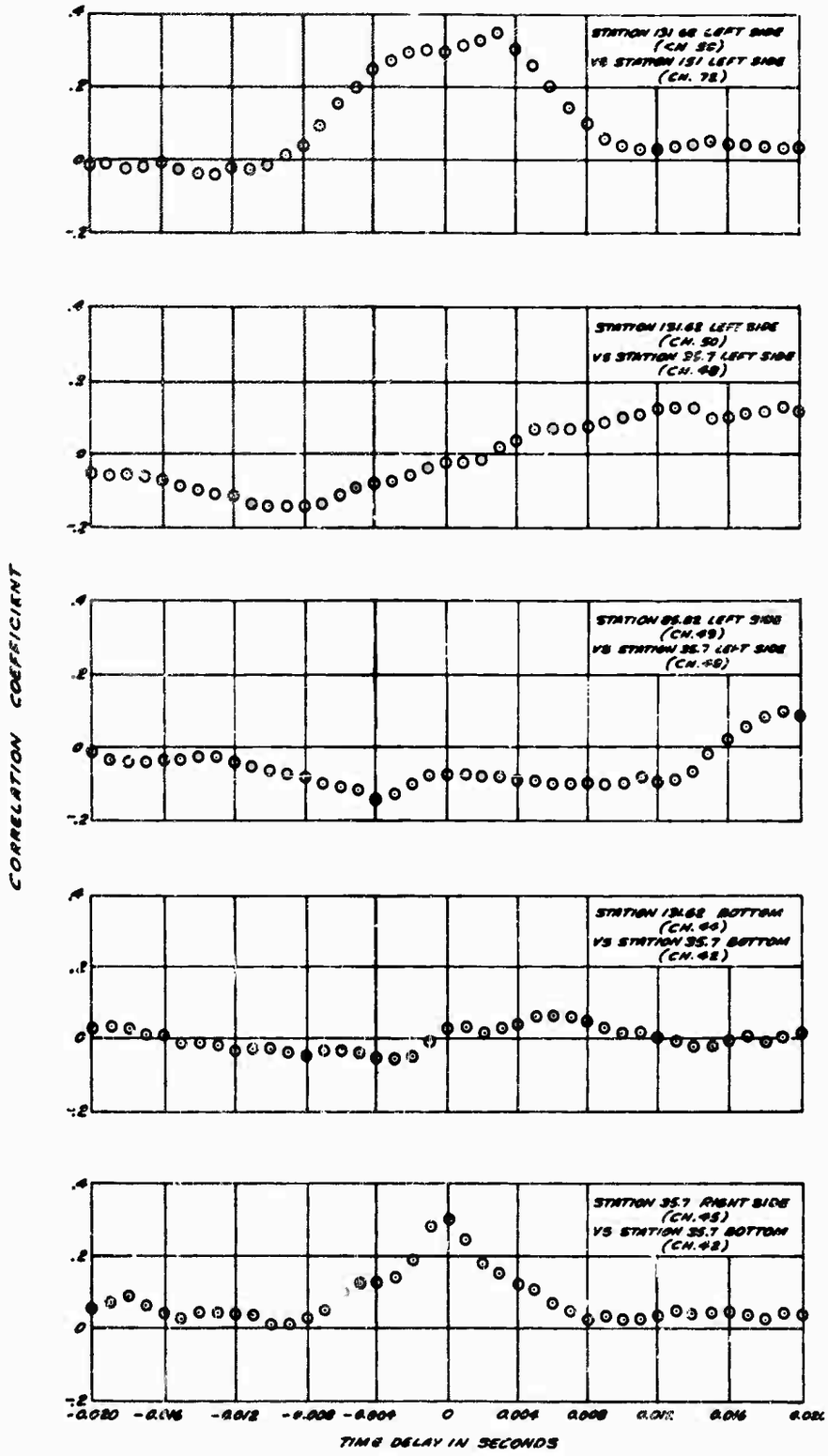

Figure 25 - Cross correlation of pressures at the missile fuselage for flight condition 67-6-3

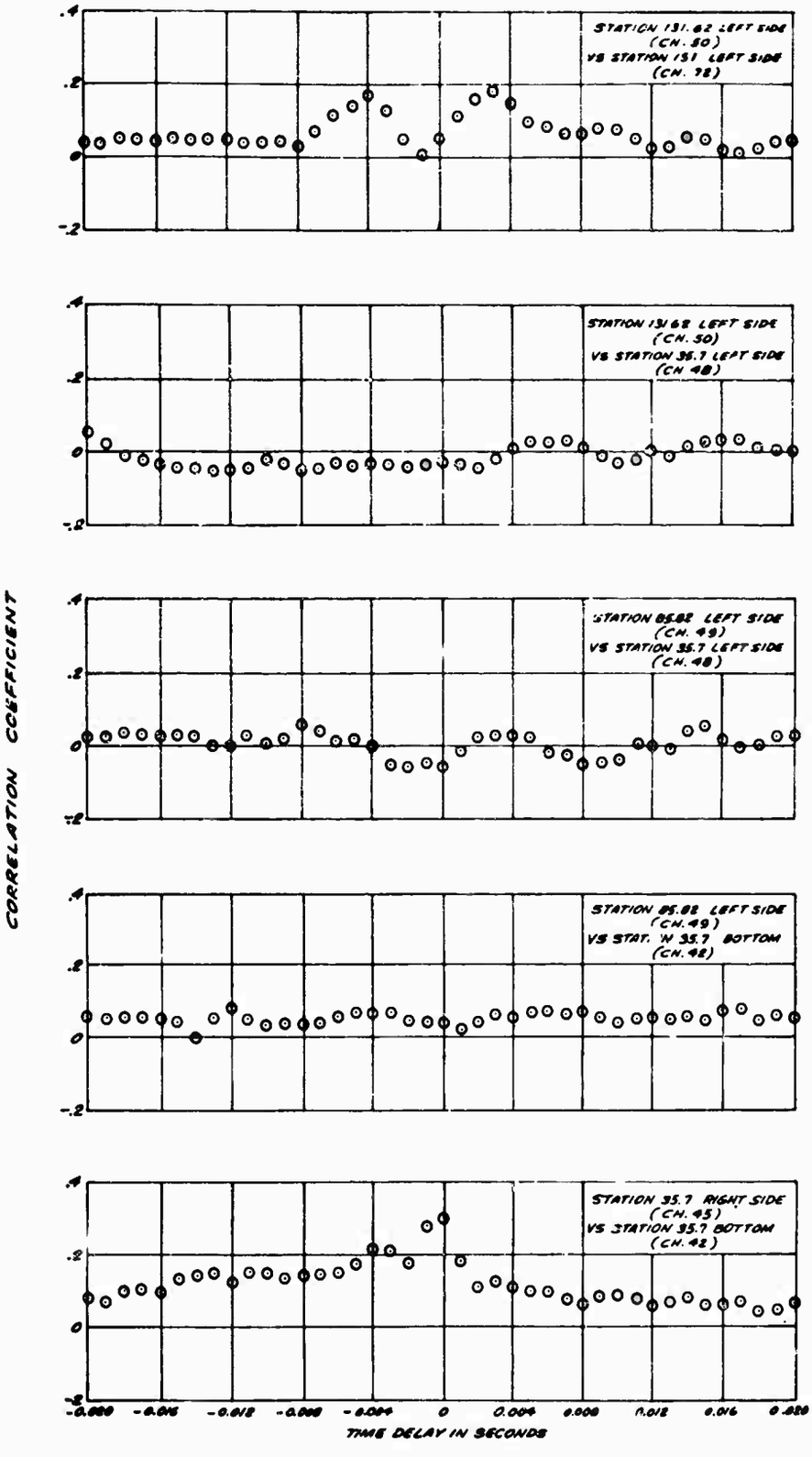

Figure 26 - Cross correlation of pressures at the missile fuselage for flight condition 67-9-5

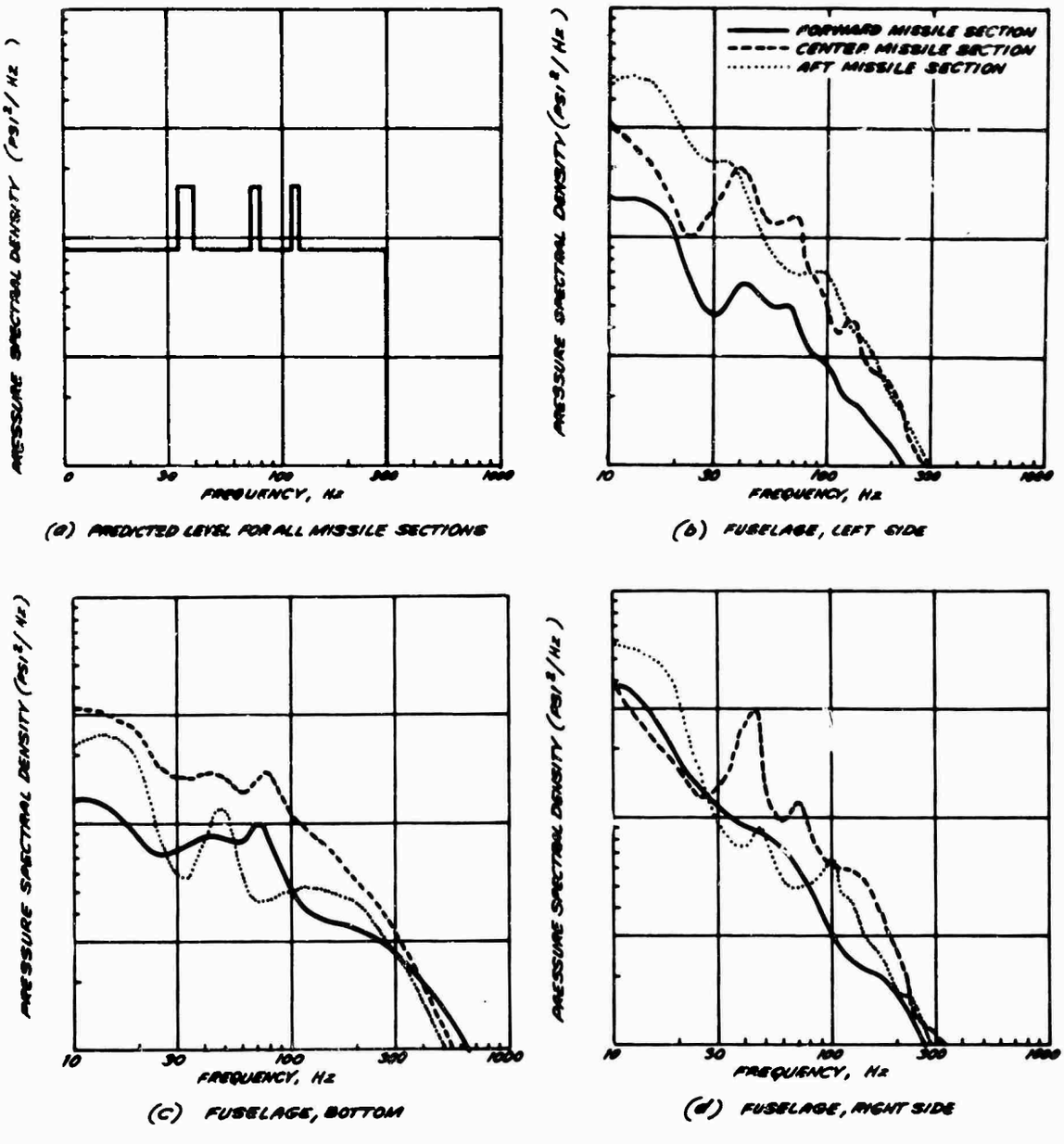

Figure 27 - Comparison of predicted bay pressure spectral density with mean data measured at the missile fuselage surface for oscillatory pressure design conditions

TABLE 1
Summary of RMS pressures

FLIGHT NO.	AIRCRAFT PARAMETERS: ALTITUDE h FEET	MACH NUMBER	DYNAMIC PRESSURE q (LBS/FT²)	AIRCRAFT ANGLE OF ATTACK DEGREES	WING SWEEP ANGLE Λ DEGREES	STRAIN GAGE PRESSURE DATA RMS PRESSURE PSI RMS (5 - 500 Hz): CH 42	CH 43	CH 44	CH 45	CH 46	CH 47	CH 48	CH 49	CH 50	MICROPHONE DATA RMS PRESSURE PSI RMS (5-2000H⁻): CH 71	CH 72
67-1-1	38780	.97	300	4.5	50	—	—	—	—	—	—	—	—	—	.076	.125
67-1-5	17120	.60	280	4.3	26	—	—	—	—	—	—	—	—	—	.089	.114
67-2-1	2000	.45	250	5.8	26	.122	.133	.112	.102	.112	.102	.051	.102	.133	.099	.114
67-2-8	29430	1.10	535	7.85	72	.163	.214	.194	—	—	—	—	—	—	.140	.162
67-2-5	36000	1.30	565	6.57	72	.245	.245	.165	.224	.245	.163	.122	.173	.224	.166	.221
67-3-1	17000	.65	557	3.5	30	.184	.288	.224	.214	.255	.235	.143	.204	.255	.166	.230
67-3-2	17000	.55	896	5.8	50	.245	.316	.265	.296	.316	.265	.173	.245	.337	.198	.296
67-3-3	10000	.70	500	3.6	50	.224	.275	.240	.216	.285	.235	.133	.214	.306	.188	.260
67-3-5	2000	.60	500	.6	50	.214	.245	.184	.184	.235	.173	.112	.184	.245	.172	.229
67-6-1	2000	.85	995	3.6	50	.337	.438	.357	.367	.416	.388	.234	.367	.510	.304	.398
67-6-5	2000	.95	1245	2.83	72	.416	.510	.426	.561	.612	.548	.416	.488	.561	.344	.510
67-6-5	2000	.70	675	6	50	.255	.296	.245	.245	.275	.224	.153	.245	.306	.214	.292
67-7-2	10000	.70	500	⊕⊕⊕	26	.194	.250	.189	.163	.194	.163	.102	.184	.234	.174	.224
67-7-5 ⊕	10000	.70	500		26	.204	.367	.204	—	—	—	.112	.245	.204	.186	.254
67-8-2 ⊕	17000	1.15	1020		72	.632	.550	.570	.530	.653	.367	.255	.428	.520	.470	.435
67-8-3 ⊕⊕	17000	1.15	1020		72	.551	.561	.367	.572	.643	.347	.286	.377	.460	.435	.398
67-6-1 ⊕⊕	10000	.70	500		26	.204	.265	.204	.194	.234	.163	.112	.204	.245	.181	.236
67-6-2	22000	1.05	660		72	.194	.275	.230	—	—	—	.143	.184	.246	.188	.260
67-8-5 ⊕	22000	1.05	660		72	.214	.316	.306	—	—	—	.133	.184	.275	.210	.276
67-9-4 ⊕⊕	22000	1.05	660		72	.184	.265	.234	.255	.265	.224	.133	.194	.263	.210	.262
67-6-5	17000	1.15	1020		72	.372	.540	.398	.480	.500	.336	.240	.378	.500	.488	.452

⊕ 0.5 g PUSHOVER MANEUVER ⊕⊕ 2.5g PULLUP MANEUVER ⊕⊕⊕ DATA NOT AVAILABLE FOR FLIGHTS 67-7-2 THROUGH 67-8-5

TABLE 2
Comparison of Predicted Bay Missile Oscillatory Pressure Design Levels with Measurements on the Missile Fuselage

Missile Location	Random Pressure Levels, dB (Re 0.0002 Microbars) 2 - 500 Hz			
	Predicted Level (All Sections)	Left Side	Bottom	Right Side
Forward Missile Section	165	162.7	166.2	167.2
Center Missile Section	165	165.8	168.1	168.2
Aft Missile Section	165	168.1	166.1	166.9

The pressure data in Table 1 shows that forward of the wing, high rms pressures occur on the side of the missile near the bay walls, whereas aft of the wing the high rms pressures occur near the bay centerline. For straight and level flight, the pressures on the missile adjacent to the bay opening were usually greatest near the forward wing attachment. In all cases, pushover maneuvers caused these pressure levels to increase. The microphone data showed higher pressure readings usually occurring at the aft portion of the missile radome bulkhead near the bay opening. Photographs of the tufts within the bay indicated for many flight conditions forward flow within the bay near the bay floor.

COMPARISONS WITH PREDICTIONS

The measurements during these flight tests provided data needed for the refinement of initial unsteady pressure predictions and the upgrading of missile and launcher structural design criteria. The oscillatory pressure environment for design of the PHOENIX in the F-111B bay is illustrated in Figure 27a. Figure 27b, c, and d show measured pressure spectral density data, extrapolated to the same design condition. The data tend to be much higher than the predicted levels at the low frequencies, and drop off to lower levels at the higher frequencies. In the frequency band of major fuselage resonances, the measured oscillatory pressure spectra are generally 1.5 to 2 times the predictions. Overall random pressure levels are compared in Table 2 for a selected condition. The levels change with location on the missile, but generally they are quite close to the predicted overall level.

In general, there was basic agreement between dynamic loads measured and predicted. Errors in predicting the magnitude and spectral density of the pressures along the missile for loads studies were compensated by conservative estimates for the spatial coherence. The bending and torsion loads on the control surface near the bay floor and centerline were 10-15% higher than predicted while the measured values on the other three control surfaces were generally less than predicted. The resultant of the vertical and lateral fuselage bending moments were close to predicted moments. A direct comparison of predicted and measured wing bending moments could not be made since the measurements were taken on a wing whose fuselage attachment was different from that analyzed. No structural damage to the missile occurred during the flight test program even though the total time the bay doors were open was several times that required for missile design.

CONCLUSIONS

The paper has described the captive flight measurements program of a PHOENIX missile in the weapons bay of an F-111B aircraft, the approach used to make early estimates of the fluctuating pressure field, and the recent measurements. The major conclusions are as follows:

1. The design concept of the PHOENIX missile measurement system being self-contained and dependent on the mother aircraft only for power and on/off control was proven to be a good approach.

2. The PHOENIX T-20 bay measurements program was highly successful in both quantity and quality of data acquired.

3. The criteria used to predict the unsteady pressures in the F-111B bay and to establish PHOENIX design loads were adequate for that design but may not apply for other missiles or other bays.

4. A more refined analytical-experimental approach needs to be developed to estimate the dynamic loads and vibratory responses for missiles housed in an open weapons bay.

ACKNOWLEDGEMENTS

The writers of this report wish to acknowledge the help of those members of the Space Systems Division, Flight Test Division, Aeronautical Systems Division, and the Missile Systems Division of Hughes Aircraft Company who contributed to the success of this program.

REFERENCES

1. "XAIM-54A T-20/F-111B Weapons Bay Environmental Measurements Post Flight Evaluation Report" by T. M. Kiwior and R. P. Mandich, TPM Section R-3.3.2.3.1, 1 April 1968.

2. "Success and Failure with Prediction and Simulation of Aircraft Vibration" by A. J. Curtis and N. G. Tinling, Shock and Vibration Bulletin 39 (to be published).

3. "Captive Missile Response Due to Random Pressures" by H. L. Leve, pg. 698-709, from Symposium Proceedings: Structural Dynamics of High Speed Flight, ACR-62, Volume I, Aerospace Industries Associated (Office of Naval Research), Los Angeles, California, April 1961.

4. "A Theoritical and Experimental Investigation of the Acoustic Response of Cavities in an Aerodynamic Flow", WADD-TR-61-75, by H. E. Plumbee, J. S. Gibson, L. W. Lassiter, March 1962.

5. "PHOENIX Missile Response Report" by R. J. Oedy and J. B. Yows, PMS-49/2222, July 1965 (Conf).

Mr. Mustain (McDonnell Douglas Corp.): The question I have is on correlation. Did you make a check to see what happened to the vibration responses in the missile along with the correlation? For instance, if you had a correlated field, were the vibration levels greater or could you make any distinction there at all?

Mr. Mandich: Are you talking about the measurements or the original predictions?

Mr. Mustain: The actual measurements - not the predictions. Did you have a higher vibration level on your accelerometers in a correlated field or an uncorrelated field?

Mr. Mandich: We measured the correlation that actually occurred in the bay. The correlation was about 0.3 for close separations and then it dropped off with distance. We were using actual measurements so we did not have fully correlated or fully uncorrelated fields. We did the original analysis from missile loads- we made those two limiting cases.

Mr. Mustain: You still did not answer my question. In correlation studies it is quite often said that in most cases the response is with a correlated field. But this is not always the case and here you have an example of actual measurements. It is hard to find actual measurements of correlated fields and check against the vibration. You have a vibration data, and you have measurements for the acoustic correlation. You can look at the data to see if the correlated field or the uncorrelated areas give you a greater response.

Mr. Mandich: We have not gone back to check.

Mr. Mustain: I would suggest you do it and I would certainly like to know how your answers come out.

LUNAR ORBITER FLIGHT VIBRATIONS WITH COMPARISONS TO FLIGHT ACCEPTANCE REQUIREMENTS AND PREDICTIONS BASED ON A NEW GENERALIZED REGRESSION ANALYSIS

By Sherman A. Clevenson
NASA Langley Research Center
Langley Station, Hampton, Va.

This paper presents detailed flight-measured vibration data obtained during the five successful flights of the Lunar Orbiter and compares these data with vibration levels specified as flight acceptance requirements. These data are also compared with predictions based on results of a recently developed regression analysis of vibration data compiled for a number of major launch vehicles. It is shown that the flight acceptance requirements were adequate but due to unexpectedly low random vibration flight inputs, the random acceptance requirement is considered severe. For establishing vibration requirements utilizing a proven launch vehicle, the regression analysis does not provide as good as a basis as does flight vibration measurements from prior flights of the launch vehicle. However, the regression analysis may be useful in estimating vibration levels for new and untried launch vehicles.

INTRODUCTION

Five successful Lunar Orbiter spacecraft were launched during the period of August 6, 1966, through August 1, 1967, whose mission was to secure topographic data of nearly all of the moon's surface. Prior to their flights, the spacecraft underwent qualification and flight acceptance tests. During their flights, the spacecraft were subjected to environmental inputs from the launch vehicle, one of the most severe being vibration. During each flight, vibration measurements were continuously obtained using accelerometers which allow the determination of peak vibrations for critical conditions of lift-off, transonic speeds, booster engine cut-off, booster engine staging, sustainer engine cut-off, vernier engine cut-off and horizon sensor fairing ejection, shroud jettison, Atlas-Agena separation, Agena first and second ignition and burnout, and spacecraft separation.

The purpose of this paper is to present results of the analyses of the flight vibration measurements and to compare these data to flight acceptance test requirements. In addition, these data are compared with the results of a recently developed regression analysis technique for predicting random vibration levels for any spacecraft.

SYMBOLS

a	indication of low signal amplitude or less than 2 cycles for frequency analysis
b	indication of no available data
c	indication of a pulse peak amplitude
d	indication of the changeover from accelerometers to position indicators
C	damping
C_{cr}	critical damping
f	frequency, Hz
FAT	flight acceptance tests
g	acceleration
g_{peak}	peak acceleration
g_{p-p}	double amplitude acceleration
g^2/Hz	acceleration squared per Hz
G(f)	average power spectral density;

$$G(f) = b_1(f)x_1 + b_2(f)x_2 + \ldots b_N(f)x_N = \sum_{i=1}^{N} b_i(f)x_i$$

b_i	ith coefficient
$f(x)_i$	ith variable parameter
Hz	hertz, cycles per second
rms	root mean square
sec	seconds
t	time, sec
Q	amplification factor
λ	logarithmic decrement

PROJECT DESCRIPTION

The Lunar Orbiter spacecraft were launched by Atlas-Agena-D launch vehicles (supplied by General Dynamics Corporation and Lockheed Missile and Space Company, respectively) under the overall project management of the Boeing Company, which, in turn, was under contract to NASA-Langley Research Center. Each spacecraft weighed a nominal 380 kilograms (853 pounds), and in its flight configuration, with all elements fully deployed (see fig. 1), spanned 5.21 meters (17.1 feet), and was 2.08 meters (6.83 feet) high.

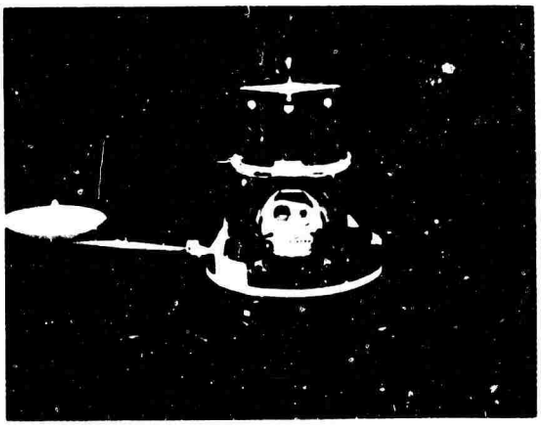

Figure 1.- Lunar Orbiter spacecraft.

Flight Acceptance Test Requirements

The philosophy for the flight acceptance test (FAT) requirements for Lunar Orbiter was that the input test levels to the spacecraft be as high as any that would be experienced in flight. This is in contrast to a sometimes used philosophy of FAT requirements to test at very low levels to assess workmanship in construction. If the spacecraft to be flown can successfully withstand the expected flight environment before flight, one can have considerable assurance that it will withstand the actual flight environment. It should be understood that a prototype spacecraft would have had prior qualification tests at levels which were higher than FAT requirements to show that the design was adequate.

Sinusoidal vibrations.- The sinusoidal test levels pertaining to the Flight acceptance Test (FAT) were basically derived from a detailed review of about 25 previous Atlas and Thor-Agena flights. (Since the time that the FAT levels were established, considerably more data have been compiled by the Lockheed Missile and Space Company and are found in ref. 1.) The flight data from only six flights which had the greatest vibration levels were used as the bases for determining shock spectra response levels for Q's of 5, 10, and 30. Q is the amplification factor of the response of a mass of a single-degree-of-freedom system and is equal to $C_{cr}/2C$, the ratio of the critical damping to twice the damping of the system ($C_{cr}/2C = 1/2\lambda$). To obtain the equivalent sinusoidal test levels for the system with these assumed Q's, the response values from the shock spectrum results were divided by the Q used, namely 5, 10, and 30. The resulting equivalent sinusoidal spectrum levels were statistically evaluated to determine the 95 percent levels, and since these values were determined from only six flights, they were enveloped. In order that essentially all damped systems be subjected to flight vibration levels, the enveloped Q = 5 lines were used as the basis of the Flight Acceptance Test (FAT) levels. Because of the limited data and since only a single-degree-of-freedom system was considered, an uncertainty multiplying factor of 1.25 was applied to obtain the FAT requirements. These resulting FAT levels for both the longitudinal and transverse directions are compared with flight results in a later section.

Random vibrations.- The flight acceptance test requirement for random excitation was

determined from an enveloping of the power spectral density plots derived from flight data of previous Agena flights for both lift-off and transonic speeds. Only one test for both lift-off and transonic speeds was required at these test levels. It was expected that the overall rms acceleration level would be very conservative. It was also expected that the shape of the random test spectrum would agree with subsequent flight data. This conservatism is not too objectionable for test purposes in that the spacecraft acts as its own filter and responds primarily at its own resonances.

Flight Vibration Measurements

All vibration data were transmitted continuously on channels utilizing the telemetry of the Agena vehicle. A total of eight accelerometers were used (see fig. 2): four were mounted near the Agena forward ring (approximately

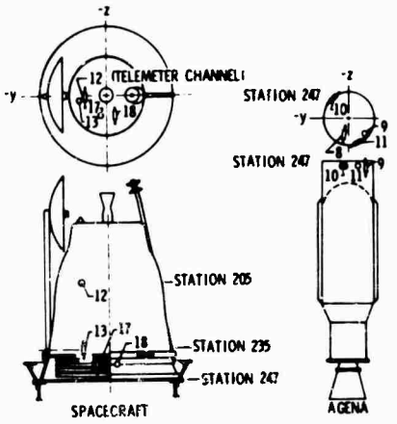

Figure 2.- Accelerometer locations. Spacecraft in undeployed condition.

TABLE 1.- Flight Instrumentation List

Telemetry Channel Number	Direction of Measured Acceleration	Location	Accelerometer Frequency Response (cps)	Accelerometer Calibration Range (g's)	Channel Frequency Response* (cps)
8	Transverse	Agena Forward Ring	0-45	±5	45
9	Longitudinal	Agena Forward Ring	0-60	-4 to +12	60
10	Tangential	Agena Forward Ring	0-80	±5	80
11	Tangential	Agena Forward Ring	0-110	±5	110
12	Transverse	Spacecraft	5-800	±10	160
13	Longitudinal	Spacecraft	5-1100	±10	220
17	Longitudinal	Spacecraft Adapter	20-2000	±20	790
18	Transverse	Spacecraft Adapter	20-2000	±20	1050

*With standard filters

station 247) to measure the longitudinal, tangential and transverse responses; two were installed in the spacecraft adapter (approximately station 238) to measure longitudinal and transverse excitation, and two were installed within the spacecraft, one to measure longitudinal acceleration at the foot of the photosubsystem (approximately station 235) and one to measure transverse accelerations at the base of the oxidizer tank (approximately station 205). The same two accelerometers in the spacecraft were used both during FAT and during flight. The flight instrumentation list is given in table 1 in which the acceleration telemeter channel, direction of response, location, accelerometer frequency response and calibration range and telemeter frequency response using standard filters are given. For the analyses of Lunar Orbiter vibration data, the standard filters were replaced with filters that had twice the frequency band width characteristics of the standard filters.

Data Analyses

The method of data analysis utilized depended on the desired form of the results. The real time analog data of instantaneous vibration level as a function of time were obtained by recording the instantaneous levels on oscillograph records. Amplitudes were determined from the calibrations, and frequencies could be determined to over 1000 Hz. To obtain power spectral density values and shock spectra, the data were digitized at the rate of 8,000 and 7,000 samples per second, respectively, and stored on magnetic tape. The tapes were used as inputs to a digital computer program to obtain auto-correlation, probability density, and power spectra functions and to a separate program to obtain shock spectra.

REGRESSION ANALYSIS-TECHNIQUE FOR PREDICTING VIBRATION LEVELS

The Measurement Analysis Corporation, under contract to Langley Research Center, recently developed a new procedure for predicting the random vibration environment for generalized spacecraft. The method utilizes a regression analysis of flight vibration data previously compiled by Langley for all major launch vehicles. Previous studies of this type have been made for aircraft and captive airborne missiles. Mahaffey and Smith (ref. 2) presented one of the earliest documented procedures followed by Brust and Himmelblear (ref. 3) and Curtis. Piersol and Van Der Laan developed a general prediction rule for all classes of military aircraft. The current study included data from the following vehicles: Agena (excluding Lunar Orbiter); Atlas (E and F series); Minuteman; Saturn I; Thor; Thor/Asset; Thor/Delta; Titan I, II, IIA, and IIIC. The data are generally in the form of power spectra for lift-off, Mach 1, and maximum dynamic pressure. The basic approach used assumed that the power spectrum for the vibration environment in a spacecraft can be described by a linear equation of the form

$$G(f) = b_1(f)x_1 + b\ (f)x_2 + \ldots b_N(f)x_N = \sum_{i=1}^{N} b_i(f)x_i$$

where $G(f)$ is the average power spectral density, b_i is the coefficient of the i^{th} parameter, and $(f)x_i$ is the i^{th} parameter being used to describe the vibration. Studies have been made for both the thrust and transverse axes. The primary parameters which the analysis determined as significant are air density, nozzle exit area, exhause gas velocity, ambient and local speeds of sound, surface weight density, and dynamic pressure. Prediction curves with a 97.5 percent upper prediction limit for space vehicle vibration on basic structure have been established for lift-off, transonic flight, and maximum dynamic pressure conditions. The actual power spectrum may have peaks which exceed the octave band averages by a wide margin. However, past studies of average power spectra in octave bands versus narrow band power spectra indicate that most spectral peaks will be no more than 7 db higher than the octave band average. Details of this analysis are given in reference 4.

RESULTS AND DISCUSSION OF FLIGHT MEASUREMENTS

The results and discussion will be presented in two sections. The first section will concern real time measurements of acceleration levels and frequencies at various times during the launch phase. Random vibrations will also be discussed. The second section will contain comparisons of flight measurements with flight acceptance test levels and with the results of predictions based on the regression analysis.

Real Time Measurements

Flight time history.- Nominal flight time histories for the eight accelerometers are given in figure 3 for the first 400 seconds of flight (through Agena first ignition).

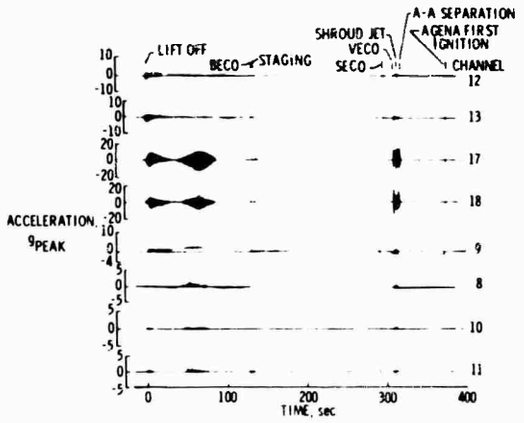

Figure 3.- Nominal flight time history.

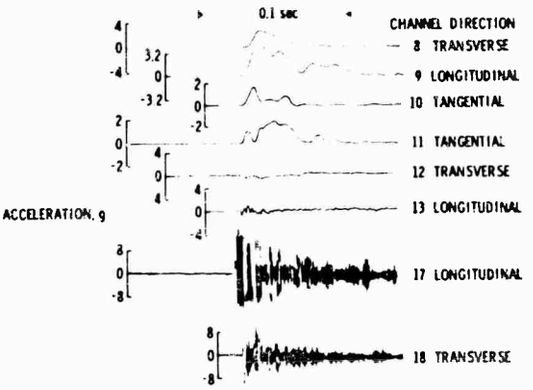

Figure 4.- Response at Atlas-Agena separation. Lunar Orbiter V.

The time scale is too compressed for accurate analyses of the data. However, the responses are as expected with bursts of acceleration occurring on the record. Some of the significant flight events are indicated. The traces are identified by telemeter channels which are listed in table 1. Channels 17 and 18, the longitudinal and transverse accelerometers in the adapter, were responsive to the higher frequencies and indicated the largest vibrations. Acceleration magnitudes and frequencies obtained from high-speed oscillograph recordings will be discussed in the next section.

Peak vibration levels at significant events.- During the launch phase of the Lunar Orbiter flights, vibration levels and predominant frequencies were determined for the following events:

Lift Off
Transonic Speed
Booster Engine Cut Off (BECO)
Booster Engine Staging (BES)
Sustainer Engine Cut Off (SECO)
Vernier Engine Cut Off (VECO) and Sensor Fairing Jettison
Shroud Jettison
Atlas-Agena Separation
Agena First Ignition
Agena First Burn-Out
Agena Second Ignition
Agena Second Burn-Out
Agena Lunar Orbiter Spacecraft Separation

From table 2, it may be noted that peak vibration levels and response frequencies are reasonably similar for these events from flight to flight for the five flights of Lunar Orbiter.

Figure 4 shows the representative responses of the accelerometers on Lunar Orbiter V at Atlas-Agena separation. It should be noted that 1000 cps oscillations and below may be easily determined. The peak-to-peak and pulse acceleration levels are determined from the calibrations. It is apparent from this representative example that only a few cycles of oscillation are available for determining response frequencies. The top four traces on figure 4 are good examples of pulses. In some instances, flight data were not available due to lack of appropriate flight magnetic tapes or due to electronic difficulties either in the original tapes or in the recovery of the data. For example, on the flight tapes of Lunar Orbiter I from all receiving stations there were no data on channel 12 until the channel was switched to another transducer. Prior to Agena-Lunar Orbiter spacecraft separation, telemeter channels 9, 12, and 13 were switched to dash-pot type position indicators to record the spacecraft separation. Thus, no vibration data were recorded for this event on these three channels. In addition, since the telemeter was in the Agena, no further vibration information was available from the spacecraft.

Random vibrations.- From figure 3, it was noted that high vibration levels for more than a few seconds occurred at lift-off and then again at times 55 to 65 seconds of flight. These levels are attributed to random excitation: at lift-off the vibration is attributed to acoustic coupling and at 55-65 seconds (transonic speeds) the vibration is attributed to aerodynamic buffeting.

Power spectral density analyses were made for telemeter channels 12 and 13 in the

TABLE 2
Amplitudes and Approximate Frequencies of Flight Transients

Lunar Orbiter	I		II		III		IV		V	
Item / Channel	g_{p-p}	f	g_{p-p}	f	g_{p-p}	f	g_{p-p}	f	g_{p-p}	f
LIFT-OFF										
8	2.5	3.0	1.4	5.5	0.5	a	b	b	0.6	5
9	0.7	a	1.6	42.0	0.5	a	b	b	1.1	5
10	1.0	a	0.9	82.0	0.5	a	b	b	1.0	a
11	1.0	a	1.2	570.0	1.5	a	b	b	1.0	a
12	b	b	3.1	5.5	0.5	a	b	b	1.7	a
13	1.0	520	1.9	400.0	1.5	a	b	b	1.4	5
17	14.0	1000	12.8	960.0	26.0	1000	b	b	17.0	1000
18	14.0	1000	10.5	960.0	10.0	1000	b	b	12.0	900
TRANSONIC SPEEDS										
8	2.8	3.0	0.9	29.0	2.5	a	1.8	a	2.4	a
9	1.3	a	2.0	34.0	1.5	a	1.2	a	3.0	a
10	1.0	56.0	0.8	a	0.5	a	1.4	a	1.0	a
11	1.3	91.0	0.6	a	0.8	a	1.0	a	1.3	a
12	b	b	0.6	a	a	a	0.1	a	0.7	a
13	0.8	500	1.7	a	0.6	400	0.3	400	0.7	a
17	12.0	1000	8.8	960.0	26.0	1000	14.0	1000	17.0	1000
18	12.5	1000	6.5	960.0	1[illegible].0	1000	7.0	1000	17.0	1000
BOOSTER ENGINE CUT-OFF										
8	1.1	9.9	0.1	62	a	a	0.3	a	0.3	a
9	3.9	a	0.9	15	a	a	1.2	15	0.7	a
10	1.9	66.0	0.9	63	1.0	64	1.4	61	1.7	65
11	2.3	66.0	1.2	63	1.6	67	1.7	62	2.0	65
12	b	b	0.5	a	1.0	a	0.7	a	0.7	a
13	3.0	1.2	0.7	34	1.0	a	1.4	59	1.4	19
	1.5	16.0	1.9	14	1.0	a	1.4	59	1.4	19
	1.0	65.0								
17	0.1	1000	0.2	960	0.5	a	0.5	1000	1.3	a
18	0.1	1000	0.4	960	0.5	a	0.5	1000	1.2	a
BOOSTER ENGINE STAGING										
8	0.5	a	0.5	38	0.5	a	0.6	a	0.7	38
9	0.4	a	0.5	32	0.3	a	0.7	35	0.5	38
10	2.5	390	1.2	69	0.5	a	0.9	71	0.7	a
11	3.0	390	1.0	35	0.9	a	0.8	71	[illegible].0	a
12	b	b	1.5	35	1.0	a	1.4	35	1.7	34
13	1.0	a	0.5	444	0.7	400	1.4	35	1.1	a
17	0.6	a	3.7	950	4.0	1000	1.7	1000	2.4	1000
18	0.6	a	1.4	950	2.0	1000	1.4	1000	1.7	a

TABLE 2.- Continued.

Lunar Orbiter	I		II		III		IV		V	
Item / Channel	g_{p-p}	f	g_{p-p}	f	g_{p-p}	f	g_{p-p}	f	g_{p-p}	f
SUSTAINER ENGINE CUT-OFF										
8	0.3	a	a	a	0.5	a	0.2	a	0.2	a
9	2.6	a	a	a	0.4	a	0.6	a	0.4	a
10	0.2	a	0.2	a	0.3	82	0.4	80	0.2	a
11	0.4	80	0.2	a	0.6	82	0.4	80	0.2	a
12	b	b	0.5	a	0.4	a	1.0	a	1.0	a
13	1.2	a	0.8	81	0.4	a	1.4	a	1.4	24
17	0.7	a	a	a	0.6	a	0.7	a	0.2	a
18	0.7	a	a	a	0.6	a	0.8	a	0.2	a
VECO AND SENSOR FAIRING JETTISON										
8	4.7	c	4.5	c	4.0	c	3.1	c	3.5	c
9	5.9	c	4.0	c	6.4	c	5.4	c	5.5	c
10	4.0	c	1.1	c	0.6	a	1.9	c	1.3	110
11	5.0	c	2.7	c	2.5	a	3.5	c	3.3	110
12	b	b	0.9	100	0.5	a	1.0	a	0.7	a
13	1.5	460	5.2	400	2.0	a	2.8	a	2.8	175
17	20.0	990	13.0	960	34.0	1000	29.0	1000	28.0	900
18	20.0	990	10.5	960	38.0	1000	31.0	1000	33.0	900
SHROUD JETTISON										
8	3.8	c	3.1	c	2.5	c	3.6	c	3.5	c
9	5.6	c	4.9	c	6.4	c	5.8	c	7.0	c
10	1.9	100	2.1	c	2.0	c	2.5	c	1.3	c
11	1.7	68	1.9	c	2.5	c	2.8	c	2.6	c
			3.0	133						
12	b	b	1.0	a	0.6	a	0.6	a	0.7	a
13	4.0	490	4.8	400	3.0	400	2.8	a	3.5	a
17	24.0	1000	36.7	960	38.0	1000	35.0	900	28.0	1000
18	24.0	1000	31.9	960	36.0	1000	32.0	900	14.0	1000
ATLAS-AGENA SEPARATION										
8	1.3	c	2.4	c	3.2	c	2.1	c	1.3	c
9	4.1	c	3.2	c	3.5	c	3.4	c	4.1	c
10	1.1	c	2.7	c	1.7	c	3.5	c	1.5	c
11	1.6	c	2.1	c	2.0	c	1.8	c	2.1	c
12	b	b	0.5	a	0.6	a	0.4	a	0.3	a
13	1.4	40	2.5	400	2.0	400	1.8	a	1.4	40
17	32.0	1000	36.7	960	38.0	1000	32.0	1000	32.0	1000
18	23.0	1000	23.8	960	36.0	1000	33.0	1000	23.0	1000

TABLE 2.- Continued.

Lunar Orbiter	I		II		III		IV		V	
Item / Channel	g_{p-p}	f	g_{p-p}	f	g_{p-p}	f	g_{p-p}	f	g_{p-p}	f
AGENA FIRST IGNITION										
8	1.0	a	0.2	a	a	a	0.4	a	0.2	a
9	1.6	100	1.2	c	a	a	0.4	a	0.9	a
10	1.3	a	1.2	c	0.6	a	0.3	a	0.3	a
11	1.0	a	0.2	a	a	a	0.4	a	0.4	a
12	b	b	1.0	a	a	a	0.7	a	1.0	a
13	1.0	440	1.4	400	1.1	390	0.7	a	1.4	a
17	10.0	1000	11.0	960	22.8	1000	4.2	700	4.2	a
18	9.5	1000	6.6	960	8.2	1000	2.2	a	1.6	a
AGENA FIRST BURN-OUT										
8	0.5	55	0.4	a	2.14	43	0.7	a	0.7	a
9	0.7	86	0.6	75	0.8	73	2.0	c	1.7	c
10	0.8	85	0.7	c	0.5	73	0.7	a	0.7	a
11	0.8	430	0.7	a	2.9	a	0.7	a	0.7	a
12	b	b	0.7	40	1.9	43	2.1	400	2.1	a
13	2.0	80	3.9	c	2.8	c	3.5	c	3.0	c
	2.5	430	1.1	400						
17	2.0	1000	3.0	960	5.3	925	2.5	800	2.8	950
18	1.5	1000	1.9	960	2.0	875	1.3	800	1.6	a
AGENA SECOND IGNITION										
8	0.6	80	0.7	50	3.0	c	0.7	a	0.4	a
9	0.4	100	0.4	125	1.2	22	2.5	cc	2.5	c
10	0.5	80	0.5	125	0.7	22	0.5	a	0.4	a
11	0.7	a	0.8	125	2.8	c	0.8	a	0.7	a
12	b	b	1.8	35	1.4	42	1.7	400	1.5	a
13	3.5	a	5.1	c	2.9	c	3.5	c	3.5	c
			1.1	400						
17	2.0	1000	7.0	c	2.8	1000	2.0	800	1.6	1000
			1.5	960						
18	1.5	1000	1.0	960	2.0	1000	1.5	800	1.3	a
AGENA SECOND BURN-OUT										
8	0.9	58	0.7	50	2.8	50	0.8	a	0.7	50
9	1.5	86	1.2	72	4.0	c	4.8	a	5.0	c
10	0.9	a	0.7	a	0.7	a	0.9	a	0.7	70
11	1.0	a	0.9	a	3.4	c	0.9	a	0.7	a
12	b	b	2.5	50	2.8	a	3.0	400	3.0	38
13	7.8	c	11.0	c	7.6	c	7.0	c	7.5	c
	4.3	350	1.8	400						
17	3.0	1000	5.0	c	5.7	950	4.5	900	6.4	900
			4.0	960						
18	3.0	1000	2.8	960	4.6	950	4.5	900	2.5	a

TABLE 2.- Concluded

Lunar Orbiter	I		II		III		IV		V	
Item / Channel	g_{p-p}	f	g_{p-p}	f	g_{p-p}	f	g_{p-p}	f	g_{p-p}	f
LUNAR ORBITER SEPARATION										
8	2.5	25	2.3 4.0	c 0.76	3.71	57	2.1	c	3.5	c
9	d	d	d	d	d	d	d	d	d	d
10	1.0	104	2.2	c	1.6	44	1.8	c	0.6	c
11	0.8	82	2.1	c	1.7	173	1.8	c	1.3	c
12	d	d	d	d	d	d	d	d	d	d
13	d	d	d	d	d	d	d	d	d	d
17	20.0	1000	36.3	960	40	850	46	800	20	800
18	20.0	1000	42.5	960	40	850	b	b	b	b

a. Frequency in cps approximated from 2 or more cycles. a - indicates either a very low signal or less than 2 cycles.

b. No data available, either from lack of appropriate flight tape or from electronic difficulties.

c. Pulse peak amplitude.

d. Prior to separation, these channels were switched to position indicators to show separation.

spacecraft and 17 and 18 in the spacecraft adapter for both lift-off and transonic speeds. In addition, probability density coefficients and auto-correlation functions were determined.

Random vibration data were not always available for all channels for the same reasons the same transient data are not included. However, from the five flights, excellent repetition occurs both as to frequency content, trends, and magnitudes. In general, all spectral density levels were considerably lower in amplitude than expected. The responses within the spacecraft (channels 12 and 13) were much less than the measurements at the base of the spacecraft (channels 17 and 18), with the possible exception of the response in the longitudinal direction (channels 13 and 17) at a frequency of about 400 cps at lift-off.

To further study the nature of the random vibrations, probability density analyses (histograms) were made for each channel for both lift-off and transonic speeds (see example, fig. 5). After digitizing the data, the number of times an amplitude occurred in a narrow band width were determined. These data were standardized to an area of one and compared to the normal (gaussian) probability density function (ref. 5) (fig. 5). It may be seen that the general trend of the Gaussian curve closely follows the flight data indicating that although the probability distribution of the data is non-gaussian, the deviation is small.

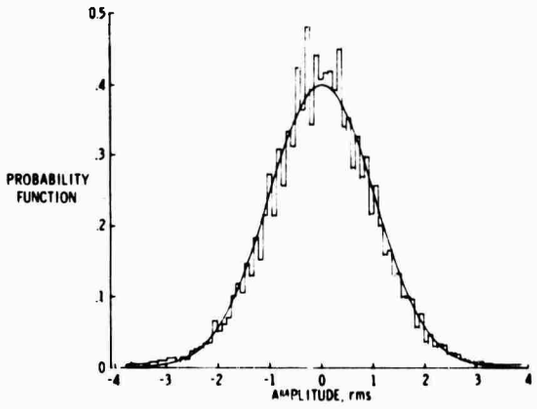

Figure 5.- Example of probability analysis in the transverse direction at lift off on Lunar Orbiter V.

An example of additional examination of the random characteristics of the random vibrations is given in figure 6 where the autocorrelation function is shown. The figure represents a narrow-band random vibration whose center frequency is 940 cps (see ref. 5). The auto-correlation functions for channels 17 and 18 were all of this nature, although though the center frequency was not always as clearly indicated. Channel 13 had the same type of auto-correlation function with a center frequency of approximately 400 cps. Channel 12, in general, had very little response; thus, the plots of probability density and auto-correlation functions indicated no particular random characteristics.

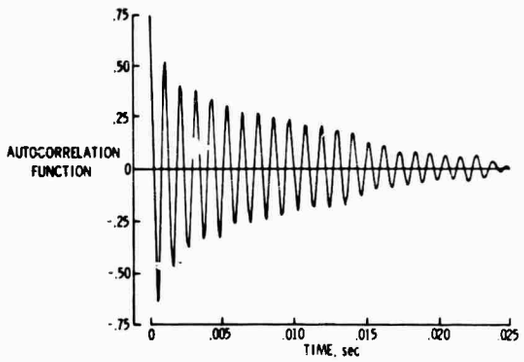

Figure 6.- Example of autocorrelation function in the transverse direction at lift off on Lunar Orbiter V.

Comparison of Results

Two comparisons of the flight data are made: (1) with the flight acceptance test (FAT) levels and (2) with the results of a regression analysis that predicts the flight vibration levels.

Sinusoidal vibrations.- To compare the flight measured levels with FAT levels, selected shock spectrum outputs from accelerometers on channels 17 (longitudinal) and 18 (transverse) for Q = 5 were divided by 5, the same Q used in determining FAT levels, to obtain an equivalent sinusoidal level. These values are shown on figure 7. It may be noted that at frequencies above 90 cps in the longitudinal direction and above 50 cps in the transverse direction that equivalent sinusoidal flight levels have exceeded the FAT requirements. These data would indicate that the FAT levels for sinusoidal vibration are certainly not overly conservative. A look at the response data within the spacecraft as discussed in the following paragraph leads to a similar conclusion.

Figures 8 and 9 show the measured responses during flight and during FAT at two positions within the spacecraft (Lunar Orbiter V). Superimposed around the FAT measurements are peak responses from the various flight transients as determined by narrow band analyses conducted by The Boeing Company. The narrow band analyses consisted of passing the transient signal through band pass filters; 2 to 15 cps, 12 to 30 cps, 20 to 50, and 40 to 80 cps. By measuring the amplitude for the resulting sinusoids, acceleration levels were determined and shown in the figures.

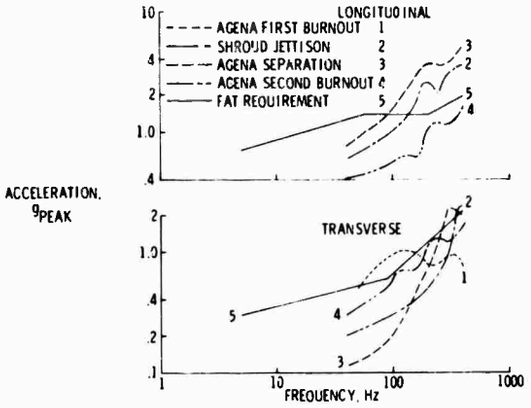

Figure 7.- Comparison of sinusoidal FAT requirements with equivalent sine levels of shock spectra from flight data (Q = 5).

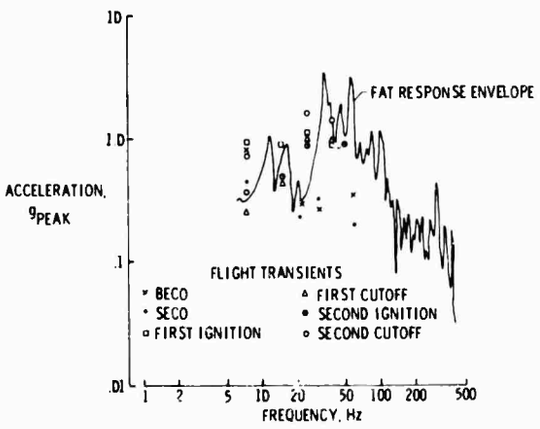

Figure 8.- Comparison of spacecraft transverse response due to sinusoidal FAT and flight inputs.

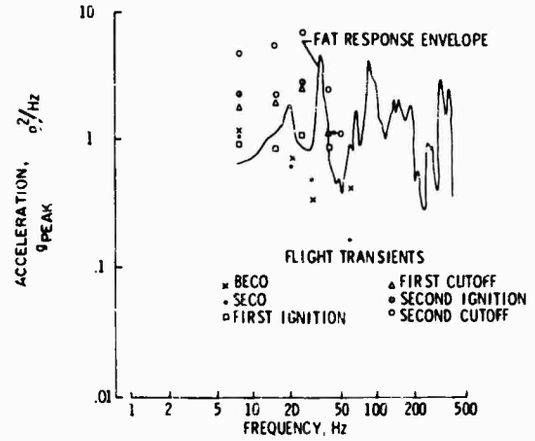

Figure 9.- Comparison of spacecraft longitudinal response due to sinusoidal FAT and flight inputs.

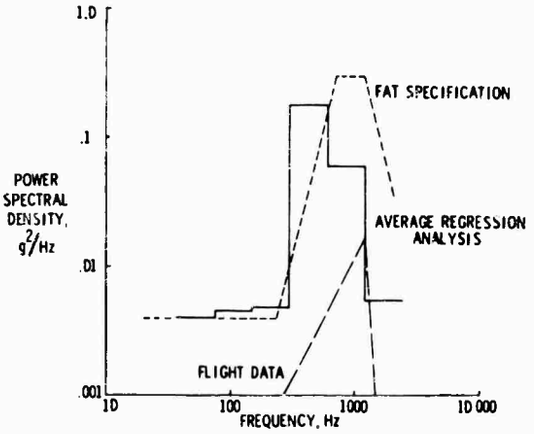

Figure 10.- Comparison of FAT, regression analysis, and flight data in the longitudinal direction at lift off.

From figure 8, it appears that the required sinusoidal FAT levels were adequate and definitely not overly severe for tests in the transverse direction. For tests in the longitudinal direction, figure 9, it appears that the sinusoidal FAT levels may not have been sufficiently high. However, when it is remembered that only the sinusoidal component of the peak response is shown and that the actual FAT consisted of slow sweep sinusoidal tests were many hundreds of cycles occur near the peak amplitude, the tests are considered to be adequate.

Random vibrations.- The random flight measured vibrations can also be compared to FAT levels for the conditions both of inputs to the spacecraft, and to the results of a new prediction technique based on a regression type analysis (figs. 10 - 14). Measurements obtained only at lift-off and during transonic speeds are considered to be of sufficient time duration to analyze as random vibration. Since the specified FAT levels were determined from an enveloping of the flight data of previous Agena flights for both lift-off and transonic speeds, it was expected that the overall test levels would be conservative.

During the flights of Lunar Orbiter, the random inputs as measured in the longitudinal and transverse directions (figs. 10-13) were more than an order of magnitude lower than the predicted values throughout the vibration spectrum. Although it was expected that the rms accelerations would be lower in flight, the maximum levels of the power spectral density were expected to be at the FAT levels. However, the spectral density levels from flight measurements were considerably lower.

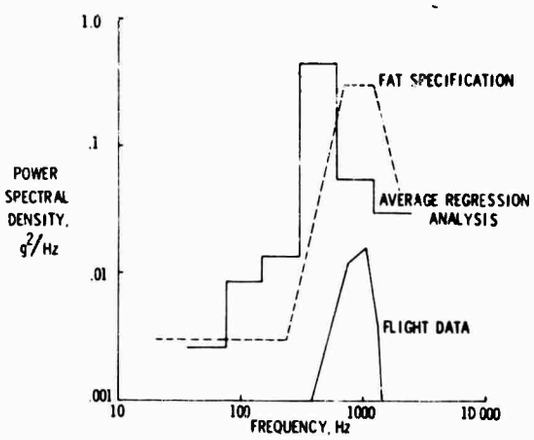

Figure 11.- Comparison of FAT, regression analysis, and flight data in the longitudinal direction at transonic speeds.

These low levels may have been due to the ogive metallic nose fairing (same fairing as used on Mariner 4 which also had low random excitation) or could have been the result of the interaction between the Lunar Orbiter spacecraft and the Atlas-Agena D launch vehicle. Since the flight input vibration levels to the spacecraft were much lower than expected, the responses within the spacecraft would be expected to be proportionally less.

For purposes of comparison, the random vibration flight data (generally interpreted as inputs to the spacecraft) measured on the five

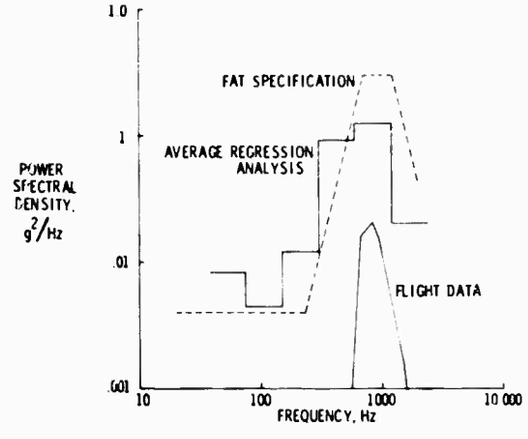

Figure 12.- Comparison of FAT, regression analysis, and flight data in the transverse direction at lift-off.

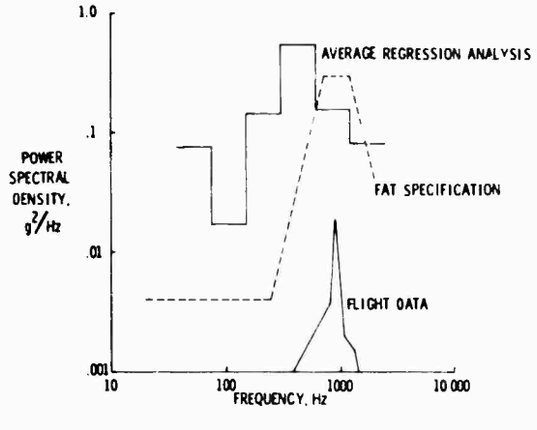

Figure 13.- Comparison of FAT, regression analysis, and flight data in the transverse direction at transonic speeds.

Lunar Orbiter flights have been enveloped in the same manner as the previous flight data that were used in estimating FAT requirements. Figures 10 and 11 show the enveloped random vibration levels in the longitudinal direction at lift off and transonic speeds, respectively, and figures 12 and 13 show the enveloped random vibration levels in the transverse direction at lift off and transonic speeds, respectively. Figure 14 shows a composite of the maximum values from figures 10 - 13. All five plots show power spectral density (g^2/Hz) versus frequency for FAT requirements, results of average

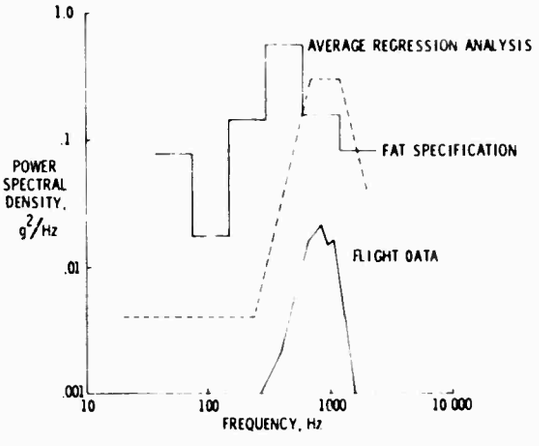

Figure 14.- Composite comparison of FAT, regression analysis, and flight data.

regression analyses, and flight data. In all instances, FAT requirements and results of the regression analysis indicate higher levels by an order of magnitude than those measured in flight (note above section pertaining to low flight inputs). The spectrum shape of the regression analyses indicates maximum energy levels in the 300 to 600 cps octave band whereas the flight data peaks at higher frequencies (see composite, fig. 14). In addition, octave band values of the regression analysis are compared to 20 cps band width values of flight data. Thus, this new method has predicted the measured environment of the Lunar Orbiter spacecraft no better than the method used to extablish FAT requirements. However, since it has considered many more pertinent variables than other prediction methods, it appears that the method could be used effectively as a first step for any new or untried launch vehicle. As evidenced by the comparison of the shape of the spectrum (see fig. 14) between FAT requirements and flight data, the use of previous flight data from the same launch vehicle still appears to be the better way of estimating FAT requirements. Enveloping of the data results in a certain amount of conservatism which is considered necessary in view of the many unknown responses in flight and because of the difference in responses from spacecraft to spacecraft.

Comparisons of the response within the spacecraft due to the application of the FAT random requirements with the measurements obtained during the flight of Lunar Orbiter V are shown in figures 15 and 16 for the transverse and longitudinal directions, respectively.

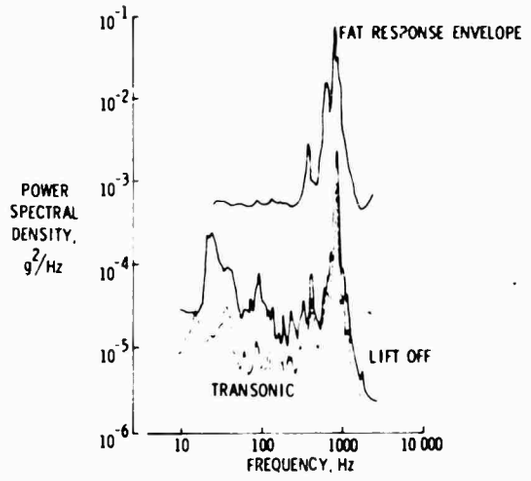

Figure 15.- Comparison of spacecraft transverse response due to random FAT and flight inputs.

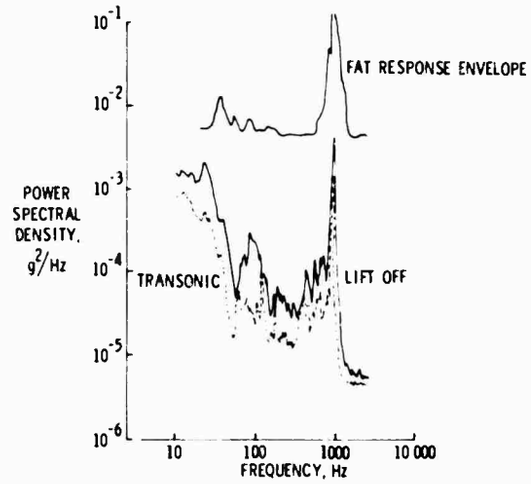

Figure 16.- Comparison of spacecraft longitudinal response due to random FAT and flight inputs.

These data were reduced by Boeing Company. The top curves of these figures show the responses (power spectral density, PSD) due to the application of the maximum FAT random inputs and the lower curves are the results of PSD analyses of the flight data. These data indicate that the trends of the responses within the spacecraft in flight are the same as those that occur during FAT. Since the flight inputs were more than an order of magnitude less than FAT levels, the responses within the spacecraft were accordingly less by an order of magnitude.

CONCLUDING REMARKS

This paper has presented detailed vibration measurements from five successful Lunar Orbiter flights including peak acceleration values and predominant frequencies that occurred during the various transients, and results of power spectral density analyses during lift-off and transonic speed conditions. It has discussed the origin of the flight acceptance test requirements and shown then to be adequate. Since the flight inputs were lower than expected, the FAT random vibration levels are considered severe. The flight data were also compared to the results of a new prediction method based on a regression analysis. For establishing vibration requirements utilizing a proven launch vehicle, the regression analysis does not provide as good a basis as does flight vibration measurements from prior flights of the launch vehicle. However, the analysis may be useful in estimating vibration levels for new and untried launch vehicles.

REFERENCES

1. Houston, Allan B.: Study to Define Agena Vibration and Acoustic Environment. NASA CR-66196.

2. Mahaffey, P. R.; and Smith, K. W.: Method for Predicting Environmental Vibration Levels in Jet Powered Vehicles. Noise Control, Vol. 6, No. 4, 1960.

3. Brust, J. M.; and Himelblau, H.: Comparison of Predicted and Measured Vibration Environments for Skybolt Guidance Equipment. Shock and Vibration Bulletin No. 33, Part 3, p. 231, 1964.

4. Piersol, A. G.; and Van Der Laan, W. F.: A Method for Predicting Launch Vehicle Vibration Levels in the Region of the Spacecraft Adapter. NASA CR 1227, 1968.

5. Bendat, Julius A.; and Piersol, Allan G.: Measurement and Analysis of Random Data. Published by John Wiley and Sons, Inc., New York, 1966, pp. 16 -21 and 160 - 161.

Mr. Bendat (Measurement Analysis Corp.): I think that was a very fine paper and it is very apropos to some of the remarks of the Chairman earlier on the need for analysis and engineering requirements to be considered together as a pair. Because there were certain analytical results available which did not quite agree with the experimental results and you had an opportunity to consider the reasons for the differences. The mathematical model which someone might use requires a great deal of care and interpretation. There is really no such thing as a sine wave in nature - nothing can persist indefinitely like a sine wave. There is no such thing as a Gaussian process in nature - I would say that any amplitude could be exceeded no matter how large it might be, so you have compromises right at the very start. If there are significant results that might be predicted you should use all the tools that are available. In some of the plots that were made in this paper, as well as the preceding paper, I did not notice complete mention of bandwidths, record lengths and other such parameters that would help one in putting some standard error on the measurements. These are the kinds of considerations that are brought to bear, together with all the engineering understanding of the problem before you get the final answers.

Mr. Delchamps (Bell Telephone Laboratories): Have you done any distribution analysis on the peaks of the transient? You were picking a maximum and I just wondered where this was in the distribution of the peaks which you found when you did your spectrum analysis.

Mr. Clevenson: We found primarily that the distribution of peaks occurred at the natural frequencies that were shown up during the sinusoidal tests. During the flight acceptance test, various resonances occurred and the same peaks occurred during the analysis of the random tests. So we can pretty much expect that whatever resonances are there, these frequencies are going to show up as maximum response.

Mr. Delchamps: All right for the frequencies, I was thinking about the distribution of levels. In other words, you took a level that was one of the high levels, and it was there 60 or 70 or 80 percent of the time, or maybe only 30 percent. Or maybe just a peak.

Mr. Clevenson: I very carefully specified that the table of values in the report gives the peak values of the transients as obtained from high speed oscillograms.

Mr. Delchamps: O.K. I think it would be interesting to see the distribution of peak levels in that transient to find out whether this was an event, or two events, or a number of events in a few more events - in the same manner that you would look at the distribution of amplitudes in a random sample to find out if you have a Gaussian density function.

Mr. Clevenson: We did not do what you are asking. However, I think we could to that. We have all the various transients and we could combine them and determine an amplitude spectrum from them. I assume you mean from all of the amplitudes - all of the transients - not the amplitudes within one transient.

Mr. Delchamps: Both. When you pick the maximum, the natural question is: what else was there? That is what I was trying to ask. Maximums, as Dr. Bendat pointed out, are at infinity, really, except that we do not measure them when they are there, unfortunately, since we are non-linear we do not see them either in the real world.

Mr. Clevenson: Maximums is what we have measured and they are really there.

Mr. Delchamps: I give up - you are right.

VIBRATION AND ACOUSTIC ENVIRONMENT CHARACTERISTICS OF THE SATURN V LAUNCH VEHICLE

Clark J. Beck, Jr. and Donald W. Caba
The Boeing Company

This paper presents representative examples of vibration and acoustic data from flights of the Saturn V launch vehicle and static firings of Saturn V launch vehicle stages. The purpose of the paper is to provide vibration and acoustic environment characteristics which are pertinent to the design of launch vehicles.

Comparisons of vibration spectra are presented which illustrate differences between flight and static firing environments, effects of mass loading on the vibration environment, vibration transmission through structure, and the effects of fluid flow rate on vibration level.

Comparisons of acoustic data are presented which indicate differences between static firing and flight acoustic environments, differences in the acoustic environment internal and external to the vehicle, and variations in sound pressure level due to engine exhaust direction.

Flight vibration and acoustic time histories are presented. The time histories are compared with time histories of dynamic pressure and Mach number to illustrate the correlation between these parameters and the vibration and acoustic environment.

INTRODUCTION

The Saturn V launch vehicle consists of three stages, the S-IC, S-II, and S-IVB (Figure 1). To date there have been approximately 30 static firings of the flight stages. Over 3,00 vibration measurements have been made during these static firings. In addition about 400 vibration measurements were taken during the first two flights of the Saturn V vehicle. This paper presents representative examples of vibration and acoustic data from flights of the Saturn V launch vehicle and static firings of Saturn V launch vehicle stages. The purpose of the paper is to provide vibration and acoustic environment characteristics which are pertinent to the design of launch vehicles.

STATIC FIRING AND FLIGHT VIBRATION ENVIRONMENTS

The vibration environment of a stage during static firing and flight can differ radically as illustrated in Figure 2. This figure shows the spectrum of a typical measurement taken during S-IVB static firing as compared with a spectrum of the same measurement during the liftoff period of the Saturn V. Note the large level difference between 10 and 500 hertz. This difference is attributed to the structure response to dissimilar acoustic noise fields produced by the engines of the stage and the launch vehicle. The S-IVB has one engine producing over 200,000 pounds thrust while the S-IC has five engines producing over 7.5 million pounds of thrust.

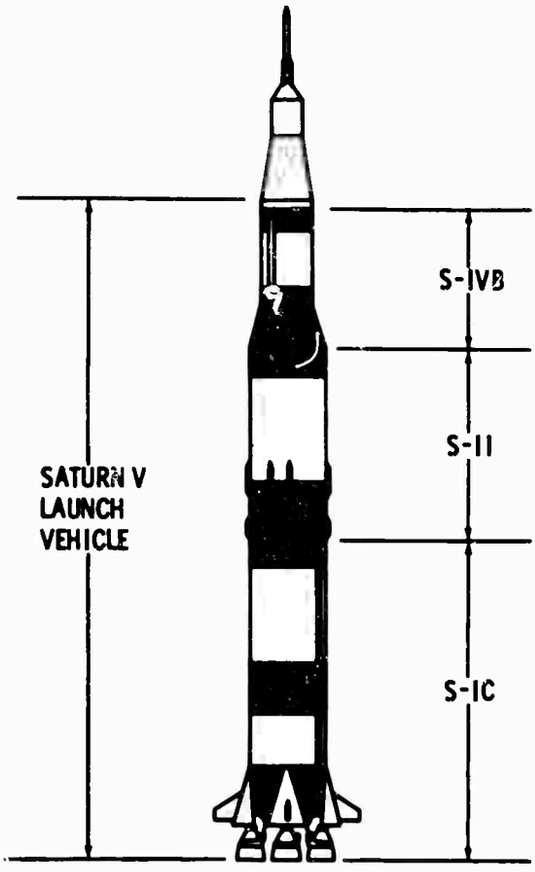

Figure 1: SATURN V SPACE VEHICLE

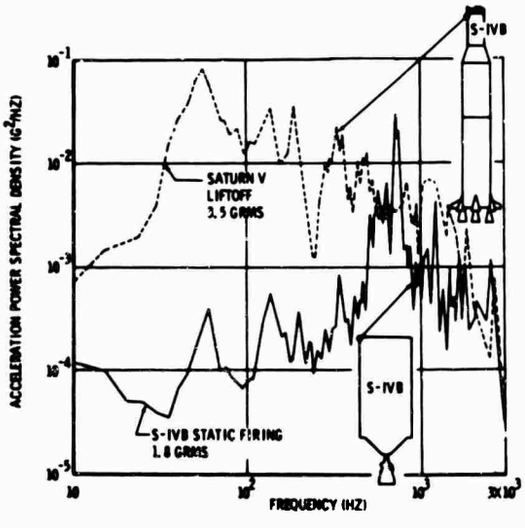

Figure 2: COMPARISON OF S-IVB VIBRATION ENVIRONMENT DURING S-IVB STATIC FIRING AND SATURN V LIFTOFF

Figure 3 illustrates the comparison of spectra from the same measurement for S-IVB static firings, Saturn V launch, and flight at Max q (Maximum Dynamic Pressure). This figure shows that the vibration environment during Max q flight differs from both the static firing and liftoff environments.

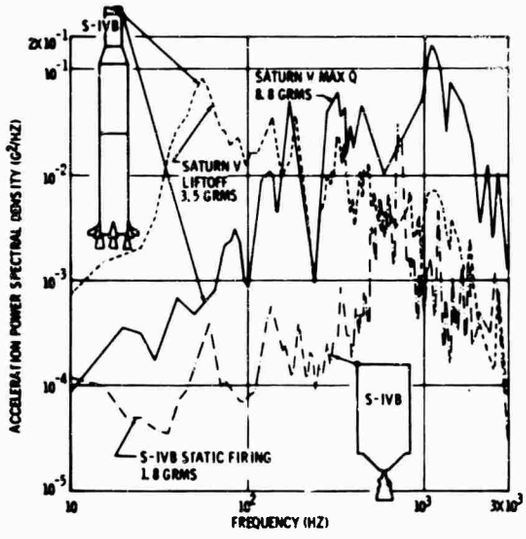

Figure 3: COMPARISON OF S-IVB VIBRATION ENVIRONMENT DURING S-IVB STATIC FIRING, SATURN V LIFTOFF AND SATURN V MAX Q

MASS LOADING EFFECTS

Mass loading has a significant effect on the vibration environment as illustrated in Figure 4. The figure shows the difference between two measurements located on the S-IC LOX bulkhead. The dotted spectrum is a measurement located on a portion of the bulkhead which is one-fourth inch thick and of uniform mass distribution. The solid spectrum is from a measurement located next to a massive fitting (approximately 54 pounds) on the bulkhead. The overall vibration level for the mass loaded bulkhead is approximately one-third of that for the unloaded bulkhead.

Figure 5 also illustrates mass loading effects resulting from liquid level variations in a tank. When considering vibration levels on a tank, it is very important that the vibration levels be considered as a function of liquid level. The solid line on Figure 5 shows the spectrum level when liquid is above the measurement while the dotted spectrum is the vibration level with liquid below the measurement. The liquid mass attenuates the overall vibration level by a factor of approximately four.

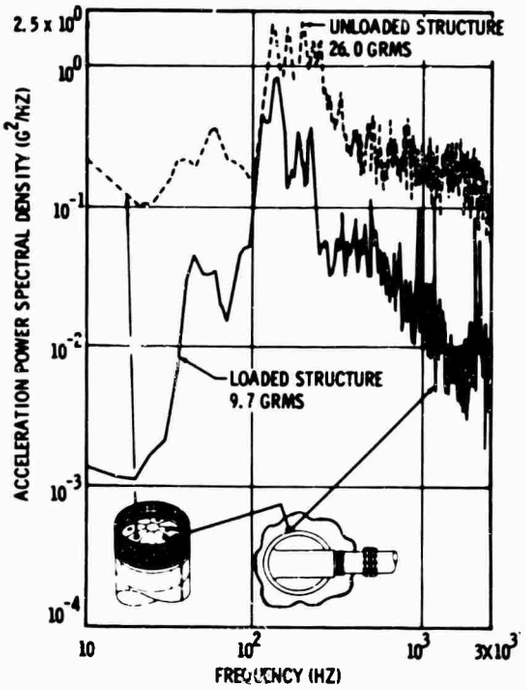

Figure 4: COMPARISON OF LOADED AND UNLOADED STRUCTURE VIBRATION ENVIRONMENTS

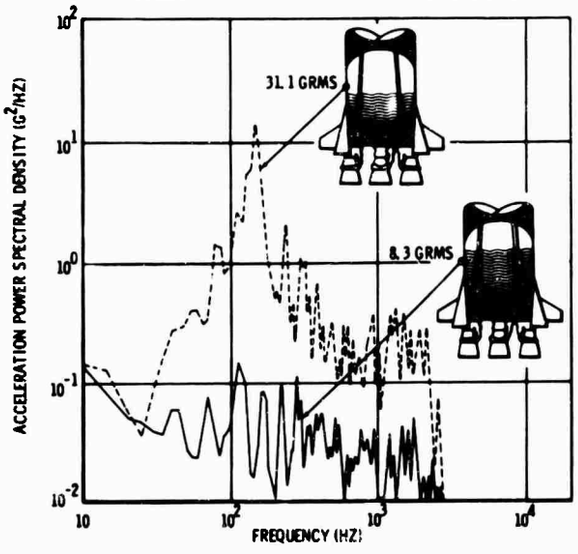

Figure 5: EFFECTS OF LIQUID LEVEL IN A TANK ON THE VIBRATION ENVIRONMENT DURING STATIC FIRING

VIBRATION TRANSMISSION THROUGH THE STRUCTURE

Vibration transmission through a structure is illustrated in Figure 6. The figure shows the vibration spectrum for various locations, along the S-II thrust cone. A measurement (A) located about 28 inches up the thrust cone from where the engines are mounted indicates a level of 5.5 Grms. Another measurement (C) about 60 inches further up the thrust cone shows a level of 1.6 Grms. A third measurement (B) located between measurements A and C shows a level of 2.4 Grms. The B spectrum is not plotted, but it falls between the two. The vibration source for this example is considered to be the J-2 engines since the measurements were taken during S-II powered flight. During S-II powered flight, acoustic noise levels are low and hence vibration due to acoustic noise is insignificant.

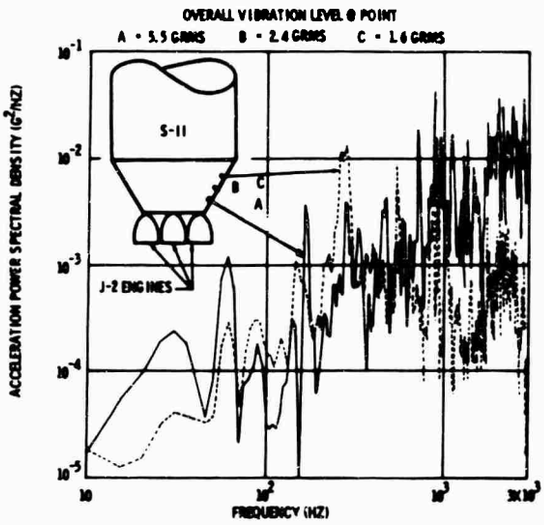

Figure 6: VIBRATION TRANSMISSION THROUGH STRUCTURE

FLUID FLOW EFFECTS

Figure 7 shows the effect of fluid flow rates on the vibration environment. The data shown in this figure were obtained by recording the vibration level resulting from LOX flowing through a 6-inch diameter line. Note that the vibration level increases exponentially with an increase in flow rate. A metalic bellows in this line failed while LOX was being pumped through the line. The failure was close to the vibration measurement point shown in Figure 7.

STATIC FIRING AND FLIGHT ACOUSTIC ENVIRONMENTS

The characteristics of the acoustic environment associated with a large launch vehicle can vary widely. The acoustic environment differences between a stage static firing and launch vehicle liftoff are shown in Figure 8. The environment differences, as discussed previously, are the result of dissimilarities in the size and number of engines on the S-IVB stage and the Saturn V launch vehicle. The difference in the overall sound pressure level is

approximately 6 db with the significant level differences occurring below 500 hertz.

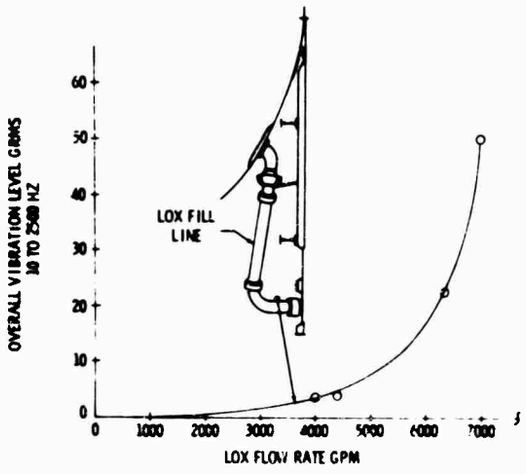

Figure 7: VARIATION IN VIBRATION LEVEL DUE TO FLUID FLOW RATE

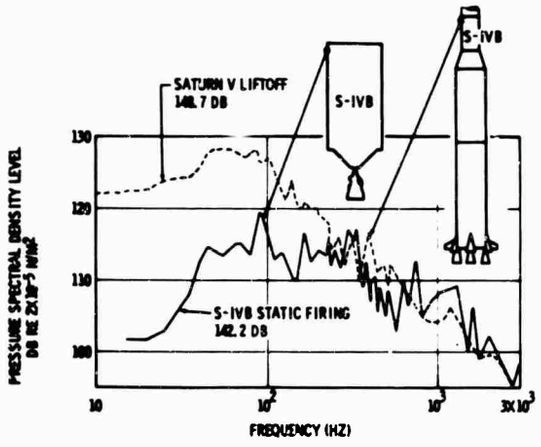

Figure 8: COMPARISON OF ACOUSTIC ENVIRONMENT DURING S-IVB STATIC FIRING AND SATURN V LIFTOFF

Other interesting characteristics of the acoustic environment are shown in Figures 9 and 10. Figure 9 shows the typical variation in the acoustic sound pressure level due to the shadowing effect of the stage. The overall sound pressure level drop due to the shadowing effect of the stage is generally 8 to 10 db. Two acoustic measurements taken during a static firing of the S-IC stage are shown in Figure 9. The measurements were located externally, one on the same side to which the engine exhaust was deflected and the other 180 degrees away. The solid spectrum is the one of the exhaust side and the dotted spectrum is the one taken on the opposite side.

Figure 10 shows the variation in the acoustic spectrum from measurements internal and external to the launch vehicle. A typical variation in overall sound pressure level is 8 to 10 db.

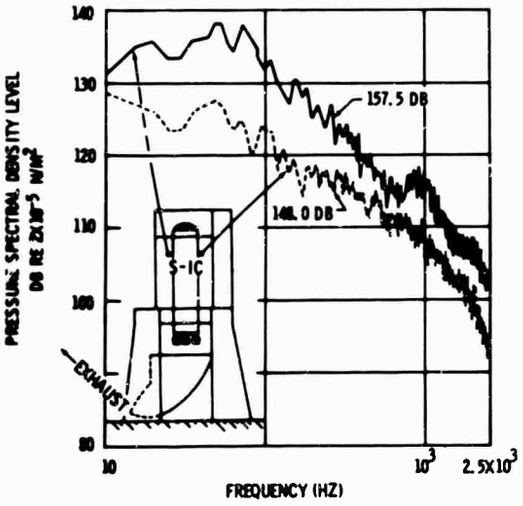

Figure 9: EFFECT OF STAGE SHADOWING ON THE ACOUSTIC ENVIRONMENT

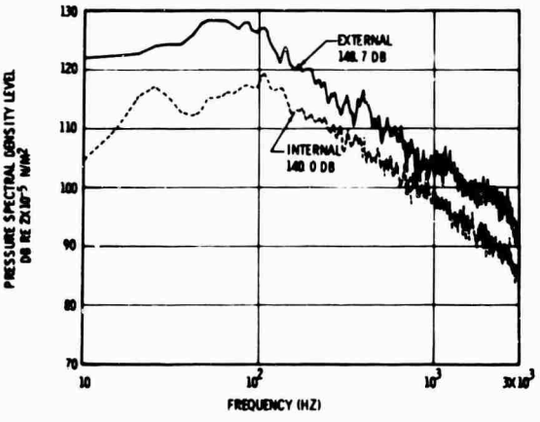

Figure 10: COMPARISON OF INTERNAL AND EXTERNAL ACOUSTIC ENVIRONMENTS

FLIGHT VIBRATION AND ACOUSTIC TIME HISTORIES

The acoustic environment of a launch vehicle is time variant as illustrated in Figure 11. The data shown in this figure came from a microphone mounted externally near the top of the S-II stage. The sound pressure level time history for this particular location has three distinctive features. First, the sound pressure level near time zero increases rapidly and then decreases as the vehicle speed in-

creases. This is characteristic of the liftoff environment. Second, the sound pressure level increases and decreases at a rate coincident with the variation in dynamic pressure. Third, the sound pressure level increases rather abruptly at the critical Mach Number ($M_{CR} \simeq 0.8$). This increase is attributed to the presence of a normal shock wave near the microphone location. Figure 12 shows data from a vibration transducer at a location similar to the microphone location. The vibration environment has the same distinctive features as the acoustic environment with one exception. The structure responds more readily to the liftoff acoustic environment than to the flight acoustic environment.

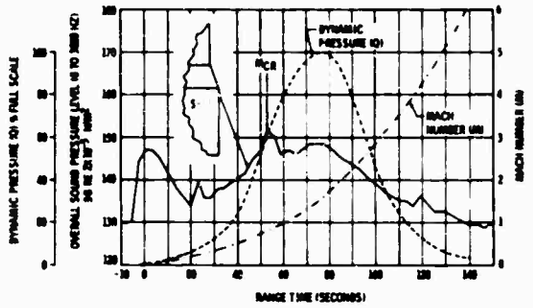

Figure 11: CORRELATION BETWEEN ACOUSTIC ENVIRONMENT AND AERODYNAMIC PARAMETERS

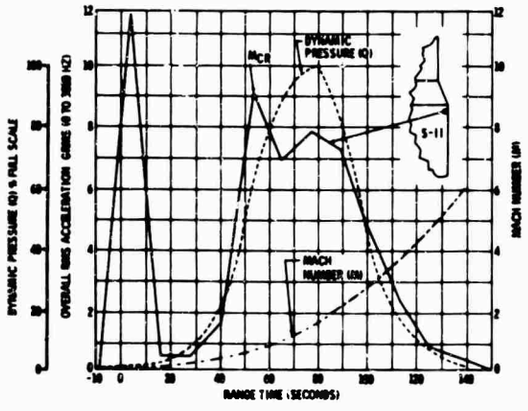

Figure 12: CORRELATION BETWEEN VIBRATION ENVIRONMENT AND AERODYNAMIC CHARACTERISTICS

CONCLUSIONS

The vibration and acoustic data in this paper are presented to provide an idea of the environmental levels associated with a large launch vehicle. The data are also selected to provide an insight into how the environmental characteristics are influenced by operating conditions. The reader should realize that the data presented represents a small sample of the available data. However, the examples discussed are characteristic of the larger body of data. These characteristics should be considered in the design of launch vehicles and equipment. An extensive bibliography has been included with this paper to provide a list of documents which contain a majority of the Saturn V data.

ACKNOWLEDGEMENTS

The data described in this paper were generated under National Aeronautics and Space Administration contracts.

BIBLIOGRAPHY

Saturn V Statistical Analysis for Vibration and Acoustic Environment-Static Firing;
October 2, 1967; D5-15569-1; Revision A;
The Boeing Company.

Saturn V Statistical Analysis for Vibration and Acoustic Environment-Static Firing;
February 26, 1968; D5-15569-2;
The Boeing Company.

Saturn V Statistical Analysis for Vibration and Acoustic Environment-AS-501 and AS-502 Flight;
September 3, 1968; D5-15569-3;
The Boeing Company.

Saturn S-IC-501 Static Test Vibration and Acoustic Data;
March 1967; D5-13644-1; Revision A;
The Boeing Company.

Saturn S-IC-502 Static Test Vibration and Acoustic Data;
February 1967; D5-13644-2;
The Boeing Company

Saturn S-IC-503 Static Test Vibration and Acoustic Data;
October 1967; D5-13644-3;
The Boeing Company.

Saturn S-IC-504 Static Test Vibration and Acoustic Data;
January 1968; D5-13644-4;
The Boeing Company.

Saturn S-IC-505 Static Test Vibration and Acoustic Data;
July 1968; D5-13644-5;
The Boeing Company.

Saturn S-IC-501 Flight Vibration and Acoustic Data;
August 1968; D5-13851-1;
The Boeing Company.

Saturn V Post Flight Vibration and Acoustic Test Data Report; AS-501;
February 1968; D5-15572-1;
The Boeing Company.

Saturn V Post Flight Vibration and Acoustic Test Data Report, AS-502;
June 1968; D5-15572-2;
The Boeing Company.

DISCUSSION

Mr. Bendat (Measurement Analysis Corp.): I hope you will accept my comments objectively, but there are many many questions that your paper raises which are typical of other questions I have heard. There are so many open ended areas which would lead one to feel that these results are only a start and in many cases misleading. You show that the data is non-stationary in some of the later slides, and yet in the earlier slides you were doing spectral analysis as if the data had been entirely stationary. There is just no way to reconcile those two matters. If the data is non-stationary, all your spectral results are wrong. There is no way to interpret the results properly. You are interested in variations which are dependent on time and you have removed time from consideration by the ordinary spectral analysis. Furthermore, as the chairman has mentioned a couple times earlier, there is nothing noted here about any amplitude properties, and frequently amplitude properties will reveal completely separate and distinct information. You have amplitude fluctuations which are also a function of time and cannot be handled in the usual way. But even when the data is stationary, which you may be able to justify in certain specialized cases, even there, if the data is not Gaussian the amplitude information reveals further properties that are not revealed in this spectral density information. Here you have a case of lift-off and dynamic pressures and rapidly changing dynamic environments which are not stationary, and you cannot use stationary methods to describe the environment. The fact that you compare something that was done in the past incorrectly with something that is being done incorrectly today still does not make a good comparison.

Mr. Caba: The measurements which you spoke of as being done in the past incorrectly were made on a static firing, and were quite stationary, and those that were compared to flight data were chosen during the lift-off period at a portion on the oscillograms that appeared to be stationary in the data reduction which showed data distribution which appeared to have a Gaussian distribution.

Mr. Woolam (Southwest Research Institute): One problem which you touched on and passed over rather rapidly is the failure of the metal bellows used in piping. This seems to me to be a very serious problem. We have done some work at Southwest Research Institute on vibration frequencies of bellows, which is exactly the same problem - they are predictable. The problem is the cryogenic temperatures. Failures are quite rapid and there is a good case for a good application of some sort of damper or damping material. Cryogenic temperatures are not favorable for most typical damping materials. It is quite a serious problem and, I think, one which should be considered at this time. You might make some comments further on the work on the failures of flexible baffles.

Mr. Caba: The baffles themselves caused the turbulence, and we applied the telescoping sleeve to cut down the turbulence and this seemed to solve our problem.

THE BLAST FIELD ABOUT THE MUZZLE OF GUNS

Peter S. Westine
Southwest Research Institute
San Antonio, Texas

The blast wave propagated from the muzzle of a gun imparts a severe transient load to any structure or personnel in the vicinity. This paper outlines a procedure for estimating the maximum pressure field, impulse field, and entire transient pressure history emitted from the muzzle of a gun. Experimental test data from test firings from pistols, rifles, grenade launchers, howitzers, and naval guns establish the validity of this procedure for developing the blast field at any arbitrary location around the muzzle of a gun.

INTRODUCTION

As a result of detonating an explosive or of firing a projectile from a gun barrel by igniting a propellant, a pressure wave of finite amplitude is propagated into the surrounding atmosphere. Such a pressure wave causes a transient load to be imparted to any structure or person in the vicinity. In this paper, we restrict ourselves to predicting the entire muzzle blast history at any location around a gun. The procedure which is developed takes full advantage of the similitude laws for scaling blast to predict the blast field about most weapons from a small number of experimental observations. The similitude law which this study uses is closely related to the scaling law of Hopkinson [1] because the same assumptions are required concerning the propagation of a blast under sealevel atmospheric conditions.

Hopkinson's law of 1915 was developed for scaling the blast field about conventional explosive charges under sealevel conditions. Hopkinson scaling assumes that heat conduction and viscosity may be neglected. In addition, gravitational effects are assumed to be minimal. This law for the propagation of a blast with only one spatial coordinate (propagation from a spherical charge) states that peak overpressure will scale as Eq. (1) and scaled impulse as Eq. (2)

$$P = f\left(\frac{R}{W^{1/3}}\right) \tag{1}$$

$$\frac{I}{W^{1/3}} = f\left(\frac{R}{W^{1/3}}\right) \tag{2}$$

where

P = peak overpressure

R = standoff distance

W = charge weight

I = total positive impulse

Because the density of most charges varies little, $W^{1/3}$ is directly proportional to the diameter of the charge, d. Therefore, another method of stating Hopkinson's law is to substitute the charge diameter for $W^{1/3}$ into Eqs. (1) and (2) and note that P and I/d are unique functions of standoff distance in charge diameters.

$$P = f\left(\frac{R}{d}\right) \tag{3}$$

$$\frac{I}{d} = f\left(\frac{R}{d}\right) \tag{4}$$

During World War II, a considerable research effort was directed towards selecting the most powerful explosive for shells and bombs. This effort required the development of recording instrumentation capable of measuring free-air blast. The reduced data from these studies substantiated that Hopkinson scaling was the proper similitude law for scaling

the blast fields under ambient sea level conditions. Actually, Hopkinson's law is a special case of a more general law proposed by Sachs [2] to account for the effect of changes in ambient air pressure and temperature on overpressure and impulse. A review of Sachs' scaling would show that the left-hand terms in Eqs. (3) and (4) are nondimensional if atmospheric conditions are added to the pi terms; however, this review will not discuss Sachs' contribution as altitude conditions are not included in this study.

Apparently Reynolds at Princeton and the Navy at David Taylor Model Basin were the first to apply Hopkinson scaling to determine the blast field about guns [3, 4]. Princeton applied Hopkinson scaling to obtain the peak pressure monitored by gages in a panel under a gun, while the Navy considered free-field overpressures and impulses about naval guns. Both groups noted that if geometric similarity existed to the extent that

$$\frac{M_1}{M_2} = \frac{E_1}{E_2} = \left(\frac{c_1}{c_2}\right)^3 = \left(\frac{\ell_1}{\ell_2}\right)^3 \qquad (5)$$

and

$$V_1 = V_2 \qquad (6)$$

where

M = mass of the projectile

E = energy in the propellant

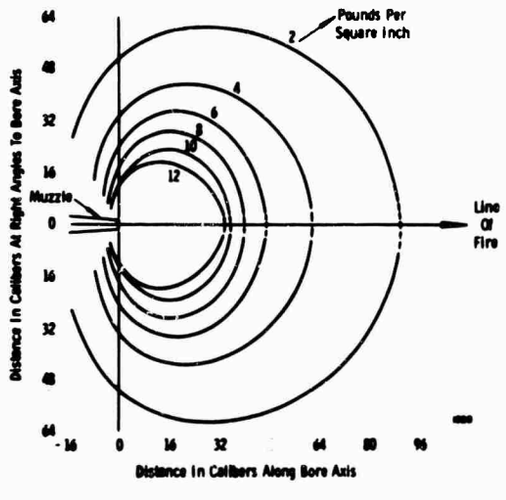

Fig. 1 - Pressure about guns, Navy technique

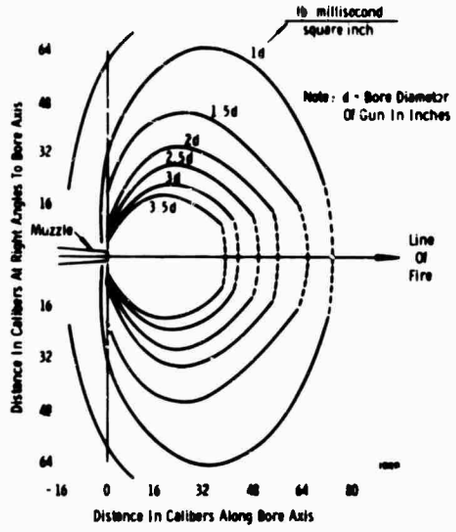

Fig. 2 - Impulse about guns, Navy technique

c = caliber of weapon

ℓ = length of bore

V = velocity of the projectile

and the subscripts denote specific weapons, then the distribution curves for maximum pressure should be identical, provided the distances are measured in calibers. The Navy drew the additional conclusion that the distribution curves for impulse should be identical, if the impulse divided by the caliber of the gun were plotted against distance in calibers. Plots of isobars of constant pressure and isoclines of I/c were constructed from the Navy data with an abscissa of $\frac{L_{\parallel}}{c}$ and an ordinate of $\frac{L_{\perp}}{c}$ for a 30"/50 caliber naval gun, Figs. 1 and 2. These results correlated well with a 16"/45 caliber naval gun, since the deviation from true replica scaling, Eqs. (5) and (6), in the interior ballistics of the two weapons averages only 15%. In the past, the Navy felt that the length of the barrel could be disregarded in the scaling, but this observation, based on insufficient data, is incorrect as will be demonstrated later in this paper. These scaling observations made in the mid-40's on the blast field about guns are correct, provided the interior ballistic restrictions expressed by Eqs. (5) and (6) are maintained. The plots shown in Figs. 1 and 2 are Hopkinson's law, Eqs. (3) and (4) for spherical charges, extended to the blast field about weapons by requiring dynamic and geometric similarity to be maintained, Eqs. (5) and (6).

Unfortunately, this scaling by calibers is satisfied in only a few cases and then accidentally. In order for the Navy's simulation to include all weapons, a large number of plots would be required with a systematic variation in propelling charge, projectile mass, barrel length, and muzzle velocity. Fortunately, some procedures are available for eliminating several variables.

Armour Research Institute attempted to represent the blast field about a weapon by assuming that some equivalent weight of spherical explosive charge could be located on the bore axis at a distance, r_o, from the muzzle [5]. The distance r_o evidently corresponded to the location of the stationary shock associated with the so-called "bottle" at the muzzle of a gun. To create an approximation to the peak pressures, Armour created a "reduced energy", W,

$$W = n(E - 1/2MV^2) \tag{7}$$

where n is a correlation or fudge factor for a gun that is multiplied by the energy in the propellant minus the kinetic energy in the projectile to obtain an energy going into the blast. This reduced energy is an approximation of the available energy in the blast. It ignores the important temperature losses and a few other trivial energy losses. Actually, this "pseudo energy" is a fairly accurate representation of the energy going into the blast because a first-approximation would be to assume that the significant energy losses are nearly a constant percentage of available energy. Armour applied Hopkinson's law as expressed in Eq. (1) to determine the pressure distribution over a plate, except that they rewrote this equation as

$$P = f\left(\frac{h}{W^{1/3}} \ , \ \frac{L}{W^{1/3}} \ , \ \frac{x}{W^{1/3}}\right) \tag{8}$$

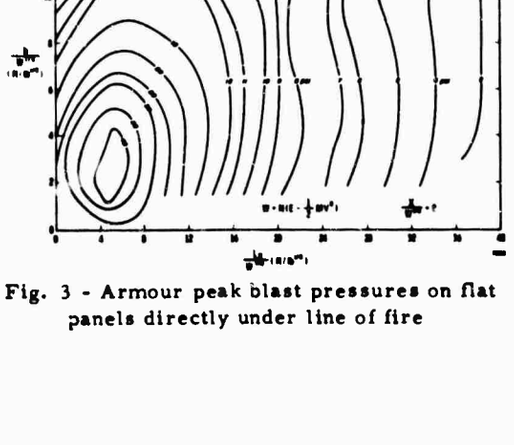

Fig. 3 - Armour peak blast pressures on flat panels directly under line of fire

Because of the extra spatial coordinates, Armour presented their results as shown in Fig. 3, and tested the technique with data from caliber .50, 20-mm, 37-mm, and 3.00-in. gun with $\frac{x}{W^{1/3}} = 0$. Their results were excellent for predicting pressures, within 20%, but only because all guns tested possessed virtually the same barrel length in calibers $\frac{\ell}{c}$. Had Armour tested a grenade launcher, a caliber .45 pistol, or other stubby gun, their predictions would have been poor. At that time, data were not available to show that $\frac{\ell}{c}$ should be considered. In addition, Armour did not consider the impulse field about the muzzle of a gun.

In retrospect, observe that all of these early techniques used Hopkinson's law to simulate the blast field about weapons. The use of this law has been correct except that restrictions do arise. The Navy could use Figs. 1 and 2 because many of their guns were replica models of themselves and possessed similarity. The weakness in the Navy's technique is that for Figs. 1 and 2, $\frac{M}{c^3}$, $\frac{W}{c^3}$, V, and $\frac{\ell}{c}$ all remained invariant. The Armour approach eliminated the need to maintain $\frac{M}{c^3}$, $\frac{W}{c^3}$, and V as constants, but assumed $\frac{\ell}{c}$ was insignificant. The new technique which is about to be demonstrated does not make the unjustified assumption that barrel length is insignificant, and incorporates the effects of both pressure and impulse in the analysis.

NEW SCALING FOR BLAST ABOUT WEAPONS

Another method for rendering data nondimensional and including the length of the gun barrel involves writing the Hopkinson scaling law as

$$\frac{Pc^3}{W} = f\left(\frac{L_{\parallel}}{c} \ , \ \frac{L_{\perp}}{c} \ , \ \frac{\ell}{c}\right) \tag{9}$$

and

$$\frac{Ic^2}{W} = f\left(\frac{L_{\parallel}}{c} \ , \ \frac{L_{\perp}}{c} \ , \ \frac{\ell}{c}\right) \tag{10}$$

These scaling equations follow readily from a similitude analysis that includes such parameters as standoff distance perpendicular to line of fire, $L_{\perp}$; standoff distance parallel to line of fire, $L_{\parallel}$; length of gun barrel; caliber of weapon; side-on overpressure; side-on impulse;

and energy in the blast. Eq. (9) states that a nondimensionalized pressure is a function of geometric similarity. Eq. (10) states that a nondimensionalized impulse is a function of geometric similarity. [Actually, Eq. (10) is not nondimensional because the pi term $\frac{Ic^2}{W}$ should be written as $\frac{Ic^2a}{W}$, where a is the velocity of sound. Eq. (10) has been written as a scaling parameter with dimensions because the velocity of sound remains essentially invariant, and no need exists to include a dimensional constant, sound velocity, in the solution.]

If the pi term $\frac{\ell}{c}$ were assumed to be insignificant, Eqs. (9) and (10) would represent an alternate method of presenting the Armour approach. Actually, the Armour assumption that $\frac{\ell}{c}$ is insignificant was poor and based on too few experimental observations, as will soon be apparent. The term W in Eqs. (9) and (10) is the energy in the blast. For our purposes, we will approximate this equation much as Armour approximated it, but no fudge factor, n, will be needed. Let Eq. (11) define the energy in the blast:

$$W = E - 1/2MV^2 \qquad (11)$$

All that is required to evaluate Eqs. (9) and (10) and develop the functional relationship is free-field blast data from weapon firings. Although numerous weapon firings have been conducted, the great majority of these experiments had instrumentation located behind blast shields, in the hatches of tanks, in pillboxes, or with other obstacles interfering with the measurements of blast in a true free-field. Fortunately, some testing has been conducted without introducing diffraction, refraction, and reflections. These limited data have been used to create the following observations concerning the free-field blast about guns.

FREE-FIELD BLAST PRESSURE

In Fig. 4, one observes isobars of constant nondimensional pressure on a plot with a

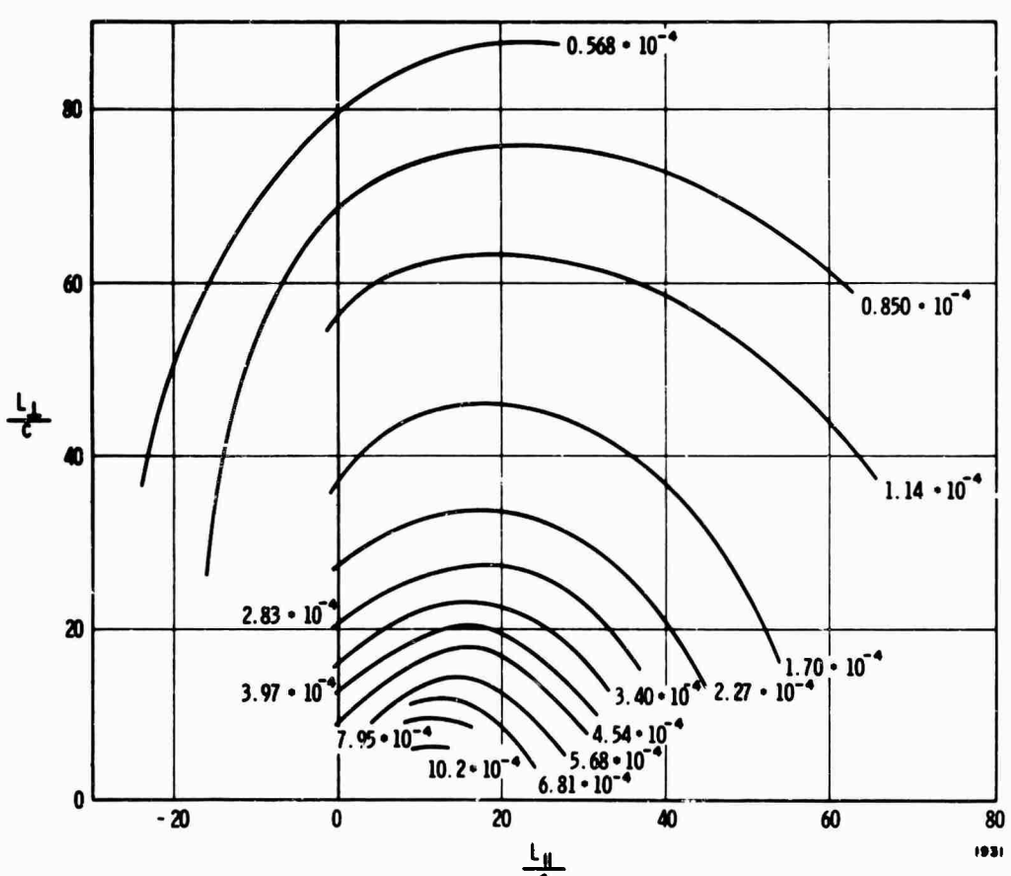

Fig. 4 - Isoclines of side-on pressure, $\frac{Pc^2\ell}{W}$

nondimensional distance from the line of fire as an ordinate and a nondimensional distance from the muzzle along the line of fire as an abscissa. This presentation for free-field blast was created after experimentally observing that the precise equation for free-field blast pressure, Eq (9), could be approximated by multiplying $\frac{Pc^3}{W}$ by $\frac{\ell}{c}$ to form Eq. (12):

$$\frac{Pc^2\ell}{W} = f\left(\frac{L_\perp}{c} \quad , \quad \frac{L_\parallel}{c}\right) \tag{12}$$

Fig. 4 is a plot of Eq. (12), using the experimental data generated by Shapiro and Rich for a 20-mm aircraft gun [9]. Note that Fig. 4 employs Hopkinson scaling and incorporates the effects of barrel length in the solution with an empirical observation. Virtually all experimental observations before 1960 were on guns with large barrel lengths, $\frac{\ell}{c}$. Armour and others concluded that the length of the barrel mattered little because these early observations were made with long-barreled weapons. Very recent test firings on a high-velocity, 40-mm grenade launcher [8], on a low-velocity grenade launcher [6], and on caliber .45 pistol [6], do not correlate on a plot of $\frac{Pc^3}{W}$ as a function of $\frac{L_\perp}{c}$ and $\frac{L_\parallel}{c}$, as suggested by Armour scaling. Only after the length of barrel has been included in an analysis by multiplying $\frac{Pc^3}{W}$ by $\frac{\ell}{c}$ can the free-field blast pressures around all weapons be reduced to a common factor, Eq. (12).

Fig. 5 is a plot of $\frac{Pc^2\ell}{W}$ versus $\frac{L_\perp}{c}$ for fourteen different weapons with $\frac{L_\parallel}{c} = 0$. Notice that excellent correlation exists and ℓ/c varies from 8.8 up to 92.0 for the weapons plotted in Fig. 5. The grenade launchers and pistol would not correlate had we plotted $\frac{Pc^3}{W}$ versus $\frac{L_\perp}{c}$ for $\frac{L_\parallel}{c} = 0$. The variation in weapon characteristics is much greater in Fig. 5 than the variation in weapon characteristics for earlier scaling efforts. This evaluation of the scaling for blast pressures about weapons uses data from guns firing both supersonic and subsonic projectiles; the largest caliber divided by the smallest caliber is a factor of 18.5; the greatest energy divided by the least energy is a factor of 430; the standoff distance covers two orders of magnitude, and barrel lengths vary by more than an order of magnitude. The correlation is excellent especially when one considers that the data come from various sources [4, 6-9] whose authors had no thought of testing the scaling law of Eq. (12). Had muzzle velocity been measured, the rounds been hand loaded, bomb calorimeter tests been conducted on all powders, etc., a greater degree of correlation could perhaps have been obtained.

These observations on the scaling of peak pressure have required some assumptions. All the assumptions inherent in Hopkinson scaling for peak pressures are present in this analysis. In addition to assuming a weapon under sea level ambient conditions with heat conduction, viscosity, and gravitational effects minimal, we assume that the shock is sufficiently weak so that the ratio of specific heats in air may be considered a constant. This assumption requires overpressures of under approximately 300 psi for the scaling to be rigorously correct. Inasmuch as a 300-psi overpressure is extremely high, and the other assumptions associated with Hopkinson scaling are relevant, this scaling for peak overpressures seems very appropriate.

Because of a lack of information concerning the specific impetus of various propellants, a constant value was assumed for all powders, $350,000 \frac{ft\text{-}lb}{lb}$. Of even greater consequence was the assumption that the ratio of specific heat equaled 1.25 for all ignited propellants. The ratio of specific heat plays a prominent role because the specific energy in the propellant is calculated by dividing the specific impetus by the ratio of specific heat minus one. Undoubtedly, the lack of precise information for calculating the energy in the blast created the greatest scatter in the experimental scaling results seen in Fig. 5. In addition, different values for available energy in the same propellant depend upon the measurement technique used to determine the energy. Virtually no reports presenting experimental blast data indicate the quantity or type of propellant. For these reasons, the propelling energy could only be estimated in developing the blast observations presented in Fig. 5.

Personal discussions with naval personnel have indicated that a gun can emit a significant muzzle flash, especially if flash suppressors are not present in the powder. A second shock wave will be propagated if a weapon flashes. The peak overpressures associated with the second front often exceed the overpressures in the initial shock waves. Our application of Hopkinson scaling does not model these secondary explosions caused by unexpended oxygen-starved propellant igniting outside the barrel.

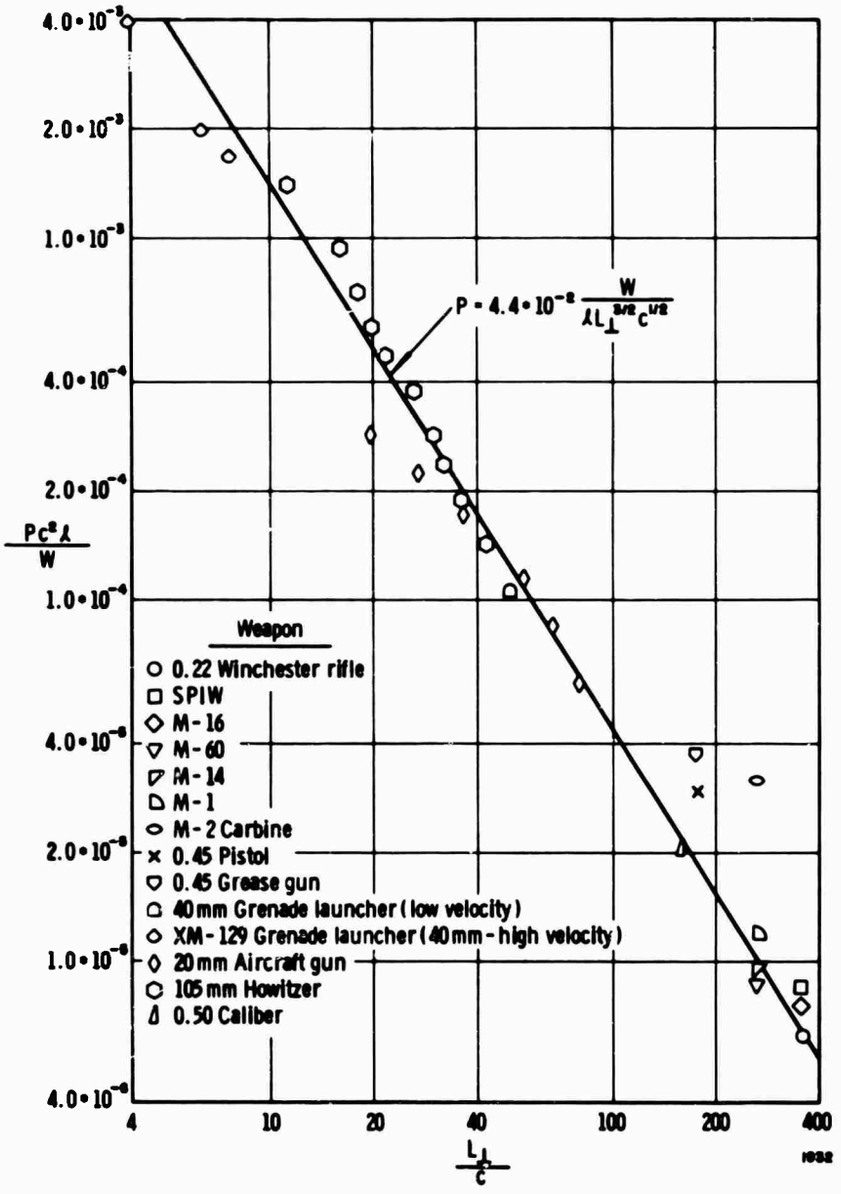

Fig. 5 - Scaled side-on pressure versus scaled standoff for Army guns

Fortunately, the secondary flashing phenomena are most pronounced in large caliber weapons such as naval guns; however, some small caliber weapons will flash; but, usually in the smaller caliber weapons, the second shock front is not as pronounced. Flashing is a phenomenon that can modify these experimental results.

In Fig. 6, one observes scaled free-field blast pressures as a function of $\frac{L_{\perp}}{c}$ with $\frac{L_{\parallel}}{c} = 0$ for eight different naval guns reported in Refs. [4, 10-12]. As was the case with the fourteen different Army weapons, these naval weapons appear to form a unique function. An oddity arises in that the naval guns all appear to give a lower scaled pressure than the Army weapons for a given $\frac{L}{c}$. The discrepancy is not enromous considering the art of blast measurements; nevertheless, the discrepancy is apparent. At $\frac{L_{\parallel}}{c} = 0$, Army pressures range

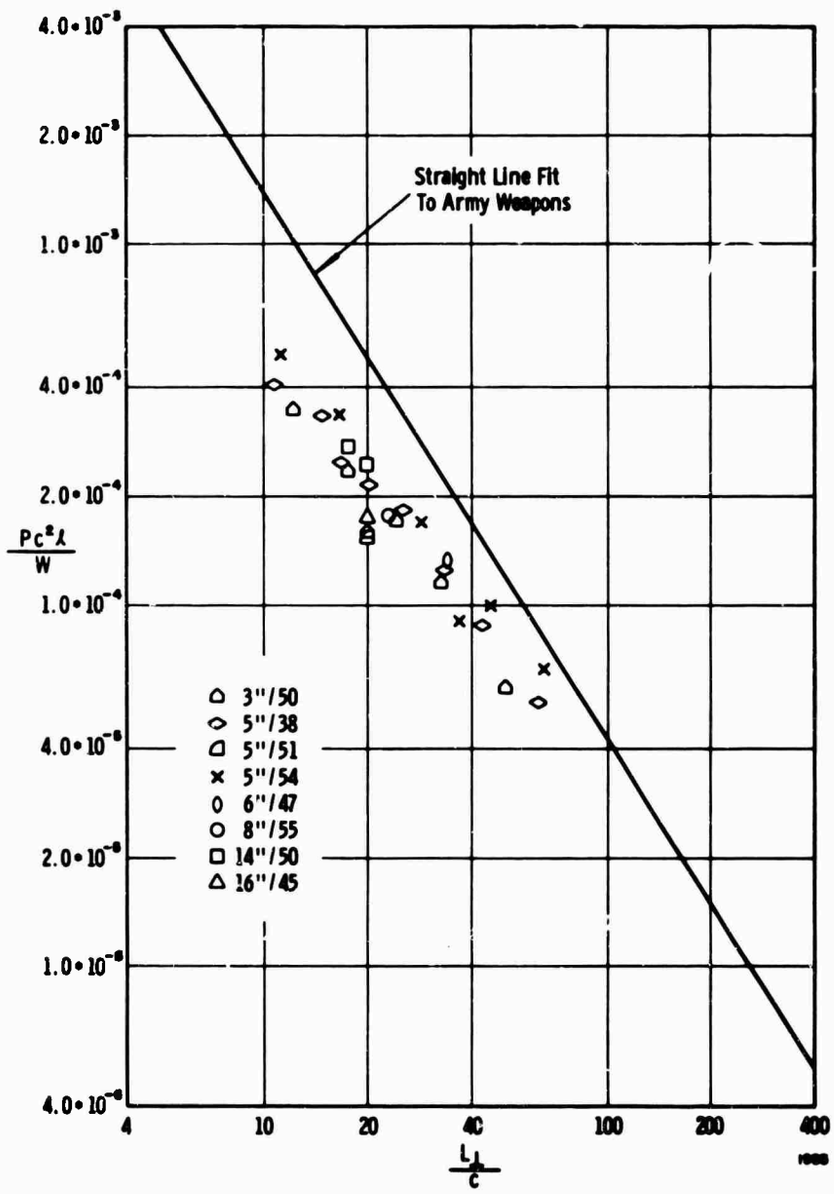

Fig. 6 - Scaled side-on pressure versus standoff for naval guns

from 1.5 times Navy pressure at $\frac{L_\perp}{c} = 70$, to 2.5 times Navy pressures at $\frac{L_\perp}{c} = 15$. This phenomenon is not easily explained but may be the results of: (1) muzzle flashing which seems more prevalent in naval guns, (2) much of the naval data being old, relative to the more recent army data with newer instrumentation giving more accurate (and higher) pressure peaks, (3) an average specific impetus for naval powders which are usually single base propellants and lower than the average specific impetus used in calculating data points for the double base propellants used in Army weapons, or (4) combinations of these possible explanations. Little detailed background information is presented on each experiment, so no more adequate explanation can be offered for lower-scaled pressures in naval guns than Army guns. This oddity could probably be explained had experiments been more completely reported;

nevertheless, with eight naval guns scaling pressures excellently as a group, and fourteen Army weapons scaling pressures excellently as another data sample, one should not discredit these experimental observations made on scaling free-field blast pressures about weapons.

FREE-FIELD SIDE-ON IMPULSE

In Fig. 7, one observes isoclines of constant scaled impulse on a plot with a nondimensionalized distance from the line of fire as an ordinate and a nondimensionalized distance from the muzzle along the line of fire as an abscissa. This presentation for scaled free-field impulse was created after experimentally observing that the precise equation for free-field impulse, Eq. (10), could be approximated by multiplying $\frac{Ic^2}{W}$ by $\left(\frac{\ell}{c}\right)^{3/4}$ to form Eq. (13):

$$\frac{Ic^{5/4}\ell^{3/4}}{W} = f\left(\frac{L_\perp}{c} \ , \ \frac{L_{||}}{c}\right) \qquad (13)$$

Fig. 7 is a plot of Eq. (13) using the experimental data generated by Shapiro and Rich for a 20-mm aircraft gun [9]. Actually, Eq. (13) is not r dimensional as the pi term $\frac{Ic^{5/4}\ell^{3/4}}{W}$ should have the velocity of sound to the first power in the expression. Eq. (13) has been written as a scaling parameter with dimensions because the velocity of sound remains invariant with no need to include a dimensional constant in the expression. Caution should be used in applying the appropriate dimensions to all impulse data. Note that Fig. 7 employs Hopkinson scaling and incorporates the effects of barrel length in the solution through an empirical observation similar to the observation used to develop the pressure scaling.

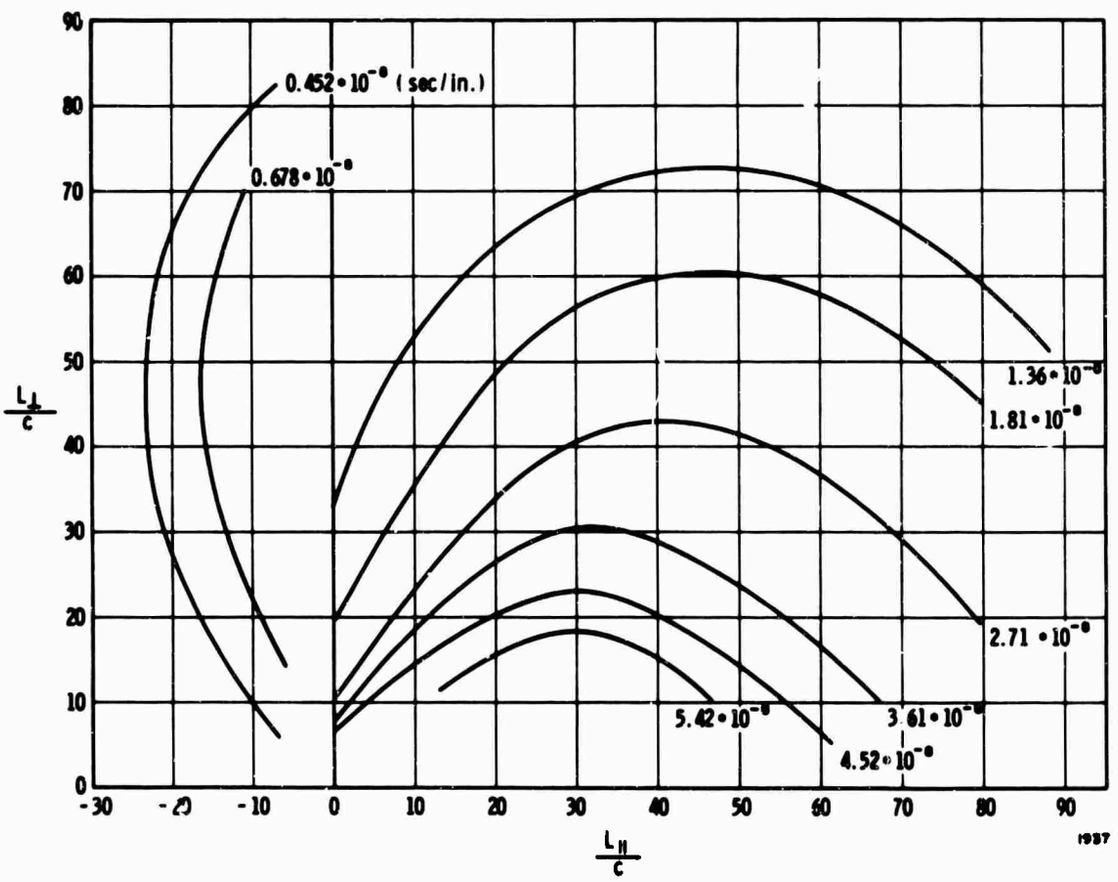

Fig. 7 - Isoclines of constant scaled impulse, $\frac{Ic^{5/4}\ell^{3/4}}{W}$

Fig. 8 is a plot of $\frac{I c^{5/4} \ell^{3/4}}{W}$ versus $\frac{L_\perp}{c}$ for sixteen different weapons with $\frac{L_\parallel}{c} = 0$. Notice that excellent correlation exists for both Army and naval weapons and for short-barrelled as well as long-barrelled weapons. These experimental data come from Refs. [4, 6, and 10] as virtually no one else reports experimentally observed impulses in the free-field along a line through the muzzle and 90 deg to the line of fire. A slight tendency exists for the naval weapons to scale lower than the Army weapons. As was the case in discussing the scaling of free-field pressures in Army and naval weapons, this phenomenon can not be explained, but may be the results of: (1) muzzle flashing which seems more prevalent in naval guns, (2) the naval data being old relative to the Army data, (3) an average specific impetus which is lower in naval powder, or (4) combinations of these phenomena. Under the worst conditions, the scaled Army impulses are only 1.33 times the Navy impulses. The discrepancy in scaling impulse for naval guns and Army weapons is much less pronounced than the discrepancy with respect to scaling their respective peak pressures.

TRANSIENT PRESSURE HISTORY

The engineer or designer who must analyze the structural response of a panel or other structural component is interested in knowing the shape of the transient load applied to the structural element for all instants in time. Fortunately, a curve-fitting procedure exists that approximates the shape of the transient load from a knowledge of impulse and peak pressure. The Friedlander equation with specific values assigned to the constants fits experimental data very well in predicting the

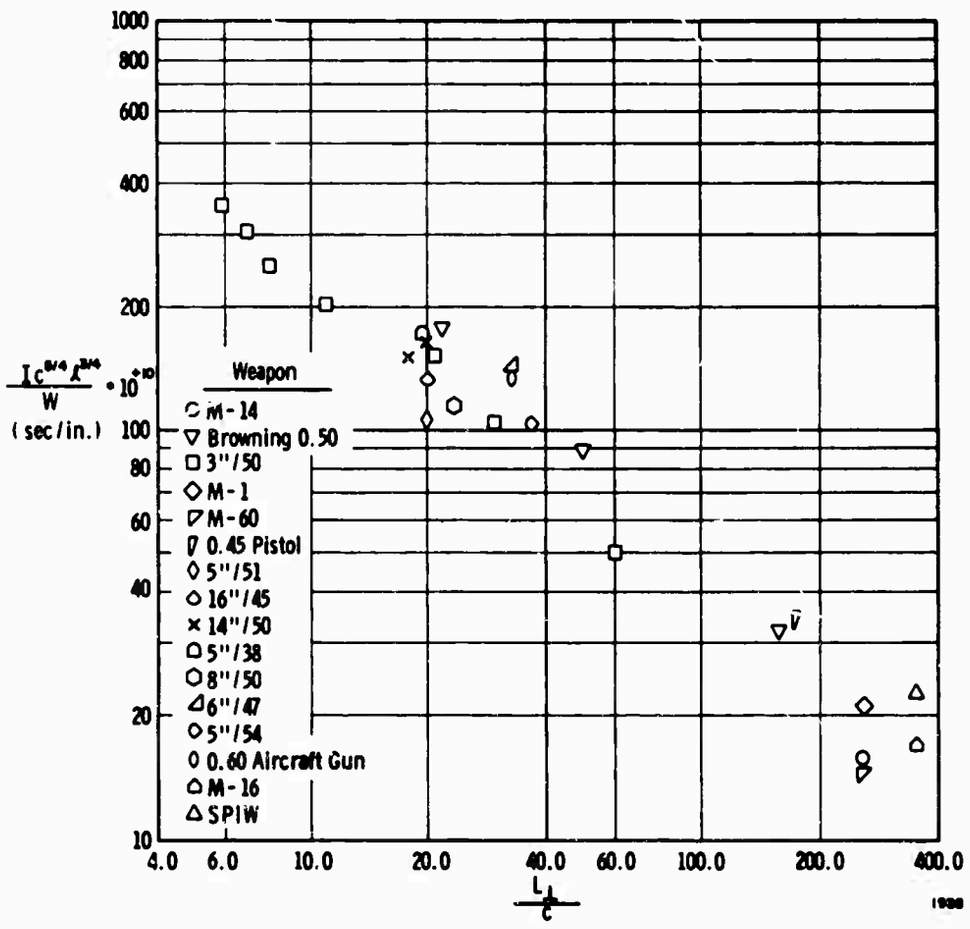

Fig. 8 - Scaled side-on impulse versus scaled standoff

shape of the blast wave emitted from a H. E. charge [13]. This equation has the form:

$$p(t) = P\left(1 - \frac{t}{T}\right)e^{-t/T} \quad \text{for } 0 < t < T \qquad (14a)$$

$$p(t) = 0 \qquad \text{for } t > T \qquad (14b)$$

Such an equation describes our experimental observations extremely well. The integrated form of Eq. (14) gives a maximum positive impulse of

$$I_{max} = \frac{PT}{e} \qquad (15)$$

Because I, P, and e are all known, the duration of loading T is found upon substituting in Eq. (15). The shape of the applied transient load then follows from Eq. (14). Fig. 9 compares the curve fit expressed by Eq. (14) to experimentally observed loads measured about

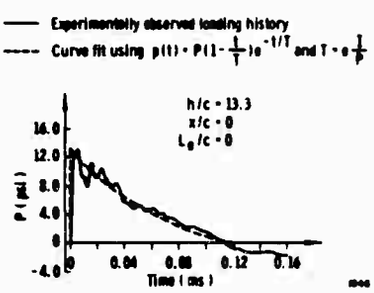

Fig. 9 - Comparison of curve-fit to observed loading history

a caliber .45 pistol. Any error which exists in applying Eq. (14) does not exceed the error in the isoclines of maximum impulse or isobars of peak pressure which determine the duration of loading or time constant, T. Other curve-fitting equations have been evaluated [14] about H. E. charges, but none appear to improve on matching experimental observations without compounding analytical efforts. In addition to being easily applied, this procedure estimates the duration of loading with greater accuracy than is available in the experimental observations on pressure and impulse. The technique slightly overestimates the duration of the positive loading phase, but usually by less than 8%.

CONCLUDING COMMENTS

Although this paper has dealt exclusively with side-on or free-field blast about guns, the report [15] which this paper abstracts considers the actual load imparted to a panel or other structural component in the blast field. In addition, the report discusses the blast field about guns with muzzle brakes, flash suppressors, and similar devices which direct the flow of gases emitted from the barrel. Other discussion in the report centers on the blast field about recoilless weapons and rockets. This information has been deleted from this paper in the interest of brevity, but may be found in Ref. [15].

A procedure has been described for estimating the blast field about weapons. For the more conventional closed-breech weapons, this procedure is well developed and only requires a knowledge of the amount and type of propellant, the weight of the projectile, the velocity of the projectile, the length of the gun barrel, the caliber of the weapon, and the position in space or on a panel for determining the blast field. Graphs are presented which permit estimates of peak pressure and impulse. The report shows that the transient pressure history may be approximated by the Friedlander equation with specific values which are functions of peak pressure and impulse assigned to the time constants. Experimental data on weapons ranging from pistols to naval guns substantiate these observations. This information constitutes the first necessary step in a transient analysis of a panel or other structural element being loaded by the blast wave emitted from the muzzle of a gun.

ACKNOWLEDGMENTS

This author is indebted to many individuals for supplying experimental data on muzzle and breech blast about weapons. The contract technical monitor, Mr. O. T. Johnson, at Ballistic Research Laboratory, acquired many firing reports; Mr. Harry Rich and Dr. W. W. Murray from Naval Ship Research and Development Center, Washington, D.C., furnished information on naval guns; Mr. Edward Briggs, Sr., from Fort Sam Houston, provided ballistic data on Army weapons; Mr. Don Lince and Mr. George Garinther, of Human Engineering Laboratory, supplied unreported test data about eleven different weapon systems; and Mr. Robert Geene, from Interior Ballistics Laboratory at BRL, furnished data on interior ballistics in Army weapons. Without the information contributed to this program by these individuals, the scaling considerations presented in this paper would be only a hypothesis.

Many SwRI personnel contributed by offering opinions and suggestions for improving the observations reported in this paper. The author extends special recognition to Dr. W. E. Baker, project manager; Mr. P. A. Cox; and Mr. Sandor Silverman, who as authors of other aspects in the overall program on structural response of helicopters to muzzle blast, furnished many pertinent and constructive suggestions. The cooperation of these individuals and others is greatly appreciated.

REFERENCES

1. B. Hopkinson, "British Ordnance Board Minutes 13565," 1915.

2. R. G. Sachs, "The Dependence of Blast On Ambient Pressure and Impulse," Ballistic Research Labs., Rept. No. 466, Aberdeen Proving Ground, Maryland, 1944.

3. George T. Reynolds, "Muzzle Blast Pressure Measurements," Rept. No. PMR-21, Princeton University, April 15, 1944.

4. U. S. Navy Gun Blast Committee, "Survey Of Research On Blast," First Interim Report, 1946, pp. 15-25

5. H. J. Barton, R. J. Heyman, and T. Schiffman, "Correlation Of Muzzle-Blast Pressures Over Flat Surfaces," Armour Research Foundation of Illinois Institute of Technology (Undated, but apparently in mid-1950's).

6. George Garinther and Donald Lince, Unpublished Data, Human Engineering Laboratory, Aberdeen Proving Ground, Maryland.

7. Ernest Stuckal, "Technical Feasibility Study and Preliminary Design Airmobility Artillery," Vol. 1, USSAVLABS Tech. Rept. 66-7, March 1966

8. Charles O. Bateman, "Blast, Flash, Gas, and Erosion Studies M134, XM129, and XM140 Weapons," Frankfort Arsenal, Philadelphia, Pa., June 1967.

9. Nathan Shapiro and Harry Rich, "Measurement of Muzzle Blast From the 20 mm and the Short Barrel Caliber 0.60 Aircraft Guns," NA810-059, TED-TMB-DE-201, David Taylor Model Basin, May 1949, Report C-45.

10. Preliminary Letter Report, Subject 3"/50 Gunfire Free Field Blast Measurement; preliminary report on, (a) Test Plan for Land-Based 3"/50 Caliber Gunfire Test at NWL, Dahlgren (SMS-FS-117) of 22 May 1967, (b) ORDTASK No. 201- RDT&E-30-67 of 7 July 1967, From U.S. Naval Weapons Laboratory, Dahlgren, Va., To Naval Ordnance Systems Command, Washington, D.C., Reference WDEI: WPB: efl 8310.

11. M. F. Walther, "Gun Blast From a 5"/54 Gun," N. P. G. Report No. 1608, Weapons Development and Evaluation Laboratory, U.S. Naval Proving Ground, Dahlgren, Va., July 30, 1958.

12. M. F. Walther, "Gun Blast From a 5"/38 Gun," N. P. G. Report No. 1307, U.S. Naval Proving Ground, Dahlgren, Va., Nov. 26, 1954.

13. C. K. Thornhill, "The Shape of a Spherical Blast Wave," A.R.D.E. Memorandum (B) 41/59

14. N. H. Ethridge, "A Procedure for Reading and Smoothing Pressure-Time Data from H. E. and Nuclear Explosions," BRL Memorandum Report No. 1961, September 1965.

15. Peter S. Westine, "Structural Response of Helicopters to Muzzle and Breech Blast, Volume I, Free Field Blast About Weapons," Southwest Research Institute Contract No. DAAD05-67-C-0201 with U. S. Army Ballistic Research Laboratories, Not Yet Published (Unclassified but limited distribution).

SPECIFICATIONS: A VIEW FROM THE MIDDLE

T. B. Delchamps
Bell Telephone Laboratories, Incorporated
Whippany, New Jersey

Specifications were the subject of extended panel discussions during the 31st and 34th Symposia. Virtually all of the traditional elements of conflict within and between the various government and industrial agencies of supply, procurement, and use are represented in the transcripts. An effort will be made to organize this collection of viewpoints as a basis for further discussion. Since consensus in these matters is not a reasonable expectation, the common goal of providing reliable working hardware depends upon a thorough understanding of diverse views, justified in their own context, and upon our collective ability and willingness to apply a substantial measure of skill and judgment in resolving differences or achieving suitable compromise.

INTRODUCTION

In lieu of moderating a panel session on shock-and-vibration specifications at this symposium, the writer agreed to undertake a critical review of panel sessions on the same subject which were held during the 31st and 34th Symposia. For added interest, the session entitled "Optimum Balance Between Component and Systems Testing" from the 31st Symposium, has been included. Representative comments appearing on 39 pages of text have been literally torn from context, and arrayed, with commentary, in a manner that will hopefully display them in a new and useful perspective. In general, quotation marks are reviewer's license since it is understood that most of the material was edited for clarity prior to publication in the proceedings. Some freedom has been exercised in evaluating the panelists' intent, but names have been withheld to protect the guilty.

WHAT IS A SPECIFICATION?

First, because the panelists didn't, let's attempt to distinguish between specifications and standards, and then dispense with further discussion of the latter. Standards are usually broad in content and offer an array of alternatives for doing a general class of work. Specifications, on the other hand, usually provide detailed instructions covering how a specific job must be done. Specifications draw support from standards but tend to become autonomous in the context of a particular program. Some specifications, MIL-S-901 for example, spring full blown, like Aphrodite from the foam, without significant help from prior guiding standards. Such specifications tend to go it alone, and although their ancestry is frequently in question, their impact on the society of things is often dramatic, sometimes devastating, but almost always useful. In general, specifications are ambivalent, since they serve as the focus for both agreement and dispute. Good specifications are keystones of success -- poor specifications are wellsprings of failure. Good specifications are trustworthy, loyal, helpful, etc. -- poor specifications are not.

Now let's look in on the specification panelists at the 31st and 34th Symposia and see if we can pan some nuggets of insight from their stream of consciousness. We'll cover various general subject areas in the following order: FUNCTION, TECHNICAL BASIS,

FLEXIBILITY, RISK/RESPONSIBILITY/COST, and TEST CRITERIA.

FUNCTION OF SPECIFICATIONS

First, our panelists generally agreed that specifications should function to protect both buyer and supplier at all levels of military procurement, with the focus and flexibility of requirements narrowing from systems offices in the direction of the suppliers of component parts. The transcripts confirm that the system contractor usually enjoys considerable freedom in establishing environmental design criteria and in passing his requirements down the line, with appropriate multipliers to allow for resonant buildups and as a tribute to conservatism. The component supplier, however, unless he manufactures inertial instruments, frequently receives the final requirements with detached amusement and skepticism, but with no substantial concern prior to test, since he wouldn't know how to go about designing to the specification anyway.[1] Nevertheless, in the belief that this might be a straightforward exercise, one panelist observed that: "Some problems could be traced to component manufacturers who failed to put the specification numbers into their design." [2] Perhaps this indictment reflects a degree of over-optimism regarding the quality and character of component design technology, at least where the environment is concerned.

There were valiant attempts, particularly at the 34th Symposium, to distinguish between specifications as design criteria and as test requirements. Various types of tests which the designer must anticipate were mentioned, though not discussed in depth, and it was generally agreed that to the extent the designer can respond a priori to test criteria, he must make the effort. Usually, however, "you try to get the equipment as rugged and strong as you can under practical, yet economical conditions. If it is relatively easy to make the equipment much stronger, you do so. If it is difficult, you go only to what you think the conditions might be."[3] It was pointed out that shipboard shock-test requirements admitted no direct design interpretation and that somehow, the designer must be given early guidance of greater sophistication than impending trial by hammer. [4] Yesterday's discussion on this subject indicates that considerable progress has been made in this direction during the ensuing years.

TECHNICAL BASIS FOR SPECIFICATIONS

Next, what did our panelists consider the most important single ingredient of good specifications? Not surprisingly, nothing was said about either legal subtlety or literary excellence. The panelists views are made quite clear by such statements as: "first, one must acquire data"[5] and "the hope was that one could anticipate the vibration that the system and components would experience by analyzing or obtaining data from similar operating systems." [6] Further: "Special emphasis should be placed on the prediction of the environment." [7] And finally: "there have been rather successful attempts to predict, using models and subscale tests, what the response is going to be at the component level for future systems." [8] Needless to say, the ideal situation is one in which direct measurement of the environment at points of interest forms the basis for design and testing specifications. Since this is clearly not possible in the early stages of many programs, we must be diligent and imaginative in making our predictions, we must permit our specifications to respond to new information, and our first priority must be to obtain the required information by direct measurement at the earliest opportunity.

FLEXIBILITY OF SPECIFICATIONS

This brings us to one of the more difficult questions discussed by our panelists, namely: to what extent should we, can we, or must we, allow our specifications to breathe-in new information? Let's listen to the panelists: "We try to update our specifications just as early as we possibly can."[9] "They need to be fairly constantly revised as work proceeds." [10] "We refine (the specification) again after the first series of flights and again after a later series of flights." [11] Surprisingly, nowhere in these transcripts is there any reference made to cost impact of changes in scope-of-work midway through a program. It would seem clear, however, that responsibility rests ultimately with the originators of the top environmental spec in any given situation. This accounts for the tendency toward over-conservatism found in early equipment and component specifications, which prompts, though does not necessarily justify such glib comments as: "To have a really good

specification, you shouldn't be throwing in these ignorance factors unless there is good cause." [12] We'll all have to recognize that there almost always is good cause, however, we must carefully avoid being capricious in establishing our margins.

The possibility of simply specifying that the equipment function and survive in the service environment, without defining that environment, was considered at some length. [13] This works fine at the system level where the prime contractor usually bears major responsibility for defining the service environments and has the experience to back it up, however, there seems to be no practical alternative to being more specific in component specifications, while maintaining some fluidity until the environments have ultimately been confirmed. At the same time we must remain sensitive to the potential penalties in cost and time associated with careless, inadequate or tardy environmental definition.

Another aspect of flexibility concerns implementation of specifications, rather than content. I refer specifically to deviations and waivers, the Scylla and Charybdis of good specsmanship. One panelist remarked: "We do waive certain specifications when it is justified by the contractor." [14] From another transcript I surmised that such negotiations usually take place in a steambath: "In our debates we could all be stark naked and it would still be obvious who the contractor and who the government people were." [15] Clearly, the spectrum of waivers and deviations, both temporary and permanent, spreads from full engineering justification, through expediency, to unwarranted risk. Unfortunately, timing and cost factors frequently force decisions in such matters toward the wrong end of this spectrum.

Other observations were: "His request for a change was denied by the legal people even though it was supported by reliable field data and the government technical representatives were in agreement." [16] And: "If the contractor does not take exception to the spec at the time he makes the proposal, that is his responsibility." [17] Further: "It might be worthwhile for the panel to consider the question of how much preliminary engineering it is justifiable for a company to do in order to search out, ahead of time, the exceptions they need to take to the specifications." [18] At that point, someone changed the subject. My own view is that it's not basically a question of justification, but rather, one of contractor obligation to himself and to his customer. We all know that it frequently costs money to discharge our obligations. If one is in the business, he ought to be required to know something about it.

A most interesting and instructive exchange involved that favorite focus of controversy, Navy shock test requirements. Apparently, there is equipment presently at sea which has never survived the rigors of MIL-S-901: "The requirement was waived when they bought the equipment --." [19] Such equipment would probably not survive the combat environment, and indeed, some has "turned out to be so bad that it required a special crew of people to keep it operating in a number 3 sea state."[20] Such waivers are presumably temporary and clearly fall in the "expedient" category. Our Navy has an immediate job to do, and such statements as "The fact that they are letting this equipment go to sea indicates that they admit that the specification is inadequate" [21] seem ill-advised and unwarranted.

RISK, RESPONSIBILITY AND COST

These three elements in the specification domain are intimately entwined, like the convolutions of a well-formed pretzel. Direct and indirect reference to these three appear about 25 times in the transcripts. One panelist commented: "If you're selling, you want to get the best price with the least restriction. If you're buying, you want the most restrictions." [22] Sometimes it gets more complicated: "It would be necessary to establish a group of ground rules on the amount of risk you wish to take, the probability requirements for the function of this piece of equipment, and how much money you want to spend." [23]

Now some of my best friends are statisticians -- and while I know I can't function effectively without them, I am dismayed by the extent to which their mystique has become a substitute for engineering judgment, rather than its reinforcement, the role originally intended. While it is sometimes true that risk can be quantized within a statistical framework, in the final

analysis it is sound engineering that pays off. Who is responsible for sound engineering, statisticians or engineers? Although the answer seems obvious, and even our statisticians agree, the obvious response does not appear to enjoy universal acceptance within the engineering profession, as indicated by statements like the following: "With a proper application of probability theory, we could devise a test -- which would have associated with it a confidence level and all the other regalia that quality control requires. Within that level of confidence you could perform your design and hope that your test would simulate what you had designed into your vehicle and equipment"[24] whatever that means.

By taking certain literary liberties, I have pieced together this dialogue: "Are contracts currently being written so that it is the legal responsibility of the contractor to produce an item which will perform satisfactorily in service operation?"[25] Answer: "We wrote a requirement that the total system should work in a given manner with one associate contractor becoming responsible for the system. The remaining contractors were responsible for delivering their equipment to him."[26] But unfortunately: "The systems contractor will not accept responsibility for a failure if it's not his equipment, -- (and) you can't expect each man to guarantee the performance of his single piece of equipment when he has no idea what the associated contractors will do to his equipment after it is delivered." [27] At the systems level, incentive contracting (regardless of what else you may say about it) has clearly improved this situation since 1963. One would hope that component suppliers are no longer so lacking in information and skill that they cannot assume some burden of responsibility. Good specifications, of course, are of fundamental importance here.

Risk, responsibility, and cost, were all implied in the following tale of one observer: "Those who knew what the problems were, bid high, throwing in lots of contingencies, because they could anticipate problems of shipping, handling, and so on. The lower bidder, who didn't know or care about those things, was likely to get the award." [28] Nobody popped up with an answer to this dilemma, however, the answer would seem to lie in the extent to which we allow good engineering judgment to prevail in a cost-conscious climate. This is seldom easy, and is often impolitic, but with a measure of courage, and with due care in the selection of potential suppliers, in the preparation of specifications, and in the evaluation of proposals, catastrophe should be avoidable in nine out of ten cases.

TEST CRITERIA

Let's begin with an apt comment by one of the chairmen: "Test procedures and the specs which call for them are not moral questions. It is not a question of fair or unfair tests, but of useful tests and tests which are not useful." [29] Such tests, in the broadest sense, should include those identified as either development, design qualification, (flight) acceptance, or reliability demonstration. Although the transcripts show general agreement on the intent of tests in each of these categories, a variety of opinions erupted concerning their implementation. Both the problems and the controversy spring directly from our limited ability to predict, measure, and reproduce in the laboratory, the environments of concern. More specifically, at the very moment we are taking costly and imaginative steps toward overcoming ignorance of the environment and refining testing techniques, we must concurrently design, build, and evaluate hardware which will perform its intended function in the real world.

With regard to prediction: "Because of the mounting arrangements of the pump and variations of the propellant burning, it is almost impossible to predict the vibration spectrum and magnitude." [30] And: "Vibration specifications are based a good deal on insufficient actual measurements." [31] Finally: "There is no such thing as a predictable real environment -- because they are all different, therefore the tests you devise must be a conglomerate of the real environments." [32] Regarding simulation technique: "the field vibration environment is probably omnidirectional, whereas your simulation equipment is usually unidirectional."[33] And: "we are now concerned with conditions like separation shock caused by explosive hardware which results in requirements of 5,000 g's with durations of 1/4 millisecond." [34] I don't believe that any of us here today has yet developed a fully-satisfactory laboratory technique for handling this one.

One of the transcripts contains a brief flurry regarding the use of sine testing, identified as a "diagnostic" tool, for design-qualification purposes. It was argued (by implication) that virtual absence of periodic components in the service environment should invalidate sine testing as a qualification requirement. [35] The man from Marshall heartily disagreed,[36] and his position would seem fully justified. Sine testing is universally recognized as an essential development tool, and confirmation of its effective prior use is clearly admissable as a qualification requirement.

In one way or another, all of the items just discussed contribute variability to the testing process and force us to balance our lack of testing skill and knowledge of the environment with appropriate design and testing margins. This does not absolve us, however, from recognizing the merit in the argument of one panelist: "The vibration test specification should be such that when an item of equipment passes the test that is specified it should function with reasonable certainty in the service environment. Also, a good test specification should be such that if an item of equipment functions in a service environment, we would like to think that it would pass the specified test." [37] Nevertheless, my personal view is that I would rather see a bad specification in the latter sense, than tempt the Fates by cutting margins to the bone. Dr. Vigness put it nicely when he said: "Run it through a vibration or a shock test, find out what fails, and correct it. Do that several times and be sure that it is at least several times as strong as the value specified for the completed equipment. Don't worry if it's a lot stronger because sometimes this can be accomplished with only a little bit of effort." [38] Although this comment may have been made with shipboard equipment in mind, it has a more solid ring to me than the assurance that: "Once you have the variance, the standard deviation, and some assumed sampling distribution, it is possible to establish a test level which will, with a reasonable degree of confidence, include all the vibration levels you've anticipated in that area of the vehicle." [39] I guess all you have to do is anticipate the levels and the computer will take care of the rest.

CONCLUSION

It is the hope of any reviewer that he brings his audience a sometimes pleasing, sometimes stimulating, and sometimes downright irritating mixture of his own and his subjects' views and prejudices. In wading through the welter of crosscurrents evoked by the subject of shock and vibration specifications, I have not attempted to touch on all topics and attitudes represented in the transcripts, but rather, I have tried to provide a sampling of certain key viewpoints on subjects of general interest. Perhaps I have not been entirely fair in the execution, and for this I apologize. Nevertheless, if I have in any way helped to distill or clarify some of the material contributed by the panelists (while adding my own measure of bias) then I am pleased.

REFERENCES

Reference Number	Bulletin Number	Page Number	Reference Number	Bulletin Number	Page Number
[1]	31-II	283	[21]	34-4	157
[2]	31-II	279	[22]	31-II	291
[3]	31-II	288	[23]	31-II	301
[4]	34-4	157	[24]	31-II	296
[5]	34-4	156	[25]	31-II	292
[6]	31-II	277	[26]	31-II	292
[7]	34-4	156	[27]	31-II	292
[8]	31-II	278	[28]	31-II	292
[9]	34-4	159	[29]	31-II	280
[10]	34-4	153	[30]	31-II	276
[11]	31-II	290	[31]	34-4	154
[12]	34-4	156	[32]	31-II	298
[13]	31-II	292	[33]	31-II	296
[14]	31-II	291	[34]	34-4	155
[15]	34-4	154	[35]	34-4	161
[16]	31-II	290	[36]	34-4	161
[17]	31-II	290	[37]	34-4	156
[18]	31-II	290	[38]	31-II	288
[19]	34-4	157	[39]	34-4	160
[20]	34-4	158			

GPO 872-334